

Transcriptomic Assessment of Quinone Mediated Hepatic Oxidative Stress

Thesis submitted for the degree of

Doctor of Philosophy (PhD)

at the University of Leicester

By

Joel D Parry BSc.

MRC Toxicology Unit

University of Leicester

December 2007

UMI Number: U495643

All rights reserved

INFORMATION TO ALL USERS

The quality of this reproduction is dependent upon the quality of the copy submitted.

In the unlikely event that the author did not send a complete manuscript and there are missing pages, these will be noted. Also, if material had to be removed, a note will indicate the deletion.



UMI U495643

Published by ProQuest LLC 2013. Copyright in the Dissertation held by the Author.
Microform Edition © ProQuest LLC.

All rights reserved. This work is protected against
unauthorized copying under Title 17, United States Code.



ProQuest LLC
789 East Eisenhower Parkway
P.O. Box 1346
Ann Arbor, MI 48106-1346

ABSTRACT

Transcriptomic Assessment of Quinone Mediated Hepatic Oxidative Stress

Joel D Parry, MRC Toxicology Unit, University of Leicester

Several important anti-cancer drugs contain quinone moieties. Quinones can be chemically highly reactive and cause redox cycling, sulphhydryl arylation or interact with reducing centres such as the mitochondrial electron transport chain. This chemistry may be essential for anticancer pharmacology, but the associated toxicity also restricts use and affects development of drugs with quinone-related metabolites. Quinone based drugs are complex structures with multiple chemical properties. Therefore in this work to further understand quinone toxicity in drugs simpler structures with defined chemistry were used as tools. To discern mechanistic insight transcriptomic investigations were undertaken in rat hepatocytes and *in vivo* mouse liver exposed to a range of prototypical quinones. Genes important in response to quinone exposure were identified and analysed using several bioinformatic tools.

Transcriptomics in hepatocytes could not differentiate quinone redox effects from other interactions, although 22 'quinone signature genes' indicated a coordinated response to redox stress. A central role for mitochondria as targets of quinone interaction was confirmed, the transcriptomic profile indicating optimisation of energy metabolism and suppression of intrinsic apoptosis. *Pim1* and *Pim3* kinases were central to this response, confirmed in follow up experiments.

Pharmacokinetics from mice treated *in vivo* with 25mg/kg DMNQ or menadione intraperitoneally indicated DMNQ to be more widely distributed and better suited as an *in vivo* redox model compound than menadione. However, *in vivo* redox challenge from DMNQ in the liver was transient and insufficient to cause oxidative damage. The findings indicate that DMNQ has utility for studying redox stress *in vivo*, although a repeat dosing approach is required in future.

The findings add to the knowledgebase of quinone toxicity. Particularly the increased responsiveness and sensitivity of hepatocytes *in vitro* compared to *in vivo* which may lead to an erroneous perception of toxicity if *in vitro* systems are studied alone.

ACKNOWLEDGMENTS

It is difficult to know where to start when it comes to acknowledging those who have helped, guided, inspired, motivated, and supported me throughout the duration of this thesis. I will start by thanking my academic supervisors at the MRC Toxicology Unit, Tim Gant and Andy Smith. They have both shown great patience over the years and in the run up to submission, the speed with which chapters were critiqued was truly impressive. Also thanks to Amy Pointon for all the livers extracted on my behalf. Hopefully I will be able to return the favour one day.

I also owe a debt of gratitude to my industrial supervisor (and line manager at GSK for the last five years) Jon Lyon. Jon has been hugely supportive and on the odd occasion when the task in front of me seemed unachievable, he was always there to coach me through. I would also like to recognise the fact that GSK (my employer) have funded my research and also to thank Angus DeSouza, Elisabeth George and Ron Tyler. These people originally gave me the opportunity to undertake this thesis. Thanks also to the folks I have managed over the last few years (Gino, Jackie, Dan, Rhi, Steve and Laura) for being so understanding and putting up with periods of neglect.

A number of people within GSK have been of huge help during the course of this thesis. Firstly, thanks to my CPT colleagues Tracy Walker, Anita Naidoo, Denise Nemitz and Chloe Day. You have trained me in *in vitro* techniques and were always on hand to sort that damn SpACE[®] autoanalyser out! I also thank Joanne 'HPLC guru' Charlewood for her help with setting up the quinone exposure assays and analysing the data. My colleagues from DMPK, Simon Parry and Steve Hood, were also of great help in educating me on the interpretation of the exposure data. Thanks to Chris Clayton and Adam Taylor in the Discovery Technology Group. Chris first mentored me in the ways of transcriptomics and Adam has been of enormous help with the analysis of my GeneChip[®] data over the last year. Lastly, thanks to Andy Winkley, the other half of the 'IPT part-time PhD student self-help group'. It's always been good to know that someone else was equally miserable at the same time.

I would also like to thank my close friends (Scott, Marc, Steve, Maca, Guy and Andy) for being so understanding. I've lost count of the times I have been unable to make a birthday celebration, or social gathering, as I have had work to do. Sorry. Thanks also to my parents, Marcia and Tom and brother Teifyon, for your support and encouragement. Finally, thanks to my ever loving wife Susannah. You have endured the full spectrum of my emotions and kept me focussed, at times when I was unable to remain so on my own. It's been a difficult year and I could not have got through it without your support and love. Thank you!

P.S. Thanks to Kenco and Twinings for their Costa Rican Blend and 1706 Strong Tasting Tea, respectively. These beverages kept me going.

CONTENTS

ABSTRACT	2
ACKNOWLEDGMENTS	3
CONTENTS	4
LIST OF FIGURES	7
LIST OF TABLES	11
ABBREVIATIONS	13
CHAPTER 1. GENERAL INTRODUCTION	18
1.1. Introduction to Quinones	19
1.1.1. Human Exposure to Quinones	20
1.1.2. Quinones in Medicine	21
1.1.3. Quinone-Related Toxicity	23
1.2. Redox Cycling and Oxidative Stress	27
1.2.1. Redox Cycling	28
1.2.2. Oxidative Damage to Cellular Macromolecules	29
1.3. The Cellular Response to Oxidative Stress	31
1.3.1. Glutathione Synthesis, Regulation and Function	32
1.3.2. Transcriptional Responses to Oxidative Stress	37
1.4. Transcript Analysis, Transcriptomics and Microarrays	42
1.4.1. Stanford-Type Microarrays	45
1.4.2. Affymetrix GeneChips®	47
1.5. Thesis Rationale and Aims	53
CHAPTER 2. MATERIALS AND METHODS	55
2.1. Hepatocyte Monolayer Culture Methodology	56
2.1.1. Isolation of Rat Hepatocytes Using the Ex Vivo ‘Wedge’ Perfusion Method	56
2.1.2. Determination of Hepatocyte Viability and Cell Number	57
2.1.3. Plating, Attachment and Recovery of Hepatocytes	58
2.1.4. Treatment of Hepatocyte Monolayers	59
2.2. Transfection of Hepatocyte Monolayer Cultures with Small Interfering RNA	60
2.2.1. Transfection Complex Preparation	60
2.2.2. Transfection of Rat Hepatocyte Monolayers	61
2.3. Assessment of Hepatocyte Viability Using LDH Leakage	62
2.3.1. Sampling Culture Media and Hepatocyte Monolayers	62
2.3.2. Running the LDH Assay	63
2.4. Assessment of Liver Damage by Measurement of Plasma Alanine Aminotransferase Levels	64
2.4.1. The ALT Assay	64
2.5. Assessment of Liver Damage by Measurement of Plasma Aspartate Aminotransferase Levels	66
2.5.1. Running the AST Assay	66
2.6. Measurement of Hepatocyte Total Protein Content Using the BCA Protein Assay	68
2.6.1. Sample and Standard Curve Preparation	68

2.6.2.	Running the BCA Protein Assay	68
2.7.	Measurement of Glutathione-Related Endpoints.....	70
2.7.1.	Measurement of GSH Using the O-phthaldehyde Method	70
2.7.2.	Measurement of GSH and GSSG Using the Bioxytech GSH/GSSG-412 Assay.....	71
2.8.	Measurement of Activated Caspase 3 Activity in Hepatocyte Cultures.....	74
2.8.1.	Sample Preparation	74
2.8.2.	Running the Caspase 3 Assay.....	74
2.9.	Determination of DMNQ and MNQ Levels by HPLC	75
2.9.1.	Sample preparation	75
2.9.2.	Running the HPLC Assay	75
2.10.	Total RNA Extraction	77
2.10.1.	Hepatocyte Lysate Preparation.....	77
2.10.2.	Liver Tissue Homogenate Preparation.....	77
2.10.3.	Total RNA Extraction Using the SV Columns.....	77
2.11.	Total RNA Quantification and Quality Control	79
2.11.1.	Quantification Using UV Spectrophotometry	79
2.11.2.	Agarose Gel Electrophoresis	79
2.12.	Transcriptional Profiling Using Affymetrix GeneChip® Microarrays.....	81
2.12.1.	Preparation and Quality Control of cRNA Targets for Hybridisation to GeneChips®.....	81
2.12.2.	Hybridisation of cRNA Targets to Affymetrix GeneChips® and Scanning.....	87
2.12.3.	Downstream Analysis of Transcriptomic Data	90
2.13.	SybrMan® Real-Time Quantitative PCR.....	93
2.13.1.	Primer Design and Testing	93
2.13.2.	First Strand cDNA Synthesis	94
2.13.3.	Running SybrMan® RT-QPCR	94
2.13.4.	Statistical Analysis of RT-QPCR Data.....	96
2.14.	Buffer and Culture Media Preparation.....	97
CHAPTER 3.	EVALUATION OF THE RELATIVE CYTOTOXICITY OF SELECTED QUINONES IN RAT HEPATOCYTES.....	99
3.1.	Introduction.....	100
3.1.1.	Quinones	100
3.1.2.	Experimental design	103
3.2.	Results	105
3.2.1.	Biochemical Endpoints	105
3.2.2.	Transcriptional Changes.....	113
3.3.	Discussion	115
CHAPTER 4.	TRANSCRIPTIONAL PROFILES OF QUINONES IN RAT HEPATOCYTES	118
4.1.	Introduction.....	119
4.2.	Results	121
4.2.1.	Biochemical Endpoints	121
4.2.2.	Transcriptomic Investigations	123
4.3.	Discussion	140
4.3.1.	Biochemical Endpoints	140
4.3.2.	Transcriptional Investigations	142

CHAPTER 5.	REDOX MEDIATED TEMPORAL RESPONSES IN GENE EXPRESSION IN RAT HEPATOCYTES	155
5.1.	Introduction.....	156
5.2.	Results	158
5.2.1.	Biochemical Endpoints	158
5.2.2.	Transcriptomic Investigations	162
5.3.	Discussion	180
5.3.1.	Biochemical Endpoints	180
5.3.2.	Transcriptomic Investigations	181
CHAPTER 6.	KNOCKDOWN OF PIM3 OR GCLC TRANSCRIPTION IN RAT HEPATOCYTES RESULTS IN A QUINONE-SENSITIVE PHENOTYPE.....	195
6.1.	Introduction.....	196
6.2.	Results	200
6.2.1.	Optimisation Experiments	200
6.2.2.	Quinone Challenge of Rat Hepatocytes Transfected with <i>Pim3</i> or <i>Gclc</i> siRNAs	206
6.3.	Discussion	212
6.3.1.	Optimisation of Rat Hepatocyte Transfection and Selection of Target Gene siRNAs.....	212
6.3.2.	DMNQ and MNQ Challenge of Rat Hepatocytes With Suppressed <i>Pim3</i> or <i>Gclc</i> Expression.....	214
CHAPTER 7.	TOXICOKINETICS OF DMNQ AND MNQ IN MICE AND THE UTILITY OF DMNQ FOR STUDYING HEPATIC REDOX STRESS <i>IN</i> <i>VIVO</i>	217
7.1.	Introduction.....	218
7.2.	Results	220
7.2.1.	Quinone Assay Development	220
7.2.2.	Preliminary Investigations into DMNQ Exposure Kinetics in C57BL/6J Mice	224
7.2.3.	Toxicokinetics, Biodistribution and Hepatic Effects of Acute DMNQ or MNQ Exposure in C57BL/6J Mice.....	228
7.3.	Discussion	238
7.3.1.	Preliminary Investigations into DMNQ Exposure Kinetics in C57BL/6J mice	238
7.3.2.	Toxicokinetics, Biodistribution and Hepatic Effects of Acute DMNQ or MNQ Exposure in C57BL/6J Mice.....	240
CHAPTER 8.	GENERAL DISCUSSION	244
8.1.	The Utility of Quinone Signature Genes.....	245
8.2.	The Efficacy of Thymoquinone in Preventing Aflatoxin B ₁ -Mediated Hepatocarcinogenesis Warrants Further Investigation.....	247
8.3.	An Insight into the Key Genes Promoting Hepatocyte Survival in the Face of Quinone-Mediated Mitochondrial Toxicity.....	249
8.4.	Comparability of the <i>In Vivo</i> and <i>In Vitro</i> Hepatic Responses to DMNQ and its Utility for Studying Oxidative Stress <i>In Vivo</i>	253
8.5.	Future Work.....	256
8.6.	Conclusions.....	257
REFERENCES	259

ADDENDA CONSISTING OF 1 DATA CD

LIST OF FIGURES

Figure 1.1: Graphical representation of the mitochondrial electron transport chain	20
Figure 1.2: Quinone (menadione) metabolism and toxicity	25
Figure 1.3: Production of HO [*] Via Fenton Chemistry	29
Figure 1.4: Chemical structure of GSH (A) and GSSG (B).	33
Figure 1.5: The γ -Glutamyl Cycle.	34
Figure 1.6: Detoxification of hydroperoxides by GSHPx	35
Figure 1.7: Schematic of the adaptive response to oxidative stress.....	38
Figure 1.8: Schematic of the Nrf2-ARE pathway activation	39
Figure 1.9: Stanford-type microarray production and hybridisation	47
Figure 1.10: Photolithographic synthesis of oligos for the production of Affymetrix GeneChips [®]	48
Figure 1.11: Methodology of standard eukaryotic gene expression assay.....	50
Figure 2.1: The liver perfusion rig with three rat liver lobes <i>in situ</i>	57
Figure 2.2: LDH Assay Principle.....	62
Figure 2.3: ALT Assay Principle..	64
Figure 2.4: AST Assay Principle.....	66
Figure 2.5: Typical BSA standard curve for the BCA Protein Assay	69
Figure 2.6: The GSH Redox Cycle.....	71
Figure 2.7: Typical GSH/GSSG-412 Assay Standard Curve	73
Figure 2.8: Representative RNA 6000 Nano Labchip cRNA Quality Assessment Images.....	86
Figure 2.9: SybrMan [®] Master Plate Layout.....	95
Figure 2.10: Typical SybrMan [®] Standard Curve	96
Table 3.1: Structure and activity of the five quinones under investigation.....	101
Figure 3.1: LDH leakage and GSH depletion in rat hepatocytes as a result of 8 hours BQ exposure.	108
Figure 3.2: LDH leakage and GSH depletion in rat hepatocytes as a result of 8 hours NQ exposure.	109

Figure 3.3: LDH leakage and GSH depletion in rat hepatocytes as a result of 8 hours DMNQ exposure.	110
Figure 3.4: LDH leakage and GSH depletion in rat hepatocytes as a result of 8 hours MNQ exposure.	111
Figure 3.5: LDH leakage and GSH depletion in rat hepatocytes as a result of 8 hours TQ exposure.	112
Figure 3.6: Percent genes significantly modulated in quinone treated cultures relative to vehicle control.	113
Figure 4.1: LDH Leakage (A), GSH (B) and GSSG (C) levels in rat hepatocyte monolayers exposed to VC, BQ, NQ, DMNQ, MNQ or TQ for 1, 4 and 8 hours.	122
Figure 4.2 Overview of data analysis of transcriptional changes induced in rat hepatocytes exposed to BQ, NQ, DMNQ, MNQ or TQ for 1, 4 and 8 hours.	124
Figure 4.3 Heat map representation of <i>K</i> -means cluster analysis of 820 genes regulated significantly regulated with either BQ, MNQ, TQ or DMNQ exposure at 1, 4 and 8 hours.	126
Figure 4.4: Heat map representation of Nrf2-target genes (A) and DNA damage-related genes (B) significantly regulated with quinone exposure.	133
Figure 4.5A Confirmation of selected quinone-regulated genes in BQ, DMNQ and MNQ exposed hepatocyte cultures using SybrMan Q-PCR.	137
Figure 4.5B Confirmation of selected quinone-regulated genes in BQ, DMNQ and MNQ exposed hepatocyte cultures using SybrMan Q-PCR.	138
Figure 4.5C Confirmation of selected quinone-regulated genes in BQ, DMNQ and MNQ exposed hepatocyte cultures using SybrMan Q-PCR.	139
Figure 4.6: Quinone signature genes integrated into a model of quinone challenge	154
Figure 5.1: Percent LDH leakage in rat hepatocyte monolayers exposed to VC, DMNQ or MNQ for 1, 2, 4, 6, 8, 12, 18 and 24 hours.	160
Figure 5.2: GSH levels in rat hepatocyte monolayers exposed to VC, DMNQ or MNQ for 1, 4, 8, 16 and 24 hours.	160
Figure 5.3: GSSG levels in rat hepatocyte monolayers exposed to VC, DMNQ or MNQ for 1, 4, 8, 16 and 24 hours.	161
Figure 5.4: Media total glutathione levels in rat hepatocyte monolayers exposed to VC, DMNQ or MNQ for 1, 4, 8, 18 and 24 hours.	161
Figure 5.5: Mean profiles of clusters C1, C2, C6 and C8, decreased with DMNQ and MNQ exposure.	164

Figure 5.6: Mean profiles of clusters C3, C4, C5 and C7, increased with DMNQ and MNQ exposure.....	165
Figure 5.7: Exemplar gene profiles for cluster C1.....	168
Figure 5.8: Exemplar gene profiles for cluster C6.....	169
Figure 5.9: Exemplar gene profiles for cluster C8.....	170
Figure 5.10: Exemplar gene profiles for cluster C3.....	172
Figure 5.11: Exemplar gene profiles for cluster C4.....	173
Figure 5.12: Exemplar gene profiles for cluster C7.....	174
Figure 5.13: DMNQ and MNQ exposure in rat hepatocytes results in dysregulation of iron and haem homeostasis.	194
Figure 6.1: <i>Gapdh</i> transcription (A) and LDH Leakage (B) in rat hepatocyte monolayers exposed to 0.0, 5.0, 7.5 or 10.0 μ L/mL <i>TransIT-TKO</i> [®] in WE incomplete media for 16 hours, followed by 8 hours in fresh WE incomplete media.	203
Figure 6.2: <i>Pim3</i> transcription (A) and LDH leakage (B) in rat hepatocyte monolayers transfected with three different <i>Pim3</i> siRNAs at 25, 50, or 100nM final concentrations	204
Figure 6.3: <i>Gclc</i> transcription (A) and LDH leakage (B) in rat hepatocyte monolayers transfected with three different <i>Gclc</i> siRNAs at 25, 50, or 100nM final concentrations.	205
Figure 6.4: LDH leakage in rat hepatocyte monolayers challenged with DMNQ or MNQ following <i>Pim3</i> or <i>Gclc</i> knockdown.....	208
Figure 6.5: Activated caspase 3 activity and GSH levels in rat hepatocyte monolayers challenged with DMNQ or MNQ following <i>Pim3</i> or <i>Gclc</i> knockdown.....	209
Figure 6.6: <i>Pim3</i> (A) and <i>Gclc</i> (B) transcription in rat hepatocyte monolayers challenged with DMNQ or MNQ following <i>Pim3</i> or <i>Gclc</i> knockdown.....	211
Figure 7.1: DMNQ HPLC assay optimisation.....	221
Figure 7.2: MNQ HPLC assay optimisation.	223
Figure 7.3: Liver tissue DMNQ (A), GSH (B) and GSSG (C) levels in mice treated with Vehicle Control (n=6) or 200mg/kg DMNQ (n=5) i.p.....	225
Figure 7.4: DMNQ exposure kinetics in male C57BL/6J mice treated with 25mg/kg DMNQ in AO i.p.).....	227
Figure 7.5: DMNQ and MNQ exposure kinetics in male C57BL/6J mice treated with 25mg/kg in AO i.p.	230

Figure 7.6: Liver GSH (A) and GSSG (B) levels in mice treated with AO, DMNQ or MNQ.	232
Figure 7.7: Plasma ALT (A) and AST (B) levels in mice treated with AO or 25mg/kg DMNQ	233
Figure 7.8: Mean profiles of clusters C1, C2 and C3	236
Figure 7.9: Mean profiles of clusters C4, C5 and C6	237
Figure 8.1: Mechanisms of redox cycling quinone-mediated mitochondrial toxicity and the key response pathways regulated by rat hepatocytes to ameliorate these effects and promote survival.	250

LIST OF TABLES

Table 1.1: Quinone cofactors and their distribution in nature.....	19
Table 1.2: Quinone-related therapeutics	21
Table 1.3: Examples of one- and two-electron reductases that catalyse the reduction of the quinone moieties of quinone-containing alkylating drugs.....	23
Table 1.4: Examples of compound classes that undergo redox cycling.....	28
Table 1.5 Examples of biochemical and enzymatic antioxidants	32
Table 1.6: ARE-containing genes and their function.....	41
Table 1.7: Compounds that induce ARE-mediated transcription.....	42
Table 1.8: Open transcriptional techniques	44
Table 1.9: GeneChip® hybridisation quality control metrics.....	52
Table 2.1: Volumes of Tissue Culture Reagents Used for Different BioCoat Plate Types.....	58
Table 2.2: Test Quinone Details	59
Table 2.3: GeneChip® Supply Details.....	87
Table 2.4: Reagents and Volumes for Hybridisation Cocktail Preparation	88
Table 3.2: Concentration ranges of quinones tested in dose-ranging experiments.....	105
Table 3.3: Concentrations selected for evaluating transcriptional changes at eight hours.....	107
Table 3.4: 8 hours EC ₅₀ values and accompanying GSH depletion for the five quinones	116
Table 3.5: Optimal concentration selected for each quinone	117
Table 4.1: Selected concentration for each quinone.....	119
Table 4.2: Number of genes filtered for EASE biological theme analysis at each time point.	127
Table 4.3: EASE biological theme analysis of quinone-regulated genes.	128
Table 4.4: Number of genes filtered for IPA biological theme analysis at each time point.....	129
Table 4.5: IPA biological theme and network analysis of 1 and 4 hour time point quinone-regulated genes.....	130

Table 4.6: IPA biological theme and network analysis of 8 hour time point quinone-regulated genes.....	131
Table 4.7: Quinone Signature Genes	135
Table 5.1: EASE biological theme analysis of 804 probe sets selected for cluster analysis.....	166
Table 5.2: Confirmation of Quinone Signature Gene Regulation	175
Table 5.3: Oxidative stress response and Nrf2-target genes regulated with DMNQ and MNQ exposure.....	176
Table 5.4: Cell cycle control and DNA damage response genes regulated with DMNQ and MNQ exposure	177
Table 5.5: Energy Metabolism-Related Genes regulated with DMNQ and MNQ Exposure.....	178
Table 5.6: Iron and Haem Homeostasis-related genes regulated with DMNQ and MNQ exposure.....	179
Table 6.1: Control and Target Gene siRNA Details	198
Table 6.2: Transfection media conditions used to determine optimal <i>TransIT</i> -TKO [®] conditions for target gene knockdown	200
Table 7.1: Levels of DMNQ detected in spiked naïve mouse liver homogenates.....	222
Table 7.2: DMNQ and MNQ exposure metrics in male C57BL/6J mice	229

ABBREVIATIONS

%	-	Percent
<	-	Less than
>	-	Greater than
±	-	plus or minus
≤	-	Less than or equal to
≥	-	Greater than or equal to
µg	-	microgram
µL	-	Microlitre(s)
µM	-	Micromolar
8-oxoG	-	8-oxoguanine
A	-	Adenine
ADP	-	Adenine diphosphate
ALT	-	Alanine aminotransferase
AO	-	Arachis oil
AP-1	-	Activator protein-1
ARE	-	Antioxidant response element
AST	-	Aspartate aminotransferase
ATP	-	Adenine triphosphate
AUC	-	Area under the curve
B[a]P	-	Benzo[a]pyrene
BAD	-	BCL2-antagonist of cell death
BBB	-	Blood brain barrier
BER	-	Base excision repair
BQ	-	1,4-benzoquinone
BSA	-	Bovine serum albumin
bZIP	-	Basic-leucine zipper transcription factor
C	-	Cytidine
CCl ₄	-	Carbon tetrachloride
CDKs	-	Cyclin dependent kinases
cDNA	-	Complementary DNA
CHO cells	-	Chinese hamster ovary cells
C _{max}	-	Maximum concentration
CO ₂	-	Carbon dioxide
CoA	-	Coenzyme A

cRNA	-	Complementary RNA
C _t	-	Cycle threshold
Cy	-	Cyanine dye
CYP	-	Enzymes cytochrome P450
Cyt. <i>c</i>	-	Cytochrome <i>c</i>
DD	-	Differential display
DDIT	-	DNA damage inducible transcript
DMNQ	-	2,3-dimethoxy-1,4-Naphthoquinone
DMSO	-	Dimethylsulphoxide
DNA	-	Deoxyribonucleotide acid
D-PBS	-	Dulbeco's phosphate buffered saline
dUTP	-	Deoxyuridine triphosphate
e ⁻	-	Electron
e.g.	-	For example
EASE	-	Expression Analysis Systematic Explorer
EC ₅₀	-	Effective concentration 50 percent
EDTA	-	Ethylenediaminetetraacetic acid
EST	-	Expressed sequence tag
FA	-	Fatty acid
FD	-	Fragment display
g	-	Gram(s)
<i>g</i>	-	Gravity
G	-	Guanine
GADD	-	Growth arrest and DNA damage
gDNA	-	Genomic DNA
γ-GC	-	Gamma-glutamylcysteine
γ-GT	-	Gamma-glutamyl transpeptidase
GSH	-	Reduced glutathione
GSHPx	-	Glutathione peroxidase
GSHr	-	Glutathione reductase
GSHt	-	Total glutathione
G-site	-	GSH binding site
GSSG	-	Oxidised glutathione
GST	-	Glutathione-S-transferase
H ⁺	-	Proton
H ₂ O ₂	-	Hydrogen peroxide

HAEC	-	Human arterial endothelial cells
HBSS	-	Hank's balanced salt solution
HO [•]	-	Hydroxyl radical
HPLC	-	High performance liquid chromatography
IMS	-	Industrial methylated spirit
i.p.	-	Intraperitoneal
IPA	-	Ingenuity pathways analysis
IRE	-	Iron response element
Keap1	-	Kelch-like ECH-associated protein 1
kg	-	Kilogram(s)
LDH	-	Lactate dehydrogenase
LH	-	Unsaturated fatty acid
LH [•]	-	Lipid radical
LO [•]	-	Lipid Alkoxy radical
log P	-	Logarithm of the partition coefficient
LOH	-	Lipid aldehyde
LOO [•]	-	Lipid peroxy radical
LOOH	-	Lipid peroxide
m ²	-	Meters squared
mg	-	Milligram(s)
mL	-	Millilitre(s)
mM	-	Millimolar
MM	-	Mismatch
MNQ	-	Menadione
MPA	-	<i>Meta</i> -phosphoric acid
MPTP	-	Mitochondrial permeability transition pore
MRC	-	Medical Research Council
mRNA	-	Messenger RNA
MSB	-	Menadione sodium bisulphate
NADH	-	Reduced Nicotinamide adenine dinucleotide
NADPH	-	Reduced Nicotinamide adenine dinucleotide phosphate
NAPQI	-	<i>N</i> -acetyl- <i>p</i> -benzoquinoneimine
NCEs	-	New chemical entities
NER	-	Nucleotide excision repair
NFI	-	Nuclear factor I/C (CCAAT-binding transcription factor)
NFκB	-	Nuclear factor kappa B

nM	-	Nanomolar
NOAEL	-	No observed adverse effect level
NQ	-	1,4-Naphthoquinone
NQO1	-	NAD(P)H:Quinone oxidoreductase 1
Nrf2	-	Nuclear factor (erythroid-derived 2)-like 2
O ₂	-	Molecular oxygen
O ₂ ^{•-}	-	Superoxide anion
Oligo(s)	-	Oligonucleotide(s)
OPT	-	O-Phthaldialdehyde
p53	-	p53 tumour suppressor
PBS	-	Phosphate buffered saline
PC	-	Phosphatidylcholine
PCR	-	Polymerase chain reaction
PDC	-	Pyruvate dehydrogenase complex
PDK	-	Pyruvate dehydrogenase kinase
PEG-200	-	Polyethylene glycol-200
PM	-	Perfect match
pM	-	Picomolar
Ref-1	-	Redox factor-1
RISC	-	RNA-induced silencing complex
RNA	-	Ribonucleotide acid
RNAi	-	RNA interference
ROOH	-	Organic peroxide
ROS	-	Reactive oxygen species
rpm	-	Revolutions per minute
rRNA	-	Ribosomal RNA
R-S [•]	-	Thiyl radical
R-SH	-	Thiol moiety
RT-QPCR	-	Real-time quantitative PCR
siRNA	-	Small interfering RNA
SOD	-	Superoxide dismutase
Sp1	-	Specificity protein 1 transcription factor
SSIIRT	-	Superscript II reverse transcriptase
T	-	Thymine
TBHP	-	<i>Tert</i> -butylhydroperoxide
TBHQ	-	<i>Tert</i> -butylhydroquinone

TCA	-	Trichloroacetic acid
TF(s)	-	Transcription factor(s)
TGF β	-	Tissue growth factor beta
T _m	-	Melting temperature
T _{max}	-	Time to maximum
TNF α	-	Tumour necrosis factor alpha
Topo II	-	Topoisomerase II
TQ	-	Thymoquinone
UQ	-	Ubiquinone
UTR	-	Untranslated region
UV	-	Ultraviolet
VC	-	Vehicle control

CHAPTER 1. GENERAL INTRODUCTION

1.1. Introduction to Quinones

Quinones are diketones derived from aromatic hydrocarbons[1] and are found extensively in nature[2;3]. In prokaryotes, fungi and plants quinones are synthesized via the polyketide pathway. In mammals this pathway is absent and so endogenous quinones are produced via the oxidative metabolism of estrogens and catecholamines[3]. Physiologically quinones are utilised as redox-active cofactors which act as electron shuttles in the electron-transport chains of aerobic respiration and photosynthesis[4]. Quinone moieties are also present as redox cofactors in a number of enzymes (Table 1.1)[5].

Table 1.1: Quinone cofactors and their distribution in nature

Quinone Cofactor	Enzyme Class	Organisms
Topaquinone	Amine oxidases	Prokaryotes and eukaryotes
Lysyl topaquinone	Lysyl oxidase	Mammals
Tryptophan tryptophylquinone	Alkylamine dehydrogenases	Gram negative bacteria
Cysteinyl-tyrosyl radical	Galactose oxidase	Fungi

Adapted from McIntire, 1998[5]

Arguably one of the most important function of quinones in biological systems is as electron transfer molecules in mitochondrial respiration and photosynthesis. In the mitochondrial electron transport chain (ETC) of mammalian cells (Figure 1.1), the lipophilic ubiquinone (UQ or coenzyme Q) serves as the electron shuttle between Complex I (NADH dehydrogenase or NADH:ubiquinone oxidoreductase) and/or Complex II (succinate:ubiquinone reductase) and Complex III (bc₁-complex) of the respiratory chain[6;7]. Complexes I and II reduce ubiquinone to the hydroquinone ubiquinol. Two electrons are then shuttled through Complex III to the next electron acceptor (cytochrome *c*), with the concomitant translocation of two protons into the inter-mitochondrial membrane space, via a mechanism known as the 'Q-cycle'[6]. The corresponding electron shuttle within plants, plastoquinone is an analogue of ubiquinone[7;8]. Plastoquinone also accepts electrons from Photosystem II of the photosynthetic electron transfer chain in chloroplasts and shuttles them to the b₆-f complex.

Figure 1.1

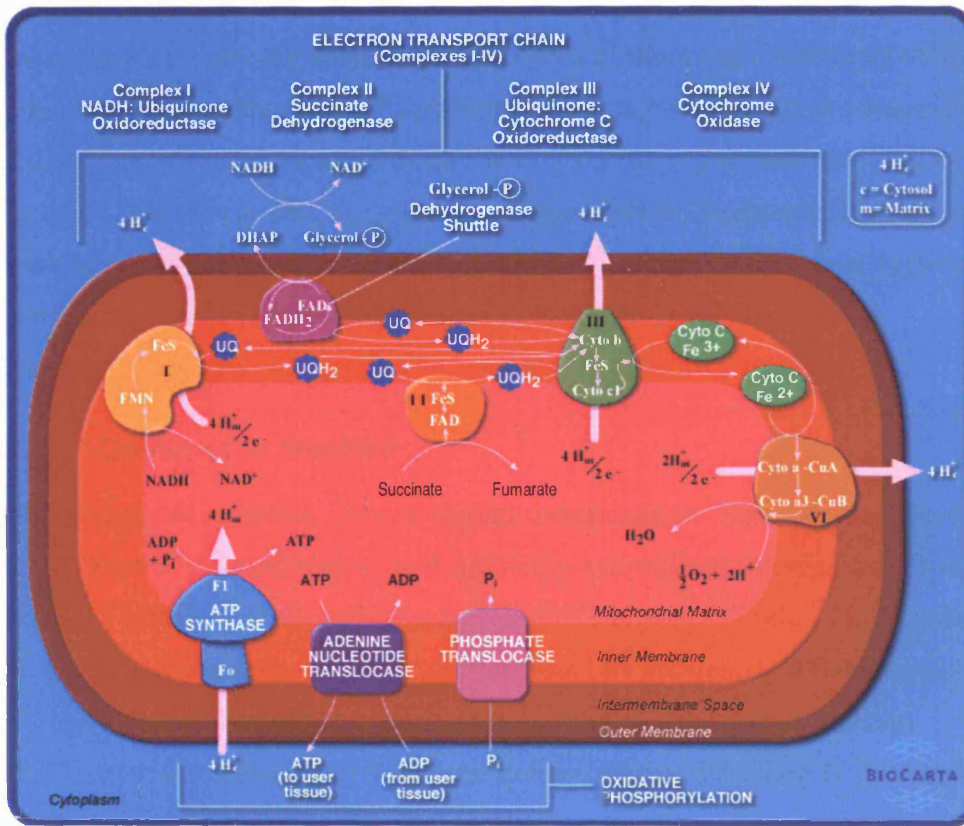


Figure 1.1: Graphical representation of the mitochondrial electron transport chain (Obtained from <http://biocarta.com>)

Energy from the transfer of electrons (white arrows) down the electron transport chain is used to pump protons (pink arrows) from the mitochondrial matrix into the intermembrane space, creating an electrochemical proton gradient across the mitochondrial inner membrane. This electrochemical proton gradient allows ATP synthase (ATP-ase) to use the flow of H^+ through the enzyme back into the matrix to generate ATP from adenosine diphosphate (ADP) and inorganic phosphate. Complex I (NADH:ubiquinone oxidoreductase) accepts electrons from the Krebs cycle electron carrier NADH, and passes them to UQ (or coenzyme Q), which also receives electrons from complex II (succinate dehydrogenase). UQ passes electrons to complex III (cytochrome bc₁ complex), which passes them to cytochrome c (cyt c). Finally cyt c passes electrons to Complex IV (cytochrome c oxidase), which uses the electrons and hydrogen ions to reduce molecular oxygen to water.

1.1.1. Human Exposure to Quinones

In addition to endogenous quinones, humans are exposed to quinones (and related compounds) from a number of sources, including diet, medicinal and environmental. As quinones are common secondary metabolites in plants, the active ingredients of many herbal remedies are quinones[9]. Extract of henna (*Lawsonia inermis*), which contains

lawsone (2-hydroxy-1,4-naphthoquinone), is used as a ‘traditional’ medicine to treat a number of inflammatory ailments. Senna (the dried leaves of *Cassia acutifolia*) has been used as an herbal laxative for hundreds of years. One of the active constituents of senna is the quinone rhein (4,5-dihydroxyanthraquinone-2-carboxylic acid)[10]. A number of plant-derived dyes also contain quinone derivatives, for example pigments extracted from henna and madder (*Rubia tinctorum*)[3]. Quinones are also common environmental pollutants[3]. Quinone derivatives of polycyclic aromatic hydrocarbons are constituents of engine exhaust fumes, cigarette smoke and urban air particulates from organic waste combustion[1;9;11].

1.1.2. Quinones in Medicine

In addition to herbal remedies, quinone-related compounds are important in modern medicine. Some of the most widely used antibiotics and anti-cancer drugs are polyketide quinones[12] belonging to the anthracycline class of antibiotics (Table 1.2). Since the early 1960s, two anthracyclines in particular, Adriamycin (doxorubicin) and Daunomycin (daunorubicin) have been amongst the most frequently prescribed chemotherapy agents[13]. Both doxorubicin and daunorubicin were originally isolated from *Streptomyces peucetius vercaesitue*[13] and exhibit activity against a number of human cancers[14]. Doxorubicin in particular, is effective in the treatment of a wide range of tumour types, including acute leukaemias and lymphomas, sarcomas, malignant neoplasms of the bladder, breast, lung, ovary, stomach and thyroid[13]. Daunorubicin is most frequently used to treat adult myelogenous leukaemia[14].

Table 1.2: Quinone-related therapeutics

Compound	Quinone Class	Clinical Use
Anthracycline antibiotics	Doxorubicin	Cancer
	Daunorubicin	Cancer
	Tetracenomycin	Antibiotic
Mitomycin quinone-containing alkylating agents	Mitomycin C	Cancer
	Porfiromycin	Cancer
Benzoquinone-containing alkylating agents	Triaziquone	Cancer
	Diaziquone	Cancer
	Carbazilquinone	Cancer

The precise mechanisms that underlie the anti-tumour activity of the anthracycline antibiotics are yet to be defined. There is evidence to suggest a number of modes of action may be involved, including direct interaction with genomic DNA, inhibition of the enzyme DNA topoisomerase II (Topo II) and perturbation of DNA and RNA synthesis[14]. Doxorubicin has been shown to interfere with Topo II activity *in vitro*[15]. Topo II catalyses the transient double strand breakage and subsequent rejoining of DNA during genome replication and repair. Doxorubicin (and other Topo II inhibitor anti-cancer agents, such as etoposide) hinders the ability of Topo II to repair the double strand breaks it makes, effectively converting the enzyme into a DNA-damaging agent[15]. Anthracyclines have also been shown to directly interact with DNA by intercalating between base pairs[14]. As potential intercalation sites become saturated, the melting temperature (T_m) of the DNA increases and affords greater stability to the DNA double helix. The intercalating mechanism can also be used to explain the inhibitory effects that anthracyclines have on DNA and RNA synthesis[14].

A second important class of quinone-related drugs are the quinone-containing alkylating agents (Table 1.2). The anti-tumour activities of this class of quinone have been known since the 1950s[16]. The most frequently prescribed quinone-containing alkylating agent is mitomycin C, first isolated from *Streptomyces caespitosus* in 1958[16]. Since the 1970s, mitomycin C has been used to treat solid tumours, such as bladder cancer and gastric, pancreatic and oesophageal carcinomas. It is also frequently used in combination with other anti-tumour agents, including doxorubicin and 5-fluorouracil.

As the class name suggests, the quinone-containing alkylating agents contain two core structural elements that are critical to their activity. The first is a redox-active quinone moiety and the second, an alkylating element that can covalently bind to cellular macromolecules. In general, quinone-containing alkylators require reduction of their quinone moiety for the alkylating group to become active[16-18]. For this reason they are often referred to as 'bioreductive alkylating agents'. Once activated, the alkylating element becomes electrophilic and can covalently bind protein and DNA. From an anti-tumour perspective, the most important interaction is with DNA, resulting in the formation of DNA-monoadducts (or DNA cross-links in the case of bifunctional alkylators). This results in induction of apoptosis and cell death.

Intracellular activation of quinone-containing alkylating agents is carried out by one- and two-electron reductases (Table 1.3). The relatively selective nature of these drugs for cancer cells is primarily due to the enhanced potential for reductive metabolism that is observed in hypoxic cells near the necrotic core of tumours. Indeed, enhanced expression of some reductases has been observed in tumours (e.g. NAD(P)H:quinone oxidoreductase (NQO1) and carbonyl reductase)[17]. The basic premise is that in hypoxic tumour cells the reduction of the quinone moiety is favoured, resulting in activation of the alkylating moiety. In healthy, well oxygenated cells, the less toxic pro-drug is regenerated through a process known as redox cycling (discussed in detail in section 1.2.1).

Table 1.3: Examples of one- and two-electron reductases that catalyse the reduction of the quinone moieties of quinone-containing alkylating drugs

Reaction	Reductase Enzyme	Subcellular Location
One-electron reduction	P450 (cytochrome) oxidoreductase	Endoplasmic reticulum
	NADH:Cytochrome b5 reductase	Mitochondrion, outer membrane
	Carbonyl reductase	Cytosol
Two-electron reduction	NAD(P)H:quinone oxidoreductase	Cytosol
	Xanthine dehydrogenase	Peroxisome

Adapted from Beall and Winski, 2000[17]

1.1.3. Quinone-Related Toxicity

Although certain quinones have clear therapeutic benefit, exposure to quinone-related compounds is associated with toxicity in a number of target organs. Common quinone-associated toxicities (in humans and animals) include haemolytic anaemia, renal and hepatic damage, immunotoxicity[9;19] and possibly neoplastic change[1]. Two predominant mechanisms are responsible for the toxic effects of quinone exposure: 1) Covalent binding to vital cellular macromolecules, and 2) oxidative stress, via redox cycling[2;20-22] (Figure 1.2). The relative importance of each of the two mechanisms varies from quinone to quinone and can depend on factors such as the level of substitution within the quinone structure, or the redox potential of the quinone[23].

Many quinones have potent electrophilic centres (e.g. the 3-carbon in 2-methyl-1,4-naphthoquinone (menadione)) that are susceptible to attack from cellular nucleophiles (e.g. protein thiols and the thiol group in reduced glutathione (GSH)) [2;20-22]. GSH (whose function and biosynthesis is discussed in detail in section 1.3.1) readily forms conjugates with quinones through its nucleophilic cysteinyl SH group[23;24], thus potentially diverting electrophilic attack from important cellular macromolecules. The rapid depletion of GSH by electrophilic quinones can disrupt the redox balance of a cell. This can both mimic oxidative stress (oxidative stress is discussed in more detail in section 1.2) and sensitize a cell to subsequent oxidative challenge[25]. Once cellular GSH reserves become depleted, protein thiols are more vulnerable to attack by electrophilic quinones. If residues critical for a protein's activity are covalently bound, this can lead to impaired function, resulting in perturbation of important cellular pathways and cytotoxicity[2;20;25]. For example, protein arylation potential has been shown to be important in menadione[26], 1,4-benzoquinone and 1,4-naphthoquinone cytotoxicity in rat hepatocytes[20;27].

Quinone-induced oxidative stress occurs due to the generation of reactive oxygen species (ROS) as a consequence of redox cycling, through either one- or two-electron reduction[21]. As mentioned previously (section 1.1.2 and Table 1.3), one electron reduction is carried out by various one-electron reductases and results in the generation of a semiquinone radical (Figure 1.2). The semiquinone radical readily autoxidises back to the parent quinone in the presence of molecular oxygen resulting in the generation of superoxide anion ($O_2^{\bullet -}$) (Figure 1.2). The downstream effects of this reaction (in terms of oxidative stress and toxicity) will be discussed in more detail in section 1.2. Two-electron transfer reduction is driven by DT-diaphorase (also known as NAD(P)H:quinone oxidoreductase (NQO1)) in animals[28]. This reaction is generally considered to be non-toxic and results in the generation of a relatively stable hydroquinone (or quinol). Hydroquinones are cleared from the body through conjugation with sulphate or glucuronic acid, producing conjugates that are more readily excreted in the urine[9;28].

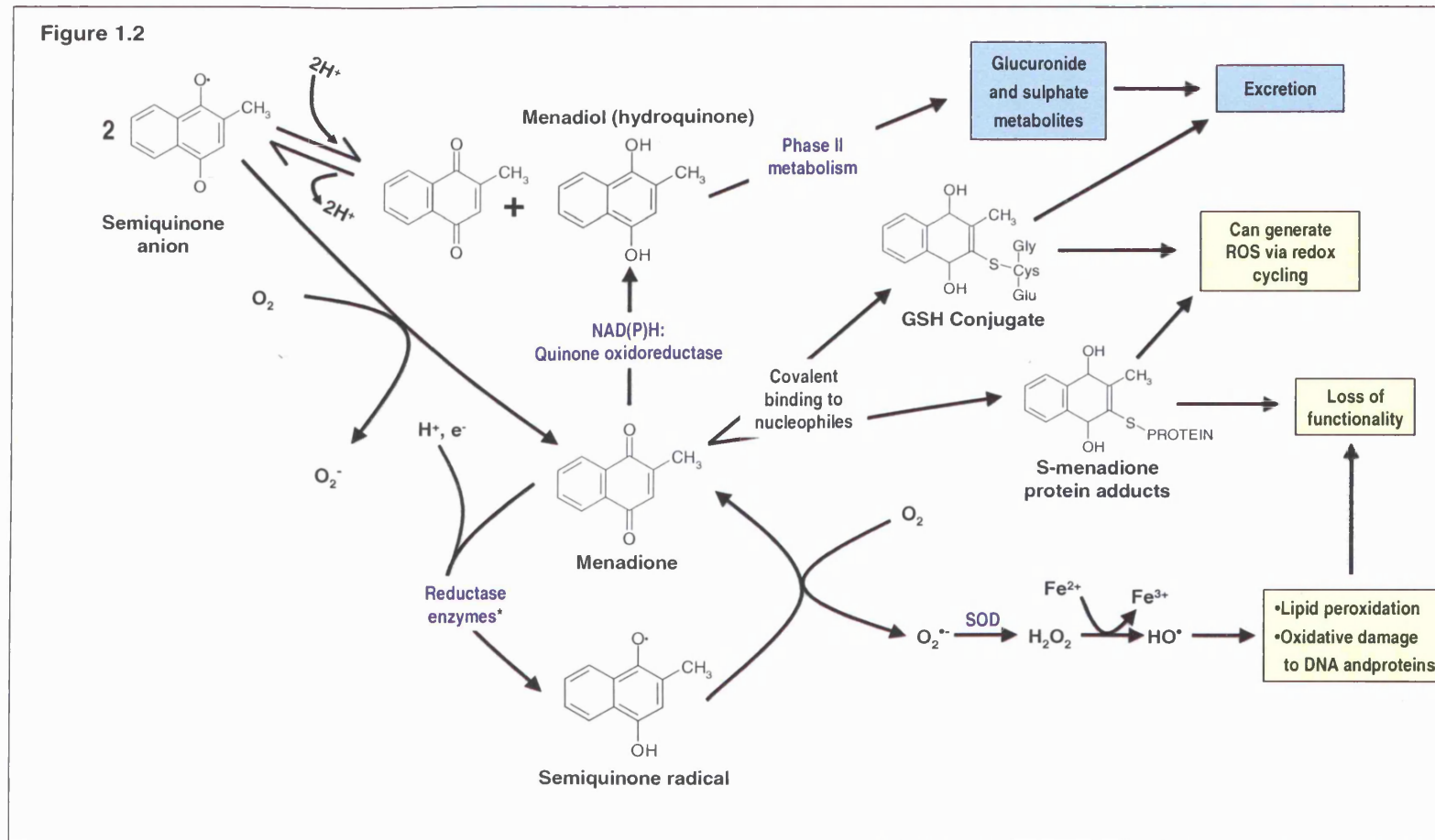


Figure 1.2: Quinone (menadione) metabolism and toxicity

Quinones can undergo one electron reduction to the semiquinone radical which readily autooxidises to the parent quinone in the presence of molecular oxygen (redox cycling), with the concomitant generation of ROS via Fenton chemistry. Alternatively the parent quinone can undergo two-electron reduction (catalysed by NQO1) to form the hydroquinone, which can also undergo redox cycling to the parent quinone via a disproportionation reaction that generates the semiquinone anion. Electrophilic centres (for example the 3-carbon of menadione) can readily react with cellular nucleophiles such as the thiol moieties of GSH or cysteinyl residues within proteins. The GSH conjugate or protein-quinone adducts can also redox cycle via a disproportionation reaction with the parent quinone, similar to that shown for the hydroquinone. Quinones can be eliminated through direct conjugation to GSH, the conjugate being excreted intact in the bile or converted to the mercapturic acid and excreted in the urine. Alternatively the hydroquinone undergoes sulphation or glucuronidation prior to urinary excretion. *Refer to Table 1.3

Although two-electron reduction is predominantly considered as a detoxification pathway, hydroquinones can autoxidise and cause toxicity through ROS generation[9;29] (Figure 1.2). The partially substituted quinone lawsone (2-hydroxy-1,4-naphthoquinone) induces oxidative stress (i.e. increased oxidized glutathione) in rat hepatocytes in the absence of one-electron reduction[30]. Gant *et al* demonstrated that this was probably the result of redox cycling via two-electron reduction (unpublished work, 1988). Watanabe *et al* also demonstrated that extracellular autoxidation of hydroquinones were causative in the cytotoxicity of menadione and 2,3-dimethoxy-1,4-naphthoquinone (DMNQ) to A549-S cells[31]. The degree to which this occurs is dependent upon the rate at which the parent quinone is reduced by NQO1 and the stability of the hydroquinone[9]. The autoxidation reaction often occurs through a free radical chain reaction propagated by $O_2^{\bullet-}$ [21]. A semiquinone radical is generated (along with hydrogen peroxide) which undergoes further oxidation back to the parent quinone, and further generation of $O_2^{\bullet-}$ (Figure 1.2).

In addition to oxidative stress caused by redox cycling of the parent quinone, a number of quinones are known to have redox-active GSH conjugates. GSH conjugation (discussed in more detail in section 1.3.1) is generally considered to be a detoxification of electrophilic compounds like quinones[32]. However, a number of quinones maintain equivalent redox potentials in their GSH-conjugated form (e.g. menadione and the benzoquinone metabolite of bromobenzene)[32;33] (Figure 1.2).

In addition to causing oxidative stress, redox cycling quinones also have the ability to adversely affect cellular energy metabolism. This occurs through perturbation of the normal flow of electrons along the mitochondrial respiratory chain, decreasing ATP generation. Redox cycling quinones (e.g. menadione and doxorubicin) act as alternate electron acceptors, being reduced by complex I (NADH-ubiquinone oxidoreductase). Electrons are diverted from the respiratory chain which greatly diminishes the efficiency of energy conversion, whilst simultaneously increasing substrate oxidation[34]. Quinone cytotoxicity has been demonstrated to correlate with ATP depletion in hepatocytes[35;36]

In terms of clinically relevant quinone toxicities, the cardiac changes associated with anthracycline treatment are one of the most important. Cardiac toxicity limits the clinical usefulness of doxorubicin and daunorubicin[13]. Both compounds induce chronic cumulative dose-related cardiomyopathy[13;37]. For doxorubicin an empirical safe dose

limit of 500mg/m² is used in the clinic, as the incidence of cardiomyopathy rises sharply at dose levels in excess of 550mg/m²[38]. One of the predominant mechanisms through which anthracyclines cause cardiomyopathy is thought to be oxidative stress[13]. This is partly due to redox cycling of the anthracycline quinone moiety, which undergoes one-electron reduction by complex I of the respiratory chain[34;39]. A role for oxidative stress in anthracycline cardiotoxicity has been confirmed by the protective effect of agents that reduce ROS generation. For example, co-administration of the iron chelating agent dexrazoxane has been shown to reduce anthracycline cardiotoxicity[13]. The binding of free (or loosely bound) iron reduces the potential for ROS generation through the Fenton reaction (discussed in section 1.2.1). In addition, a number of agents with antioxidant properties (e.g. vitamin E, curcumin and thymoquinone) have been shown to be cardioprotective in animal models of doxorubicin toxicity[13;37]. However, anthracycline toxicity is multifactorial with redox cycling-mediated oxidative stress being one component[38].

A number of other drugs also have quinone-related metabolites that are known to contribute to their toxicity. An important example is paracetamol, which can be metabolised to reactive *N*-acetyl-*p*-benzoquinoneimine (NAPQI) by the major enzyme cytochromes P450 (CYP) (e.g. CYP2E1, CYP1A2 and CYP3A4)[40]. Paracetamol is also metabolised to glucuronide and sulphate derivatives that are excreted in the urine. However during overdose, the proportion of paracetamol undergoing activation to NAPQI becomes so great that it overwhelms protective mechanisms and causes widespread hepatic necrosis[40].

1.2. Redox Cycling and Oxidative Stress

The term redox cycling is used to define the cyclic transition of chemicals from a reduced to an oxidised state. A diverse range of compounds can undergo redox cycling and the process is a critical element of many biological processes, such as ubiquinone in the mitochondrial respiratory chain (as discussed in Section 1.1). Redox cycling results in the production of ROS. If deregulated, redox cycling can result in potentially toxic levels of ROS formation resulting in oxidative damage to cellular macromolecules[41].

A wide range of xenobiotics can also undergo redox cycling (Table 1.4) and concomitant ROS generation. As mentioned previously, redox cycling is known to play an important role in the toxicity of quinone and quinone-related metabolites[28;42-45].

Table 1.4: Examples of compound classes that undergo redox cycling

Class	Examples
Quaternary bipyridyl compounds	Paraquat and diquat
Benzoquinones and naphthoquinones	1,4-benzoquinone, Menadione and 2,3-dimethoxy-1,4-naphthoquinone
Anthracyclines and heterocyclic quinones	Adriamycin (doxorubicin), Mitomycin C and streptonegrin
Nitro and azo compounds	Nitrofurantoin and prontosil

1.2.1. Redox Cycling

Redox cycling essentially involves one electron-reduction of a compound to form a semiquinone reactive intermediate, followed by an auto-oxidation reaction in the presence of molecular oxygen (O_2)[29;46] (Figure 1.2). During this process the intermediary compound transfers the extra electron to O_2 [29;42]. This results in the production of the parent compound (now available to undergo another round of one-electron reduction) and superoxide anion ($O_2^{\bullet-}$). The $O_2^{\bullet-}$ may undergo further one-electron reduction to form hydrogen peroxide (H_2O_2), either enzymatically (driven by superoxide dismutase (SOD)) or spontaneously [29;42;46;47]. The H_2O_2 formed is not reactive *per se*, however it is the main source of a far more reactive species in the presence of transition metal ions[41]. If the H_2O_2 formed is not detoxified by enzymes, such as catalase or glutathione peroxidase (GSHPx), formation of the hydroxyl radical (HO^{\bullet}) can result. The HO^{\bullet} is formed non-enzymatically via the Fenton reaction involving transition metal ions (e.g. iron and copper) (Figure 1.3)[42;48]. The HO^{\bullet} is one of the most reactive ROS produced as a result of redox cycling[42]. The highly reactive nature of HO^{\bullet} ensures that the species is short-lived, initiating oxidative damage to macromolecules that are within close proximity of its formation[41].

One of the key issues with redox cycling is that a disproportionate level of ROS generation can result from a relatively modest dose level. If large amounts of redox cycling compound are present, cellular defence mechanisms can become overwhelmed. This results in cytotoxic levels of ROS generation, resulting in reduced glutathione (GSH) and reduced nicotinamide dinucleotide phosphate (NADPH) depletion, lipid peroxidation and oxidative damage to proteins and DNA; a condition known as 'oxidative stress'.

Figure 1.3

Fenton Reaction Equation



Figure 1.3: Production of HO[•] Via Fenton Chemistry

1.2.2. Oxidative Damage to Cellular Macromolecules

The ensuing oxidative stress that is caused by excessive levels of ROS can result in damage to cellular macromolecules, such as lipids, nucleic acids and proteins[49]. This damage can lead to loss of functional activity of components of the cell that are essential to viability and survival. These effects result in the cytotoxicity associated with oxidative stress.

Lipid peroxidation of cellular membranes is one of the key markers of oxidative stress[50;51] and may be a contributory factor in toxicity associated with redox cycling compounds[52]. Lipid peroxidation can be divided into three phases, initiation, propagation and termination[50;51;53]. The initiation step involves the interaction of the free radicals produced by redox cycling with the unsaturated fatty acid of membrane phospholipids[44]. An unsaturated lipid (LH) is first attacked by an initiating radical (e.g. HO[•]), resulting in the formation of a lipid radical (L[•]) (via hydrogen abstraction)[42;44]. The L[•] readily reacts with O₂ to form a lipid peroxy radical (LOO[•]). LOO[•] can abstract hydrogen from a neighbouring LH within the membrane to yield the corresponding lipid hydroperoxide (LOOH), and a newly formed L[•] (which may now undergo the same process, leading to propagation of lipid peroxidation). LOOH can undergo a Fenton-type reaction (Figure 1.3) with Fe²⁺ to yield the lipid alkoxyl radical (LO[•]). The LO[•] may subsequently fragment, giving rise to a number of breakdown products (e.g. lipid aldehydes (LOH) and alkene radical). The radicals produced during the latter phase of lipid peroxidation may serve to initiate new peroxidation chains through generation of L[•][42;44;51;53].

Unrestricted lipid peroxidation quickly results in damage to cellular membranes resulting in a decrease in fluidity, an increase in permeability and adverse effects on membrane-bound protein function[50]. The reactive breakdown products produced can also initiate damage to DNA and proteins. For example, electrophilic aldehydes, such as malondialdehyde and glyoxal, are known to react with DNA to form base adducts. Also, alkenals and 4-hydroxyalkenals can covalently bind to thiol[54] groups within proteins via thioether bond formation[55].

In addition to initiation of lipid peroxidation, ROS generated through redox cycling can also cause extensive oxidative damage to DNA. Oxidative damage to DNA can take the form of both oxidised base modifications and DNA strand breaks[56]. Numerous oxidative base modifications have been identified in DNA, although by far the most abundant is 7,8-dihydro-8-oxoguanine, commonly referred to as 8-oxoguanine (8-oxoG)[57-59]. 8-oxoG is formed through reaction of HO^\bullet with guanine to form a C8-OH adduct radical, with the subsequent loss of an electron (e^-) and proton (H^+)[60]. An alternative major oxidation product of guanine may also be formed when the C8-OH adduct radical is reduced and subsequently converted to 2,6-diamino-4-hydroxy-5-formamido-pyrimidine (FaPy). The most common form of oxidized pyrimidine is thymine glycol, again a product of reaction with the HO^\bullet [60].

As well as being the most common oxidative base modification, 8-oxoG is the most critical in terms of mutagenic capacity[60]. 8-oxoG can pair with cytosine and adenine nucleotides with virtually equivalent efficiency, resulting in GC \rightarrow TA transversions. Oxidative damage to dGTP within the free nucleotide pool can also result in incorporation of 8-oxo-dGTP into genomic DNA, potentially leading to both GC \rightarrow TA and TA \rightarrow GC transversions[60].

The HO^\bullet is the ROS identified as being predominantly responsible for oxidative damage to DNA[56;59], although peroxyl radicals (e.g. LOO^\bullet , one of the products of lipid peroxidation) are also known to be involved. ROS-mediated oxidative damage to DNA has been implicated in the mutagenicity and carcinogenicity of redox cycling compounds (e.g. mitomycin C and doxorubicin)[1].

Similarly, the HO[•] is chiefly responsible for ROS-mediated oxidative damage of proteins. The HO[•] can readily abstract hydrogen from thiol (R-SH) moieties to form thiyl radical (R-S[•]). Subsequent interaction between R-S[•] modifications can yield disulphide bridges (R-S-S-R)[44]. The HO[•] can also sequentially remove hydrogen from the CH₂ groups in amino acid residues of proteins to yield a carbonyl group (Hancock, P. 2002: personal communication). Carbonyl modifications can react with amines resulting in cross-linking with other proteins or DNA. These forms of oxidative damage to proteins result in conformational changes that can adversely affect function[44].

1.3. The Cellular Response to Oxidative Stress

Mammalian cells possess an array of biochemical and enzymatic antioxidants that maintain the redox balance and protect cellular macromolecules from the damaging effects of ROS (Table 1.5). Under pro-oxidant conditions, biochemical antioxidants are rapidly utilised and a shift in the redox balance can result in oxidative stress. To counter this event, cells can mount an 'oxidative stress response'. During this response the activity and transcription of antioxidant enzymes are up-regulated, and the generation of biochemical antioxidants is increased. This enables the stressed cell to return to a state of redox balance.

Termination of lipid peroxidation can be achieved by the interaction of endogenous antioxidants (e.g. vitamin E (α -tocopherol)). Vitamin E reacts with LOO[•] to form the corresponding LOOH and α -tocopherol quinone, thus halting propagation by preventing generation of newly formed L[•]. LOOH may then undergo reaction with GSH (driven by GSHPx or phospholipid hydroperoxide GSH Peroxidase) to form LOH and oxidised glutathione (GSSG)[42;53;61].

Table 1.5 Examples of biochemical and enzymatic antioxidants

Protective Agent	Function
Superoxide dismutases	Dismutates $O_2^{\cdot-}$ to H_2O_2
Catalase	Reduces H_2O_2 to water and O_2 .
GSHPx (GSH)	Reduces H_2O_2 and organic peroxides (to water, and water and alcohol, respectively)
Phospholipid hydroperoxide GSH Peroxidase	Reduces lipid hydroperoxides to water and lipid aldehydes.
Antioxidants (e.g. vitamin E, ascorbate, retinoic acid)	Halts lipid peroxidation by reducing lipid peroxy radicals to lipid hydroperoxides
Thioredoxins	Contain redox active thiol groups that directly reduce ROS and regenerate oxidatively inactivated proteins
Ferritin and other metal ion sequestering proteins	Prevents the formation of HO^{\cdot} via the Fenton reaction

1.3.1. Glutathione Synthesis, Regulation and Function

GSH or, γ -glutamylcysteinylglycine, is a tripeptide of glutamate, cysteine and glycine (Figure 1.4) and is probably the single most important biochemical antioxidant within mammalian cells. GSH protects cells from the toxic effects of ROS by reacting with H_2O_2 and organic hydroperoxides (ROOH)[42;62]. This reaction is driven by the enzyme GSHPx and results in the generation of the oxidised disulphide form of glutathione (GSSG). Intracellular concentrations of GSH vary greatly between cell/tissue types (0.5-10mM), with one of the highest concentrations in hepatocytes (typically 4-8mM)[42]. GSH exists in two pools within the cell; cytosolic and mitochondrial. Mitochondria lack the enzymes required for GSH synthesis and therefore import GSH from the cytosol[62]. In hepatocytes, mitochondrial GSH accounts for 10-15 percent of the total cellular pool and is at a concentration of 10mM (higher than the 4-8mM range observed in the cytosol of hepatocytes)[42]. Mitochondrial GSH plays an essential role in the detoxification of H_2O_2 , an unwanted by-product of four-electron reduction of oxygen to water by the respiratory chain. There is some leakage of electrons along the respiratory chain, resulting in the production of $O_2^{\cdot-}$, and subsequently H_2O_2 [42;63]. Mitochondria lack catalase, thus GSH is solely responsible for the detoxification of H_2O_2 in these organelles[42;62]. Mitochondria do possess all the enzymes and co-factors necessary for the GSH redox cycle, ensuring the reduction of GSSG to GSH[42]. The high physiologic ROS generation within mitochondria results in a GSH:GSSG ratio of around 10:1, whereas within the cytosol it is typically 100:1[42].

Figure 1.4

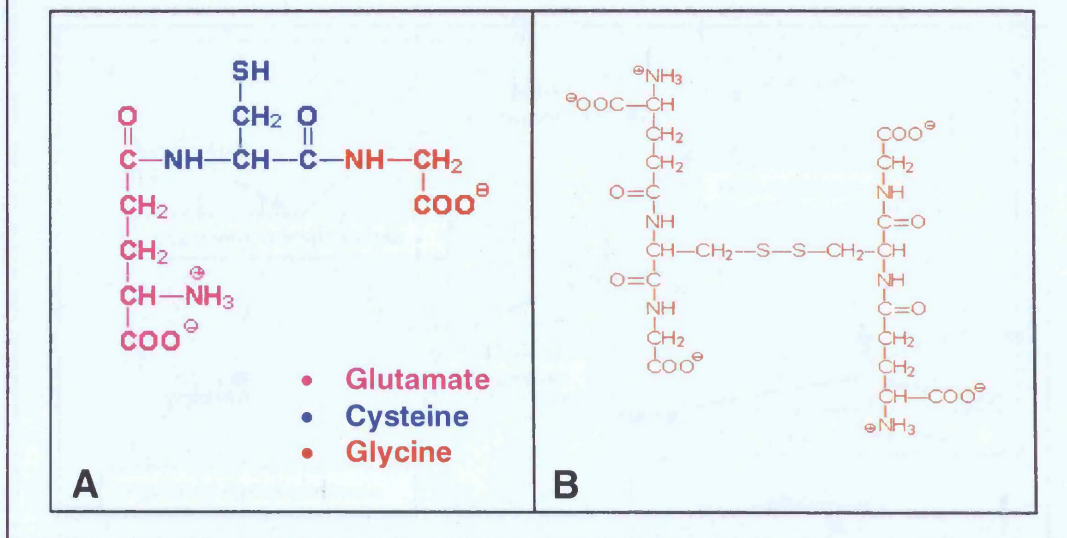


Figure 1.4: Chemical structure of GSH (A) and GSSG (B).

GSH is synthesised in virtually all mammalian cells by two ATP-requiring reactions (Figure 1.5)[64]. The first reaction is the formation of γ -glutamylcysteine (γ -GC) from glutamate and cysteine, which is catalysed by γ -glutamylcysteine synthetase. The 'second' reaction is the formation of GSH from γ -GC and glycine, which is catalysed by GSH synthetase. In mammals, γ -GC synthetase is a heterodimer composed of a heavy subunit (which is enzymatically active) and a light subunit (which is inactive and plays a regulatory role) which are thought to be bound by hydrophobic interaction[64]. GSH synthetase is a homodimer and shows substrate specificity for glycine and the cysteinyl moiety of γ -GC[64;65].

Figure 1.5

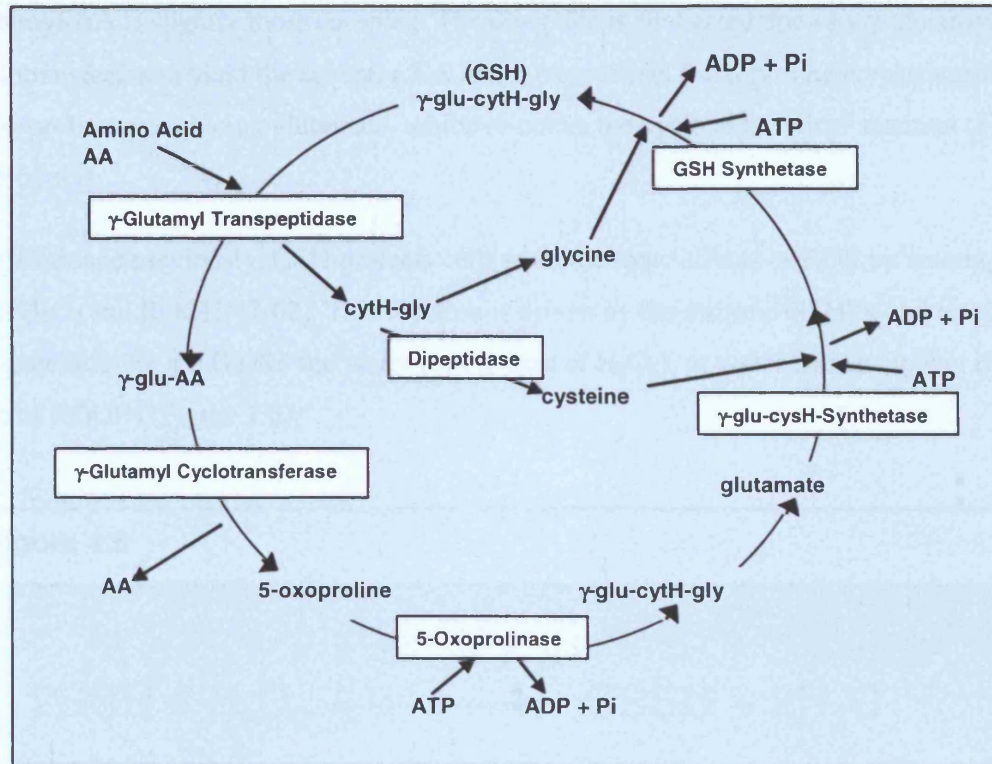


Figure 1.5: The γ -Glutamyl Cycle.

Adapted from Ristoff and Larsson[65]

γ -GC synthetase and GSH synthetase are two enzymic components of the γ -glutamyl cycle (Figure 1.5). The cycle involves four additional enzymes that are responsible for GSH degradation. Following synthesis, most mammalian cells export GSH (to a varying degree) upon which the γ -glutamyl bond is open to cleavage by γ -glutamyl transpeptidase (γ -GT)[65]. γ -GT is a membrane bound protein whose active site is found on the outside of certain organs/cells (e.g. kidney, biliary duct, intestine, pancreas, lung and lymphocytes)[62;64;66]. γ -GT is also known to be present in certain body fluids (e.g. serum, bile extract and amniotic fluid)[62]. γ -GT transfers the γ -glutamyl moiety of GSH to an acceptor amino acid (AA) with concomitant translocation of γ -glutamyl-AA and the cysteinylglycine moieties across the cellular membrane. Once in the cytosol, cysteinylglycine undergoes hydrolysis via dipeptidase resulting in the generation of

cysteine and glycine. The constituent amino acids are now available to re-enter the γ -glutamyl cycle at the 'first' and 'second' reactions respectively (Figure 1.5). The fate of γ -glutamyl-AA is slightly more complex. The dipeptide is first acted upon by γ -glutamyl cyclotransferase to yield the acceptor AA and 5-oxoproline. 5-oxoproline is rearranged by 5-oxoprolinase producing glutamate, which re-enters the cycle at the 'first' reaction (Figure 1.5)[64;65].

As mentioned previously, GSH protects cells from the toxic effects of ROS by reacting with H_2O_2 and ROOH[42;62]. This reaction is driven by the enzyme GSHPx and results in the generation of the GSSG and water (in the case of H_2O_2), or water and an alcohol (in the case of ROOH) (Figure 1.6).

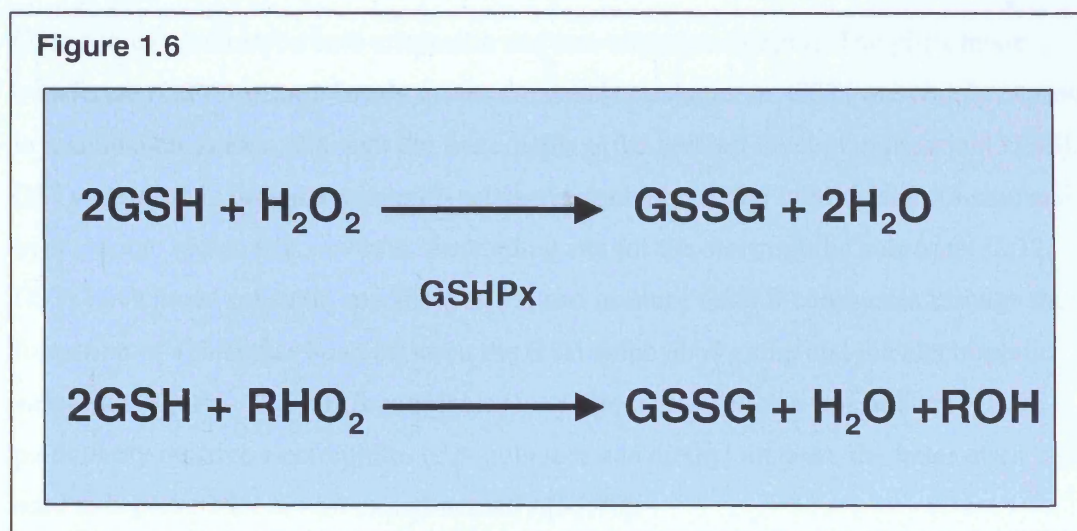


Figure 1.6: Detoxification of hydroperoxides by GSHPx

The reduction of hydroperoxides by GSHPx is an important cellular defence system and prevents the formation of the highly reactive $\cdot\text{OH}$. The GSSG formed is reduced to GSH by the enzyme GSH reductase (GSHr), at the expense of the reducing equivalent NADPH[64]. This reaction is termed the 'GSH redox cycle' and is responsible for maintaining a balance between GSH and GSSG levels within the cell that is heavily weighted towards GSH under normal physiological conditions[42;64]. Thus, the GSH to GSSG ratio in most cells is between 20:1 and 1000:1[67]. Under conditions of extreme oxidative stress the GSH redox cycle cannot maintain the normal GSH:GSSG balance as NADPH becomes depleted.

Excessive levels of GSSG are excreted by the cell and consequently intracellular glutathione is depleted[62].

The conjugation of GSH to electrophilic xenobiotics (or their metabolites) also leads to depletion of cellular glutathione. GSH is the most abundant intracellular non-protein thiol[33;68]. Conjugation of xenobiotics to GSH therefore re-directs the damaging effects of electrophilic attack away from important functional thiol groups within cellular proteins[33;66;69]. A wide range of xenobiotics undergo GSH conjugation; examples include quinones and quinone derivatives, epoxides (e.g. benzene epoxide), certain halogenated aromatic and aliphatic compounds (e.g. 3,4-dichloronitrobenzene), and unsaturated aliphatic compounds with suitable electron-withdrawing groups (e.g. diethyl maleate)[28;61;68;70;71].

GSH conjugation can be both enzymatic and non-enzymatic[68;69]. The glutathione-S-transferase (GST) enzyme family drives enzymatic conjugation. GSTs are widely expressed in mammalian tissues, although the liver displays the greatest level of expression[32;45]. GSTs are dimeric proteins with each subunit possessing a GSH binding site (G-site) and a hydrophobic region that serves as the binding site for the electrophilic substrate[32;72]. GSTs have broad substrate specificities[72] and produce GSH S-conjugates through the formation of a thioether bond between the GSH sulphhydryl group and the electrophilic substrate (Figure 1.2). GSH S-conjugates may also be formed non-enzymatically with particularly reactive electrophiles (e.g. quinones and diethyl maleate, the latter often being used to deplete GSH *in vivo* experimentally)[33;70].

The fate of the GSH S-conjugate in the liver is frequently through biliary elimination[28;45;73]. However, many GSH S-conjugates undergo further enzymic modification that results in both biliary and urinary excretion of acetylcysteine conjugates (often referred to as mercapturic acids)[28;45;68]. The γ -glutamyl and glycine moieties are sequentially removed by glutathionase and peptidase enzymes, respectively. Finally, the amino group of cysteine is acetylated resulting in the formation of the mercapturic acid derivative, which is excreted[68]. For most compounds GSH conjugation is considered to be a detoxification reaction[32;45]. However, for certain xenobiotics the reaction with GSH can lead to products that are as toxic (if not more toxic) than the parent compound[32;33;69]. Examples of such compounds include halogenated alkanes and

alkenes (e.g. dichloromethane and hexachlorobutadiene), and quinones and quinoneimines (e.g. bromobenzoquinone)[28;32;33;70].

When intracellular GSH levels are depleted cells respond by increasing synthesis. As GSH levels decrease the activity of γ -GC synthetase (the enzyme that catalyses the 'first' step in GSH synthesis) increases. GSH competitively binds to the glutamate-binding site of γ -GC synthetase blocking the binding of the substrate, and is therefore a competitive feedback-inhibitor of the enzyme. Thus, reduced GSH levels will increase γ -GC synthesis. γ -GC synthetase transcription also increases under conditions that deplete GSH (e.g. oxidative stress and the level of GSH conjugates), which may also lead to increased γ -GC synthesis. However, the rate of γ -GC synthesis is also heavily dependent upon the intracellular availability of cysteine. Because most tissues lack the ability to synthesise cysteine, in mammals the liver is heavily relied upon to meet any increased requirement by exporting GSH.

The liver acts as a GSH and cysteine reservoir due to the highly active cystathionine pathway in hepatocytes. The cystathionine pathway is highly responsive to cysteine requirement[42]. The activity of two enzymes in the cystathionine pathway appear to be modulated by oxidative stress[74]. Cystathionine β -synthase activity increases and methionine synthase activity decreases. The former catalyses the formation of cystathionine (a cysteine precursor) from homocysteine. The latter utilises homocysteine for methionine synthesis. The opposing effect that oxidative stress has on the key cystathionine-utilising enzymes means that cysteine synthesis increases[74].

1.3.2. Transcriptional Responses to Oxidative Stress

The transcription of a wide range of genes is modulated during the adaptive response to oxidative stress (Figure 1.7). A coordinated and balanced response is undertaken by increasing transcription of genes whose proteins enhance production of antioxidants and effect the repair of ROS-induced biochemical lesions, while at the same time decreasing transcription of ROS-producing systems[49].

One of the key mechanisms through which oxidative stress modulates transcription is regulation of redox-sensitive cysteinyl residues within a number of transcription factors (TF) to enhance or reduce their activity[75-77]. Positive oxidative stress sensors include

TFs such as activator protein-1 (AP-1), nuclear factor-kappa B (NF- κ B) and nuclear factor (erythroid-derived 2)-like 2 (Nrf2). Negative oxidative stress sensors include nuclear factor I/C (CCAAT-binding transcription factor) (NFI) and specificity protein 1 TF (Sp1)[49;77].

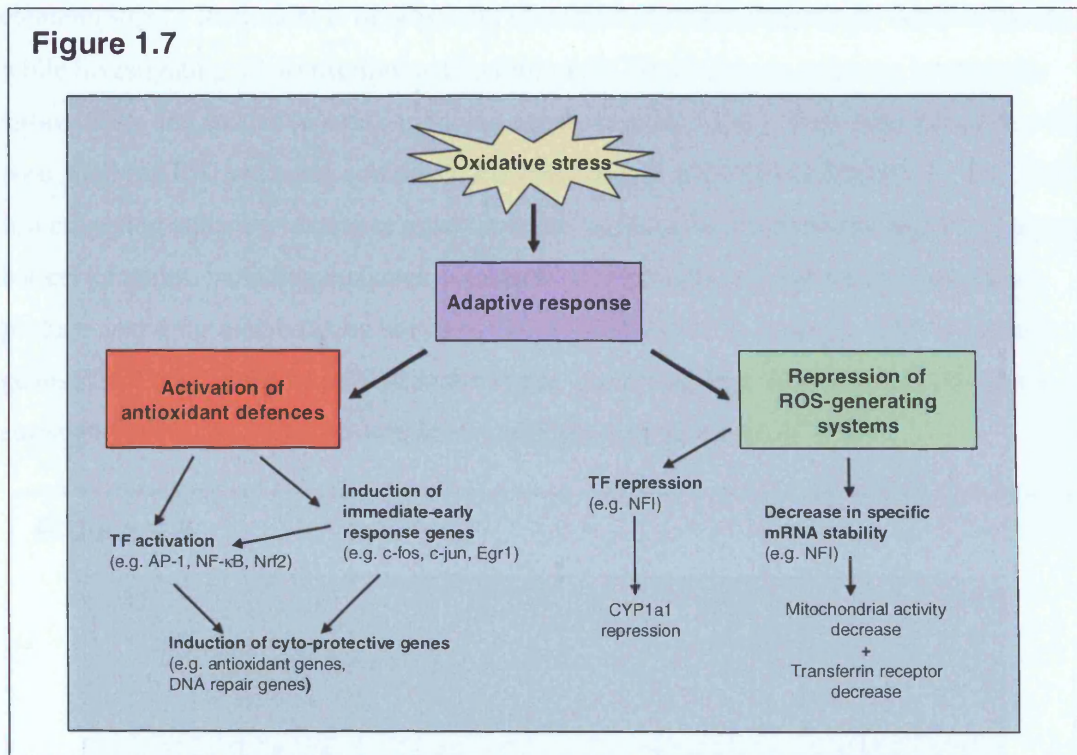


Figure 1.7: Schematic of the adaptive response to oxidative stress

Adapted from Morel and Barouki, 1999[49]

A critical modulator of redox-sensitive transcriptional regulation is a protein called Redox factor-1 (Ref-1). The Ref-1 protein is a bifunctional enzyme that is involved in DNA repair and activation of a number of stress-response TFs[76;78;79]. Ref-1 is thought to act directly on critical cysteinyl residues within the DNA binding domains of AP-1, NF- κ B, p53, activating transcription factor/cAMP-response element binding protein (ATF/CREB), hypoxia-inducible factor (HIF)-1 α and HIF-like factor[76;78]. When the redox-sensitive cysteinyl residues of these TFs are oxidised, their DNA binding capacity is generally reduced. Ref-1 is believed to carry out the reduction of the same cysteinyl residues within the TFs as part of a redox cascade within the nucleus involving thioredoxin[49], although the precise mechanism is not fully understood[78]. The result is enhanced binding of Ref-1-

regulated TFs to their respective DNA response elements and increased transcription of target genes.

One of the key pathways of gene regulation in the oxidative stress response is that of the antioxidant response element (ARE) (Figure 1.8), also known as the electrophile response element[80;81]. Rushmore *et al* originally identified and characterised the ARE in the rat, while investigating the transcriptional control of the *Gsta2* gene in response to phenolic antioxidants and oxidative stress-inducing agents (e.g. H₂O₂)[82]. They determined that the core ARE (cARE) sequence comprised the consensus 5'-RGTGACNNGC-3'. The ARE is a *cis*-acting enhancer sequence now known to be found in the promoter regions of a large battery of genes, including enzymes associated with glutathione regulation, antioxidant proteins and drug-metabolising enzymes (Table 1.6)[83;84]. In essence, ARE-regulated genes effect the control of cellular redox status, protect against the ravages of oxidative stress and aid in the detoxification of electrophilic xenobiotics[83].

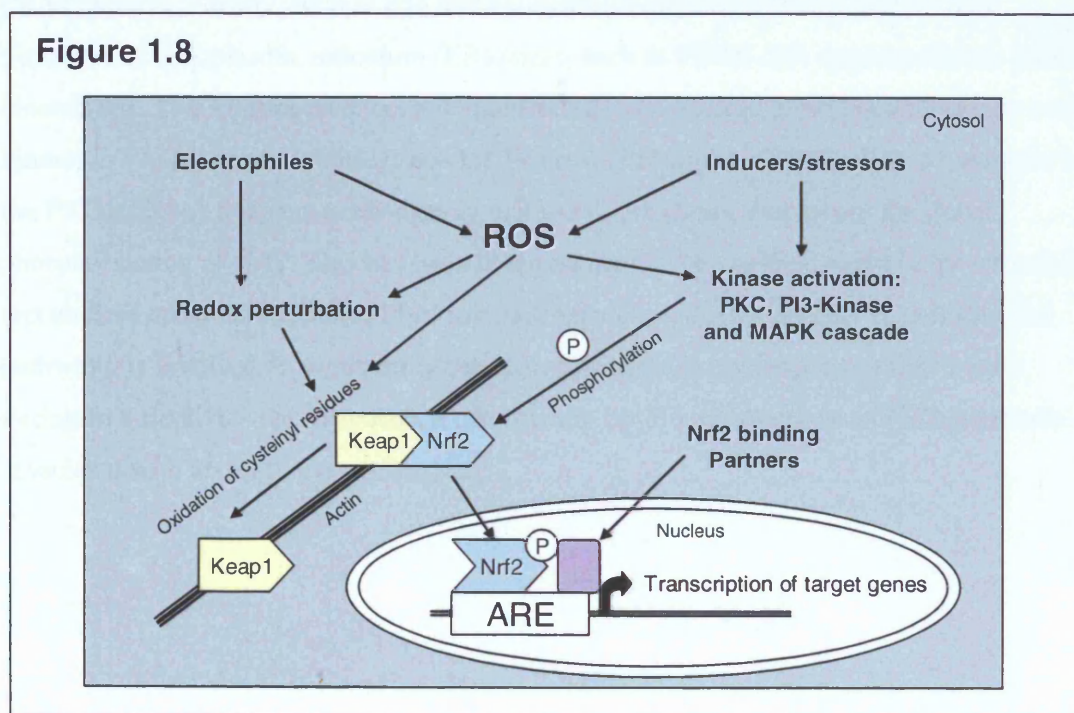


Figure 1.8: Schematic of the Nrf2-ARE pathway activation

Adapted from Lyakhovich *et al*[85]

The ARE is bound by the ubiquitously expressed Nrf2, a transcriptional activator belonging to the basic-leucine zipper (bZIP) class of transcription factors. bZIP proteins (which

include members of the AP-1 family, small Maf proteins and ATF/CREB TFs) can bind to DNA as part of homodimer and/or heterodimer complexes[77;83;86]. Nrf2 normally resides within the cytosol, where it is associated with a cytoskeletal inhibitory partner called kelch-like ECH-associated protein 1 (keap1)[84]. Keap1, which contains several highly reactive cysteinyl residues, is thought to act as a redox sensor. Under pro-oxidant conditions the reactive cysteinyl residues are oxidised to form disulphide bridges, inducing a conformational change in keap1[80;84]. This change results in the dissociation of the Keap1/Nrf2 complex, freeing Nrf2 to translocate into the nucleus, bind the ARE and initiate transcription of ARE-responsive genes (Figure 1.8).

In addition to the role that Keap1 plays in ARE regulation, phosphorylation of Nrf2 is thought to be necessary for Nrf2-mediated activation of ARE-containing genes. A number of upstream kinase pathways, responsive to a range of stressors and inducers, have been proposed as transducers of Nrf2 activity (e.g. members of the mitogen-activated protein (MAP) kinase pathway, such as p38 and extracellular-regulated kinase (ERK); and signallers of endoplasmic reticulum (ER) stress, such as PERK (ER-transmembrane protein kinase)[80]. Two kinases have been demonstrated to be critical in Nrf2 activation, protein kinase C (PKC) and phosphatidylinositol 3-kinase (PI3-kinase)[84;87]. PKC, a member of the PKC pathway that senses changes in cellular redox status, carries out the direct phosphorylation of Nrf2. This has been demonstrated to be a critical event in its activation and nuclear translocation[84]. PI3-kinase, a kinase intrinsic in a number of cell survival pathways, is involved in augmenting the actin cytoskeletal rearrangement that occurs during an oxidative stress response, a prerequisite for the translocation of Nrf2 (normally associated with actin) to the nucleus[84].

Table 1.6: ARE-containing genes and their function

Pathway/Function	Gene	Abbreviation
Phase II metabolism (glutathione conjugation)	Glutathione S-transferase A1, 2, 4 and 5	GSTA1, 2, 4 and 5
	Glutathione S-transferase M1, 2, 3 and 4	GSTM1, 2, 3 and 4
	Glutathione S-transferase P1	GSTP1
Quinone metabolism (two electron reduction)	NAD(P)H:quinone oxidoreductase	NQO1
GSH biosynthesis/redox cycle	Glutamate-cysteine ligase, catalytic subunit	GCLC
	Glutamate-cysteine ligase, modulatory subunit	GCLM
	Glutathione Peroxidase 2	GPx2
	Glutathione Reductase	GSR
Biliary secretion of GSSG	Multidrug resistance-associated protein 2	MRP2 (also known as ABCC2)
Antioxidant generation/Heme metabolism	Heme oxygenase 1	HMOX1
Antioxidant/metal chelation	Metallothionein-1 and 2	MT1 and MT2
Antioxidant	Inducible NO synthase	iNOS
	Superoxide dismutase 1 and 3	SOD1 and SOD3
Thiol redox regulation	Thioredoxin reductase 1	TXNRD1
	Thioredoxin	TXN
	Peroxiredoxin 1	PRDX1

Adapted from Morel and Barouki, Lyakhovich *et al*, and Vollrath *et al*[49;85;88]

Nrf2 is also known to have a number of binding partners that modulate ARE-binding and transcriptional activation. Members of the small Maf proteins (e.g. MafF, G and K) are able to heterodimerise with Nrf2 and enhance ARE binding. However, the Nrf2 transcriptional activation of the ARE is repressed, leading to decreased expression of ARE-responsive genes. Additional binding partners belonging of the bZIP family (e.g. CREB, c-JUN, c-FOS and activating transcription factor 4 (ATF4)) enhance both binding of Nrf2 to the ARE and transcriptional activation [83;86]. Overall, it seems that the degree of ARE-activation is optimised to the stressing agent and severity of redox perturbation. This is achieved through the coordinated response of the Nrf2/Keap1 complex, several kinase pathways and a number Nrf2 DNA binding partners.

A wide range of compounds have been shown to activate the ARE pathway (Table 1.7). They include natural and synthetic phenolic antioxidants, quinones, heavy metals, hydroperoxides, and compounds that can react directly with sulphhydryl groups (e.g. diethyl maleate)[83;85]. Common properties that these compounds possess include the ability to generate ROS through redox cycling (or metabolites that can), electrophilic moieties (that deplete GSH and/or oxidize cysteinyl residues on proteins, thus mimicking oxidative stress), or pro-oxidant activity[89].

Table 1.7: Compounds that induce ARE-mediated transcription

Compound Class	Examples	Mechanism of ARE Induction
Phenols	3-hydroxycoumarin, butylated hydroxyanisole, catechol	Metabolism to redox cycling/electrophilic derivative
Quinones	<i>tert</i> -butylhydroquinone, <i>p</i> -benzoquinone, hydroquinone	Redox cycling and GSH depletion
GSH depleters	Diethyl maleate, isothiocyanates (e.g. sulforane)	Sulphydryl group oxidation
Hydroperoxides	Hydrogen peroxide, <i>tert</i> -butyl hydroperoxide	Enhancement of ROS generation
Heavy metal atoms	Cadmium, copper, mercury, lead	Enhancement of ROS generation

Adapted from Nguyen *et al* and Lyakhovich *et al*[85;89]

1.4. Transcript Analysis, Transcriptomics and Microarrays

By comparing the transcriptional levels of genes in tissues or cells from ‘control’ and ‘test’ states, it is possible to gain insight into the mechanisms and pathways underlying the comparative phenotypes observed. There are a multitude of techniques available to researchers to undertake these types of transcriptional investigation, although they can be broadly defined as ‘open systems’ and ‘closed systems’.

Open transcriptional systems have the advantage of not requiring any prior sequence knowledge of the genes under investigation. Thus they can be used to study model organisms for which there is little genomic sequence information available and poor gene annotation. Open systems can also be used to identify previously unknown genes in model organisms for which quality genomic sequence information does exist. A number of alternative approaches are used in open systems (Table 1.8), including ‘differential display’

(DD) (more appropriately referred to as ‘fragment display’ (FD))[90], ‘tag sequencing’ and ‘subtractive/competitive hybridisation’ techniques. In general, the main disadvantage associated with open transcriptional systems is their relatively low throughput, both in terms of numbers of gene modulations that can be positively identified and the number of transcriptional comparisons that can be made. Individual techniques also have more specific drawbacks, in terms of sensitivity and false positive rates (summarised in Table 1.8).

Closed transcriptional systems include an equally diverse array of techniques, although the shared attribute is the requirement for prior sequence knowledge of the gene(s) under investigation. Closed systems include techniques that are only amenable to investigating the transcriptional levels of single (e.g. Northern blots and the ribonuclease protection assay) or small subsets of genes (e.g. real-time quantitative PCR (RT-QPCR)). At the other end of the spectrum, they include those capable of simultaneously measuring the expression levels of thousands of genes, i.e. microarrays. The later have lead to the development of ‘transcriptomics’, broadly defined as the rapid and quantitative comparison of large-scale mRNA expression profiles in biological systems.

Table 1.8: Open transcriptional techniques (adapted from Scheel *et al*[90])

Technique	Method	Sensitivity/Throughput
Fragment Display	<p>mRNA populations are used to prepare cDNA fragments which are PCR amplified and displayed by gel electrophoresis.</p> <p>A correlation between mRNA abundance and PCR fragment intensity allows identification of differentially expressed fragments.</p> <p>Differential bands must be excised, re-amplified, (cloned) and sequenced to identify the gene represented.</p>	<p>DD had poor reproducibility, sensitivity (under-representation of rare transcripts) and high false positive rate.</p> <p>Use of restriction enzymes to fragment cDNA, which is ligated to universal primers prior to PCR amplification and electrophoresis have allowed the disadvantages of DD to be overcome.</p> <p>Throughput still remains low due to the requirement to excise and sequence fragments to identify regulated transcripts.</p>
Taq sequencing	<p>Two broad methodologies available; SAGE (Serial Analysis of Gene Expression) and MPSS (Massive Parallel Signature Sequencing)</p> <p>Conversion of mRNA to cDNA, which is used to undertake SAGE and MPSS and then relies on the fact that a small sequence stretch (10-20mer) can positively identify a specific gene.</p> <p>Abundance of given gene is proportional to its sequence tag representation.</p>	<p>SAGE can be insensitive to rare transcripts unless huge numbers (<100,000) sequence tags are generated.</p> <p>MPSS allows the rapid generation of up to 1 million sequence tags, affording increased sensitivity.</p> <p>Both tag sequencing techniques are hugely expensive and low throughput in terms of mRNA populations that can be evaluated.</p>
Subtractive/competitive hybridisation	<p>Hybridisation of mRNA/cDNA from 'tester' population to excess of 'driver' population. Un-hybridised species are separated and represent up-regulated genes in 'tester' population.</p> <p>Differentially expressed mRNAs/cDNAs are then cloned and sequenced.</p> <p>Additional rounds of hybridisation can be used to enrich differentially expressed genes</p>	<p>Reversal of 'tester' and 'driver' mRNA/cDNA populations is required to identify down-regulated genes in the sample of interest.</p> <p>Susceptible to false positives and insensitive to low magnitude changes (<5 fold).</p> <p>High level of redundancy in regulated clones results in identification of only a small number of differentially expressed genes.</p> <p>Additional rounds of hybridisation can be time consuming</p>

In the last 10 years, microarrays have become an established part of the research armoury and are a powerful tool. They have been applied to further the understanding of biological processes in a range of fields, including toxicology[91-95]. Combined with the huge advances in genome sequencing and gene annotation made in recent years, they have led to the advantages of 'open' transcriptional systems becoming more or less obsolete. As genome sequencing of an increasing number of model species is completed, it is becoming practicable to use microarrays to measure transcription at a virtually genome-wide scale. This has enabled the generation of huge volumes of data, faster than ever before.

All microarray platforms utilise the ability of nucleic acids immobilised on a solid substrate ('probe') to hybridise with labelled complementary sequences in solution ('target') that have been derived from total RNA under investigation. One of the earliest microarray methods used positively charged nylon as the immobilising substrate onto which PCR products (amplified from cDNA libraries) were spotted. A radiolabelled 'target' was then hybridised, the excess washed off and binding measured using phosphorescence detection. Although relatively cheap and easily accessible, this approach has fallen out of favour in recent years due its use of radioactivity, relatively low density and poor sensitivity. It has now been almost completely superseded by two predominant microarray platforms; the Stanford-type microarray system and Affymetrix GeneChips®.

1.4.1. Stanford-Type Microarrays

The manufacture of glass slide microarrays and their application to transcriptomic investigations was pioneered by the Brown lab in Stanford University, California from 1995 onwards[90]. The first published study utilising the Stanford microarray system was an investigation of the differential expression of 45 *Arabidopsis* genes in *Arabidopsis thaliana*[96]. This early application using a low density version of the Stanford microarray was quickly followed a year later when DeRisi *et al* used the same methodology in a higher density format[97]. They evaluated the transcriptional expression of over 1000 genes in the human UACC-903 melanoma cell line under normal and tumour suppressing conditions, to identify genes that may be important in this response[97]. Since then, Brown *et al* have made available details of the design, manufacture and methodologies associated with the use of the Stanford microarray system. This has led to wide spread adoption of the system

throughout the scientific community, including the Systems Toxicology Group at the MRC Toxicology Unit, Leicester.

The Stanford system involves the printing of solutions of either PCR amplified cDNAs or short synthesised oligonucleotides (oligos) onto poly-L-lysine-coated glass microscope slides at very high density. This is carried out through the use of robotic arrayers that can print large numbers of replicate microarrays (over 100 per run) in a single run. High density printing (up to 20-30 probe spots per square millimetre)[90] is achieved by printing heads containing up to 32 metallic microquills that deposit the probe solutions onto the glass slides. The probes are then covalently bound to the glass slides using a UV-crosslinker.

To undertake transcriptomic investigations using the Stanford-type arrays, competitive hybridisation of 'control' and 'test' targets is carried out simultaneously (Figure 1.9). This process involves the synthesis of fluorescently-labelled cDNA reverse-transcribed from each total RNA sample under investigation. This is achieved through direct incorporation of dUTP labelled with one of two fluorescent cyanine dyes (Cy3 or Cy5) during reverse transcription. Alternatively, indirect labelling by incorporation of amino-allyl dUTP during reverse transcription (which can subsequently be coupled to esterified Cy3 or Cy5) can be used.

Once labelling is complete, the control and test targets are co-hybridised to the same microarray and data captured using a laser scanner capable of exciting at appropriate dual wavelengths. To account for any differences in labelling efficiency and signal intensity of the two fluorophores, the hybridisation experiment is often repeated with the targets reverse-labelled. Relative abundance of each gene is derived from the intensity of a particular spot, while differential expression between the two targets is inferred from the ratio between the two fluorescent channels.

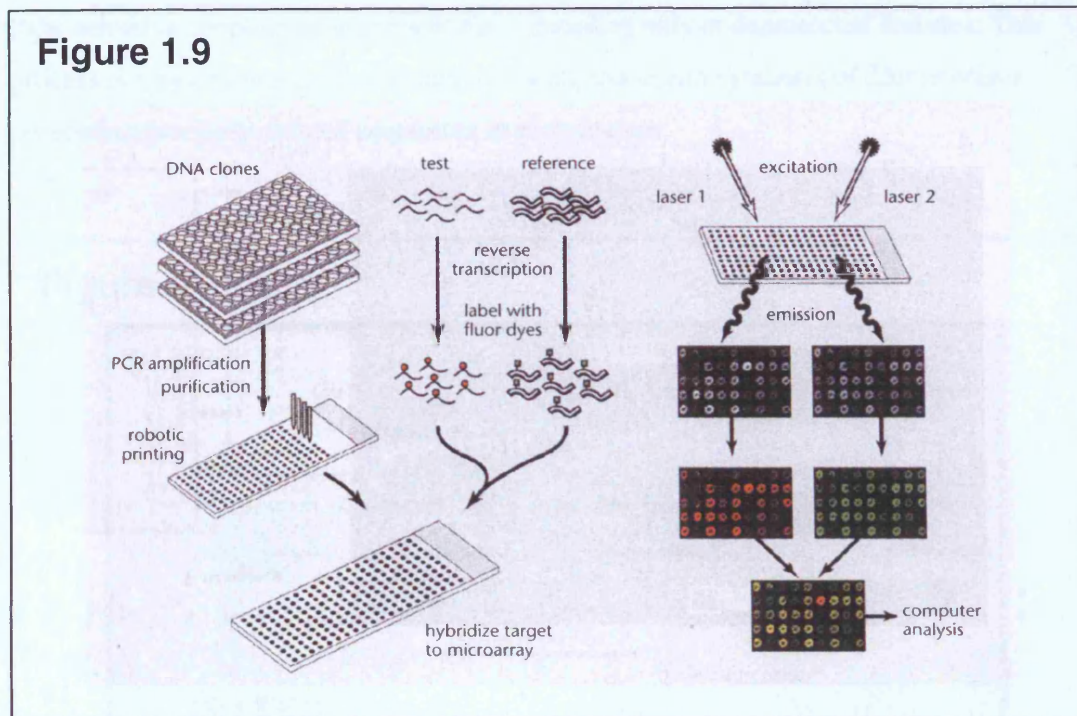


Figure 1.9: Stanford-type microarray production and hybridisation[98]

1.4.2. Affymetrix GeneChips®

Affymetrix GeneChips®, first commercially manufactured in 1994, differ from the Stanford microarray platform in two main ways. Firstly, sets of multiple 25-mer oligos are used as probes for each gene (versus a single cDNA or oligo for the Stanford platform). Secondly, the probe sets are hybridised with a single target population, thus two microarrays are required to undertake a comparison of differential gene expression.

A number of chemistries have been combined by Affymetrix to develop their GeneChip® technology. GeneChips® are manufactured using a process known as photolithography, which enables the production of microarrays with millions of probes. The photolithographic process begins with a quartz wafer being coated with a light sensitive chemical that prevents binding of nucleotides until exposed to light (Figure 1.10). Lithographic templates are used to expose or mask defined regions (or features) of the quartz wafer to light, resulting in deprotection of exposed features. The quartz wafer is submerged in a solution containing the appropriate nucleotide (which also possesses a

light-sensitive coupling group) resulting in coupling only at deprotected features. This process is repeated in a cyclic manner, allowing the *in situ* synthesis of 25mer oligos possessing precisely defined sequences at each feature.

Figure 1.10

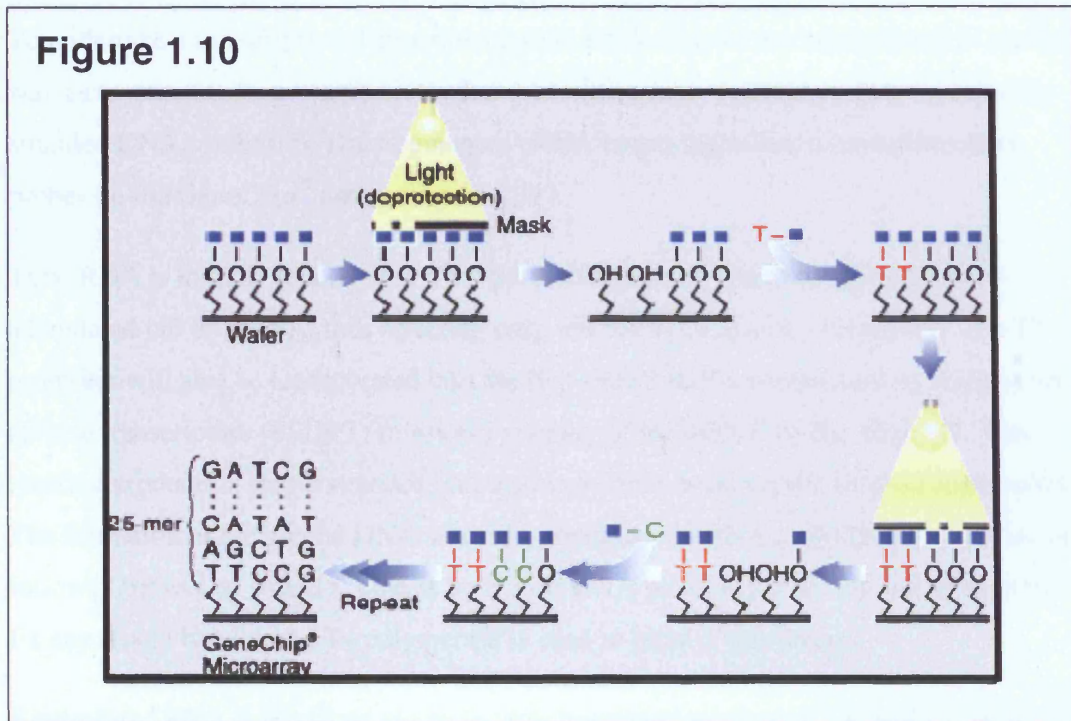


Figure 1.10: Photolithographic synthesis of oligos for the production of Affymetrix GeneChips®

The cycling between deprotection of the wafer and nucleotide addition enables tight regulation of the nucleotides added at each feature (Affymetrix image library - <http://affymetrix.com>).

The current standard GeneChips® are manufactured at a density of over 1.3 million features per microarray (approximately 5 micron dimensions), although each quartz wafer is diced into tens or hundreds of identical GeneChips® (depending on number of individual genes represented). The standard expression GeneChips® possess 22 different 25mer oligo probes (termed a 'probe set') for each gene represented, which are distributed at locations remote to each other. The probe sets are 3'-biased and designed to give the optimal balance between sensitivity and specificity for the target gene. To evaluate any potential for non-specific hybridisation, each 'perfect match' (PM) probe feature has an adjacent paired 'mismatch' (MM) probe feature. The MM probe differs in sequence from the PM probe by a single nucleotide, located in the centre of the 25mer. The MM features serve as controls

that allow the subtraction of non-specific hybridisation signals (non-specific hybridisation for the PM and MM features should be roughly equivalent) from the PM signal to derive the true signal for a particular gene.

1.4.2.1. Affymetrix GeneChip® Target Generation, Hybridisation and Scanning

To undertake a transcriptional experiment, total RNA samples are manipulated in such a way as to generate fragmented biotinylated-complimentary (c)RNA targets (via double-stranded DNA synthesis). The fragmented cRNA targets hybridise to complimentary probes on the GeneChip® arrays (Figure 1.11).

Total RNA is initially treated with a T7-(oligo-dT) primer, which binds to the poly-adenylated tail of mRNA, thus selecting only mRNA to be reverse transcribed. The T7 promoter will also be incorporated into the first strand cDNA synthesised by Superscript II reverse transcriptase (SSIIRT) following priming of the mRNA by the oligo-dT. This reaction produces a single stranded (ss) antisense DNA bound to the original input mRNA. The formation of the second DNA strand is dependant on RNA degradation by RNase H, followed by second strand synthesis by *E.Coli* DNA polymerase. *E.Coli* ligase is added to fix any strand breaks, and T4 polymerase is used to blunt 3'-overhangs.

Biotinylated RNA is produced via an *in-vitro* transcription reaction, dependant on the T7 promoter. The RNA produced is complimentary to the original sample RNA, hence the term 'cRNA'. The nucleotide substrates for the formation of cRNA are biotinylated to enable detection when hybridised to the GeneChip®. The cRNA is then fragmented into 35-200 nucleotide fragments of cRNA by metal-induced hydrolysis.

The fragmented cRNAs are hybridised to the GeneChips® overnight, excess cRNA removed by washing and the GeneChips® stained. There is a triple staining procedure to amplify the signal. First a fluorescently labelled streptavidin stain, which binds to the biotin-labelled cRNA fragments. This is followed by a biotinylated anti-streptavidin antibody, and then a repeat of the fluorescently labelled streptavidin. The GeneChip® is then placed into an Affymetrix Laser Array Scanner and the raw data captured by measurement of fluorescence signal. Scanning the GeneChip® produces a raw image data file (.dat file) which is analysed within the Affymetrix operating system (GeneChip®)

Operating Software (GCOS)) to produce a .cel file. The .cel file contains a single intensity value for each probe feature on the GeneChip®.

Figure 1.11

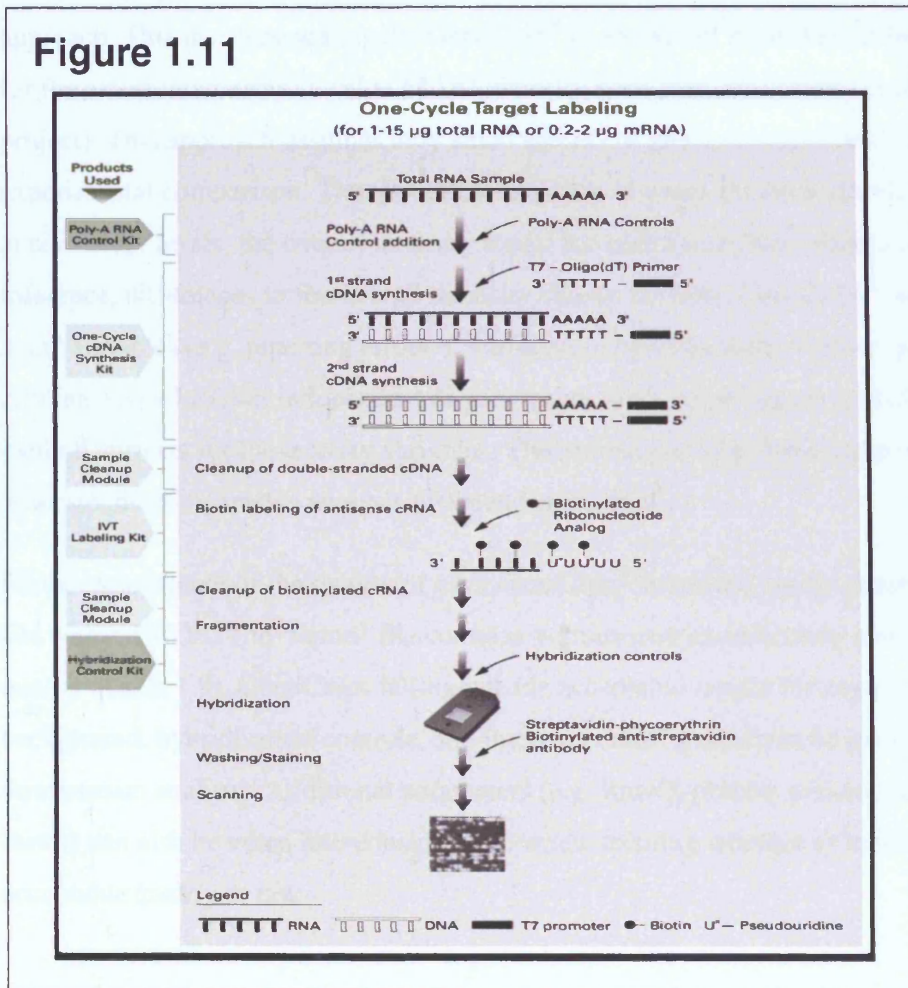


Figure 1.11: Methodology of standard eukaryotic gene expression assay.

Labelled cRNA targets derived from mRNA of an experimental sample are hybridised to nucleic acid probes attached to the quartz wafer chip. By monitoring the amount of label associated with each DNA location, it is possible to infer the relative abundance of each RNA species represented (Affymetrix image library - <http://affymetrix.com>).

1.4.2.2. Affymetrix GeneChip® Primary Analysis and Quality Assessment

Initial analysis of the GeneChip® involves inspection of the .dat file image for the presence of any obvious image artefacts (e.g. bubbles, high regional/overall background, bleached areas, scratches, etc...). The GeneChip® is then analysed by GCOS to produce a final .chp

file, which contains a single reported intensity value for each gene represented on the GeneChip[®] (this is derived from the entire probe set of 11-22 probe features for each gene).

When the .chp file is generated the GeneChip[®] data is normalised using a 'global scaling' approach. This involves scaling the GeneChip[®] to an overall mean Target Intensity Signal for the entire microarray (a value of 150 intensity units was consistently used for this project). This approach assumes only small subsets of genes are regulated within any experimental comparison. Thus, since the majority of genes for each sample are expressed at consistent levels, the overall intensity signal for each GeneChip[®] should be the same. By inference, differences in the overall intensity signals between GeneChips[®] are a result of assay variables (e.g. pipetting errors or variation in hybridisation, washing and staining efficiencies) which are independent of gene expression. Applying the global scaling method corrects for these assay variables. The normalised .chp file is used for all downstream comparative analysis between GeneChips[®].

Further assessment of the quality of each GeneChip[®] is carried out by generating a 'report' file within GCOS. The 'report' file contains various metrics indicating overall hybridisation quality (Table 1.9). GeneChips falling outside acceptable ranges for key parameters (i.e. background, hybridisation controls, and internal control genes) can be excluded from downstream analysis. Additional parameters (e.g. RawQ, percent present call and scaling factor) can also be taken into consideration when deciding whether a GeneChip[®] is of acceptable quality or not.

Table 1.9: GeneChip® hybridisation quality control metrics.

Quality Indicator	Metric	Description
Background and noise values	Average Background	No specific guidelines, although Affymetrix indicate typical background values range from 20-100 intensity units
	Raw Q value	Overall indication electrical noise, which is scanner-specific. Values between GeneChips® should be comparable.
Hybridisation controls	<i>BioB</i> (1.5pM final) <i>BioC</i> (5pM final) <i>BioD</i> (25pM final) <i>Cre</i> (100pM final)	Prokaryotic gene spikes. <i>BioB</i> equates to 1:100,000 copies and is at the limit of assay sensitivity. <i>BioB</i> should be called 'present' in 50% of arrays. <i>BioC</i> , <i>D</i> and <i>cre</i> should always be called present.
Internal control genes	Beta-actin GAPDH	Used to assess input RNA quality. Probes sets representing 3' and 5' sequence. cRNA synthesis is inherently 3'-biased, but the ratio 3':5' ratio should be <3 for at least one gene. Ratios above may indicate degraded input RNA
Percent present	%P	The number of probe sets called 'present' expressed as a percentage of the total probe sets on the GeneChip®. Replicate samples should have similar %P values and extremely low values indicate poor sample quality.
Scaling and normalisation factors	SF	Indicates the factor used to normalise the array to the Target Intensity Signal. Arrays within the same experiment should have SFs within a 2-fold range.

1.5. Thesis Rationale and Aims

Quinones moieties are important structural elements within anti-cancer medicines, in particular the anthracycline antibiotic doxorubicin. Although quinone-related compounds have clear medical value, their reactivity and associated toxicity often restricts therapeutic use. As a class quinones can exert toxicity through two predominant mechanisms, 1) redox cycling with the concomitant generation of ROS and ensuing oxidative stress, 2) electrophilic attack of cellular nucleophiles resulting in damage to cellular macromolecules. A quinone can exert toxicity through one or both mechanisms. To further understand the mechanisms and cellular processes involved in the toxicity of clinically important quinones, simpler quinone entities are frequently used as tool compounds (e.g. 2,3-dimethoxy-1,4-naphthoquinone (DMNQ) and menadione (MNQ)) which have better defined chemistry. Careful selection of quinones with defined reactivity, in terms of capacity to redox cycle and/or arylate nucleophiles, has allowed the involvement and relative importance of each mechanism to be defined based on differential effects on a number of endpoints. These include general cytotoxicity[26;99], mitochondrial perturbation[100;101], damage to the cytoskeleton[102], genomic DNA[103-105] and plasma membranes[52]. However to date no comprehensive transcriptomic investigation into the genes and pathways regulated with quinone exposure has been undertaken. Such a microarray-based transcriptional analysis would offer the opportunity to identify novel genes/control pathways important in ameliorating the response to quinone challenge. In addition, as redox cycling quinones are frequently used as redox stressors, such an investigation has the potential to further understanding of the relationship between oxidative stress and gene expression.

The overall aim of this project was to therefore identify novel genes and control pathways modulated in response to quinone exposure *in vitro* and *in vivo*. Rat hepatocyte cultures were used because historically they have been utilized as model systems for studying the cytotoxic effects of quinones at a cellular levels *in vitro*[26;27;102;104]. Thus the use of primary rat hepatocytes for investigating *in vitro* transcriptomic changes in this project allowed data generated here to be interpreted in the context of the extensive knowledgebase that exists. However a critical step in understanding the relevance of *in vitro* findings is to

undertake equivalent studies *in vivo*. For this reason transcriptional changes associated with redox cycling quinone exposure were also investigated in the livers of mice.

The overall aim of the thesis was broken down into this series of sub-objectives:

1. To test the hypothesis that it is possible to differentiate the mechanism through which quinones exert cytotoxicity using transcriptomic analysis and appropriate bioinformatics. The rationale was to show that such analysis can be used for the early screening of NCEs in drug development as well as understanding the mechanisms of quinone toxicity.
2. To undertake an investigation into the utility of DMNQ as a tool compound for studying hepatic redox stress *in vivo*. The rationale for this research is that most redox work is carried out in non-physiological *in vitro* systems. Therefore during this study the toxicokinetics and biodistribution of DMNQ in mice was defined, along with the physiological effects (changes in glutathione status and the transcriptome) of a single bolus dose at a level that did not cause acute hepatotoxicity. The advantages of DMNQ for studying redox stress *in vitro* have long been recognised[26]. It was hoped that this study would for the first time demonstrate its utility *in vivo* and that the data will form the foundation for future investigations. As such the use of DMNQ *in vivo* would give rise to opportunities for studying redox stress in multiple organs systems and could eventually lead to the relative importance of redox stress in the toxicity of clinically important quinones being better defined.
3. The use of the findings of this study to advance the understanding of relationships between oxidative stress and gene expression. The rationale for this research is that oxidative stress is a fundamental mechanism of toxicity with many pathophysiological consequences. Through its further understanding there is the implicit possibility of ameliorating further its effects in many disease states and toxicological processes.

CHAPTER 2. MATERIALS AND METHODS

2.1. Hepatocyte Monolayer Culture Methodology

2.1.1. Isolation of Rat Hepatocytes Using the Ex Vivo 'Wedge' Perfusion Method

Male Han Wistar rats (10-12 weeks old) (supplied by Charles River Labs) were killed by cervical dislocation. The fur of the rat was dampened with industrial methylated spirit (IMS) before opening the abdominal cavity, just below the rib cage. The liver was cut free of connective tissue and placed into ice cold sterile Dulbecco's Phosphate Buffered Saline (D-PBS), pH7.4 (154938, Gibco). The two to three largest lobes of the liver were perfused and hepatocytes isolated using the 'wedge' perfusion method, adapted from that of Seglan *et al*[106].

The liver lobes were cannulated via the main vein and placed onto a perfusion rig (Figure 2.1) with a heating jacket for warming buffers to 38°C. All buffers used during the perfusion procedure were aerated continuously (95% O₂, 5%CO₂) and pumped at a flow rate of 10mL/minute with a 101u Peristaltic Pump (Watson Marlow). Blood was cleared by flushing for 15 minutes with Chelating Buffer (prepared as outlined in Section 2.14). The Chelating Buffer was cleared by flushing the lobes with Hank's Balanced Salt Solution (HBSS) (14175, Gibco) for 10 minutes. Finally, the lobes were perfused for 30 minutes with Collagenase Buffer (prepared as outlined in Section 2.14). Catheters were removed and the liver lobes placed in a sterile petri dish containing William's E (WE) Complete media (prepared as outlined in Section 2.14). Unperfused regions were removed and the remainder of the lobes teased apart (using sterile forceps and spatulas) to release the hepatocytes. The cell suspension was filtered through 150µm bolting cloth into a 50mL Falcon tube and made up to 50mL with WE Complete media. The cells were spun for 2 minutes at 50 x *g* (to remove dead and non-parenchymal cells) and the pellet re-suspended in 50mL of fresh WE Complete media. This was repeated three times, after which, the cell viability was assessed by trypan blue exclusion using a haemocytometer (as outlined in Section 2.1.2).

Figure 2.1



Figure 2.1: The liver perfusion rig with three rat liver lobes *in situ*.

2.1.2. Determination of Hepatocyte Viability and Cell Number

Trypan blue is one of several stains routinely used for dye exclusion tests to determine the viability of a cell population. The test is based on the principle that viable cells actively exclude so-called 'vital' dyes (like trypan blue), whereas non-viable cells do not.

A 200 μ L aliquot of the hepatocyte cell suspension was added to 200 μ L of 0.4% trypan blue solution (T8152, Sigma) and mixed by gentle aspiration in a bijou tube. A small sample of the suspension was transferred to an improved Neubauer haemocytometer counting chamber.

Cells were counted in two random squares of the chamber and a mean total number of viable (unstained) and non-viable (blue stained) cells obtained. The total number of cells/mL and cell viability were determined using the following formulae:

- Viable cell number/mL of cell suspension =

$$\text{Mean cell count per square} \times \text{dilution factor} \times 10^4$$
- Total viable cell number =

$$\text{Number of viable cells/mL of cell suspension} \times \text{volume of cell suspension}$$
- Percent cell viability =

$$\left(\frac{\text{Total viable cells (unstained)}}{\text{total cells (stained + unstained)}} \right) \times 100$$

Cell viability for hepatocyte preparations was routinely 80-90 percent. Hepatocyte preparations with cell viability less than 75 percent were not used.

2.1.3. Plating, Attachment and Recovery of Hepatocytes

Hepatocytes were diluted with Complete WE media to the appropriate density of viable cells for the culture vessel being used (Table 2.1). An appropriate volume of hepatocytes (Table 2.1) were plated onto each BioCoat Plate well (type-I collagen-coated) (Beckton Dickinson) and attachment allowed to proceed for 2 hours in a humidified incubator at 37°C (containing 5% CO₂, 95% air). Following attachment, media was removed and the hepatocytes were washed once with sterile D-PBS (at 37°C) and an appropriate volume of WE Incomplete media (prepared as outlined in Section 2.14) added (volumes defined in Table 2.1). Hepatocytes were incubated overnight (for 16 hours) in a humidified incubator at 37°C (containing 5% CO₂, 95% air) to recover prior to treatment.

Table 2.1: Volumes of Tissue Culture Reagents Used for Different BioCoat Plate Types

Plate Type (Cat. No.)	Seeding Density	Seeding Volume	Number of Cells Seeded/Well	PBS Wash Volume	WE Incomplete Media Volume	Treatment Media Volume
12-well plate (356400)	5 x 10 ⁵ /mL	0.75mL	3.8 x 10 ⁵	0.5mL	0.75mL	0.75mL
6-well plate (356500)	5 x 10 ⁵ /mL	2mL	1 x 10 ⁶	1mL	2mL	2mL

2.1.4. Treatment of Hepatocyte Monolayers

Following the recovery incubation, WE Incomplete media was discarded and dead cells removed by washing the wells with sterile D-PBS (at 37°C) (defined in table 2.1). An appropriate volume (defined in table 2.1) of freshly prepared treatment media was added to each well. Treatment media was either Vehicle Control (WE Incomplete media/1% v/v dimethyl sulphoxide (DMSO) (154938, Sigma)) or Quinone Media (the quinones detailed in Table 2.2 were diluted in 100% DMSO before being added to WE Incomplete media to achieve the desired final concentration). Hepatocytes were incubated prior to sampling at various time points in a humidified incubator at 37°C (containing 5% CO₂, 95% air).

Table 2.2: Test Quinone Details

Quinone	Abbreviation	Purity	Supplier	Cat. No.
1,4-benzoquinone	BQ	>99%	Sigma	B1266
1,4-naphthoquinone	NQ	97%	Aldrich	15,275-7
2,3-dimethoxy-1,4-naphthoquinone	DMNQ	99%	Dr T Gant, MRC Toxicology Unit, Leicester University	Not applicable
2-methyl-1,4-naphthoquinone (menadione)	MNQ	>99%	Sigma	M5625
Thymoquinone	TQ	99%	Aldrich	27,466

2.2. Transfection of Hepatocyte Monolayer Cultures with Small Interfering RNA

To investigate the role of quinone-regulated genes in the response of hepatocytes to redox stress, the gene interference technique known as small interfering RNA (siRNA) was used. siRNA utilises the endogenous RNA interference (RNAi) post-transcriptional control pathway first observed in plants[107] and later in *Caenorhabditis elegans*[108]. The term RNAi was later coined by Ketting and Plasterk[109]. An active RNAi pathway has since been demonstrated in mammalian cells and synthetic siRNAs are routinely exploited as tools for understanding gene function[110;111]. siRNAs are short double-stranded oligoribonucleotides that associate with the RNA-induced silencing complex (RISC) and induce degradation of complementary target mRNA sequences. The result is decreased levels of the target gene mRNA and consequently, decreased protein expression[110;111]. Through the use of conventional transfection techniques, it is possible to introduce siRNAs that target a gene of interest into cells cultured *in vitro*. This can bring about suppression of both the mRNA and protein expression of that gene. Once gene suppression (or 'knockdown') has been achieved, the role of that gene can be inferred by studying phenotypic changes in the cells transfected.

2.2.1. Transfection Complex Preparation

The *TransIT*-TKO[®] siRNA transfection reagent (2155, Mirus Corporation) was used as supplied (2.5mg/mL in 100% ethanol). Lyophilised siRNAs were purchased from Ambion (details given in Chapter 6) and dissolved in siRNA Buffer (details of preparation are included in Section 2.14) to the desired working concentration. siRNA working stock solutions were stored at -80°C until required.

siRNA transfection mixes were prepared on the day of use. The *TransIT*-TKO[®] was added to WE Incomplete media (without gentamicin) at the required concentration (defined in Chapter 6), mixed well by vortexing and incubated at room temperature for 20 minutes. A volume of each siRNA working stock was added (to achieve the final concentrations detailed in Chapter 6), or an equivalent volume of siRNA Buffer for control, and the solutions mixed by gentle pipetting. The siRNA mixes were incubated at room temperature for 20 minutes to allow siRNA complexes to form. The siRNA mixes were then used for transfection as outlined in Section 2.2.2.

2.2.2. Transfection of Rat Hepatocyte Monolayers

Rat hepatocytes were prepared and viability assessed as detailed previously (Sections 2.1.1 and 2.1.2, respectively). Hepatocyte monolayers were prepared on BioCoat tissue culture plates as detailed previously (Section 2.1.3), with the exception of seeding density. A reduced seeding density of 3.5×10^5 viable cells/mL was used (equating to approximately 70 percent of standard). Following attachment and washing with sterile D-PBS, WE Complete media was added to each well (6 well plates = 1.5mL/well; 12 well plates = 0.57mL/well). The appropriate 'siRNA mix' (prepared as detailed in Section 2.2.2) was added to each well (6 well plates = 0.5mL/well; 12 well plates = 0.19mL/well) and dispersed by gently rocking the plates. Hepatocytes were incubated overnight (for 16 hours) in a humidified incubator at 37°C (containing 5% CO₂, 95% air) to allow target gene knockdown to proceed prior to treatment. Treatment of hepatocytes was carried out as outlined previously (refer to Section 2.1.4).

2.3. Assessment of Hepatocyte Viability Using LDH Leakage

The determination of enzyme leakage is frequently used to assess cell viability *in vitro*. As viability decreases and cells undergo necrotic cell death, enzymes that are normally compartmentalised within the cells leak out into the culture media. Lactate dehydrogenase (LDH) is frequently used for this purpose by measuring the levels found in the culture media and viable cells remaining in culture.

The LDH-P Assay (AE1-20, Alfa Wassermann) was used for determination of LDH levels. The assay utilises the ability of LDH to catalyse the conversion of pyruvate to L-lactate in the presence of NADH (as indicated in Figure 2.2). The rate of reaction is monitored photometrically at 340nm, the rate of NADH oxidation being directly related to the level of LDH activity within the sample.

Figure 2.2



Figure 2.2: LDH Assay Principle. In the presence of pyruvate LDH catalyses the oxidation of NADH to NAD⁺, which absorbs light at 340nm.

2.3.1. Sampling Culture Media and Hepatocyte Monolayers

At an appropriate time point, 0.25mL of hepatocyte culture media was sampled into a 1.5mL Eppendorf tube and centrifuged at 10,000 x g for 3 minutes to remove cellular debris. The supernatant was transferred to a fresh 1.5mL Eppendorf and stored at 4°C until required. This constituted the 'leaked' sample. The remaining treatment media was removed, the hepatocytes washed with 0.5mL sterile D-PBS (at 37°C) and 0.5mL of 0.1% v/v Triton-X100 (Sigma) added. Lysis was allowed to proceed at 4°C for 30 minutes and 0.25mL of hepatocyte lysate sampled into a 1.5mL Eppendorf tube and centrifuged at 10,000 x g for 3 minutes to remove cellular debris. The supernatant was transferred to a fresh 1.5mL Eppendorf tube and stored at 4°C until required. This constituted the 'lysed' sample.

2.3.2. Running the LDH Assay

The LDH-P Assay Working Reagent was prepared 10 minutes before use by reconstituting one vial of kit component R2 (lyophilised substrate containing NADH at a final concentration of 0.19mmol/L when formulated) with one vial of kit component R1 (assay buffer; 52mmol/L phosphate buffer and 0.6mmol/L pyruvate). After dissolution the Working Reagent was loaded onto the reagent store within the SpACE[®] Autoanalyser (Alfa Wassermann).

All 'leaked' and 'lysed' samples were run on the same day as they were prepared. Two-hundred microlitres of each 'leaked' and 'lysed' sample was transferred to an autanalyser cup and loaded onto SpACE[®] Autoanalyser segment. The segments were loaded onto the SpACE[®] autoanalyser and LDH-P Assay run. During the assay the SpACE[®] Autoanalyser takes 4 μ L from each sample cup and mixes it with 150 μ L of Working Reagent in a clean cuvette. The rate of reaction was measured at 340nm and the results reported by the autoanalyser in units of LDH/L. Data was expressed as LDH leaked as a percent of total. To derive this value, the following formulas were used:

- Total leaked LDH IUs per well =
 'leaked' LDH IU/L x media volume in mL
- Total LDH IUs per well =
 total leaked LDH IUs per well + 'lysed LDH IU/L x lysis volume in mL
- LDH leakage as a percent of total =
 (Total leaked LDH IUs per well/Total LDH IUs per well) x 100

2.4. Assessment of Liver Damage by Measurement of Plasma Alanine Aminotransferase Levels

Measurement of circulating levels of alanine aminotransferase (ALT) is frequently used for the diagnosis of liver disease and hepatic damage as a result of toxicity. ALT is normally compartmentalised within the tissue and so circulating levels in healthy individuals are typically low (<40U/L). When injury to hepatic tissue occurs ALT is released, resulting in an increase in blood levels of the enzyme.

The ALT Assay (AL1-205, Alfa Wassermann) was used for determination of ALT levels. The assay utilises the ability of ALT to convert α -oxoglutarate and L-alanine to L-lactate and NAD^+ (in the presence of an enzyme/coenzyme mix) (as indicated in Figure 2.3). The rate of reaction is monitored photometrically at 340nm, the rate of NADH oxidation being directly related to the level of ALT activity within the plasma sample.

Figure 2.3

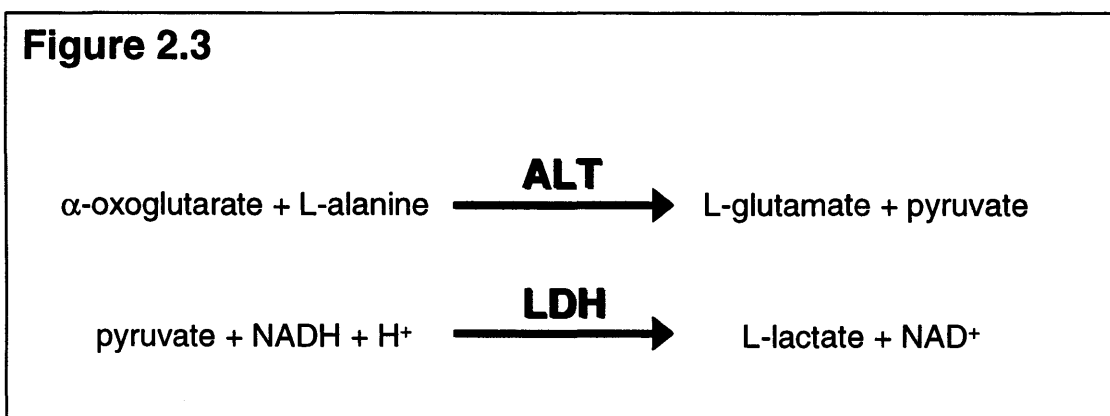


Figure 2.3: ALT Assay Principle. ALT catalyses the first reaction and the pyruvate generated is utilised by LDH in the oxidation of NADH to NAD⁺, which absorbs light at 340nm.

2.4.1. The ALT Assay

The ALT Assay Working Reagent was prepared 10 minutes before use by reconstituting one vial of kit component R2 (lyophilised substrate containing the following when formulated; 0.18mmol/L NADH, 12mmol/L α -oxoglutarate, 600U/L LDH) with one vial of kit component R1 (assay buffer; 80mmol/L tris-buffer, pH7.5 and 240mmol/L L-alanine). After dissolution the Working Reagent was loaded onto the reagent store within the SpACE[®] Autoanalyser.

Frozen plasma-EDTA samples taken from treated mice (supplied by Dr T Gant, MRC Toxicology Unit, Leicester University) were thawed and diluted in an appropriate volume of distilled water. Two-hundred microlitres of each diluted plasma sample was transferred to an autanalyser cup and loaded onto the SpACE[®] Autoanalyser segment. The segments were loaded onto the SpACE[®] autoanalyser and ALT Assay run. During the assay the SpACE[®] Autoanalyser takes 20 μ L from each sample cup and mixes it with 200 μ L of Working Reagent in a clean cuvette. The rate of reaction was measured at 340nm and the results reported by the autoanalyser in units of ALT/L.

2.5. Assessment of Liver Damage by Measurement of Plasma Aspartate Aminotransferase Levels

Measurement of circulating levels of aspartate aminotransferase (AST) is frequently used for the diagnosis of liver disease and hepatic damage as a result of toxicity. AST is normally compartmentalised within the tissue and so circulating levels in healthy individuals are typically low (<70U/L). When injury to hepatic tissue occurs AST is released, resulting in an increase in blood levels of the enzyme.

The AST Assay (AE1-36, Alfa Wassermann) was used for determination of AST levels. The assay utilises the ability of AST to convert α -oxoglutarate and L-aspartate to L-malate and NAD^+ (in the presence of an enzyme/coenzyme mix) (as indicated in Figure 2.4). The rate of reaction is monitored photometrically at 340nm, the rate of NADH oxidation being directly related to the level of AST activity within the plasma sample.

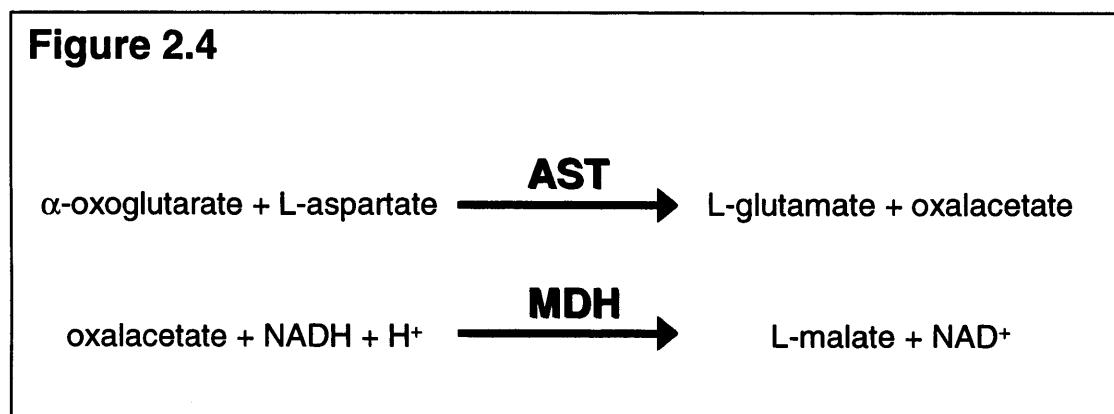


Figure 2.4: AST Assay Principle. AST catalyses the first reaction and the oxalacetate generated is utilised by malate dehydrogenase (MDH) in the oxidation of NADH to NAD^+ , which absorbs light at 340nm.

2.5.1. Running the AST Assay

The AST Assay Working Reagent was prepared 10 minutes before use by reconstituting one vial of kit component R2 (lyophilised substrate containing the following when formulated; 0.18mmol/L NADH, 12mmol/L α -oxoglutarate, 600U/L malate dehydrogenase) with one vial of kit component R1 (assay buffer; 80mmol/L tris-buffer, pH7.5 and 240mmol/L L-aspartate). After dissolution the Working Reagent was loaded onto the reagent store within the SpACE[®] Autoanalyser.

Frozen plasma-EDTA samples taken from treated mice (supplied by Dr T Gant, MRC Toxicology Unit, Leicester University) were thawed and diluted in an appropriate volume of distilled water. Two-hundred microlitres of each diluted plasma sample was transferred to an autanalyser cup and loaded onto SpACE[®] Autoanalyser segment. The segments were loaded onto the SpACE[®] autoanalyser and AST Assay run. During the assay the SpACE[®] Autoanalyser takes 20 μ L from each sample cup and mixes it with 200 μ L of Working Reagent in a clean cuvette. The rate of reaction was measured at 340nm and the results reported by the autoanalyser in units of AST/L.

2.6. Measurement of Hepatocyte Total Protein Content Using the BCA Protein Assay

Total cellular protein content was used to normalise glutathione-related endpoints (refer to Section 2.7) and activated caspase 3 data (refer to Section 2.8). Total protein levels were determined using the BCA Protein Assay Kit (2161297A, Pierce). All reagents were used as supplied. The BCA Protein Assay Kit use bicinchoninic acid (BCA) for the colourimetric quantification of total protein. The assay couples the ability of proteins to reduce Cu^{+2} to Cu^{+1} in an alkaline buffer (known as the Biuret reaction) and the reactivity of Cu^{+1} with BCA. This results in the production of a purple-coloured water soluble complex that exhibits strong absorbance at 562nm, the level of absorbance being proportional to the amount of protein in the test sample. The concentration of protein within the test sample is derived by reference to a bovine serum albumin (BSA) standard curve run at the same time.

2.6.1. Sample and Standard Curve Preparation

Sample preparation was as detailed in Sections 2.7.1.1, 2.7.2.2 and 2.8.1. The standard curve was prepared by diluting the 2mg/mL BSA Standard to the following concentrations; 2,000, 1,000, 500, 250, 125, 62.5, 31.25, 16.13, 7.81 and 0 μ g/mL. The buffer used to prepare the test samples was used as diluent (i.e. 100mM sodium hydroxide (NaOH) or Caspase 3 Assay Lysis Buffer) to control for reagent effects on the assay.

2.6.2. Running the BCA Protein Assay

Working Reagent (WR) was prepared by mixing 50 parts BCA Reagent A with 1 part BCA reagent B. Standards and test samples were added in duplicate (25 μ L/well) to a 96 well flat bottomed (black-sided) microtitre plate (6005182, Packard), along with 200 μ L of WR. The plate was mixed thoroughly on an orbital plate shaker for 30 seconds and then incubated at 37°C for 30 minutes. The plate was cooled to room temperature and the absorbance measured at 562nm using a SpectroMax 190 Plate Reader (Molecular Devices). A typical BSA standard curve is shown (Figure 2.5).

Figure 2.5

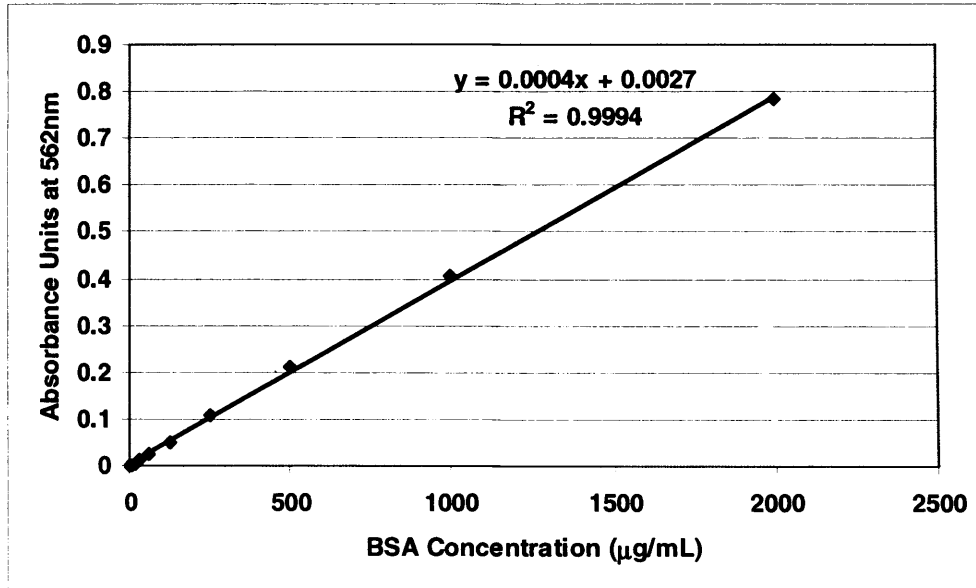


Figure 2.5: Typical BSA standard curve for the BCA Protein Assay

2.7. Measurement of Glutathione-Related Endpoints

Two alternative assays were used for measuring glutathione status within hepatocytes and liver tissue. The *O*-Phthaldialdehyde (OPT) method (outlined in section 2.7.1) was used for measuring reduced glutathione (GSH) levels during the hepatocyte dose ranging studies reported in Chapter 3. The Bioxytech GSH/GSSG-412 Assay was used for measuring both GSH and oxidised glutathione (GSSG) levels in hepatocytes and liver tissue. This method was used for the hepatocyte culture experiments reported in Chapters 4, 5 and 6, and the *in vivo* experiments reported in Chapter 7.

2.7.1. Measurement of GSH Using the O-phthaldehyde Method

The OPT method is a widely used system for assaying total cellular GSH levels. OPT becomes highly fluorescent when conjugated to GSH. The assay works on the principle that the degree of fluorescence due to OPT is proportional to the glutathione content in the sample.

2.7.1.1. Sample Preparation

At an appropriate time point, media was removed from each well of a 12 well BioCoat plate and the cells washed with 0.5mL sterile D-PBS. Two-hundred and fifty microlitres of chilled 6.5% w/v trichloroacetic acid (TCA) (304904T, BDH) was added and the plates incubated at 2-8°C for 30 minutes on an orbital shaker. The TCA lysate was transferred to a 1.5mL Eppendorf tube and centrifuged at 14,000 x *g* for 3 minutes to removed cellular debris. The supernatant was removed and stored at -70°C until required for determination of GSH levels. Following removal of the TCA sample, total cellular protein was isolated by dissolving the hepatocytes with 100µL of 1M sodium hydroxide (NaOH) (Sigma) overnight at 2-8°C. The following day, 1M NaOH extracts were diluted with 900µL of distilled water and used for determination of total cellular protein levels (outlined in Section 2.6).

2.7.1.2. Running the OPT GSH Assay

GSH levels were determined using Cobra Fara Centrifugal Autoanalyser (Roche Diagnostics). TCA extracts were thawed and 150µL samples were run with a 10µg/mL solution of OPT (P0657, Sigma) in 6.5% w/v TCA. Results were expressed as nmol/mL of GSH against a standard curve ranging from 0-32.54nmol/mL of GSH (G6013, Sigma).

GSH values were expressed against total cellular protein content (measured according to the method outlined in Section 2.6) as nmol GSH/mg total protein.

2.7.2. Measurement of GSH and GSSG Using the Bioxytech GSH/GSSG-412 Assay

The Bioxytech GSH/GSSG-412 Assay (371757, Calbiochem) was used for determination of GSH and GSSG levels. All reagents were used as supplied. GSH provides reducing equivalents for the glutathione peroxidase (*GPx*) catalysed reduction of H_2O_2 and lipid hydroperoxides to water and the respective alcohol. During this process GSH becomes oxidised to GSSG. The GSSG is recycled into GSH by glutathione reductase (*GR*) and NADPH. These two reactions are termed the 'glutathione redox cycle' (Figure 2.6). When cells are exposed to increased oxidative stress, the ratio of GSH/GSSG will decrease as a consequence of GSSG accumulation. The measurement of the GSSG level and/or the determination of the GSH/GSSG ratio is a useful indicator of oxidative stress.

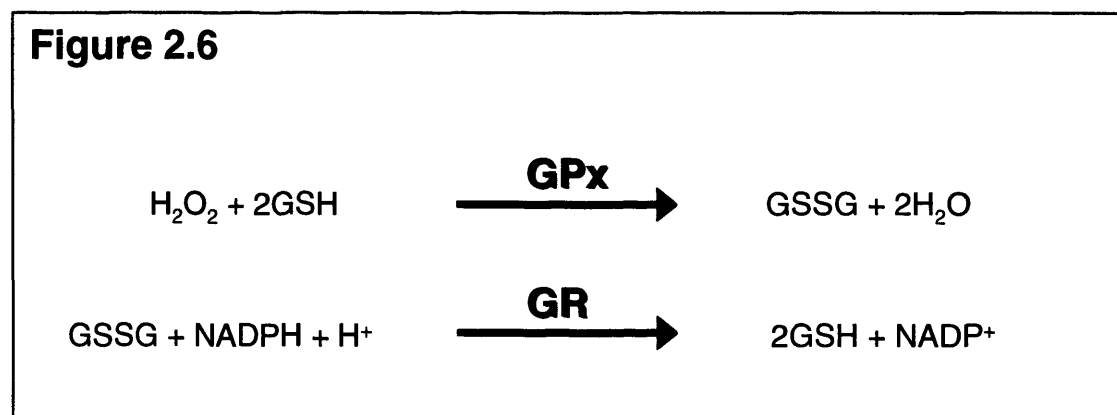


Figure 2.6: The GSH Redox Cycle. The first reaction shows the oxidation of GSH, in the presence of hydrogen peroxide (H_2O_2), catalysed by *GPx*. The second reaction shows the reduction of GSSG, in the presence of NADPH, catalysed by *GR*.

GSH reacts with the chromogen 5,5'-dithiobis-(2-nitrobenzoic acid) (DTNB) to form a product detectable at 412nm. By monitoring the rate at which the product is formed, the concentration of glutathione within a sample can be determined (with reference to standards). Total glutathione levels (GSH_t), which account for GSH and GSSG content within samples, is measured first. GSSG only levels are measured by scavenging GSH within a sample with 1-methyl-2-vinylpyridinium trifluoromethanesulphonate (M2VP). GSSG levels can then be measured by the reduction of GSSG to GSH, which is then determined by the reaction with DTNB. The rates of change in absorbance are proportional

to the GSH and GSSG concentrations. To determine the level of GSH with a sample, the GSSG value (in GSH equivalents) is subtracted from the GSH_t value.

2.7.2.1. Sample Preparation – Hepatocyte Monolayers

At an appropriate time point, media was removed from each well of a 12 well BioCoat plate and the hepatocytes washed with 0.5mL sterile D-PBS. Two-hundred and fifty microlitres of 5% w/v chilled meta-phosphoric acid (MPA) (M6288, Sigma) was added and the plates incubated at 2-8°C for 30 minutes on an orbital shaker. Supernatants were placed on ice and then stored at -80°C until required for determination of GSH/GSSG levels. Following removal of the MPA sample, total cellular protein was isolated by dissolving the hepatocytes with 100µL of 1M sodium hydroxide (NaOH) (30620, Sigma) overnight at 2-8°C. The following day, 1M NaOH extracts were diluted with 900µL of distilled water and used for determination of total cellular protein levels (outlined in Section 2.6).

MPA lysates were thawed and a total GSH_t sample was prepared by diluting 10µL of MPA lysate 1/10 to 1/40 with GSH Assay Buffer. A GSSG sample was prepared by incubating 50µL of MPA lysate with 10µL Assay Scavenger Solution at 4°C for 30 minutes prior to diluting 1/3 to 1/10 in GSSG Assay Buffer.

2.7.2.2. Sample Preparation – Liver

Liver tissue was homogenised in 10-20µL chilled 5% w/v MPA per mg of wet tissue and centrifuged at 14,000 x g to remove any precipitate. Supernatants were placed on ice and then stored at -80°C until required for determination of GSH/GSSG levels. A total GSH_t sample was prepared by diluting 10µL of MPA lysate 1/10 to 1/40 with GSH Assay Buffer. A GSSG sample was prepared by incubating 50µL of MPA lysate with 10µL Assay Scavenger Solution at 4°C for 30 minutes prior to diluting 1/3 to 1/10 in GSSG Assay Buffer.

2.7.2.3. Running the GSH/GSSG-412 Assay

All reagents provided within the GSH/GSSG-412 Assay kit were used as supplied. One-hundred and fifty microlitres of each GSH_t or GSSG sample was transferred to an autanalyser cup and loaded onto a SpACE[®] Autoanalyser segment. The segments were loaded onto the SpACE[®] autoanalyser and the GSH or GSSG variant of the assay run.

During the assay the SpACE[®] Autoanalyser takes 50 μ L of MPA sample and mixes it with equal volumes of Chromogen Solution (DNTB), Enzyme Solution (GR) and NADPH Solution. Absorbance was monitored at 408nm for 5 minutes and the rate of reaction (which is proportional to the GSH/GSSG present in the MPA solution) measured. GSH_t and GSSG levels were related to standard curves (as supplied) that were run on the same day of assay (Figure 2.7). To derive the level of GSH within a tissue, two times the GSSG value was subtracted from the respective GSH_t value. Both GSH and GSSG results were expressed in terms of nmol/mg total protein (hepatocyte data) or nmol/mg of wet tissue (liver data).

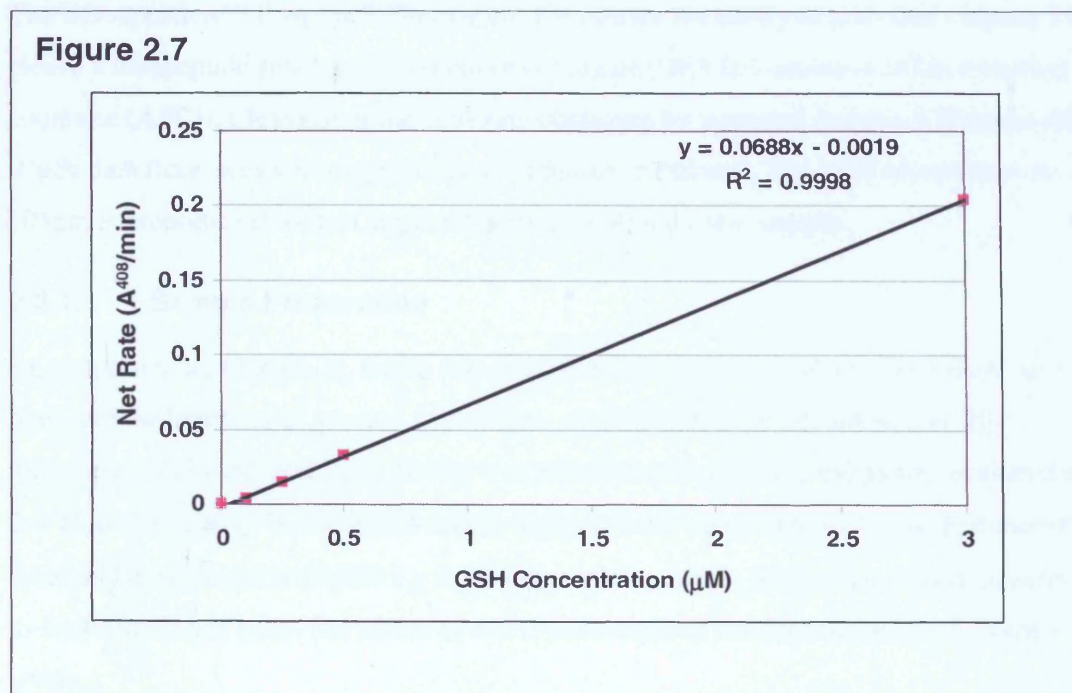


Figure 2.7: Typical GSH/GSSG-412 Assay Standard Curve

2.8. Measurement of Activated Caspase 3 Activity in Hepatocyte Cultures

Activated caspase 3 levels were assessed in rat hepatocytes to indicate overall activation of apoptosis within hepatocyte monolayers. Caspase 3 is an active cell death protease involved in the execution of apoptosis and it is activated in response to a variety of apoptotic stimuli[112]. The BD ApoAlert™ Caspase 3 Fluorescent Kit (630215, BD Biosciences Clontech) was used for the measurement of activated Caspase 3 levels in hepatocyte cultures (all reagents were used as supplied). The BD ApoAlert™ Caspase 3 Fluorescent Kit is suitable for detecting the activity of activated capsase 3 in all mammalian cell types.

The BD ApoAlert™ Caspase 3 Fluorescent Kit utilises the ability of activated caspase 3 to cleave a tetrapeptide substrate-fluorophore conjugate (DEVD-7-amino-4-trifluoromethyl coumarin (AFC)). Cleavage of the substrate conjugate by activated caspase 3 liberates AFC which then fluoresces yellow-green (peak emission at 505nm). The level of emission at 505nm is proportional to the Caspase 3 activity within the test sample.

2.8.1. Sample Preparation

At an appropriate time point, media was removed from each well of a 12 well BioCoat plate and the hepatocytes washed with 0.5mL sterile D-PBS. One-hundred and fifty microlitres of chilled Cell Lysis Buffer was added to each well and the plates incubated at 2-8°C for 10 minutes on an orbital shaker. Lysates were transferred to 1.5mL Eppendorf tubes and centrifuged at 14,000 x g to remove cellular debris. Supernatants were transferred to fresh Eppendorf tubes and stored at -80°C until required for determination of Caspase 3 levels.

2.8.2. Running the Caspase 3 Assay

Hepatocyte lysates were thawed and 50µL transferred into duplicate wells of a 96 well flat bottomed (black-sided) microtitre plate (6005182, Packard). Fifty microliters of 2 x Reaction Buffer and 5µL of the DEVD-AFC substrate (50µM final concentration) were added. The plate was incubated at 37° for 1 hour in a humidified incubator. Fluorescence was measured by reading the plate with a Spectramax 210 Fluorescence Microtitre Plate Reader (Molecular Devices) (400nm excitation filter; 505nm emission filter). Activated

caspace 3 levels were expressed as fluorescence units/mg total protein (total protein levels were measured in the same lysate samples according to the method outlined in Section 2.6).

2.9. Determination of DMNQ and MNQ Levels by HPLC

In order to investigate the toxicokinetics, tissue distribution and elimination of DMNQ and MNQ in mice, a high-performance liquid chromatography (HPLC)-based assay was developed (optimisation of the assay is detailed in Chapter 7). Tissues and plasma from DMNQ and MNQ treated mice were supplied by Dr T Gant, MRC Toxicology Unit, University of Leicester.

2.9.1. Sample preparation

Frozen tissue was weighed (approximately 100-200mg) using an analytical balance, the weight recorded and transferred to a 2mL Eppendorf tube. Tissues were homogenized in two times volume of HPLC grade water (W/0106/PB17, Fisher Scientific) at room temperature using an Ultra-Turrax T10 homogeniser (IKA). Plasma samples and tissue homogenates were mixed with two times volume of acetonitrile (H049, Romil) for 30 minutes at room temperature and centrifuged at 14,000 x g to remove any precipitate. The supernatant was removed, transferred to a fresh 2mL Eppendorf tube and dried by spinning in a SpeedVac Dryer (Eppendorf) on the medium heat setting. Dried tissue/plasma extracts were stored at -80°C until required.

2.9.2. Running the HPLC Assay

Dried tissue or plasma extracts were dissolved in 50µL of 50% v/v methanol (Assay Buffer) (prepared from HPLC grade water and HPLC grade methanol (M/4056/PB17, Fisher Scientific) per 100mg or 100µL of original starting tissue/plasma. The methanol solutions were centrifuged briefly and the supernatant loaded into Total Recovery HPLC vials (186000327c, Waters) for analysis. HPLC was performed on a 150 x 2.1mm C18 3.5µm column (WAT106005, Waters) using a 2695 HPLC Analyser with a 2487 Dual Wavelength Detector attached (Waters). Buffer A was HPLC grade water and Buffer B was HPLC grade methanol. The flow rate was set at 0.15mL/min, the column temperature was maintained at 30°C and the sample temperature was 10°C. The initial conditions were 60% Buffer A and 40% Buffer B. A gradient was run over 15 minutes to a final mix of 10% Buffer A and 90% Buffer B. This was held for 5 minutes before re-equilibrating the column

at 40% Buffer A and 60% Buffer B. The total run time was 35 minutes and the injection volume was 10 μ L. DMNQ and MNQ were monitored at 276nm and the amount of DMNQ or MNQ in each sample was determined by calibration of the system with standards of known concentration (refer to Figures 7.1C and 7.2C for example calibration curves). DMNQ and MNQ exposure data was expressed in terms of μ g/g of wet tissue (liver, kidney or brain data) or μ g/mL (plasma data).

2.10. Total RNA Extraction

Total RNA extraction from rat hepatocyte cultures and mouse liver tissue was carried out using the SV Total RNA Isolation System (Z3105, Promega). Cell or tissue lysates were first prepared (according to the methods outlined in Section 2.10.1 and 2.10.2, respectively), after which the same extraction procedure was followed (Section 2.10.3).

2.10.1. Hepatocyte Lysate Preparation

Culture media was removed and hepatocyte monolayers in 6 well BioCoat plates (BD) were washed with 1mL of sterile D-PBS). The D-PBS was removed and 150 μ L SV Lysis Buffer added to each well. Once lysis was complete, the bottom of each well wash scraped with a sterile tissue culture scraper and the contents collected to one side. The lysates were aspirated and replicate wells pooled into RNase/DNase free 1.5mL Eppendorf tubes. Genomic DNA was sheared by passing the lysates through a 19-gauge blunt-ended needle (300149, BD) four times and placed on ice. Lysates were stored at -80°C until required for total RNA extraction.

2.10.2. Liver Tissue Homogenate Preparation

Fifty to one-hundred milligrams of liver tissue was added to 700 μ L of SV Lysis Buffer in a Matrix-D Lysis Tube (Q-Biogene) and homogenised using a Ribolyser (Hybaid) for 20 seconds on speed setting 6. The homogenates were placed on ice to allow the froth to settle. Three-hundred and fifty microlitres of each homogenate was transferred to RNase/DNase free 1.5mL Eppendorf tubes and genomic DNA sheared by passing through a 19-gauge blunt-ended needle four times. Homogenates were placed on ice prior to being stored at -80°C until required for total RNA extraction.

2.10.3. Total RNA Extraction Using the SV Columns

Hepatocyte lysates or liver homogenates were thawed and 350 μ L transferred to a fresh RNase/DNase free 1.5mL Eppendorf. Seven-hundred microlitres of SV Dilution Buffer was added, mixed by inversion, and the mixture incubated at 70°C for 3 minutes. Following centrifugation at 12,000 x g for 10 minutes, the supernatant was transferred to a fresh RNase/DNase free 1.5mL Eppendorf containing 400 μ L of 95% v/v ethanol (E7023, Sigma). This mixture was loaded onto two SV RNA Isolation Tube Assemblies which were centrifuged at 14,000 x g for 1 minute. Liquid in the collection tubes was discarded, 600 μ L

of SV RNA Wash Solution applied to each column and the SV RNA Isolation Tube Assemblies centrifuged at 14,000 x g for 1 minute. The collection tubes were emptied and 50µL of SV DNase Incubation Mix (prepared from 50µL of SV Yellow Core Buffer, 5µL of SV 0.09M MgCl₂ and 5µL of SV DNase I enzyme) applied to the surface of each column membrane. SV RNA Isolation Tube Assemblies were incubated at room temperature for 15 minutes to allow DNA digestion to proceed, after which 200µL of SV DNase Stop Solution was added to each column. SV RNA Isolation Tube Assemblies were centrifuged at 14,000 x g for 1 minute, 600µL of SV RNA Wash Solution applied to each column and then centrifuged again at 14,000 x g for 1 minute. Liquid in the collection tubes was discarded and a final wash carried out by applying 300µL of SV RNA Wash Solution to each column and centrifuging the SV RNA Isolation Tube Assemblies at 14,000 x g for 2 minutes (to eliminate ethanol carry-over).

The column within each SV RNA Isolation Tube Assembly was transferred to a fresh 1.5mL RNase/DNase free Eppendorf tube and 100µL of SV Nuclease Free Water applied to the membrane. Columns were incubated at room temperature for 1 minutes and the total RNA eluted by centrifuging the column/tube assemblies at 14,000 x g for 1 minute. The columns were discarded and eluted total RNA from replicate columns pooled prior to storage at -80°C until required.

2.11. Total RNA Quantification and Quality Control

The concentration, yield and purity of each total RNA sample was determined using ultraviolet (UV) spectrophotometry. The integrity of each total RNA sample was determined by agarose gel electrophoresis.

2.11.1. Quantification Using UV Spectrophotometry

Either the Spectramax 190 UV Microtitre Plate Reader (Molecular Devices) or NanoDrop ND-1000 UV (NanoDrop Technologies) spectrophotometers were used for measuring UV absorbance of total RNA samples. The absorbance of each total RNA sample (at an appropriate dilution in Molecular Grade Water (2900136, 5Prime) at 260nm (peak nucleic acid absorbance) and 280nm (peak protein absorbance) was measured and the A_{260}/A_{280} ratio determined to indicate the level of protein contamination. Total RNA samples with a A_{260}/A_{280} ratio of 1.8 to 2.1 were considered of acceptable quality. The total RNA concentration was derived using the following formula:

- RNA concentration in $\mu\text{g}/\mu\text{L} = ((A_{260} \times 40^*) \times \text{dilution factor})/1000$

*Where 40 = the RNA extinction coefficient

2.11.2. Agarose Gel Electrophoresis

A 1% w/v agarose gel was prepared by melting 1g of Molecular Biology Grade Agarose (A4718, Sigma) in 100mL of 1 x Tris-borate EDTA (TBE) buffer (45mM tris-borate, 2mM EDTA) (T4415, Sigma). The melted gel was allowed to cool to approximately 60°C before adding 5 μL of 10mg/mL Ethidium Bromide Solution (E1514, Sigma) (final concentration of 0.5 $\mu\text{g}/\text{mL}$). The gel was mixed gently by swirling, poured onto a gel tray (containing two gel combs) and allowed to set for 30 minutes at room temperature. The set gel was transferred to an electrophoresis tank (Life Technologies) and submerged in 1 x TBE buffer.

Total RNA samples were prepared by mixing 5 μL of each total RNA sample with 1 μL of 6 x Gel Loading Buffer (G2526, Sigma) and placed on wet ice until required. Samples were loaded into wells within the gel and electrophoresis carried out for 30-45 minutes at 100 volts. To visualise total RNA staining, the gel was visualised using the GeneGenius Bioimager gel documentation system (Syngene) and the presence of intact discrete 18S and

28S ribosomal RNA (rRNA) bands indicated that the total RNA was of acceptable quality. If the rRNA bands were not present, or appeared degraded, the total RNA was discarded and a fresh isolation carried out.

2.12. Transcriptional Profiling Using Affymetrix GeneChip® Microarrays

All transcriptional investigations were carried out according to the GeneChip® Expression Analysis Technical Manual

(http://www.affymetrix.com/support/technical/manual/expression_manual.affx). The principles of the methodology are reviewed in Chapter 1 (Section 1.4.2.1).

2.12.1. Preparation and Quality Control of cRNA Targets for Hybridisation to GeneChips®

2.12.1.1. Preparation Double-Stranded cDNA

Double-stranded cDNA (ds cDNA) was prepared from total RNA using the One-Cycle cDNA Synthesis Kit (900431, Affymetrix). All reagents were used as supplied. All incubation steps were carried out using a DNA Engine Tetrad PCR Machine (MJ Research).

The following were added to a 0.75mL RNase/DNase free Eppendorf tube:

- 2µL of T7-(dT)24 primer (100pmol/µL), 1-5µg of total RNA in 9µL of Nuclease Free Water.

The tubes were centrifuged briefly to bring the contents to the bottom and incubated at 70°C for 10 minutes to allow total RNA denaturation and primer hybridisation. The tubes were cooled to 4°C and the following added to each reaction:

- 4µL of 5 x First Strand cDNA Buffer, 2µL 0.1M DTT, 1µL 10mM dNTP mix and 2µL Superscript II RT (200U/µL) (making a total reaction volume of 20µL)

The tubes were centrifuged briefly to bring the contents to the bottom and incubated at 42°C for 1 hour (to allow first strand synthesis to proceed). The tubes were cooled to 4°C and the following added to each reaction:

- 91µL of nuclease free water, 30µL of 5 x Second Strand cDNA Buffer, 3µL 10mM dNTP mix, 1µL of *E. coli* DNA ligase (10U/µL), 4µL of *E. coli* DNA polymerase (10U/µL) and 1µL of *E. coli* RNase H (2U/µL) (making a total reaction volume of 150µL)

The tubes were centrifuged briefly to bring the contents to the bottom and incubated at 16°C for 2 hours (to allow second strand synthesis to proceed). Two microlitres of T4 DNA

polymerase was added to each reaction, the tubes centrifuged briefly to bring the contents to the bottom and incubated at 16°C for 15 minutes. To stop the reaction, 10µL 0.5M EDTA (03690, Fluka) was added to each tube and the contents mixed well. The ds cDNA was either stored at -20°C until required, or cleaned-up according to the method outlined in Section 2.12.1.2.

2.12.1.2. ds cDNA Cleanup

ds cDNA was cleaned-up using the ds cDNA Cleanup Kit (900547, Affymetrix). All reagents were used as supplied.

Six-hundred microlitres of Binding Buffer was added to each ds cDNA sample, mixed thoroughly and applied to a ds cDNA Spin Column Assembly. The Assemblies were centrifuged at 14,000 x g for 1 minute and the flow through discarded. The columns were transferred to a fresh 2mL collection tube, 750µL of cDNA Wash Buffer added and the tube assemblies centrifuged at 14,000 x g for 1 minute. The flow through was discarded and the tube assemblies centrifuged at 14,000 x g for 5 minutes with the caps open (to completely dry the columns). The columns were transferred to a 1.5mL Collection Tube and 25µL of cDNA Elution Buffer applied to the membrane. The columns were centrifuged at 14,000 x g for 1 minute and the purified ds cDNA stored at -20°C until required for the *in vitro* transcription (IVT) reaction (outlined in section 2.12.13).

2.12.1.3. IVT Reaction

Biotinylated complementary RNA (cRNA) targets were generated from ds cDNA (prepared as outlined in Section 2.12.1.2) using the IVT Labelling Kit (900449, Affymetrix). All reagents were used as supplied. All incubation steps were carried out using a DNA Engine Tetrad PCR Machine (MJ Research).

The following were added to a 0.75mL RNase/DNase free Eppendorf tube:

- 20µL of ds cDNA sample, 4µL of 10 x IVT Labelling Buffer, 12µL of IVT Labelling NTP Mix and 4µL of IVT Labelling Enzyme Mix (making a total reaction volume of 40µL)

The tubes were centrifuged briefly to bring the contents to the bottom and incubated at 37°C for 16 hours to allow IVT to proceed. The cRNA was either stored at -20°C until required, or cleaned-up according to the method outlined in Section 2.12.1.4.

2.12.1.4. cRNA Cleanup

Biotinylated-cRNA was cleaned-up using the cRNA Cleanup Kit (900547, Affymetrix). All reagents were used as supplied.

To each cRNA sample, 55 μ L of Nuclease Free Water and 5 μ L of 3M Sodium Acetate (71196, Fluka) was added, making a total volume of 100 μ L. 350 μ L of cRNA Binding Buffer and 250 μ L 100% ethanol was added to each cRNA sample, mixed thoroughly and applied to a cRNA Spin Column Assembly. The Assemblies were centrifuged at 14,000 x g for 15 seconds. The flow through was reapplied to the columns and Assemblies centrifuged again at 14,000 x g for 15 seconds. The columns were transferred to a fresh 2mL collection tube, 500 μ L of cRNA Wash Buffer added and the tube assemblies centrifuged at 14,000 x g for 15 seconds and the flow through discarded. This step was repeated, followed by a final centrifugation at 14,000 x g for 1 minute with the caps open (to eliminate ethanol carry-over). The columns were transferred to a 1.5mL Collection Tube and 50 μ L of Nuclease Free Water applied to the membrane. The columns were incubated at room temperature for 1 minute and centrifuged at 14,000 x g for 1 minute to elute the cRNA. The purified cRNA was stored at -20°C until required for the quantification and fragmentation (outlined in section 2.12.1.5).

2.12.1.5. Quantification of IVT Products and Fragmentation

UV spectrophotometry (as outlined in Section 2.11.1) was used to determine the cRNA concentration and yield. For cRNA samples where sufficient yield and concentration had been achieved, fragmentation was carried out using the Fragmentation Buffer as supplied with the cRNA Cleanup Kit.

An appropriate dilution of each cRNA sample in Nuclease Free Water was prepared. The absorbance at A²⁶⁰ and A²⁸⁰ was measured and the adjusted cRNA yield calculated using the following formula:

$$\text{Adjusted cRNA yield } (\mu\text{g}) = A - (B \times C)$$

Where:

A = Total yield of cRNA according to A²⁶⁰ result (μg).

B = Starting amount of total RNA used in cDNA reaction (μg).

C = Fraction of cDNA used in IVT reaction.

For example: Start with 5 μg of total RNA, use 80% (or 4 μg) in the IVT, and the cRNA yield is 45 μg . The calculation would therefore be:

$$45 - (5 \times 0.8) = 41\mu\text{g}$$

To determine the adjusted concentration, the adjusted yield (in μg) is divided by the total volume (μL). As a guide, the minimum acceptable adjusted cRNA yield should be 4 μg per 1 μg of total RNA used for cDNA synthesis. Based on a 3% mRNA representation in total RNA, this equates to approximately a 133-fold amplification.

A volume of each cRNA sample containing 15 μg (based on the adjusted concentration) was transferred to a 0.75mL RNase/DNase free Eppendorf tube. 0.25 μL of Fragmentation Buffer was added for each 1 μL of cRNA and the tube incubated at 94°C for 35 minutes and then cooled to 4°C for 5 minutes using a DNA Engine Tetrad PCR machine. Fragmented cRNA samples were stored at -20°C until required.

2.12.1.6. Confirmation of cRNA Fragmentation

To determine whether cRNA fragmentation was successful, the size of cRNA and fragmented cRNA samples were assessed using the RNA 6000 Nano Labchip Kit (5067-1511, Agilent). Each RNA 6000 Nano Labchip contains an interconnected set of microchannels that are primed with a gel matrix. The gel matrix can then be used to separate RNA fragments within a sample based on size as they are electrophoretically driven through the microchannels. The gel matrix contains a Nano Green dye that binds to

RNA and fluoresces, the level of fluorescence being proportional to the quantity of RNA present. Electrophoresis and fluorescence detection is carried out on a 2100 Bioanalyzer (Agilent), with up to 12 RNA samples being run on each RNA 6000 Nano Labchip. All reagents were used as supplied by Agilent.

2.12.1.6.1. Gel preparation and RNA 6000 Nano Labchip Priming

RNA 6000 Nano Gel Matrix was prepared by placing 550 μ L into a Spin Filter and centrifuging at 1,500 x *g* for 10 minutes at room temperature. On the day of use, a 65 μ L aliquot of filtered RNA 6000 Nano Gel Matrix was transferred to a RNase free Eppendorf tube and 1 μ L of RNA Nano 6000 Dye Concentrate added (Gel-Dye Matrix). The Gel-Dye Matrix was mixed by vortexing and centrifuged at 13,000 x *g* for 10 minutes at room temperature. A RNA 6000 Nano Labchip was placed on the Priming Station (Agilent) and 9 μ L of Gel-Dye Matrix carefully pipetted into the 'priming well'. The plunger of the Priming Station was positioned at the 1mL graduation and the manifold closed firmly over the Labchip. The plunger was firmly depressed until it was held by the clip and priming allowed to proceed for 30 seconds, after which the clip was released. The plunger allowed to recoil for 5 seconds and then pulled back to the 1ml graduation. The Priming Station was opened, the Labchip removed and 9 μ L of Gel-Dye Matrix carefully pipetted into each of the three 'gel' wells. Labchip priming was completed by adding 5 μ L of RNA 6000 Nano Marker Buffer to wells 1-12 and the 'ladder' well.

2.12.1.6.2. Sample Preparation, Loading and Running the Labchip

Frozen cRNA and fragmented cRNA samples (prepared in Section 2.12.1.4 and 2.12.1.5, respectively) were thawed and diluted 1/10 with Molecular Biology Grade Water. Two microlitres of RNA Nano 6000 Ladder and each diluted cRNA/fragmented cRNA sample was transferred to a 0.75mL RNase free Eppendorf tube and heat denatured at 70°C for 2 minutes. The tubes were immediately chilled on ice and the contents centrifuged to the bottom at 14,000 x *g*. One microlitre of heat denatured sample was added to each sample well; the same volume of heat denatured RNA Nano 6000 Ladder was added to the 'ladder' well. The RNA Nano 6000 Labchip was placed on the Labchip Vortexer (IKA) and vortexed for 1 minute at 2,400 rpm. The Labchip was run on the 2100 Bioanalyzer within 5 minutes.

The lid of the 2100 Bioanalyzer was opened, the loaded Labchip placed into the receptacle and the lid closed carefully. The 'Nano 6000 Assay' protocol was selected within 2100 Expert Software version B.02.02 (Agilent) and electrophoresis commenced by pressing 'Start'. Once the electrophoresis was complete the results file was saved and the size profiles of each cRNA and respective fragmented cRNA sample inspected visually (refer to Figure 2.8 for representative images).

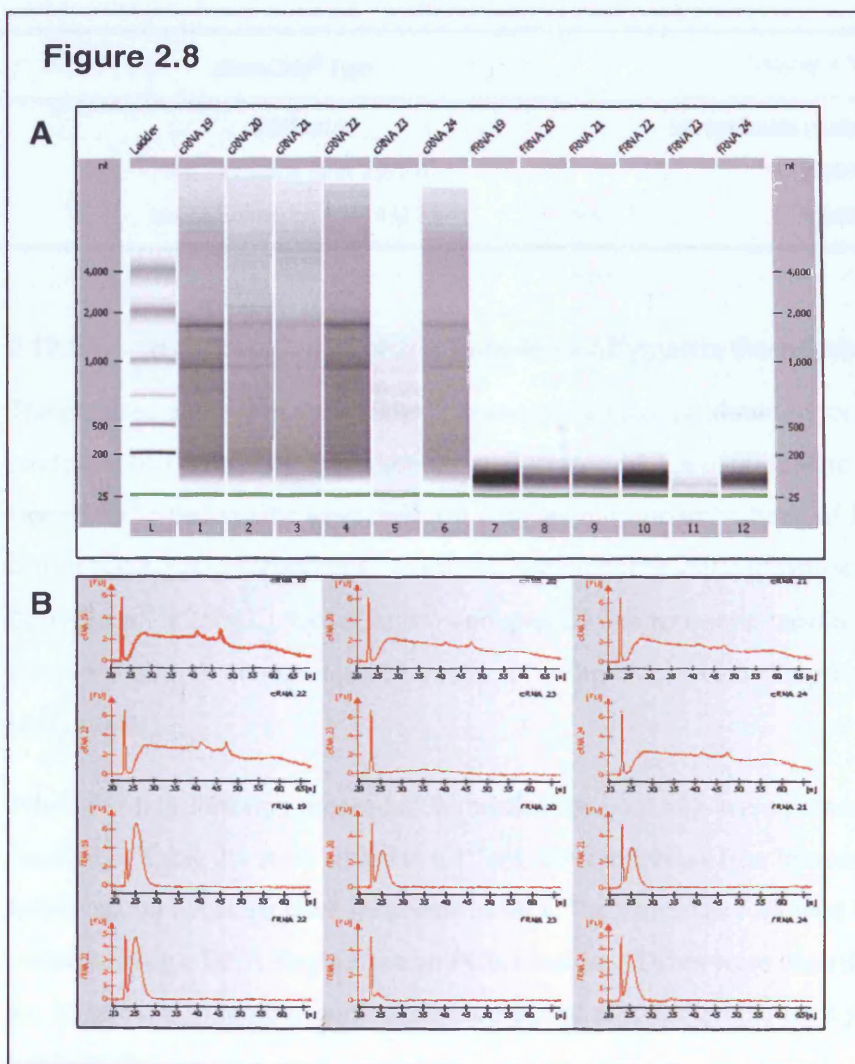


Figure 2.8: Representative RNA 6000 Nano Labchip cRNA Quality Assessment Images. Gel View (A) and Electropherogram View (B) Images.

L = RNA 6000 Nano Marker Ladder. 1-6 = cRNA samples. 7-12 = fragmented cRNA samples.

2.12.2. Hybridisation of cRNA Targets to Affymetrix GeneChips® and Scanning

Fragmented cRNA targets were hybridised to GeneChips using the GeneChip® Hybridisation, Wash and Stain Kit (900720, Affymetrix). All reagents were used as supplied. Supply details of GeneChips® used for transcriptional analysis are included in Table 2.3.

Table 2.3: GeneChip® Supply Details

GeneChip® Type	Catalogue Number
GSKRat1a	Not applicable (custom GeneChip®)
Rat Expression Array 230 2.0	900507
Mouse Expression Array 430 2.0	900497

2.12.2.1. Hybridisation of cRNA Targets to Affymetrix GeneChips®

The required number of GeneChips® were allowed to equilibrate to room temperature for a minimum of 1 hour. The upper septum was vented with a p100 pipette tip and the GeneChip® filled via the lower septum with an appropriate volume of Pre-Hybridisation Buffer (GSKRat1a GeneChips® = 160µL, Rat Genome 230 2.0/Mouse Genome 430 2.0 GeneChips® = 250µL). GeneChips® were placed in a rotisserie rack and incubated at 45°C for a minimum of 10 minutes with rotation (~60rpm) in a GeneChip Incubator (Affymetrix).

While pre-hybridisation proceeded, hybridisation cocktails were prepared. The reagents detailed in Table 2.4 were added to a 1.5mL RNase/DNase free Eppendorf tube. The hybridisation cocktails were incubated at 99°C for 5 minutes followed by 45°C for 5 minutes using a DNA Engine Tetrad PCR machine. Tubes were centrifuged at 14,000 x g for 10 minutes to remove particulates and stored at room temperature just prior to hybridisation.

Table 2.4: Reagents and Volumes for Hybridisation Cocktail Preparation

Reagent	GSKRat 1a GeneChip®	Rat Genome 230 2.0/Mouse Genome 430 2.0 GeneChip®	Final Concentration
Fragmented cRNA	10µg	15µg	0.05µg/µL
Control Oligo B2	3.3µL	5µL	50pM
20 x Hyb Controls	10µL	15µL	1.5, 5, 25 and 100pM spikes
DMSO	20µL	30µL	
2 x Hyb Mix	100µL	150µL	1 x
Nuclease Free Water	Up to 200µL	Up to 300µL	

GeneChips® were removed from the incubator and the Pre-Hybridisation Buffer removed. The upper septum was vented with a p100 pipette tip and the hybridisation cocktail applied to the GeneChip® via the lower septum. For GSKRat 1a GeneChips® a volume of 130µL was used, for Rat Genome 230 2.0/Mouse Genome 430 2.0 GeneChips® a volume of 200µL was used. GeneChips® were placed in a rotisserie rack and incubated at 45°C for 16 hours (or overnight) with rotation (~60rpm) in a GeneChip® Incubator (Affymetrix).

2.12.2.2. Washing and Staining of Affymetrix GeneChips®

GeneChips® were removed from the incubator and the hybridisation cocktail removed and discarded. The upper septum was vented with a p100 pipette tip and the GeneChip® filled via the lower septum with an appropriate volume of Wash Buffer A (GSKRat 1a GeneChips® = 160µL, Rat Genome 230 2.0/Mouse Genome 430 2.0 GeneChips® = 250µL). GeneChips were stored at room temperature until staining and washing was commenced. Prior to commencing staining and washing, the Fluidics Station 450 (Affymetrix) was primed with the appropriate wash buffers (Wash Buffer A = low stringency wash, Wash Buffer B = high stringency wash, used as supplied). Each GeneChip fluidics module was selected within the operating software GeneChip® Operating Software (GCOS) version 1.2 (Affymetrix). Priming was initiated by running the 'PRIME' protocol.

Staining Cocktail 1 (contains Streptavidin-phycoerythrin conjugate (SAPE)), Staining Cocktail 2 (contains biotinylated anti-Streptavidin antibody) and Array Holder Buffer stocks were allowed to come to room temperature. For each GeneChip® to be stained,

600µL of Staining Cocktail 1, 600µL of Staining Cocktail 2 and 800µL of Array Holder Buffer were dispensed into 1.5mL Eppendorf tubes. The Experimental details and barcode for each GeneChip® were entered in Experiment Manager within MAS. To commence staining and washing, Experiment Files were selected from Fluidics Manager within MAS and the appropriate wash protocol run (GSKRat1a GeneChips® = FS450_0004, Rat Genome 230 2.0/Mouse Genome 430 2.0 GeneChips® = FS450_0001). GeneChips® were loaded into cassette holders on the appropriate Fluidics Station 450. The aliquoted staining reagent tubes were placed into the appropriate positions below each cassette holder, as outlined below:

- **Position 1:** Staining Cocktail 1
- **Position 2:** Staining Cocktail 2
- **Position 3:** Array Holding Buffer

The needle lever was pressed down to the 'engaged' position and the staining protocol automatically commenced. When the wash protocol was completed, the LCD window at the top of each fluidics module states 'EJECT CARTRIDGE'. The cassette lever was pressed to the 'down' position to eject the GeneChip® which was removed for scanning. Prior to scanning the GeneChips® were checked for the presence of bubbles. If bubbles were present, GeneChips® were vented, the solution completely removed and replaced with 250µL of Wash Buffer A.

2.12.2.3. Scanning of Affymetrix GeneChips®, Primary Analysis and Quality Assessment

To scan the GeneChips®, Scanner Control within MAS was opened and the 'autoloader' function selected. Stained GeneChips were loaded (up to 30 at a time) onto the autoloader of a GeneChip® Scanner 3000 (Affymetrix) and scanning commenced by clicking 'start scan' within Scanner Control. The GeneChips® were automatically scanned, producing a .dat file (as outlined in Section 1.4.2.1.). Once scanning was completed, the hybridisation image for each GeneChip® was manually inspected for gross defects. GeneChip® .dat files that were of acceptable visual quality were analysed using the 'batch analysis function' within GCOS to generate .chp, .cel and .rpt files (as outlined in Chapter 1, Section 1.4.2.2).

Hybridisation quality was assessed by reviewing the metrics generated within the .rpt file and the quality assessed according to the thresholds defined in Table 1.9.

2.12.3. Downstream Analysis of Transcriptomic Data

To undertake comparison analyses of different treatment conditions the normalised .chp file for GeneChips[®] of acceptable quality (as defined in Table 1.9) were imported into Rosetta Resolver[®] (build versions 5.1 and 6.0 were used during the course of this thesis) (Merck Sharpe Dohme). Rosetta Resolver[®] is an integrated microarray data repository system that enables the storage, annotation and statistical analysis of GeneChip[®] experiments[113]. Upon import of .chp files Rosetta Resolver[®] associates individual probe set intensities with gene annotations. To analyse the data, Rosetta Resolver[®] uses a proprietary error model that is specific to the GeneChip[®] type being analysed[114]. The concept of the error model is to account for experimental error without the need to perform large numbers of replicate experiments. The error model is an empirical intensity-based method for obtaining a conservative estimate of the signal variability within a small replicate data set[114]. To determine the average signal, and whether a particular probe set is significantly expressed above background (absolute analysis), Rosetta Resolver[®] computes the average PM minus MM value for the each probe pair. As part of this analysis the error model is used to define the variability of each probe set intensity[114]. Significance of expression is determined by comparing the average signal of each probe set to the average signal of negative controls within the GeneChip[®]. Probe sets where the error-normalised difference in signal is significantly different are called as present (or significantly expressed).

To undertake comparative analysis between control ('baseline') and treatment ('test'), replicate arrays are defined for any number of groups and the 'RatioBuild' function used. The RatioBuild function automatically performs comparisons between all pairs of baseline and test groups and produces a consensus result for ratio of change (relative to baseline) and significance of change[113]. During the course of this analysis, a global normalisation is applied to all replicate GeneChips[®] and ratio of change computed from the group mean intensity for each probe set. To determine the significance of change, the error of the ratio of change is computed by combining the modelled error of individual probe sets and the variability of the actual replicates signals. With increasing numbers of experimental replicates, the relative contribution that the modelled error makes to the analysis

decreases[114]. The analysed data can then be exported by using the 'TrendSet' function within Rosetta Resolver[®]. The user defines all comparisons within the data set and selects thresholds for ratio of change and significance (P-value). An arbitrary threshold can also be set for the number of comparisons in which the ratio of change and significance thresholds must be met. This data can then be exported to Excel or as tab-delimited files for downstream data analysis.

The complexity of the data generated by microarray experiments necessitates the use of bioinformatics tools to aid interpretation and help confer biological meaning. To this end, transcriptional data exported from Rosetta Resolver[®] were analysed using cluster analysis and biological theme analysis tools. Cluster analysis is a collective term for a number of methods that group objects (gene change profiles in this case) that behave similarly into respective categories. Thus, cluster analysis enables the user to identify structure within the data. Although a number of alternative methods are available (e.g. hierarchical, self organising maps and expectation maximisation), *k*-means clustering was used to analyse transcriptional data within this thesis.

k-means clustering groups objects into a user-defined number of clusters (the *k*-value). This process starts with objects randomly distributed into *k* clusters. The software then starts to move objects between the different clusters with two main aims: 1) minimise the variability within a given cluster, 2) maximise variability between each cluster. ArrayMiner version 5.3.2 (Optimal Design) was used for *k*-means cluster analysis. Once the analysis is fully optimised the mean profiles for each cluster can be examined within ArrayMiner.

ArrayMiner reports a 'percent fit' value for each gene that gives an indication of the goodness of fit of a particular gene within a cluster. This value can be used to gauge the successfulness of the analysis. If a large proportion of genes have low percent fit values the analysis should be repeated with the *k*-value adjusted upwards. This is an iterative process that allows the data set to be segregated into an optimum number of clusters.

To help confer biological meaning upon the clustered genes, biological theme analysis was carried out. This provides a high level overview of the functional classes of genes and pathways significantly overrepresented within a data set. Two alternative methods, Expression Analysis Systematic Explorer (EASE) and Ingenuity Pathway Analysis (IPA), were used. EASE identifies terms/phrases that describe a statistically significant number of

genes in the query list that are overrepresented when compared to the entire gene population (i.e. the GSKrat1a gene set). The output is based upon gene ontology terms (GO terms) recognised by the Gene Ontology Consortium (<http://geneontology.org>). To determine the significance of the gene categories identified as being overrepresented within the data set EASE applies a modification of the Fisher exact test. This yields an 'EASE probability score' that weights significance in favour of GO terms supported by more genes[115].

Unlike EASE which is freely available within the public domain, IPA (Ingenuity Inc.) is a proprietary analysis system that must be subscribed to. IPA segregates groups of genes within the query set into networks defined by known interactions amassed from the literature[116]. In addition, biological themes are conferred to the networks by again utilising a modified version of the Fisher exact. Rather than using GO terms, IPA uses proprietary 'function terms' to assign overrepresented gene categories within the gene list. IPA also has the added advantage of being able to identify canonical pathways that are significantly regulated within the data[117].

2.13. SybrMan[®] Real-Time Quantitative PCR

Real-time quantitative PCR (RT-QPCR) is routinely used for measuring the expression levels of small numbers of specific transcripts. It is also frequently utilised for the confirmation of genes identified as being differentially expressed by microarray analysis. In this regard it has the advantages of increased sensitivity versus the different microarray platforms and is relatively low cost.

A number of alternative methodologies are available, SybrMan[®] (Applied Biosystems) RT-QPCR being one of them. All RT-QPCR platforms enable the real-time measurement of PCR amplification of a specific target sequence, or 'amplicon'. This enables the quantification of amplicon generation during the exponential phase of amplification. In the case of SybrMan[®] RT-QPCR, this is monitored by the incorporation of a fluorescent dye (SybrGreen[®]) as double-stranded PCR product is generated. The system allows the time at which the level of fluorescence (from a particular reaction) passes a threshold (known as the cycle threshold, or C_t) to be determined. The higher the copy number of a target sequence within a reaction, the faster the fluorescence passes the set threshold. By comparing the C_t values for different reactions, it is possible to determine the relative level of the target sequence that was in the sample. It is possible to determine the copy number of the target transcript in a test sample by reading its C_t value against a standard curve generated under the same PCR conditions. Species-specific genomic DNA (gDNA) standard curves are frequently used as they will always contain the intended target sequence.

2.13.1. Primer Design and Testing

Transcript-specific primers were designed using Primer Express version 2.0 (Applied Biosystems). Transcript sequences, obtained from the Ensembl Genome Browser database (<http://www.ensembl.org/index.html>), from individual exons were imported into Primer Express and assays designed using default rules. Primers had melting temperatures (T_m) of 58-60°C. Prior to running any test samples, the efficiency and specificity of the primer pairs for each gene were tested using rat gDNA. Using the dissociation curve analysis, the appearance of a single amplified peak was confirmed.

2.13.2. First Strand cDNA Synthesis

Prior to RT-QCPR, total RNA samples were first reverse transcribed to first strand complementary DNA (cDNA). cDNA was generated from 1-5µg of total RNA using the Superscript Synthesis for First Strand cDNA Kit according (12371-019, Invitrogen). All reagents were used as supplied. Reverse transcription was carried out in the presence (reverse transcriptase (RT) plus reaction) and absence (RT minus reaction) of Superscript II reverse transcriptase. The following were added to an RNase/DNase free Eppendorf tube:

- 1-5µg total RNA, 2µL Random Hexamers (50ng/µL), up to 11µL with Nuclease Free Water

The mixture was heated to 70°C for 10 minutes to linearise the RNA using a DNA Engine Tetrad PCR Machine (MJ Research). Samples were placed on ice for 1 minute and then centrifuged to collect contents at the bottom of the tube. The following was then added to each reaction:

- 2µL 10x RT Buffer, 2µL 25 mM MgCl₂, 2µL 0.1M DTT, 1µL 10mM dNTP mix, 1µL RNaseOUT Inhibitor, 1µL SuperScript II RT.

The samples were centrifuged to collect contents at the bottom of the tube, placed on the DNA Engine Tetrad PCR machine and incubated at 25°C for 15 minutes, 42°C for 50 minutes and 70°C for 15 minutes. Samples were briefly placed on ice, 1µL of RNase H added (total volume/reaction = 21µL), centrifuged to bring the contents to the bottom of the tube and incubated for 20 min at 37°C on the Engine Tetrad PCR machine. Following synthesis, the cDNA was made up with Nuclease Free Water (to give a final cDNA concentration of 10ng/µL) and stored at -20°C until required.

2.13.3. Running SybrMan® RT-QPCR

The PCR primer pairs for each assay were diluted to 1µM in Molecular Grade water and dispensed into 0.75mL Screen Mate (4273, Matrix Corporation) tubes housed within a Latch Rack (Matrix Corporation) master plate (according to the configuration outlined in Figure 2.9). The master plate was used to produce replicate plates by dispensing 5µL of each 1µM primer pair into 96-well optically clear microtitre plates (4306737, Applied Biosystems) with a Plate Mate Plus™ (Matrix Corporation). These pre-dispensed plates were referred to as 'Arrayed SybrMan Plates'.

Figure 2.9

	1	2	3	4	5	6	7	8	9	10	11
A	<i>MafK</i>	<i>MafB</i>	<i>Jun</i>	<i>Fos</i>	<i>Okl38</i>	<i>Pim3</i>	<i>Cebpd</i>	<i>Cebpa</i>	<i>Egr1</i>	<i>Atf3</i>	<i>Mat2a</i>
B	<i>Cyp 1a1</i>	<i>Hmox1</i>	<i>iNos</i>	<i>Ddit4</i>	<i>Myd116</i>	<i>Ddit3</i>	<i>Ba</i>	<i>Gapdh</i>	<i>18S</i>		
C	<i>MafK</i>	<i>MafB</i>	<i>Jun</i>	<i>Fos</i>	<i>Okl38</i>	<i>Pim3</i>	<i>Cebpd</i>	<i>Cebpa</i>	<i>Egr1</i>	<i>Atf3</i>	<i>Mat2a</i>
D	<i>Cyp 1a1</i>	<i>Hmox1</i>	<i>iNos</i>	<i>Ddit4</i>	<i>Myd116</i>	<i>Ddit3</i>	<i>Ba</i>	<i>Gapdh</i>	<i>18S</i>		
E	<i>MafK</i>	<i>MafB</i>	<i>Jun</i>	<i>Fos</i>	<i>Okl38</i>	<i>Pim3</i>	<i>Cebpd</i>	<i>Cebpa</i>	<i>Egr1</i>	<i>Atf3</i>	<i>Mat2a</i>
F	<i>Cyp 1a1</i>	<i>Hmox1</i>	<i>iNos</i>	<i>Ddit4</i>	<i>Myd116</i>	<i>Ddit3</i>	<i>Ba</i>	<i>Gapdh</i>	<i>18S</i>		
G	<i>MafK</i>	<i>MafB</i>	<i>Jun</i>	<i>Fos</i>	<i>Okl38</i>	<i>Pim3</i>	<i>Cebpd</i>	<i>Cebpa</i>	<i>Egr1</i>	<i>Atf3</i>	<i>Mat2a</i>
H	<i>Cyp 1a1</i>	<i>Hmox1</i>	<i>iNos</i>	<i>Ddit4</i>	<i>Myd116</i>	<i>Ddit3</i>	<i>Ba</i>	<i>Gapdh</i>	<i>18S</i>		

Figure 2.9: SybrMan® Master Plate Layout

Notes: *MafK* = v-maf musculoaponeurotic fibrosarcoma oncogene family, protein K; *MafB* = v-maf musculoaponeurotic fibrosarcoma oncogene family, protein B; *Jun* = Avian sarcoma virus 17 (v-jun) oncogene homolog; *Fos* = FBJ murine osteosarcoma viral oncogene homolog; *Okl38* = Pregnancy-induced growth inhibitor; *Pim3* = Serine/threonine-protein kinase pim-3; *Cebpd* = CCAAT/enhancer binding protein, delta; *Cebpa* = CCAAT/enhancer binding protein, alpha; *Egr1* = Early growth response 1; *Atf3* = Activator transcription factor 3; *Mat2a* = Methionine adenosyltransferase II, alpha; *Gclr* = Glutamate-cysteine ligase, regulatory; *Cyp1a1* = Cytochrome P450, subfamily I, member A1; *Hmox1* = Heme oxygenase (decycling) 1; *iNos* = Inducible nitric oxide synthase; *Ddit4* = DNA damage inducible transcript 4; *Myd116* = Myeloid differentiation 116; *Ddit3* = DNA damage inducible transcript 3; *Ba* = Beta actin (control gene); *Gapdh* = glyceraldehyde-3-phosphate dehydrogenase (control gene); *18S* = 18S ribosomal (control gene)

A master mix for each cDNA sample was prepared on the day of use. For each PCR reaction to be run (plus a 10 percent overage) the following reagents were added to a 1.5mL Eppendorf tube:

- 12.5µL 2x SybrMan® Universal Mastermix (Applied Biosystems), 2.5µL molecular grade water and 5µL Template Solution*

Three-hundred and sixty microlitres of each master mix was transferred to a 0.75mL Screen Mate tube and placed within a Latch Rack for dispensing into the Arrayed SybrMan Plates. The template master mix Latch Rack was placed on a BioMek FX (Beckman Coulter), along with an appropriate Arrayed SybrMan Plates, and the master mixes dispensed. Plates were sealed with a plastic optical cover (ABGene) and spun in a microtitre plate centrifuge at 1000 rpm for 30 seconds. Plates were placed in a 7900 ABI machine autoloader (Applied Biosystems) and run at default running conditions for 40 cycles. Data was saved and

analysed using the 7900 SDS Sequencer Software version 2.2.2 (Applied Biosystems). C_t values were exported as tab-delimited text files for each plate for downstream analysis using TaqMan Toolkit (Brian Bond, GSK R&D).

*Template solutions were either gDNA standards, RT plus or RT minus cDNA samples generated from total RNA samples. Sufficient volumes were prepared to allow all genes to be run four times for genomic DNA (gDNA) standard curve templates, three times for RT plus cDNA samples, and on a single occasion for RT minus cDNA samples.

2.13.4. Statistical Analysis of RT-QPCR Data

Within Excel, standard curve data was plotted for each gene (Figure 2.10) and copy numbers for individual cDNA samples derived in relation to this data. The appropriate RT minus copy number was subtracted from each of the triplicate RT plus copy numbers and an average copy number derived from these three values. Group mean fold changes in gene expression for each gene were derived in relation to the control group data and significance determined by carrying out an analysis of covariance (ANACOVA) and post-hoc Dunnett's T-test, using TaqMan Toolkit. Ribosomal 18S expression data was used as the covariant for data analysis (housekeeper gene).

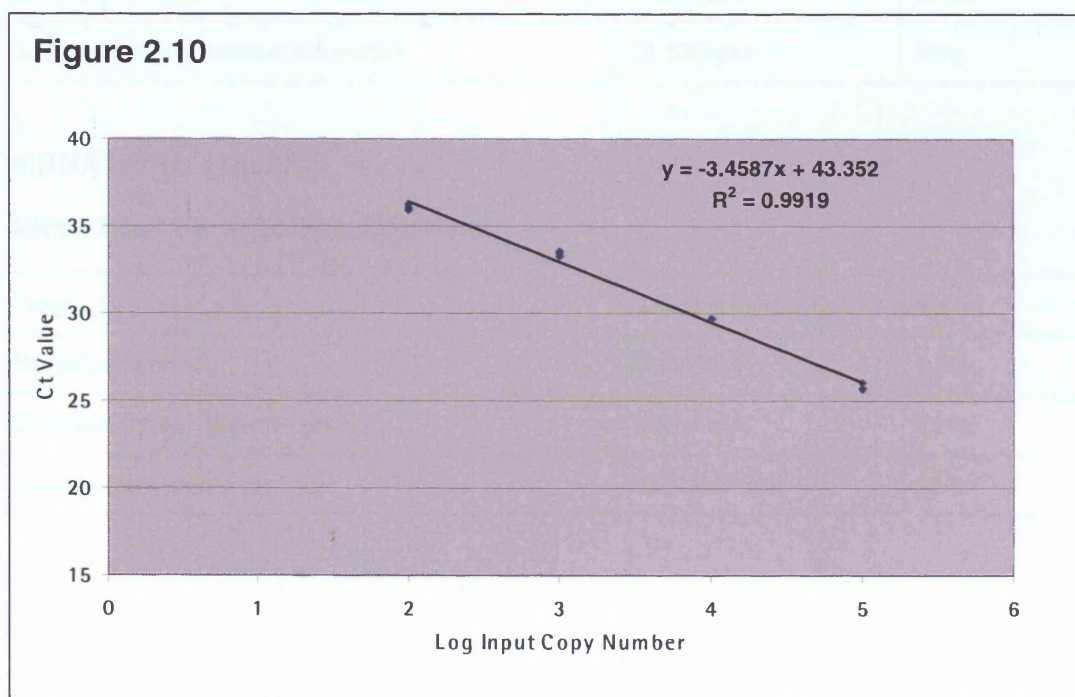


Figure 2.10: Typical SybrMan[®] Standard Curve (*Pim3* serine/threonine kinase)

2.14. Buffer and Culture Media Preparation

Chelating Buffer (500mL):

0.5mM EGTA in HBSS

Reagent	Catalogue Number/Supplier	Volume
Hanks Balanced Salt Solution (w/o Ca ²⁺ , Mg ²⁺ , phenol red) (HBSS)	14155-048/Gibco	490mL
25mM ethylene glycol-bis(β-aminoethyl ether) N,N,N',N'-tetraacetic acid (EGTA), pH7.4	03777/Sigma	10mL

Collagenase Buffer (100mL):

2mM calcium chloride/0.5mg/mL collagenase in HBSS

Reagent	Catalogue Number/Supplier	Volume/Quantity
HBSS	14155-048/Gibco	100mL
1M Calcium Chloride	275844L/BDH	200μL
Collagenase (from <i>Clostridium histolyticum</i>)	C0130/Sigma	50mg

siRNA Buffer (100mL):

55mM Tris/110mM Sodium Chloride

Reagent	Catalogue Number/Supplier	Volume
1M Tris Buffer, pH 7.5	93372/Fluka	5.5mL
5M Sodium chloride (Molecular Grade)	71386/Fluka	2.2mL
Molecular grade water	2900136/5Prime	92.3mL

WE Complete Media (500mL):

William's E media/10% foetal calf serum/50µg/mL Gentamicin

Reagent	Catalogue Number/Supplier	Volume
WE Media (with Glutamax)	32551/Gibco	450mL
Gentamicin (10mg/mL)	15750-045/Gibco	2.5mL
Foetal calf serum (heat inactivated)	10108-165/Gibco	50mL

WE Incomplete Media (500mL):

William's E media/50µg/mL Gentamicin

Reagent	Catalogue Number/Supplier	Volume
WE Media (with Glutamax)	32551/Gibco	500mL
Gentamicin (10mg/mL)	15750-045/Gibco	2.5mL

**CHAPTER 3. EVALUATION OF THE RELATIVE CYTOXICITY OF
SELECTED QUINONES IN RAT HEPATOCYTES**

3.1. Introduction

In order to investigate transcriptional responses it is necessary to identify a chemical concentration which evokes some response but does not overtly harm the cell. The purpose of the work in this chapter was to select a concentration of each quinone that was sub-cytotoxic, based on the assessment of conventional endpoints (e.g. lactate dehydrogenase (LDH) leakage). The overall aim of this study was to identify an appropriate concentration for each quinone that would be used for subsequent transcriptomic investigations using Affymetrix GeneChip[®] microarrays.

3.1.1. Quinones

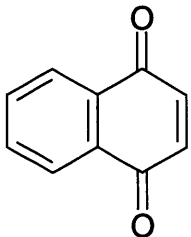
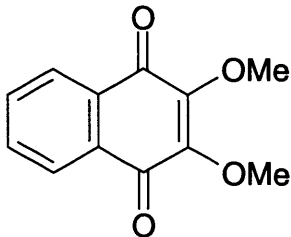
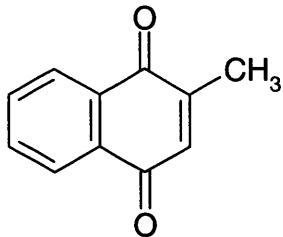
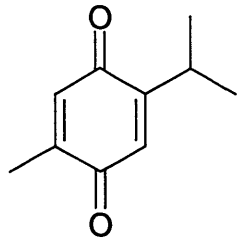
Five compounds belonging to the benzo- and naphthoquinone classes were selected for this study (Table 3.1). They were 1,4-benzoquinone (BQ), 1,4-naphthoquinone (NQ), 2,3-dimethoxy-1,4-naphthoquinone (DMNQ), menadione (MNQ) and thymoquinone (TQ). The five quinones were selected based on their varied chemical and cytotoxic properties (e.g. redox potential and electrophilic potency) and for their well documented use in primary hepatocyte cultures.

The benzene derivative BQ is well documented as a pure arylator [20;22;118] and has been shown to be cytotoxic in rat hepatocytes at concentrations between 5-100 μ M [30;102;118]. BQ has been demonstrated to induce marked and rapid reduced glutathione (GSH) depletion in hepatocytes from a number of species [119] and its toxicity is believed to be predominantly due to reactivity with cellular protein thiols [102]. As discussed in section 1.1.3, there is some evidence that the GSH conjugates of BQ undergo redox cycling [32;33] which potentially could result in a certain level of oxidative stress.

NQ possesses electrophilic centres at the 2 and 3 positions of the naphthalene ring structure and is a potent arylator [27]. NQ has been shown to be more cytotoxic than BQ in rat hepatocytes [27;35;100] and Miller *et al* [27] demonstrated that the 4 hour IC₅₀ was between 50 and 75 μ M. NQ does have the capacity to redox cycle [27], although its cytotoxicity has been primarily attributed to its arylating potential [100]. Henry and Wallace [100] also demonstrated that the capacity for NQ to redox cycle in rat hepatocytes

is concentration dependent. At concentrations $\leq 4\mu\text{M}$ redox cycling was the predominant reactivity, whereas at concentrations $>4\mu\text{M}$ cytotoxicity was primarily due to arylation.

Table 3.1: Structure and activity of the five quinones under investigation

Quinone	Structure	Notes on activity
BQ		Potent arylator $E^0 = +78\text{mV}$ [119]
NQ		Potent arylator; also redox cycles $E^0 = -140\text{mV}$ [120]
DMNQ		Pure redox cyler $E^0 = -183\text{mV}$ (T Gant, pers. comm.)
MNQ		Redox cyler and arylator $E^0 = -203\text{mV}$ [120]
TQ		Superoxide scavenger; arylator $E^0 = \text{not available}$

E^0 = redox potential – relates to the normal hydrogen electrode

The only pure redox cycling quinone used during this study was DMNQ, which was first synthesised by Gant *et al* [26]. It is a fully substituted naphthoquinone with methoxy groups at the 2- and 3-positions which block arylating potential. DMNQ has a redox cycling capacity roughly equivalent to that of menadione [26] and has been used as a model compound for studying the effects of redox cycling-induced oxidative stress in a wide range of *in vitro* systems [104;118;119;121]. Miller *et al* [27] demonstrated that rat hepatocytes were relatively insensitive to the redox cycling effects of DMNQ. No cytotoxicity was observed over 4 hours of exposure at concentrations of up to 300µM. Thor *et al* [102] and Stubberfield and Cohen [30] did observe decreased hepatocyte viability with 3 hours exposure to DMNQ at concentrations between 200 and 500µM. Both groups demonstrated up to 50 percent cytotoxicity, although the relative cytotoxicity of other quinones tested (e.g. BQ and menadione) was far higher in both studies.

MNQ, more commonly known as menadione, is a naphthoquinone analogue of vitamin K [122]. Vitamins K₁ (phylloquinone) and K₂ (menaquinone), the naturally occurring analogues, act as cofactors for the carboxylation of glutamate residues on vitamin K-dependent (VKD) proteins [122;123]. VKD proteins are involved in coagulation factor activation (e.g. factors V, VII and X, prothrombin and fibrinogen), bone metabolism, and inhibition of arterial wall calcification [123].

As with the previous three quinones, MNQ cytotoxicity has been extensively studied in rat hepatocytes [25-27;30;102;118;124]. Possessing an electrophilic centre at the 3-position, MNQ is an arylator that also has the capacity to extensively redox cycle [26;27]. MNQ exposure between 50 and 200µM results in marked cytotoxicity to rat hepatocytes within 2 hours [25;30;102;124]. Although MNQ has potent redox cycling activity, inducing increased levels of oxidised glutathione (GSSG) in rat hepatocytes [26;118;124] its cytotoxicity is believed to be primarily due to arylation of intracellular thiols [26].

TQ (2-isopropyl-5-methyl-1,4-benzoquinone) is a benzoquinone that forms the active constituent of *Nigella sativa* seed extract [125;126]. *N sativa* extract has been used as an herbal remedy for conditions such as asthma and rheumatism for centuries [126]. TQ is an analogue of *tert*-butylhydroquinone (TBHQ), a compound known to be an activator of the nuclear factor-kappa B (NF-κB) and nuclear factor (erythroid-derived 2)-like 2-antioxidant response element (Nrf2-ARE) pathway (reviewed in Section 1.3.2). Badary *et al* [126] have

shown TQ to be a potent superoxide scavenger that can inhibit lipid peroxidation *in vitro* at concentrations around 10-20 μ M. However, they also showed that TQ has some pro-oxidant activity at high concentrations (400 μ M), as evidenced by enhancement of bleomycin-ferric induced DNA damage.

Additional evidence for the antioxidant properties of TQ comes from *in vivo* studies investigating its protective properties in models of doxorubicin cardiotoxicity. Nagi and Mansour [127] showed that pre-treatment with 10mg/kg/day orally protected rats from the acute effects of doxorubicin (assessed by significant reductions in serum enzymes including lactate dehydrogenase and creatine kinase). Similarly al-Shabanah *et al* [128] demonstrated that pre-treatment with 8mg/kg/day TQ orally ameliorated doxorubicin-induced cardiotoxicity in mice. Both groups suggest the superoxide scavenging properties of TQ, and its ability to diminish lipid peroxidation, are responsible for the effects observed.

Khalife and Lupidi [129] have shown that TQ has the potential to arylate cellular thiols. They demonstrated that TQ can react non-enzymatically with GSH under physiological conditions, resulting in the generation of a glutathionyl-dihydroquinone product. This reactivity suggests that TQ has the potential to be cytotoxic to hepatocytes *in vitro*, although the concentration and exposure time are yet to be defined. No studies have been published investigating the cytotoxicity of TQ in primary hepatocyte cultures. However, a number of groups have published studies investigating the cytotoxicity of TQ in tumour cell lines, with IC₅₀ values in the order of 50 to 400 μ M [130-133].

The cytoprotective role of TQ in rat hepatocytes has been evaluated by Daba and Abdel-Rahman [125]. They reported that pre-incubation of hepatocytes with 1000 μ M TQ reduced cytotoxicity associated with exposure to the hydrogen peroxide generator *tert*-butyl hydroperoxide (TBHP). Reduced cytosolic enzyme leakage and decreased GSH depletion was observed in hepatocytes pre-incubated with TQ, the latter consistent with the superoxide scavenging capacity demonstrated by Badary *et al* [128].

3.1.2. Experimental design

Dose-ranging experiments were carried out to identify an appropriate concentration for each quinone. This was defined as the concentration that caused a marginal level of

cytotoxicity (assessed by percent LDH leakage) and/or at least a fifty percent decrease in total glutathione levels. Dose ranging investigations were carried out using 8 hours of quinone exposure, at which point LDH leakage and total glutathione levels were assessed. An 8 hour exposure period was selected as subsequent transcriptomic investigations were to be undertaken with terminal sampling at this time point. The cytotoxic effects were evaluated over a broad range of quinone concentrations, with guidance being taken from the extensive knowledgebase that existed for at least four of the compounds. As mentioned in section 3.1.1, TQ had not previously been demonstrated as cytotoxic in rat hepatocytes and for this reason a wider range of concentrations were tested.

Previous work (not reported in this thesis) indicated extremely variable transcriptional responses in rat hepatocyte monolayer cultures exposed to BQ and DMNQ. This involved the treatment of hepatocytes immediately following the post isolation attachment period. In the hope of reducing this variability, hepatocyte monolayer cultures used for all studies reported in this thesis were allowed an overnight recovery period prior to quinone exposure. During the first 24 hours of culture hepatocytes undergo dedifferentiation, resulting in a more foetal phenotype and rapid loss of enzymes cytochrome P450 (CYP) expression[134]. However, this was not considered problematic as the quinones used in this investigation do not require CYP-mediated activation to exert their toxicity.

To aid selection of the appropriate concentration for each quinone, transcriptional responses were assessed. As a gross indicator of the magnitude of transcriptional response, the number of genes modulated after 8 hours exposure to two selected concentrations of each quinone (a sub-cytotoxic and marginally-cytotoxic) was determined. This was undertaken using GSKrat1a Affymetrix GeneChip[®] microarrays. The GSKrat1a is a custom GeneChip[®] originally designed in 2002. They contain probe sets representing approximately 6400 fully annotated rat genes and approximately 2500 rat expressed sequence tags (ESTs).

3.2. Results

Rat hepatocytes were prepared and cultured according to the methodology outlined in Section 2.1. Two dose ranging experiments were carried out and LDH leakage (experiments 1 and 2) and total GSH levels (experiment 1 only) were assessed following eight hours exposure to each of the five selected quinones. The concentrations evaluated for each quinone are detailed in Table 3.2.

Table 3.2: Concentration ranges of quinones tested in dose-ranging experiments

Quinone	Experiment 1 Concentration (μM)	Experiment 2 Concentration (μM)
BQ	0, 5, 10, 25, 50, 75, 100, 200	0, 5, 10, 25, 50, 75, 100, 200
NQ	0, 1, 5, 10, 25, 50, 75, 100	0, 1, 5, 10, 25, 50, 75, 100
DMNQ	0, 1, 5, 10, 25, 50, 75, 100	0, 1, 10, 50, 100, 150, 200, 250
MNQ	0, 1, 5, 10, 25, 50, 75, 100	0, 1, 5, 10, 25, 50, 75, 100
TQ	0, 10, 50, 100, 250, 500, 1000, 2000	0, 1, 5, 10, 25, 50, 75, 100

3.2.1. Biochemical Endpoints

LDH leakage was assessed in triplicate cultures using the method outlined in Section 2.3. Total GSH levels were assessed using the *O*-Phthaldialdehyde method (outlined in Section 2.7.1.). Results of LDH leakage and GSH depletion from the two dose-ranging experiments are presented for BQ (Figure 3.1), NQ (Figure 3.2), DMNQ (Figure 3.3), MNQ (Figure 3.4) and TQ (Figure 3.5).

No increase in LDH leakage over media controls was observed with BQ exposure until a concentration of $75\mu\text{M}$ was reached (Figure 3.1A and B). LDH leakage rapidly increased at concentrations above $75\mu\text{M}$ BQ, with approximately 100 percent LDH leakage at $200\mu\text{M}$. GSH levels were slightly increased (approximately 5-15%) at lower concentrations of BQ (5- $10\mu\text{M}$), a trend that was rapidly reverted at concentrations greater than $25\mu\text{M}$ (Figure 3.1C). Almost complete GSH depletion was observed at sub-cytotoxic/marginally cytotoxic concentrations of BQ (50- $75\mu\text{M}$), although the onset of marked cytotoxicity at concentrations above these levels was rapid.

The effects of NQ and MNQ exposure on rat hepatocytes were very similar to those observed with BQ, although the steepness of the dose responses were more pronounced. One and 5 μ M NQ exposure did not cause any increase in LDH leakage (Figures 3.2A and B), although slight increases in GSH levels were observed (Figure 3.2C). At concentrations above 5 μ M GSH was rapidly depleted and cytotoxicity was manifest, with approximately 100 percent LDH leakage observed at concentrations greater than 10 μ M. The effects of MNQ exposure were almost identical (in terms of shape of dose response) (Figures 3.4A, B and C), although cytotoxicity was not observed until a concentration of 25 μ M was achieved (Figures 3.4A, B and C).

Surprisingly the cytotoxicity of TQ to rat hepatocytes was relatively high, when compared to the other quinones tested. As the cytotoxicity of TQ had not been previously evaluated in rat hepatocytes, a wide range of concentrations were assessed initially (0 to 2000 μ M). At 100 μ M TQ approximately 80 percent LDH leakage (Figure 3.5A) and 100 percent GSH depletion (Figure 3.5C) were observed. In a subsequent dose range experiment lower concentrations of TQ were assessed, again with marked cytotoxicity (approximately 100 percent LDH leakage) being observed at 100 μ M (Figure 3.5B). Overall TQ concentrations of 1 to 25 μ M were sub-cytotoxic, with concentrations above this level resulting in a steady increase in LDH leakage until 100 percent cytotoxicity was observed at 100 μ M. These results indicate that TQ is more cytotoxic to rat hepatocytes than the pure arylator BQ, although less cytotoxic than MNQ or NQ.

Of the five quinones investigated, only DMNQ (the pure redox cycler) failed to cause any increase in LDH leakage at the concentrations tested (up to 250 μ M) (Figures 3.3A and B). As with all the arylating quinones, the lowest concentrations of DMNQ tested did result in a slight (5-10 percent) increase in GSH levels (Figure 3.3C). However, increasing concentrations of DMNQ only resulted in a gradual depletion of GSH levels, with approximately 55 percent GSH depletion observed at 100 μ M. This finding fits with the lack of cytotoxicity observed with DMNQ, as almost complete GSH depletion was required before marked cytotoxicity was observed with the other four quinones tested.

Based on the results of the dose ranging experiments, transcriptional responses to each quinone were evaluated at the two concentrations detailed in Table 3.3. Both concentrations were around, or just below, the threshold of cytotoxicity. The exception was DMNQ, which

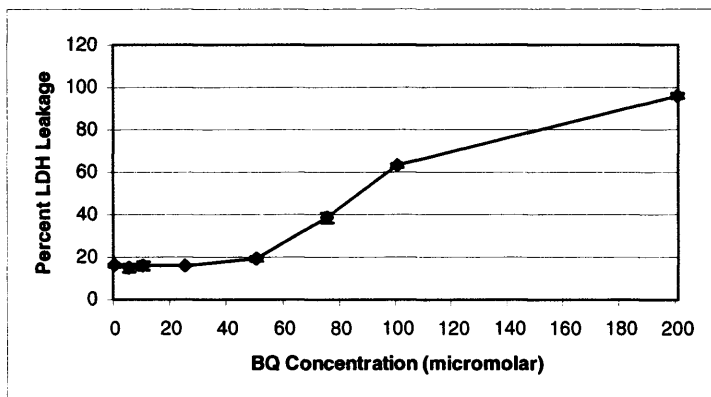
did not induce cytotoxicity at any of the concentrations tested following eight hours exposure. Instead, the lowest concentration demonstrated to induce greater than 50 percent total glutathione depletion was selected as the lower test concentration. The next concentration up was selected as the higher concentration.

Table 3.3: Concentrations selected for evaluating transcriptional changes at eight hours

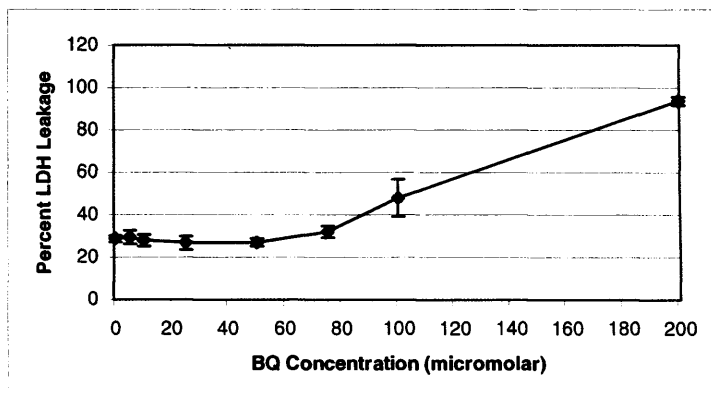
Quinone	Lower Concentration (μM)	Higher Concentration (μM)
BQ	50	75
NQ	5	10
DMNQ	100	150
MNQ	10	25
TQ	25	50

Figure 3.1

A



B



C

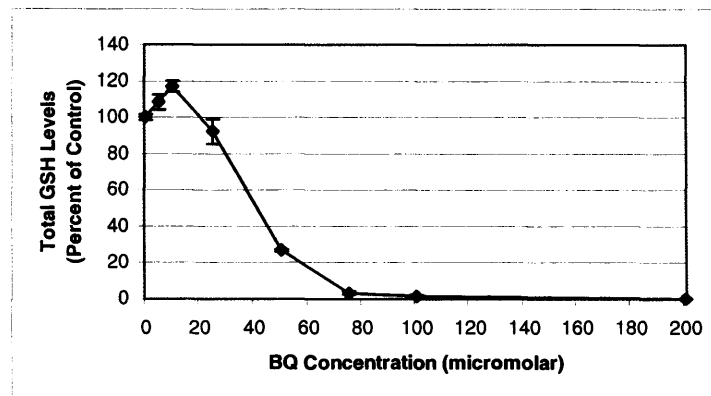


Figure 3.1: LDH leakage and GSH depletion in rat hepatocytes as a result of 8 hours BQ exposure.

LDH leakage as a percent of total (two experiments; A and B) and GSH (single experiment; C) in rat hepatocyte monolayers exposed to BQ for 8 hours. Results are mean of triplicate wells \pm SD.

Figure 3.2

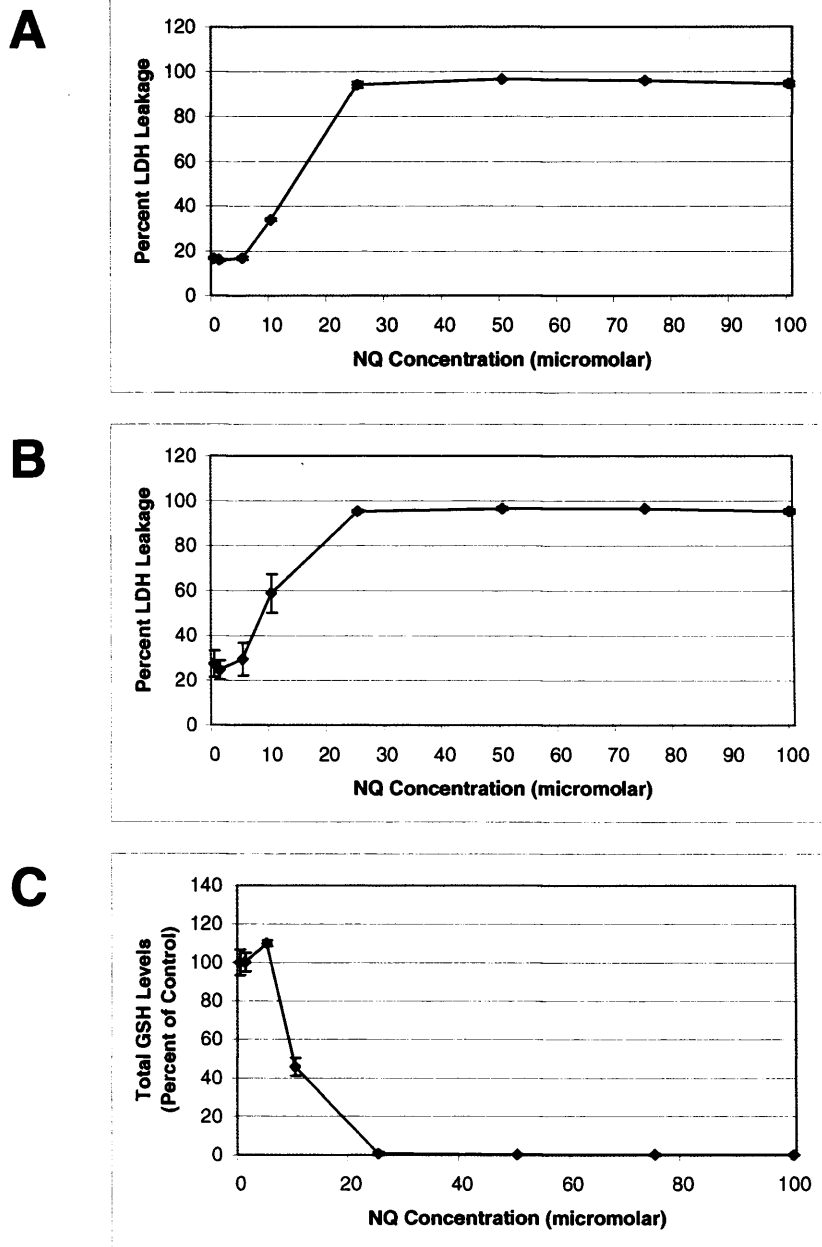


Figure 3.2: LDH leakage and GSH depletion in rat hepatocytes as a result of 8 hours NQ exposure.

LDH leakage as a percent of total (two experiments; A and B) and GSH (single experiment; C) in rat hepatocyte monolayers exposed to NQ for 8 hours. Results are mean of triplicate wells \pm SD.

Figure 3.3

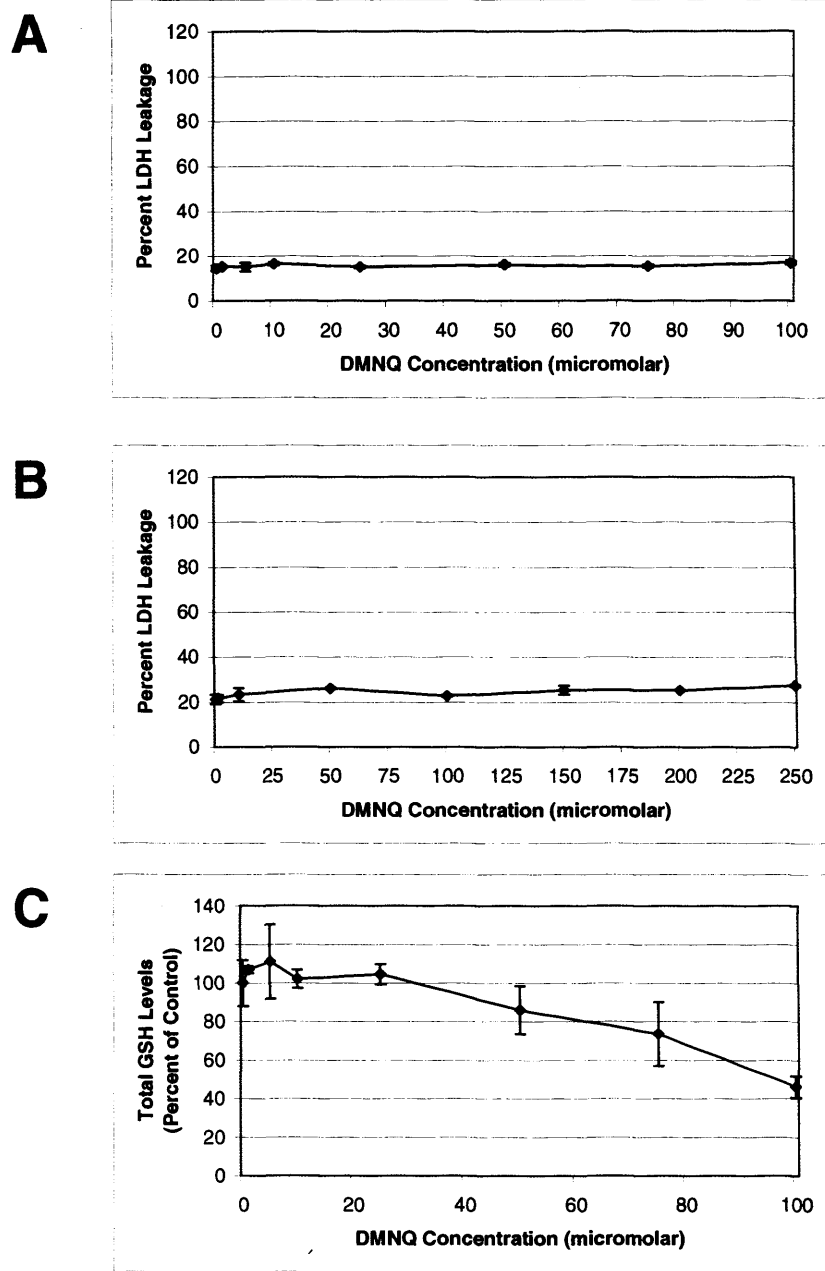


Figure 3.3: LDH leakage and GSH depletion in rat hepatocytes as a result of 8 hours DMNQ exposure.

LDH leakage as a percent of total (two experiments; A and B) and GSH (single experiment; C) in rat hepatocyte monolayers exposed to DMNQ for 8 hours. Results are mean of triplicate wells \pm SD.

Figure 3.4

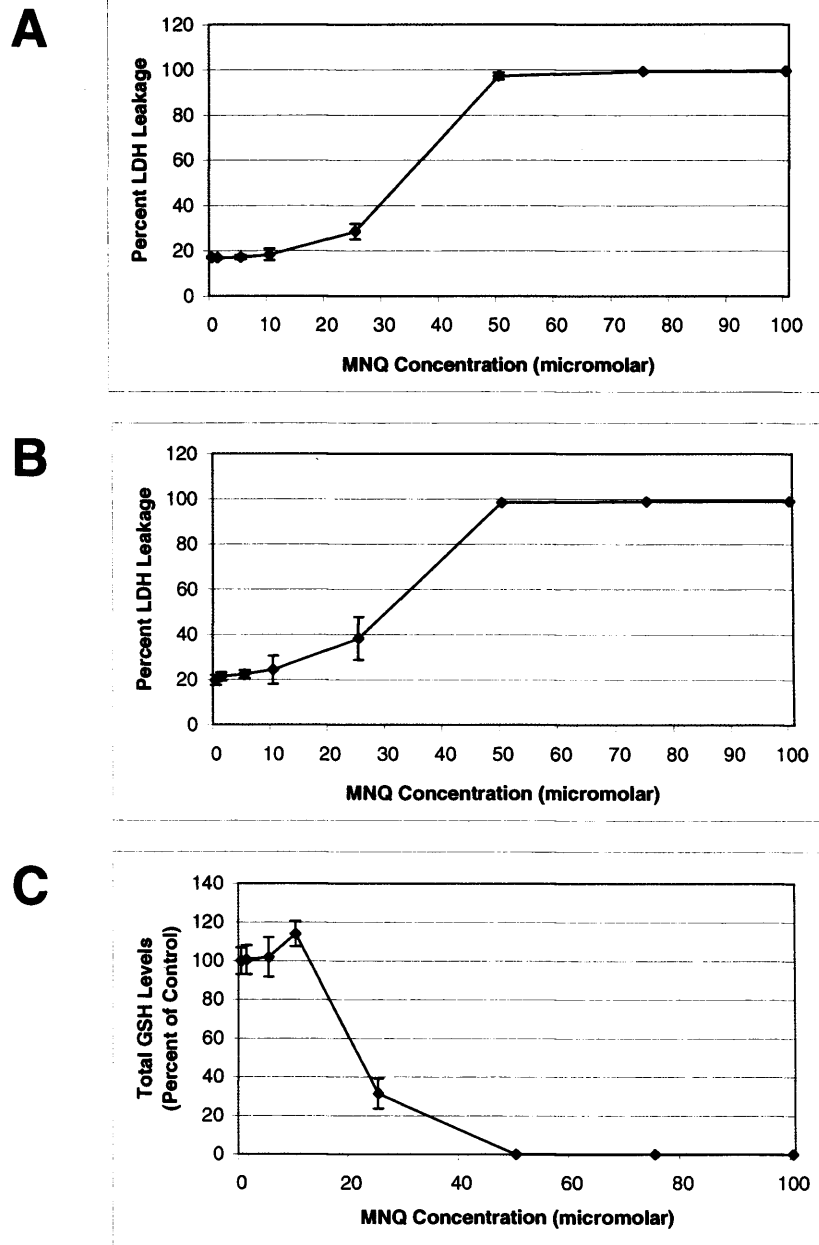


Figure 3.4: LDH leakage and GSH depletion in rat hepatocytes as a result of 8 hours MNQ exposure.

LDH leakage as a percent of total (two experiments; A and B) and GSH (single experiment; C) in rat hepatocyte monolayers exposed to MNQ for 8 hours. Results are mean of triplicate wells \pm SD.

3.2.2. Transcriptional Changes

To select the appropriate concentration for each quinone, transcriptional responses were evaluated following 8 hours exposure. Triplicate cultures were exposed to either vehicle control (VC) or the two concentrations of each quinone (detailed in Table 3.3). Total RNA was isolated (according to the method outlined in Section 2.10) from pooled triplicate cultures for each treatment. Biotinylated-cRNA targets were prepared for each pooled total RNA and the fragmented cRNA targets hybridized to a single GSKrat1a GeneChip for each sample (according to the method outlined in Section 2.12).

To evaluate the magnitude of transcriptional response with each quinone concentration, pairwise comparisons of VC and quinone exposed culture were carried out using the RatioBuild function in Resolver (outlined in Section 2.12.3). The number of genes significantly modulated ($p = \leq 0.01$) at an arbitrary threshold ($\geq \pm 2$ -fold) was used as a metric (Figure 3.6).

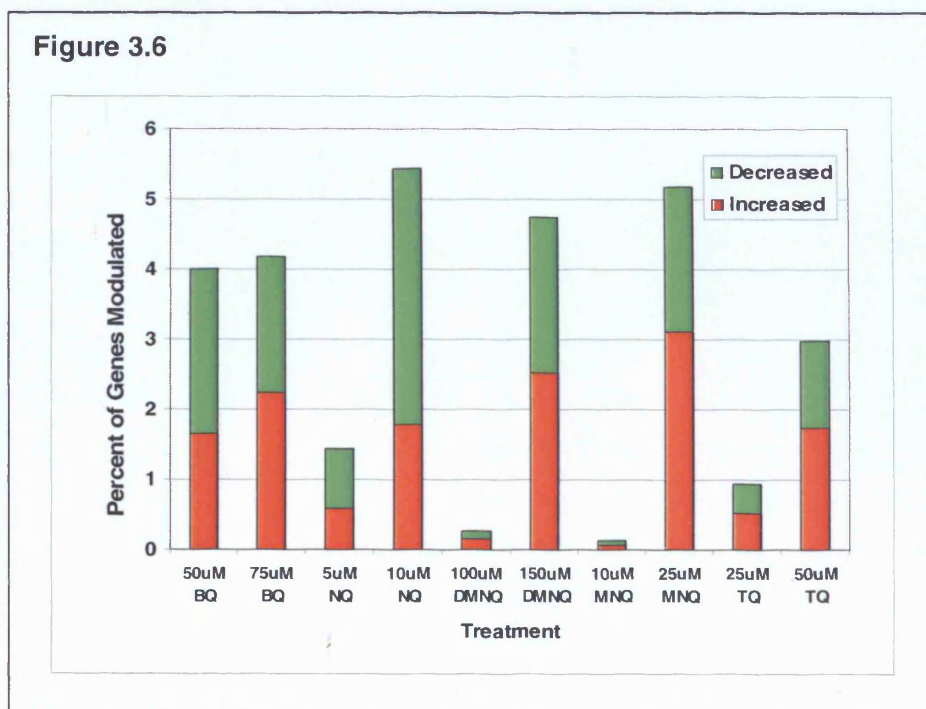


Figure 3.6: Percent genes significantly ($P < 0.01$) modulated by ≥ 2 -fold in quinone treated cultures relative to vehicle control.

With all five quinones, the higher concentration tested resulted in a greater transcriptional response. The difference in transcriptional response between the lower and higher concentrations was marked with NQ, DMNQ, MNQ and TQ. The two concentrations tested for BQ resulted in transcriptional parity (in terms of total modulations). Based on these data it was decided that the higher concentration tested for each quinone (detailed in Table 3.3) would be used for all subsequent transcriptional investigations in rat hepatocyte cultures.

3.3. Discussion

The overall aim of the experiments described in this chapter was to determine appropriate quinone concentrations for subsequent transcriptomic studies. Dose ranging experiments were carried out to identify a concentration for each quinone that was on the threshold of cytotoxicity, whilst evoking transcriptional responses of comparable magnitude between the quinones. This was achieved by determining the relative cytotoxicity of each quinone using LDH leakage and then evaluating the transcriptional responses of hepatocytes exposed to two concentrations around the threshold of cytotoxicity.

Concentration-dependent cytotoxicity was observed with four of the five quinones tested (NQ, MNQ, TQ and BQ) and all quinones induced concentration-dependent GSH depletion. Dose-ranging experiments yielded the following cytotoxicity ranking (based on LDH leakage after 8 hours of exposure) for the five quinones tested:

NQ > MNQ > TQ > BQ >>> DMNQ

This ranking is broadly in line with data published by other workers, in as much as the three potent arylating quinones (i.e. NQ, MNQ and BQ) were far more cytotoxic to rat hepatocytes cultures than DMNQ [20;22;26;119].

Approximate EC₅₀ values are presented in Table 3.4, along with an indication of the accompanying level of GSH depletion. Cytotoxicity was demonstrated in rat hepatocytes for all quinones known to have the potential to arylate (i.e. BQ, NQ, MNQ and TQ). With all four of these quinones, cytotoxicity was preceded by a marked depletion of total GSH. GSH depletion (~60%) was observed with DMNQ at 100µM. As discussed earlier (Section 3.1.1), DMNQ is a pure redox cyler and the GSH depletion observed will have been due to increased GSSG generation as a result of ROS. Interestingly, there was no accompanying cytotoxicity observed suggesting that the mechanism through which GSH is depleted is an important factor in rat hepatocytes survival. It appears that eight hours of exposure is sufficient time for cytotoxicity to develop with arylating quinones, whereas the exposure period is too acute for redox cycling alone (and increased oxidative stress) to become cytotoxic (as is the case with DMNQ).

Table 3.4: 8 hours EC₅₀ values and accompanying GSH depletion for the five quinones

Quinone	Approximate EC ₅₀ (μM)	GSH Depletion at EC ₅₀ (Percent)
BQ	90	>95
NQ	12.5	~60
DMNQ	>250	>60
MNQ	35	>75
TQ	70	>30

EC₅₀ values are approximate and based on LDH leakage

A significant finding during the dose ranging experiments was the relative cytotoxicity of TQ. With an EC₅₀ of approximately 70μM, TQ was ranked as being more cytotoxic than BQ. Based on the literature (summarised in Section 3.1.1), it had been anticipated that the superoxide scavenging properties of TQ would confer a reduced cytotoxicity ranking relative to the other quinones tested. This was not the case and as mentioned earlier, cytotoxicity was preceded by GSH depletion. It is considered likely that the GSH depletion was due to direct binding of TQ to the thiol group of GSH, a reactivity previously demonstrated[129]. The TQ cytotoxicity data produced in these experiments contradict the findings of Daba and Abdel-Rahman [125]. They noted that 1mM TQ did not cause increased cytotoxicity (as assessed by cell viability and enzyme leakage) relative to vehicle control treated cultures. It was also found that 1mM TQ protected rat hepatocytes from 2mM TBHP-related cytotoxicity and abrogated TBHP-induced GSH depletion.

The 1mM concentration of TQ used by Daba and Abdel-Rahman was far higher than the approximate EC₅₀ of 70μM determined in this study. However, they only exposed rat hepatocytes to TQ for up to 2 hours [125]. In addition, freshly isolated hepatocyte suspensions were used, versus the 16 hours old hepatocyte monolayer cultures in this study. These differences in experimental design, particularly exposure time, most likely account for the conflicting findings. TQ has been shown to be cytotoxic to HEP-2 cells (a human laryngeal cell line), also causing GSH depletion [131]. Overall, the findings of this study may indicate that TQ has the potential to be hepatotoxic *in vivo*, due to its GSH depleting capacity. Obviously *in vivo* experiments are needed to confirm or refute this.

A consistent observation made for the four quinones with arylating activity was an increase (approximately 10%) in GSH levels at the concentration preceding that at which marked depletion of GSH was observed. A similar response was observed with DMNQ, although a more gradual depletion of GSH levels was observed with increasing concentration. This finding is most likely due to an adaptive response to quinone exposure that overcompensates for the level of challenge, resulting in a net enhancement in GSH synthesis. As quinone concentration increases, the balance rapidly shifts resulting in GSH depletion.

As a gross indicator of the magnitude of transcriptional response, the number of genes modulated after 8 hours exposure to two concentrations (a sub-cytotoxic and marginally-cytotoxic) of each quinone was assessed (Figure 3.6). With the exception of BQ exposure (which led to similar responses at both concentrations), the magnitude of transcriptional response was far greater at the marginally-cytotoxic concentration. The decision was made to proceed with transcriptional investigations using the marginally-cytotoxic concentration for each quinone using a time course of three time points. I believe this approach strikes a balance by: 1) Ensuring sufficient challenge of rat hepatocytes to evoke a reliable transcriptional response, 2) allowing the identification of transcriptional changes important in responding to quinone challenge, rather than modulations perhaps more indicative of overt cytotoxicity. The concentrations selected for each quinone for future transcriptomic investigations are summarised in Table 3.5.

Table 3.5: Optimal concentration selected for each quinone

Quinone	Selected Concentration (μM)
BQ	75
NQ	10
DMNQ	150
MNQ	25
TQ	50

**CHAPTER 4. TRANSCRIPTIONAL PROFILES OF QUINONES IN
RAT HEPATOCYTES**

4.1. Introduction

In this study the transcriptional responses of rat hepatocyte monolayer cultures exposed to 1,4-benzoquinone (BQ), 1,4-naphthoquinone (NQ), 2,3-dimethoxy-1,4-naphthoquinone (DMNQ), menadione (MNQ) or thymoquinone (TQ) were examined using concentrations on the threshold of cytotoxicity. The overall aim was to produce transcriptional profiles for each compound and identify genes and pathways consistently regulated in response to quinone exposure. It was hypothesised that consistent regulation of genes/pathways may indicate key response mechanisms through which hepatocytes seek to ameliorate quinone toxicity and oxidative stress. In addition, through the selection of quinones I sought to determine whether it was possible to differentiate the mechanism through which cytotoxicity was exerted (i.e. arylation versus redox cycling) based on transcriptional response.

The dose-ranging experiments described in Chapter 3 were carried out to identify an appropriate concentration for each quinone. A single concentration was selected for each quinone that was on the threshold of causing cytotoxicity following 8 hours exposure (Table 4.1). The exception was DMNQ, which was not cytotoxic at up to 250 μ M. However, marked GSH depletion was observed by 8 hours with >75 μ M DMNQ. It was felt that the selected concentration of 150 μ M would present a significant redox challenge to the exposed hepatocytes. In addition, 150 μ M DMNQ resulted in a gross transcriptional response in line with the other selected quinone concentrations (Figure 3.6).

Table 4.1: Selected concentration for each quinone

Quinone	Selected Concentration (μ M)
BQ	75
NQ	10
DMNQ	150
MNQ	25
TQ	50

Transcriptional responses were investigated using the GSKrat1a Affymetrix GeneChip[®] microarrays (described in section 3.1.2). For each quinone, responses were evaluated

following 1, 4 and 8 hours of exposure. The 1 hour time point was needed to allow an assessment of the early transcriptional response. The 4 and 8 hour time points were chosen to evaluate adaptive changes made by the rat hepatocytes once quinone challenge, and potentially oxidative stress, was established. Biochemical endpoints were assessed throughout the time course for each quinone to provide context to the transcriptional changes observed. LDH leakage was measured as an indicator of overall cytotoxicity. Glutathione endpoints (GSH and GSSG levels) were measured to provide an indication of the degree of challenge the rat hepatocytes were undergoing, in the absence of cytotoxicity. The additional inclusion of GSSG as an endpoint in this study provided an indirect assessment of the oxidative challenge.

The complexity of the data generated by microarray analysis necessitates the use of bioinformatics tools to help confer biological meaning. To this end, transcriptional data were analysed using the Expression Analysis Systematic Explorer (EASE) and Ingenuity Pathway Analysis (IPA) biological theme analysis tools (outlined in Section 2.12.3). Responses in pathways expected to be transcriptionally regulated with quinone exposure were also evaluated. As discussed in Section 1.3.2, quinones are known inducers of the nuclear factor (erythroid-derived 2)-like 2-antioxidant response element (Nrf2-ARE) pathway due to their electrophilic nature. Additionally, oxidative stress induced by redox cycling quinones may exacerbate Nrf2-ARE pathway activation. Quinone-induced oxidative stress may also result in oxidative DNA damage (as outlined in Section 1.2.2). Thus, genes involved in both the Nrf2-ARE pathway and DNA damage response were identified within the transcriptomic data sets and their regulation evaluated.

4.2. Results

Rat hepatocyte monolayer cultures were exposed to either vehicle control (VC) or the selected concentration of each of the five quinones for eight hours (according to the methodology outlined in Section 2.1). At 1, 4 and 8 hours cultures were sampled for LDH leakage, GSH and GSSG levels, and total RNA.

4.2.1. Biochemical Endpoints

LDH leakage, and GSH and GSSG levels were determined as outlined in Sections 2.3 and 2.7.2, respectively. Triplicate cultures exposed to either VC (n = 6 replicate experiments per time point) or the selected concentration of each of the five quinones (n = 3 replicate experiments per time point, except DMNQ where n = 2) were sampled.

No significant increase in LDH leakage was observed at 1 and 8 hours with any of the five quinones (Figure 4.1A), as expected. GSH levels were decreased with BQ (significantly at 8 hours), DMNQ (4 and 8 hours) and MNQ (significantly at 1, 4 and 8 hours) exposure (Figure 4.1B). No significant changes in GSH levels were observed at 1, 4 or 8 hours with NQ and TQ exposure. Increases in GSSG levels were observed following 1 hour exposure to BQ, NQ, DMNQ and MNQ (all significant with the exception of DMNQ, where n = 2), the later two quinones inducing the more marked responses (Figure 4.2B). Increased GSSG levels persisted with DMNQ and MNQ exposure until 4 hours and by 8 hours GSSG levels in all quinone exposed cultures were not significantly different from VC levels (Figure 4.1C).

Figure 4.1

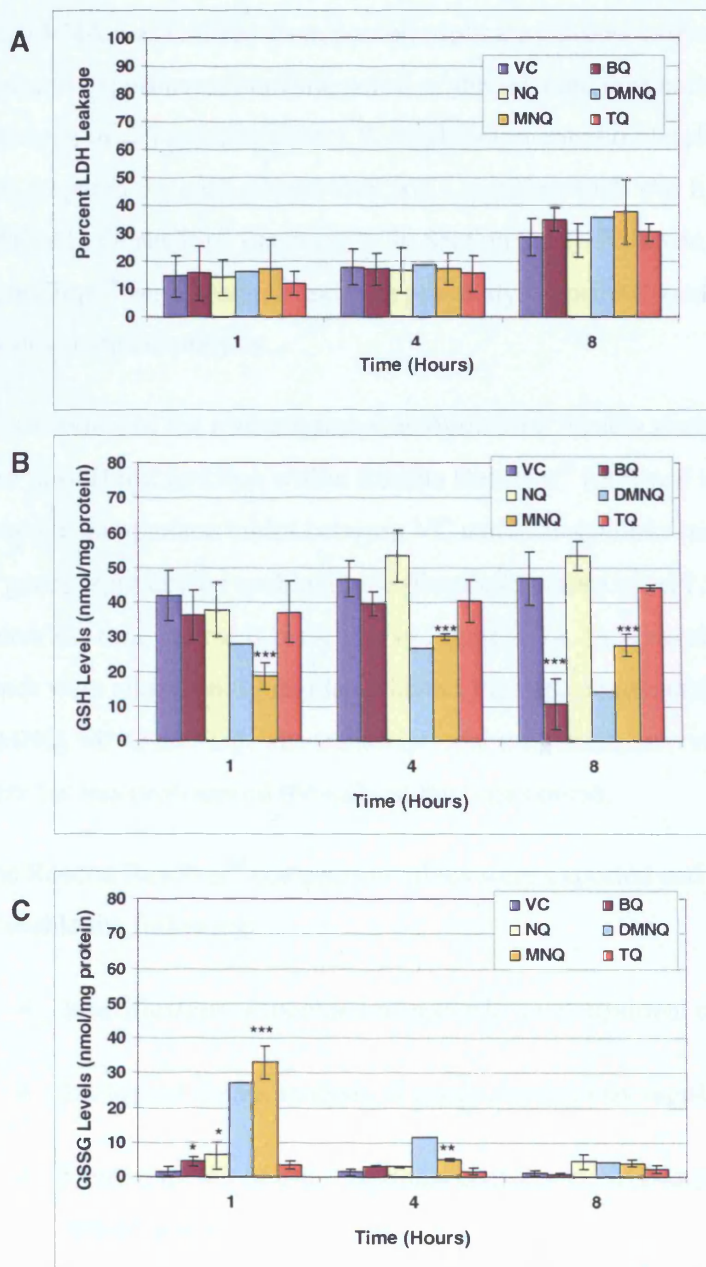


Figure 4.1: LDH Leakage (A), GSH (B) and GSSG (C) levels in rat hepatocyte monolayers exposed to VC, BQ, NQ, DMNQ, MNQ or TQ for 1, 4 and 8 hours.

Results are mean values \pm SD (VC n=6, quinones n=3, except DMNQ treated cultures, n=2). ANOVA and post-hoc Dunnett's T-test. * = P<0.05, ** = P<0.01, *** = P<0.001 versus VC. Quinone concentrations as in Table 4.1.

4.2.2. Transcriptomic Investigations

Total RNA was isolated from pooled triplicate cultures exposed to either VC (n = 6 replicate experiments per time point) or the selected concentration of each of the five quinones (n = 3 per time point). A single fragmented biotinylated-cRNA target synthesis was prepared for each pooled total RNA sample which was hybridised onto a single GSKrat1a GeneChip[®] (as outlined in Section 2.12). Following hybridisation and washing, GeneChips[®] were scanned and data pre-analysed prior to transfer to the Resolver database for downstream analysis.

An overview of the transcriptional analysis used for this study is summarised in Figure 4.2. The RatioBuild function within Rosetta Resolver[®] (outlined in Section 2.12.3) was used to generate comparison tables between VC and each quinone treated group. The total number of genes regulated by each quinone (threshold values of $>\pm 1.5$ -fold change and $p \leq 0.05$) across the time course is presented in Figure 4.3A. In general, comparable numbers of genes were significantly regulated across the time course in cultures exposed to BQ, DMNQ, MNQ and TQ. The transcriptional responses observed in cultures exposed to NQ were far less pronounced throughout the time course.

The Rosetta Resolver[®] comparison tables were exported and the data filtered within Excel to enable the following:

- Identification of mechanism-specific transcriptional changes.
- Biological theme analysis of genes consistently regulated with quinone exposure.
- Determination of transcriptional changes in Nrf2-target genes and DNA damage-related genes.
- Identification of ‘quinone signature genes’, consistently regulated at multiple time points with quinone exposure.

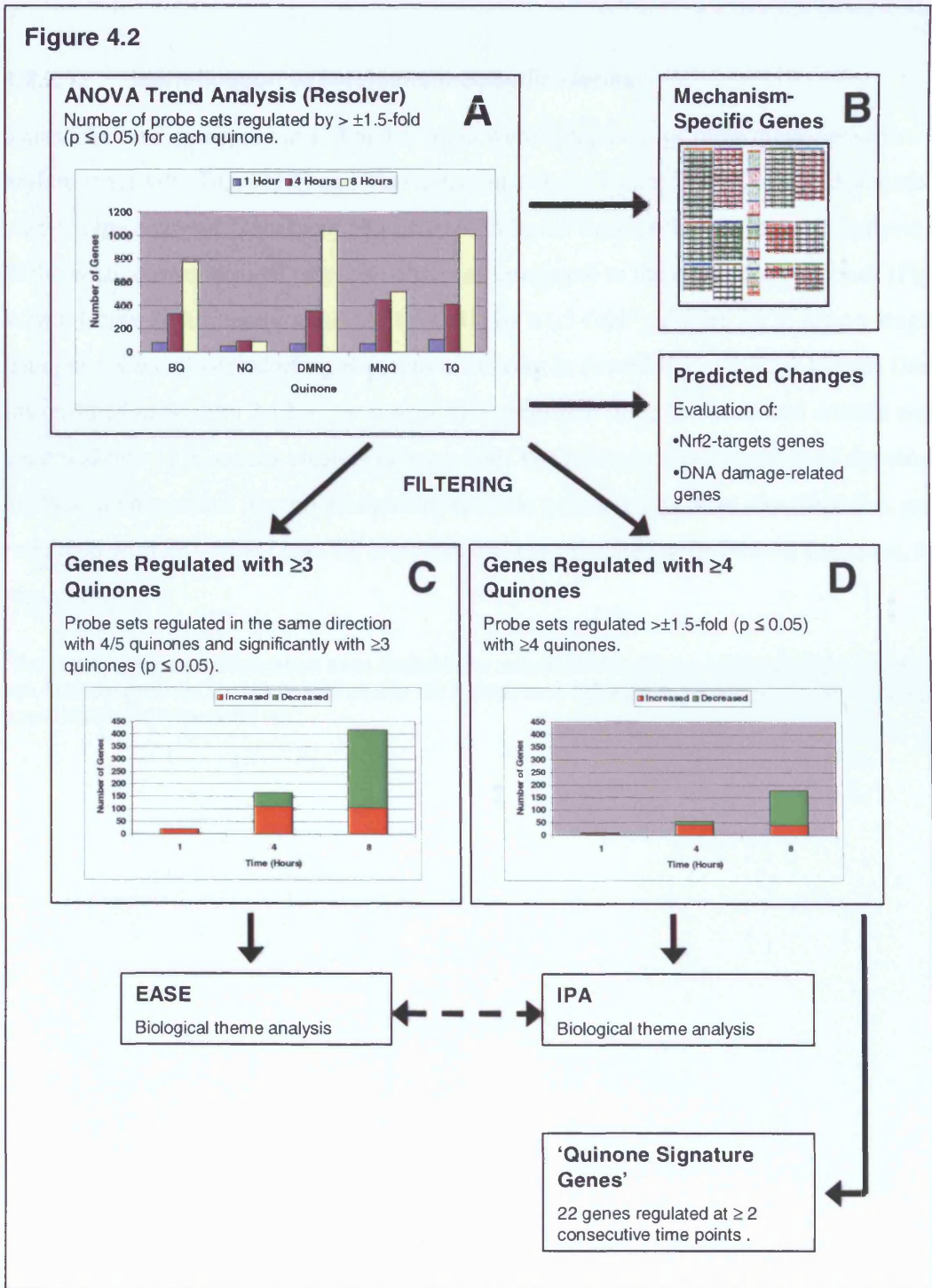


Figure 4.2 Overview of data analysis of transcriptional changes induced in rat hepatocytes exposed to BQ, NQ, DMNQ, MNQ or TQ for 1, 4 and 8 hours.

A: Summary of the number of probe sets regulated by each quinone at 1, 4 and 8 hours. B: K-means cluster analysis was undertaken to identify mechanism-specific genes. C and D: Probe sets consistently regulated with quinone exposure were analysed using EASE and IPA to identify key biological themes. The same probe sets were further filtered to identify 'quinone-signature genes'.

4.2.2.1. Identification of Mechanism-Specific Genes

Transcriptional responses at 1, 4 and 8 hours were compared for three quinones with arylating activity (BQ, MNQ and TQ) to the pure redox cycler DMNQ, using *K*-means cluster type analysis. Data from NQ exposed cultures were excluded from the analysis due to the weak transcriptional response observed compared to the other four quinones (Figure 4.2A). Genes significantly regulated ($p < 0.01$) by ± 1.5 -fold* or more for at least a single data point were clustered using *K*-means clustering in ArrayMiner v5.3.2 (Optimal Design) (as outlined in Section 2.12.3). A total of 820 genes that fitted the threshold criteria were clustered into 12 *K*-means clusters (Figure 4.3). The heatmap representation of the cluster analysis demonstrates that no mechanism-specific gene clusters were identified (i.e. genes regulated with BQ, MNQ and TQ exposure and not regulated with DMNQ exposure, or visa versa).

*The selection criteria are different from those detailed in the analysis overview (Figure 4.2) to reduce the false detection rate. More stringent selection criteria were used for this analysis as no further filtering (based on consistency of regulation across treatments) were carried out.

Figure 4.3

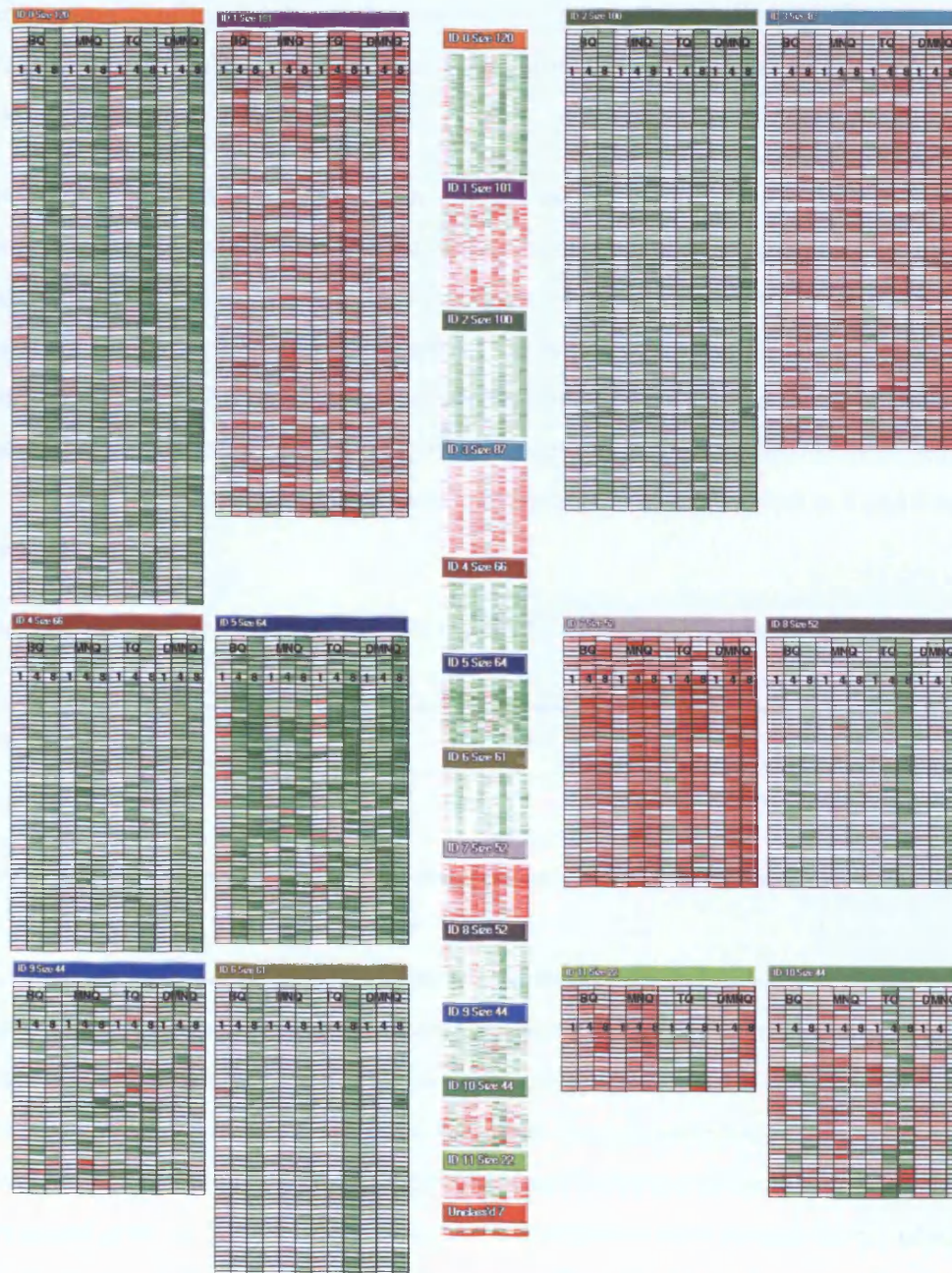


Figure 4.3 Heat map representation of K-means cluster analysis of 820 genes regulated significantly ($p < 0.01$) regulated ± 1.5 -fold with either BQ, MNQ, TQ or DMNQ exposure at 1, 4 and 8 hours.

Central heat map represents the entire data set of 820 clustered genes segregating to 13 clusters (clusters ID0 to ID11 and 'unclassified genes'). The number of genes within each cluster is indicated by 'Size n '. Larger heat maps represent enlarged images of clusters ID0 to ID11. The quinone identity and time (in hours) is indicated at the top of each enlarged cluster image.

4.2.2.2. Biological Theme Analysis

Genes consistently regulated with quinone exposure were identified and the lists of regulated genes analysed on a per time point basis using two alternative methods, EASE and IPA (described in Section 2.12.3).

Genes regulated in the same direction with at least 4/5 quinones (and significantly with 3/5 quinones) were selected for EASE analysis. The number of genes passing this filter are indicated in Table 4.2. The gene lists (containing Genbank accession numbers) were analysed using the categorical overrepresentation function of EASE and the output is presented in Table 4.3. An EASE Score cut-off of 0.05 was applied, with the exception of the 1 hour time point. At 1 hour there were no gene categories at the selected EASE Score cut-off and so gene categories that were subsequently overrepresented at 4 and 8 hours are shown.

Table 4.2: Number of genes filtered for EASE biological theme analysis at each time point.

Direction of Change	1 Hour	4 Hours	8 Hours
Increased	19	109	106
Decreased	1	57	310

EASE analysis indicated possible induction of transcriptional regulation and activity at 1 hour. These and similar categories were significantly overrepresented in the increased gene set at 4 hours. In addition, genes involved in cell proliferation and nucleic acid metabolism were increased at 4 hours. By 8 hours, there was strong overrepresentation of genes involved in DNA metabolism and replication, and S-phase cell cycle control in the decreased gene set. Transcriptional regulation categories were present in the increased gene set at 8 hours, though were less well represented than at 4 hours. Interestingly, genes involved in regulation of apoptosis were increased at 8 hours.

Table 4.3: EASE biological theme analysis of quinone-regulated genes.

System	Gene Category	1 Hour	4 Hours	8 Hours
Biological Process	Cell proliferation		0.0214	
	DNA metabolism			0.0079
	DNA replication			0.0076
	DNA replication and chromosome cycle			0.0163
	Metabolism		0.0475	0.0244
				0.00365
	Nucleoside, nucleotide and nucleic acid metabolism			0.0138
	Protein-disulfide reduction			0.0554
	Regulation of apoptosis			0.0543
	Regulation of transcription	0.1150	0.0047	
	Regulation of transcription - DNA-dependent	0.1100	0.0038	
	S phase of mitotic cell cycle			0.0076
	Transcription	0.1230	0.0020	
Transcription - DNA-dependent	0.1150	0.0047		
Cellular Component	Actin cytoskeleton			0.0490
	Intracellular			0.0377
	Nucleoplasm		0.0333	
	Nucleus	0.1740	0.00538	0.0308
			0.055	
	Transcription factor complex		0.0204	
Molecular Function	Adenyl nucleotide binding		0.0203	
	ATP binding		0.0171	
	Binding		0.0165	
	DNA binding	0.1170	0.00158	
			0.0134	
	MAP kinase phosphatase activity		0.0423	
	Nucleic acid binding	0.1850	0.00548	
			0.030338	
	Protein tyrosine/serine/threonine phosphatase activity		0.0560	
Transcription factor activity		0.0039	0.0408	
Transcription regulator activity		0.0013		

The table shows the results of EASE analysis for genes consistently regulated with quinone exposure (as defined in Figure 4.3). Gene categories with an EASE score of ≤ 0.05 are shown*, giving an overall indication of the gene functions regulated with quinone exposure. Direction of change is indicated by the EASE score font colour (Red = increased, Green = decreased).

*Except for the 1 hour time point, where no significant gene categories were identified. Gene categories significantly regulated at later time points are shown for reference.

As an additional tool for investigating biological themes overrepresented with quinone exposure, IPA analysis was used (as outlined in Section 2.12.3). A more stringent filter was applied to genes selected for IPA analysis, as outlined in Figure 4.2C. The Affymetrix probe set identification numbers and consensus direction of modulation for the genes passing the filter criteria were imported into IPA on a per time point basis. The number of genes imported into IPA are indicated in Table 4.4.

Table 4.4: Number of genes filtered for IPA biological theme analysis at each time point.

Direction of Change	1 Hour	4 Hours	8 Hours
Increased	6	42	40
Decreased	1	14	137

The gene lists were categorized by IPA based on biological functions and mapped into interacting networks, which were ranked by score. The networks (presented in Tables 4.5 and 4.6) indicate functional association between the genes present and are ranked by score for each time point. To confer biological meaning, the top three functions associated with each network is included.

Only a single network was identified at 1 hour, with the key functions being cellular movement and cell-to-cell interaction (Table 4.5). Three networks were identified at 4 hours where genes involved in cell cycle control and proliferation/growth were heavily represented (Table 4.5). Genes implicated in cell death were also represented in a single network (4 hour II). Six networks were identified at 8 hours (Table 4.6) and consistently represented functions included cell growth/proliferation control, DNA repair, cell morphology, and cell death. Genes implicated in cancer were also well represented, although it is recognised that this is a broad category.

Table 4.5: IPA biological theme and network analysis of 1 and 4 hour time point quinone-regulated genes.

Network ID	Genes in Network	Score	Focus Genes	Top Functions
1 hour I	ACAT2, AGTR1, ALOX5AP, CEBPD , CEBPG, CLDN4, CPB2, cyclic AMP, DGCR6, DUSP6, EPHA2 , F3 , FBLN5, G6PC , GCLC, GCLM, HPR, IL31, IL1B, IL1RL1, ITGAX, JUNB , Mapk, MIA, MMP8, PDGF BB, PIM3 , PTX3, RGS3 , SFTPD, SLC37A4, SLC7A1, TLR9, TNF, YARS	20	7	Cellular Movement, Inflammatory Disease, Cell-To-Cell Signaling and Interaction
4 hour I	Akt, Ap1, CEBPB , CHKA , Creb, CTGF, DUSP5 , DUSP6 , EGR1 , ERK1/2, ETS, FOS , FOSL1 , GDF15 , HMOX1 , Ige, Jnk, MAFK , MAP3K4 , Mapk, MAT2A , Mek, Mek1/2, P38 MAPK, Pdgf, PDGF BB, PI3K, PIAS3 , Pkc(s), PPP1R15A (includes EG:23645) , Ras, STAT, Tgf beta, VEGFA , ZFP36	39	17	Cellular Growth and Proliferation, Cell Morphology, Cell Cycle
4 hour II	ALPP, BAG4, BAZ1A , BCL2L11 , beta-estradiol, CEBPG, CLDN4, EPHA2 , FAS, GDF15 , GPX1, GSR, HSD17B1, Hsp70, HSPA2 , HSPA1B , hydrogen peroxide, IL1B, LCN2, OKL38 , PHF17, PIGR, PIM3 , PLK3 , PPBP, PRKRA, PSMD14, PTPN13, PTPRN, SLA, SNCG, SPN, TFRC , VHL, ZBTB7A	25	12	Cell Death, Cancer, Cellular Movement
4 hour III	BRD2 , CD19, CDK8, CEBPE, CSF3R, DAB2, EIF5A, FOSL1 , GFI1, GHR, HAS2, HNRPC, HOXB4, LAMP2, MAFG , MAP3K12, MT1E, MYC, NFE2, NME2, NMI, PITX2, PRG2 (includes EG:5553), PRKCH, PRTN3, RBP1, retinoic acid, RPS6, RPS7, S100B, SLC5A3 , SPI1, TFRC , TGM1 , ZBTB7A	10	6	Cellular Growth and Proliferation, Cellular Development, Immune and Lymphatic System Development and Function

The table shows the IPA network analysis output for genes consistently regulated with quinone exposure (as defined in Figure 4.2C). Direction of change is indicated by the gene name font colour (**Red** = increased, **Green** = decreased). Genes in 'black' text have known interactions with other members of the network, based on the IPA knowledgebase. The score is the negative log of *P* and indicates the likelihood of the focus genes in a network being found together due to chance (a cut off score of 3 was used, equating to $p < 0.001$). Focus genes refers to the number of genes within a network transcriptionally regulated with quinone exposure. Top functions indicates the three key biological themes represented within each network.

Table 4.6: IPA biological theme and network analysis of 8 hour time point quinone-regulated genes.

Network ID	Genes in Network	Score	Focus Genes	Top Functions
8 hour I	ACTN1, ADM, AKR7A2, Ap1, CEBPB, Creb, CTGF, DDIT3, DUSP5, EGR1, ERK1/2, ETS, FOS, FOSL1, GDF15, HMBS, Igfbp, IGFBP1, IL1, MAFK, Mapk, Mek, Mek1/2, Mmp, MMP11, Pdgf, PDGF BB, PDGFC, PI3K, Pkc(s), Ras, RPS6KA1, TAGLN, Tgf beta, ZFP36	36	19	Cellular Growth and Proliferation, Cell Morphology, Cancer
8 hour II	14-3-3, ACACA, Akt, APAF1, BAAT, Ck2, FSTL1, GPAM, HBEGF, HMOX1, Hsp70, HSPB8, INSIG1, INSIG2, Jnk, LIG3, MAP3K4, MEKK, NPHS1, NR1H4, P38 MAPK, PARP2, PIP5K2A, Pka, POLB, RNA polymerase II, SLC20A1, SNCG, TACC2, TFIIF, TFRC, TLR3, TRAF7, TRIAP1, XRCC1	29	16	DNA Replication, Recombination, and Repair, Gene Expression, Cardiovascular Disease
8 hour III	ACACA, AMD1, ANAPC1, ANKRA2, CDC2, CDC16, CDC27, CDC23 (includes EG:8697), CLU, CNKSR3, CTNNB1, DBH, FLCN, FOSL1, FZR1, GDF15, GH1, GLRX, GPAM, hydrogen peroxide, INTS7, LOC219854, LPHN2, LRP2, MAGI2, MAP4, NFYB, OKL38, PCCA, PRDX1, PRKAA2, PRKAB1, SFN, SLC20A1, TSC1	29	16	Cancer, Cell Death, Reproductive System Disease
8 hour IV	BET1, BET1L, DAD1, DNAJB9, DUSP5, F2, FLRT3, FOXP1, GCNT1, GDF15, GOLGB1, GOSR2, IL2, IL15, ITGAM, KDELR3, KLRD1, KLRK1, MOG, PDLIM4, PTPN13, RAB8A, RNH1, SCFD1, SEC22A, SERTAD1, SLC12A7, STX5, TGFB1, TRIM24, UPP1, VDP, XBP1, YKT6, ZHX1	24	14	Cellular Growth and Proliferation, Hematological System Development and Function, Immune Response
8 hour V	ACVR1B, ACVR2B, ADH1C (includes EG:126), Arf, ARF5, BTBD2, CLTC, COPB1, CRIM1, DBP, dihydrotestosterone, GBF1, GGA2, INHBA, INHBC, INHBE, IRS4, KCTD3, MAP4, MARK1, MCM5, MYCN, OCRL, POLA1, PRIM1, PRIM2A, RAB14, RAPGEF6, RPS3A, SLC25A37, SMARCB1, SNX9, TAGLN, TP53, YWHAG	22	13	Viral Function, DNA Replication, Recombination, and Repair, Cancer
8 hour VI	AHNAK, ALDOA, ARD1A, beta-estradiol, CDH1, CHCHD8, CTSH, CUBN, ECT2, FRK, GTF2H4, IL6, KITLG (includes EG:4254), MGP, MNAT1, MYO7A, NAT2, NFIB, Nuclear factor 1, OSBPL1A, PARD6B, PARD6G, PDLIM4, PLCL2, PPP1R9B, PREB, PRL, RAC1, RB1, retinoic acid, RPS7, SLC10A1, SLC5A3, SLC5A5, VEZT	20	12	Cancer, Cell Morphology, Cellular Growth and Proliferation

The table shows the IPA network analysis output for genes consistently regulated with quinone exposure (as defined in Figure 4.2C). Direction of change is indicated by the gene name font colour (Red = increased, Green = decreased). Genes in 'black' text have known interactions with other members of the network, based on the IPA knowledgebase. The score is the negative log of P and indicates the likelihood of the focus genes in a network being found together due to chance (a cut off score of 3 was used, equating to $p < 0.001$). Focus genes refers to the number of genes within a network transcriptionally regulated with quinone exposure. Top functions indicates the three key biological themes represented within each network.

4.2.2.3. Transcriptional Responses in Nrf2-Target and DNA Damage-Response Genes

Genes known to be transcriptional targets of the Nrf2-ARE pathway were identified in the RatioBuild comparison tables and those significantly regulated in at least one quinone treatment group are presented (Figure 4.4A). Similarly, the transcriptional regulation of genes encoding proteins and enzymes known to be involved in DNA repair and regulating the response to DNA damage were assessed (Figure 4.4B).

Induction of Nrf2-target genes was observed in hepatocyte cultures exposed to BQ, DMNQ, MNQ and TQ, primarily at 4 and 8 hours. The most consistently regulated gene was *heme oxygenase 1 (Hmox1)*, with >4-fold increases observed at 4 and 8 hours.

Increased transcription of *Gclc* and *Gclm*, subunits of γ -GC synthetase, was noted in BQ, MNQ and TQ exposed cultures at 4 and/or 8 hours. *Gclc* alone was increased in DMNQ treated cultures at 4 hours. The GST subunit *Gstm4* was increased at 8 hours in quinone-treated cultures for which significant GSH depletion (Figure 4.1B) was observed (i.e. BQ, DMNQ and MNQ).

Of the five quinones tested, TQ evoked the most marked transcriptional response in Nrf2-target genes. Increased transcription of additional antioxidant (*catalase (Cat)* and *glutathione reductase (Gsr)*) and phase II metabolism (*Nqo1*) genes were also noted at 8 hours. Only NQ failed to evoke an induction of Nrf2-target genes, although slight decreases in the transcription (1.5 to 2-fold) of *Hmox1*, *Nqo1* and *Gclc* were noted at 1 hour.



Figure 4.4: Heat map representation of Nrf2-target genes (A) and DNA damage-related genes (B) significantly regulated with quinone exposure ($P < 0.05$, fold change ≥ 1.5 -fold).

There were no significant changes in the transcription of genes encoding enzymes and proteins that directly carry out DNA repair (e.g. *Ogg1*, *Ape1*, DNA polymerases). However transcriptional regulation of six genes belonging to the Growth Arrest and DNA Damage (GADD) and DNA Damage-Induced Transcript (DDIT) families of transcription factors, which regulate responses to DNA damage, was observed (Figure 4.4B).

The most striking responses in GADD/DDIT gene regulation were in DMNQ and MNQ exposed hepatocytes. BQ exposure resulted in a slightly less marked effect. Increased transcription of *Ddit3*, *Ddit4*, *Gadd45 α* , *Gadd45 β* and *Gadd45 γ* , and *Myeloid differentiation 116 (Myd116)* were observed at one or more time points with DMNQ, MNQ and BQ. Notably, *Ddit4* was increased at 1, 4 and 8 hours with all three quinones.

TQ exposure did result in some induction of GADD/DDIT family genes (*Ddit3*, *Gadd45 β* , *Gadd45 γ* and *Myd116*), although the increases were of lower magnitude than those seen with DMNQ, MNQ and BQ. The concentration of NQ used resulted in a negligible transcriptional response of the GADD family of genes, which was in line with changes observed in Nrf2-target genes.

4.2.2.4. Quinone Signature Genes

Quinone-regulated gene sets analysed in IPA were further filtered to produce a focussed set of genes for detailed functional interpretation (as outlined in Figure 4.2). Genes modulated in at least two consecutive time points were identified and defined as 'quinone signature genes'. Twenty-two genes fitted the stringent selection criteria and they represented diverse biological functions including; transcription factors, protein kinases, regulators of lipid and glucose metabolism, cell growth/proliferation control, and the oxidative stress response (Table 4.7). With the exception *LOC498331* (similar to protein tyrosine phosphatase), all the quinone signature genes were increased in expression with quinone exposure. *Ephrin receptor A2 (Epha2)* and the *serine/threonine kinase Pim3 (Pim3)* were increased from 1 hour, perhaps suggesting a role in the early response to quinone exposure.

Table 4.7: Quinone Signature Genes

Genbank Number	Gene Symbol	Gene Description	Gene Ontology Description	1 Hour	4 Hours	8 Hours
NM_012580	<i>Hmox1</i>	<i>Heme oxygenase (decycling) 1</i>	Antioxidant/iron binding activity			
NM_031659	<i>Tgm1</i>	<i>Transglutaminase 1</i>	Cell-cell adhesion/peptide cross-linking			
AA818380	<i>Mylip</i>	<i>Myosin regulatory light chain interacting protein</i>	Cytoskeletal protein binding			
J05571	<i>Mat2a</i>	<i>Methionine adenosyltransferase II, alpha</i>	Glutathione biosynthesis			
NM_031836	<i>Vegfa</i>	<i>Vascular endothelial growth factor A</i>	Growth factor activity/response to hypoxia			
AJ001290	<i>Slc5a3</i>	<i>Solute carrier family 5, member 3</i>	Myo-inositol:sodium symporter activity			
AI236754	<i>Okl38</i>	<i>Pregnancy-induced growth inhibitor</i>	Negative regulation of cell growth			
AA800613	<i>Zfp36</i>	<i>Zinc finger protein 36</i>	Negative regulation of myeloid cell differentiation			
NM_017127	<i>Chka</i>	<i>Choline kinase alpha</i>	Phosphatidylcholine biosynthesis			
AI058759	<i>Epha2</i>	<i>Ephrin receptor A2</i>	Plasma membrane receptor			
M58040	<i>Tfrc</i>	<i>Transferrin receptor</i>	Plasma membrane transferrin receptor			
AI175045	<i>Pdk4</i>	<i>Pyruvate dehydrogenase kinase, isoenzyme 4</i>	Histidine kinase activity/glucose metabolism			
NM_022602	<i>Pim3</i>	<i>Serine/threonine-protein kinase pim-3</i>	Protein serine/threonine kinase activity			
AI172186	<i>Brd2</i>	<i>Bromodomain containing 2</i>	Protein serine/threonine kinase activity			
AF013144	<i>Dusp5</i>	<i>Dual specificity phosphatase 5</i>	Protein tyrosine phosphatase activity			
AA818197	<i>LOC498331</i>	<i>Similar to protein Tyr phosphatase</i>	Structural molecule activity/CD95 (Fas)-associated phosphatase			
NM_024125	<i>Cebpb</i>	<i>CCAAT/enhancer binding protein (C/EBP), beta</i>	Transcription factor activity			
NM_012551	<i>Egr1</i>	<i>Early growth response 1</i>	Transcription factor activity			
AI072183	<i>Fos</i>	<i>FBJ murine osteosarcoma viral oncogene homolog</i>	Transcription factor activity			
NM_012953	<i>Fosl1</i>	<i>Fos-like antigen 1</i>	Transcription factor activity			
AA799744	<i>Mafk</i>	<i>v-maf musculoaponeurotic fibrosarcoma oncogene family, protein K</i>	Transcription factor activity			
NM_019216	<i>Gdf15</i>	<i>Growth differentiation factor 15</i>	Transforming growth factor beta receptor signaling pathway			

Direction of change is indicated by the cell colour (Red = increased, Green = decreased). Quinone signature genes were consistently regulated (4/5 quinones, $p < 0.05$, fold change ≥ 1.5 -fold) in more than one time point consecutively.

4.2.2.5. SybrMan Confirmation

Regulation of 18 genes, including eight quinone signature genes (*Mafk*, *Fos*, *Egr1*, *Cebpa*, *Okl38*, *Pim3*, *Hmox1* and *Mat2a*), were verified using SybrMan[®] RT-QPCR (according to the methodology outlined in Section 2.13). Transcriptional responses were evaluated at 1, 4 and 8 hours for cultures exposed to either BQ, DMNQ or MNQ (Figures 4.5A to 4.5C). In general, a high level of concordance between SybrMan[®] RT-QPCR and GeneChip[®] data was observed (Figures 4.5A to 4.5C). Transcriptional regulation was confirmed for all eight of the quinone signature genes verified (*Mafk*, *Fos*, *Egr1*, *Cebpa*, *Okl38*, *Pim3*, *Hmox1* and *Mat2a*) plus *Jun*, *Atf3*, *Cebpd*, *Cyp1a1*, *Ddit3*, *Ddit4* and *Myd116*. Transcriptional regulation of *Gclm* and *iNos* was not confirmed by SybrMan[®] Q-PCR.

Figure 4.5A

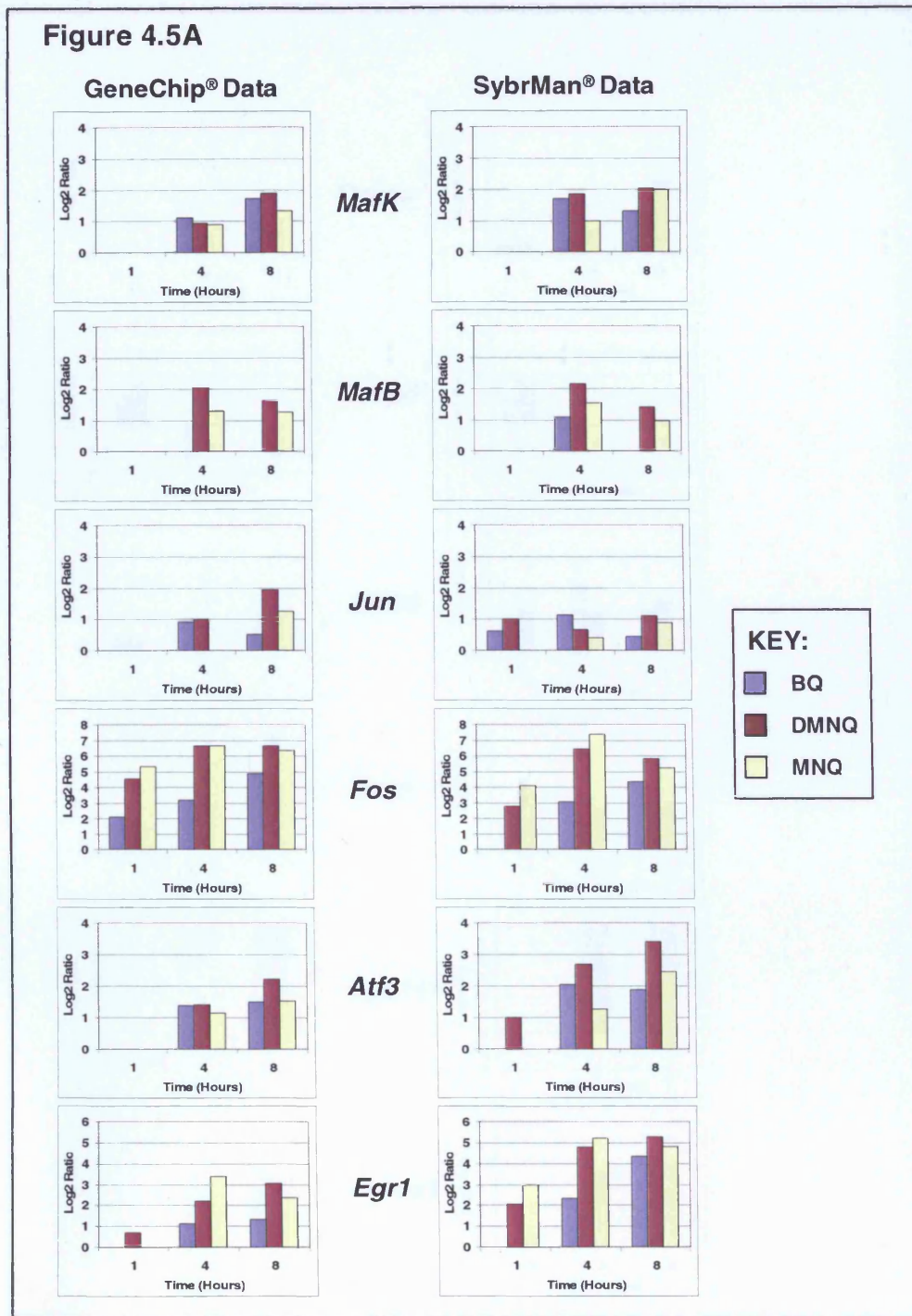


Figure 4.5A Confirmation of selected quinone-regulated genes in BQ, DMNQ and MNQ exposed hepatocyte cultures using SybrMan Q-PCR.

The figure shows GeneChip® and confirmatory SybrMan® log₂ ratio data in quinone exposed cultures relative to VC for *Mafk* (small *mafK*), *Mafb*, *Jun* (*v-jun sarcoma virus 17 oncogene homologue*), *Fos* (*FBJ murine osteosarcoma viral oncogene homologue*), *Atf3* (*activating transcription factor 3*) and *Egr1* (*early growth response 1*).

Figure 4.5B

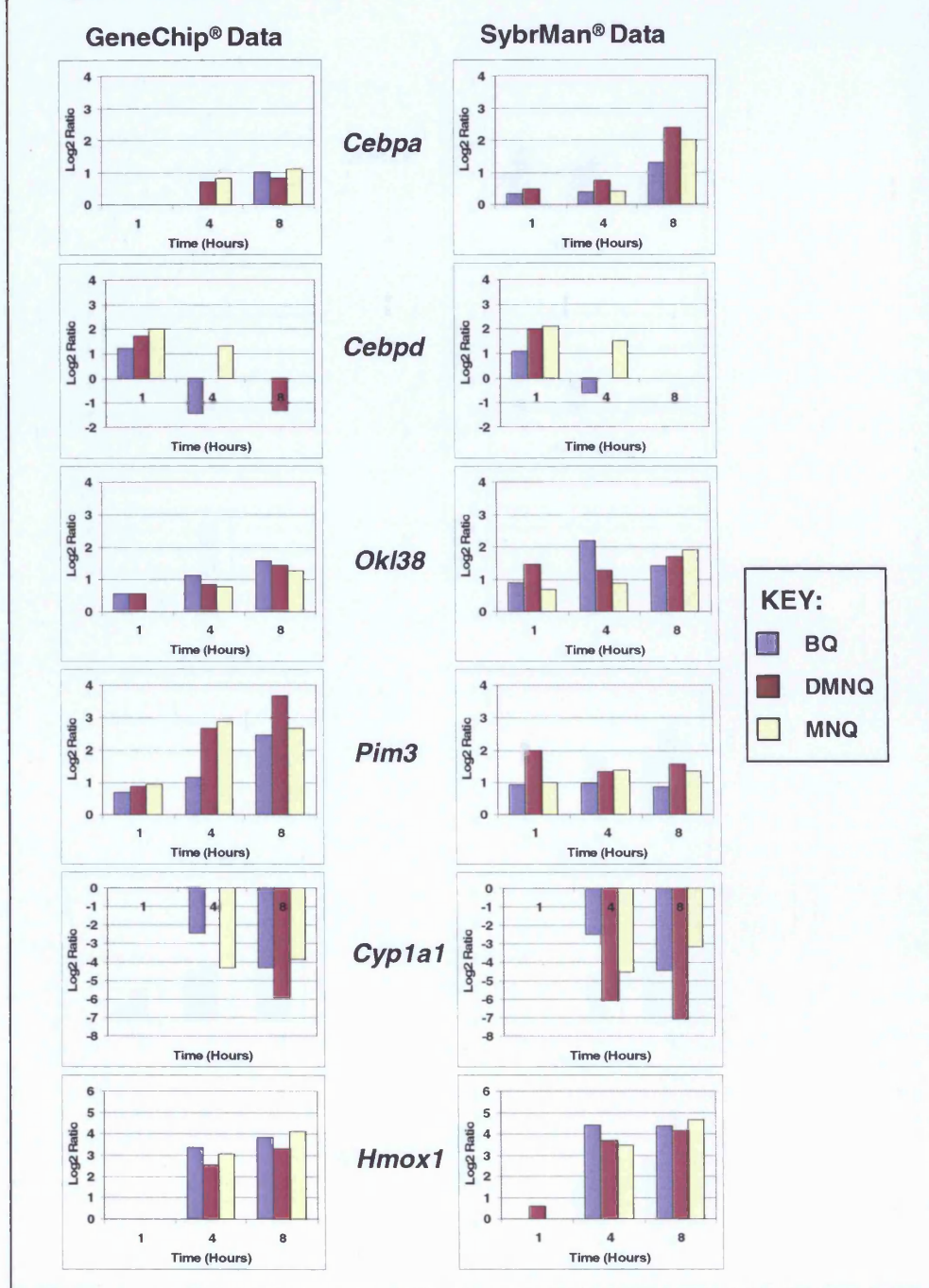


Figure 4.5B Confirmation of selected quinone-regulated genes in BQ, DMNQ and MNQ exposed hepatocyte cultures using SybrMan Q-PCR.

The figure shows GeneChip® and confirmatory SybrMan® log₂ ratio data in quinone exposed cultures relative to VC for *Cebpa* (CCAAT/enhancer binding protein (C/EBP), beta), *Cebpd*, *Okl38* (pregnancy-induced growth inhibitor), *Pim3* (serine/threonine-protein kinase pim3), *Cyp1a1* (cytochrome P450 1a1) and *Hmox1* (heme oxygenase (decycling) 1).

Figure 4.5C

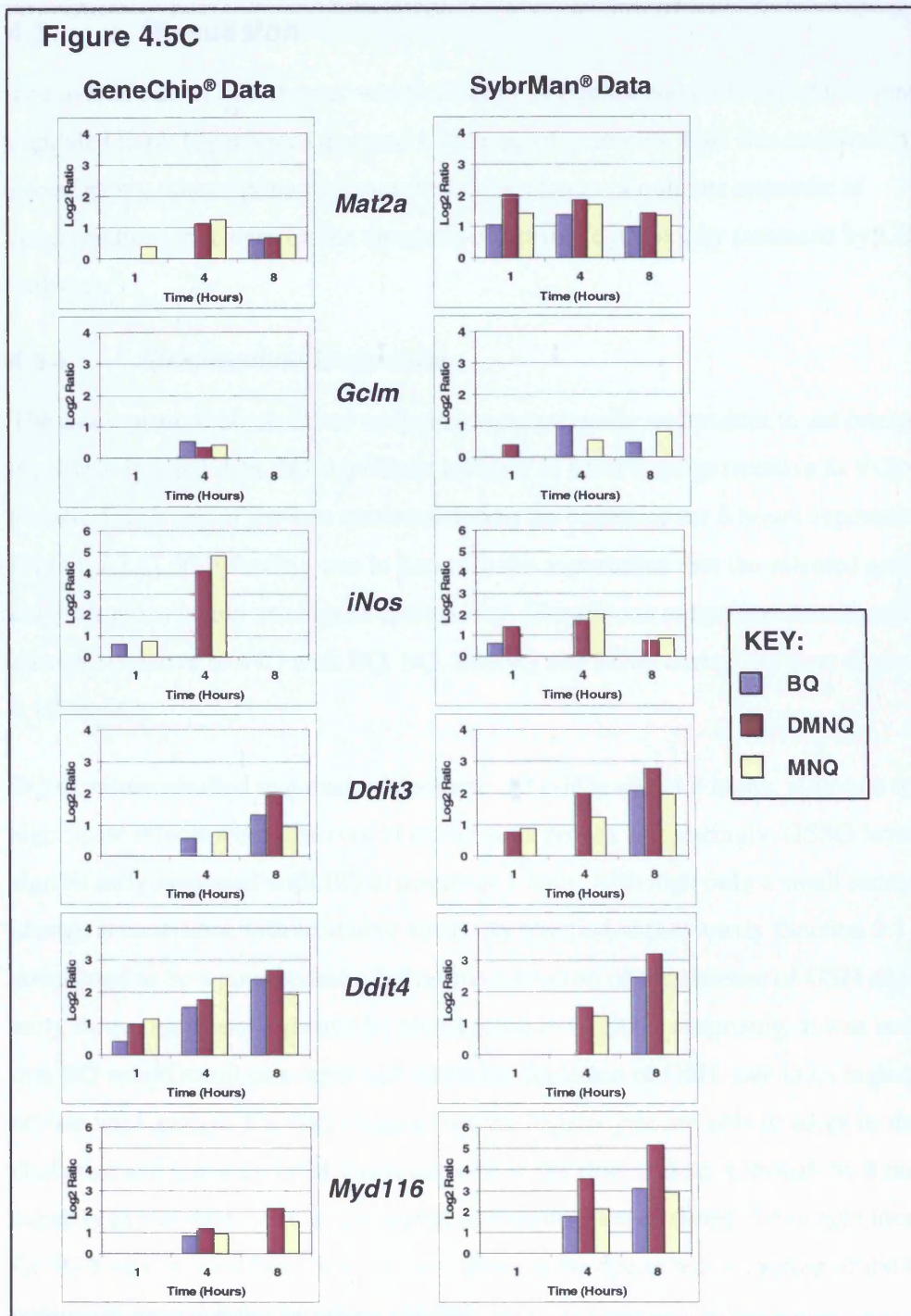


Figure 4.5C Confirmation of selected quinone-regulated genes in BQ, DMNQ and MNQ exposed hepatocyte cultures using SybrMan Q-PCR.

The figure shows GeneChip® and confirmatory SybrMan® log₂ ratio data in quinone exposed cultures relative to VC for *Mat2a* (methionine adenosyltransferase II, alpha), *Gclm* (γ -GC synthetase, modulatory subunit), *iNos* (inducible NO synthase), *Ddit3* (DNA-damage inducible transcript 3), *Ddit4* and *Myd116* (myeloid differentiation 116).

4.3. Discussion

The overall aim of this chapter was to identify key genes and pathways consistently regulated in rat hepatocytes exposed to a range of quinones. This was undertaken by investigating transcriptional changes over eight hours of quinone exposure at concentrations that were on the threshold of causing cytotoxicity (assessed by LDH leakage).

4.3.1. Biochemical Endpoints

The assessment of biochemical endpoints were primarily undertaken to aid interpretation of the transcriptional data. No significant increase in LDH leakage (relative to VC) was observed with any of the five quinones during the course of the 8 hours exposure period (Figure 4.1A). This finding was in line with the expectation that the selected quinone concentrations would not induce cytotoxicity. Glutathione endpoints were significantly changed (relative to VC) with BQ, NQ, DMNQ and MNQ during the time course (Figures 4.1B and C).

BQ exposure resulted in a marked decrease in GSH levels at 8 hours, although no significant effects were observed at earlier time points. Interestingly, GSSG levels were significantly increased with BQ exposure at 1 hour. Although only a small increase, the change is consistent with oxidative stress. As mentioned previously (Section 3.1.1), BQ is considered to be a pure arylator. Initial consideration of the absence of GSH depletion at early time points, accompanied by the increase in GSSG is surprising. It was anticipated that BQ would result in a rapid and sustained depletion of GSH, due to its high capacity to arylate thiol groups. The data suggest that the hepatocytes are able to adapt to the BQ challenge and maintain GSH levels early on in the time course, although by 8 hours their capacity to maintain GSH levels appear to become overwhelmed. The slight increase in GSSG levels observed at 1 hour is most likely to be due to redox cycling of the GSH conjugate, as suggested by others [32;33].

NQ exposure did not result in any significant GSH depletion. This was not in agreement with the findings of the dose ranging studies, where 10 μ M NQ resulted in >50% GSH depletion at 8 hours (Figure 3.2C). The reasons for this lack of response may simply be a function of inter-experiment variability due to the steepness of the NQ dose response curve.

As with BQ, a slight increase in GSSG was observed at 1 hour, again consistent with an oxidative stress challenge.

MNQ resulted in the most marked effect on GSH levels, with significant decreases at 1, 4 and 8 hours. This finding is consistent with the dual reactivity of MNQ, resulting in GSH depletion through both direct arylation of the thiol group and via redox cycling (as outlined in Section 3.1.1). MNQ and DMNQ exposure resulted in marked increases in GSSG levels at 1 hour, with significant increases still present at 4 hours (Figure 4.2B). The degree to which MNQ and DMNQ increased GSSG levels is in line with their capacity to redox cycle, relative to the other quinones tested. It is worth noting that as GSSG levels in DMNQ exposed hepatocytes returned to control levels, significant GSH depletion was observed. DMNQ is a pure redox cyler and does not have the capacity to arylate the thiol group in GSH (as discussed in section 3.1.1). Taken together, these findings suggest that hepatocytes exposed to DMNQ (and most likely MNQ) are exporting any excess GSSG formed at 4 and 8 hours into the culture media. This would redress the redox imbalance caused by markedly increased GSSG levels. To confirm this, it would be necessary to assess total glutathione levels in culture media at each time point.

Only TQ exposure failed to significantly change GSH or GSSG levels at any time point. Although TQ has been shown to have the potential to arylate the thiol group in GSH [129], the concentration used in this study was not sufficient to overwhelm the hepatocyte capacity to respond to this challenge. This result confirms the minimal effect on GSH levels observed with 8 hours exposure to TQ in the dose ranging study (Figure 3.5C). A lack of effect on GSSG levels was expected and is entirely consistent with the known antioxidant/superoxide-scavenging properties of TQ (discussed in Section 3.1.1).

Overall, the expected effects on LDH and GSH/GSSG levels were observed with all compounds. As intended, none of the selected quinone concentrations caused cytotoxicity. An oxidative stress was observed with four of the five quinones, with BQ, DMNQ and MNQ also inducing marked GSH depletion. Based on the biochemical data, TQ did not result in any significant challenge. This may in part be due to its antioxidant properties.

4.3.2. Transcriptional Investigations

Overall the transcriptional responses induced by each quinone were comparable in magnitude, with a steady increase in the number of significantly regulated genes over time (Figure 4.2A). NQ exposed hepatocytes were the exception to this trend, which exhibited comparatively weak transcriptional responses from 4 hours onwards. When considered alongside the lack of effect on glutathione endpoints at 4 and 8 hours (Figures 4.1B and C), it is likely that the 10 μ M concentration used for NQ was too low. For this reason, downstream analysis focused on genes consistently regulated by the majority of quinones, rather than the limited numbers common to all five (Figures 4.2B and C).

4.3.2.1. Identification of Mechanism-Specific Genes

I sought to determine whether it was possible to identify genes/pathways that differentiate the mechanism through which quinones exert toxicity. Cluster analysis of genes regulated by three quinones with arylating reactivity (BQ, MNQ and TQ) and the pure redox cycler DMNQ was carried out (Figure 4.3). The analysis failed to identify any gene clusters specifically associated with the arylating quinones or DMNQ. This finding indicates that in rat hepatocyte cultures it is not possible to differentiate the mechanistic reactivity of quinones based on transcriptional changes. The inability of transcriptional analysis to differentiate the mechanistic reactivity of quinones is most likely due to the ability of arylators and redox cyclers to induce oxidative stress. Quinones with redox cycling capacity induce oxidative stress through enhanced ROS generation. Arylating quinones have the capacity to mimic oxidative stress induced by redox cycling quinones through GSH depletion and potentially redox cycling of their GSH-quinol conjugates.

4.3.2.2. Biological Theme Analysis

Applying biological theme analysis provided a high level functional overview of the transcriptional response to quinone exposure. In general EASE and IPA yielded common themes, giving greater confidence in the combined output. Early changes indicate transcriptional regulation with increased expression of TFs. This was followed by regulation of cell proliferation/growth control and nucleic acid metabolism genes (and Nrf2-target gene induction, discussed in section 4.3.2.3). By 8 hours genes involved in the DNA repair, cell cycle control and regulation of cell death/apoptosis are the predominant themes.

Overall, the results are typical of the classical cellular response to oxidative stress. Oxidative challenge leads to activation of signalling cascades and TFs, resulting in induction of oxidative stress response genes (Figure 1.7). These effect DNA repair, halt cell cycle progression and detoxify ROS. Depending on the severity of the oxidative insult and whether damage can be repaired, cells survive or die. At 8 hours the biological theme analyses for this study suggest the outcome could be either way.

4.3.2.3. Transcriptional Responses in Nrf2-Target and DNA Damage-Response Genes

With the exception of TQ, exposure of hepatocytes to the selected quinones resulted in a detectable oxidative challenge. Thus, coordinated transcriptional regulation of genes involved in antioxidant defenses and DNA damage response was anticipated. To evaluate this, genes involved in these response pathways were extracted from the data set and significantly regulated genes presented (Figure 4.4A and B).

One of the key elements in protecting cells from the ravages of oxidative stress is the Nrf2-ARE pathway. As discussed in Section 1.3.2, activation of the Nrf2-ARE pathway results in the transcription of a battery of genes involved in antioxidant generation, ROS detoxification and phase II drug metabolism (Figure 1.8 and Table 1.6). Indeed, quinones are among a diverse group of electrophilic compounds that are known to induce the pathway (Table 1.7). Data produced in this study indicate exposure of rat hepatocytes to quinones at concentrations on the threshold of cytotoxicity results in only a limited induction of Nrf2-target genes. Comparison of the Nrf2-target genes significantly regulated in this study (Figure 4.4A) to the battery of genes known to contain AREs (Table 1.6) supports this suggestion. The quinones that had the most marked effect on GSH and GSSG levels (MNQ, DMNQ and BQ) elicited relatively weak responses in Nrf2-target genes. It is also worth noting that *Nqo1*, the gene that encodes NQO1 (an enzyme important in the detoxification of quinones)[28;135], was only transcriptionally increased with TQ exposure.

An important finding is that TQ was the most potent inducer of the Nrf2-target genes in this study. By 8 hours six Nrf2-target genes were increased with TQ exposure (*Cat*, *Hmox1*, *Gclc*, *Gclm*, *Gsr* and *Nqo1*) in the absence of evidence of oxidative challenge (Figure 4.1C). The relative potency of TQ to induce Nrf2-target genes may account for some of its

cytoprotective properties reported in a variety of models of oxidative stress. As mentioned earlier (Section 3.1.1), TQ can inhibit lipid peroxidation [126;136], protect hepatocytes from TBHP-induced oxidative stress [125] and ameliorate cardiotoxicity associated with doxorubicin treatment [127;128]. All of these workers have cited the superoxide scavenging properties of TQ as the underlying mechanism of cytoprotection. The data generated in this study suggest that TQ's potency as a Nrf2-target gene inducer would also contribute to its cytoprotective properties.

The Nrf2-target genes that gave the most consistent transcriptional responses were *Hmox1*, *Gclc* and *Gclm*. The protein product of *Hmox1* catalyzes the rate limiting step in heme catabolism, resulting in the formation of biliverdin, carbon monoxide and free iron [137]. The action of *Hmox1* results in enhanced elimination of free heme (itself a prooxidant) and generation of products with antioxidant properties (e.g. biliverdin) [138]. Increased transcription of *Hmox1* has been demonstrated in rat hepatocytes exposed to an anoxia/reoxygenation model of oxidative stress [139]. *Gclc* and *Gclm* code for the protein subunits that form the heterodimeric enzyme γ GC synthetase (also known as γ GC ligase (GCL)), which catalyzes the rate limiting step in glutathione synthesis (discussed in Section 1.3.1). Increased transcription of *Gclc* and *Gclm* is consistent with enhanced GSH synthesis in response to quinone exposure.

The weak transcriptional response in Nrf2-target genes indicates that a more marked oxidative challenge, or indeed cytotoxicity, may be required to induce this pathway fully. Desaint *et al* [140] observed an almost identical response in two human breast cancer cell lines (MCF-7 and MCR-9) exposed to sub-cytotoxic oxidative stress (induced by H₂O₂); increased transcription of *Hmox1*, *Gclc*, *Gclm* and *thioredoxin reductase 1 (Trr1)* but no other Nrf2-target genes.

Based on the transcriptional findings, it appears that quinone exposure resulted in some form of DNA damage, as evidenced by induction of a number of GADD/DDIT genes (Figure 4.4B). These genes are a family of transcriptional regulators involved in augmenting the response to DNA damage [141], which is typically manifest by induction of growth arrest. This allows the cell time to attempt repair of damaged DNA or initiate apoptosis if the damage is too extensive [142;143].

The transcriptional responses in DNA damage-related genes were far more pronounced in hepatocytes exposed to quinones inducing marked increases in GSSG levels (i.e. DMNQ and MNQ), suggesting a correlation with the degree of oxidative stress. The association of GADD-related gene induction with oxidative stress is well documented [141;144]. And both DMNQ and MNQ have previously been shown to induce DNA damage at sub-cytotoxic concentrations in rat hepatocytes and a human myeloid leukaemic cell line (K652) [104;145].

Ddit4 (also known as RTP801) was most consistently regulated in hepatocytes exposed to quinones inducing marked GSH depletion (MNQ, DMNQ and BQ). Increased transcription was observed at 1, 4 and 8 hours with these quinones and was not noted in hepatocytes exposed to NQ or TQ, suggesting a correlation with the severity of quinone challenge. *Ddit4* was first described by Shoshani *et al* [146] as an hypoxia-inducible factor 1 (HIF-1)-responsive gene that protected dividing cell lines (PC12 and MCF7) from oxidative stress-induced apoptosis. Interestingly, they also noted that *Ddit4* over-expression was pro-apoptotic in terminally differentiated (i.e. non-dividing) cells, such as neuron-like PC12 cells. Whether *Ddit4* induction in hepatocytes exposed to MNQ, DMNQ and BQ in this study is a pro- or anti-apoptotic signal is unclear. LDH leakage data (Figure 4.1A) confirmed that there was no overt cytotoxicity in hepatocyte cultures exposed to these quinones. However, it is worth noting that hepatocytes do not proliferate *in vitro*, unless induced to do so [147] and so the *Ddit4* signal may be pro-apoptotic.

4.3.2.4. Quinone Signature Genes

This transcriptomic study has enabled the identification of a core set of 22 'quinone signature genes' that were significantly regulated co-ordinately with quinone treatment. This relationship suggests a critical role in the hepatocyte homeostatic response to quinone challenge and oxidative stress. The quinone signature genes represent a range of biological functions and pathways (indicated in Table 4.7). However, they can be broadly defined as genes involved in the immediate-early response, antioxidant response, maintenance of cellular integrity and homeostasis, pro-survival signalling, growth arrest and pro-apoptotic signalling. In general quinone signature genes correlate with the known cellular response to quinone challenge, the one exception being *Tfrc*.

Regulation of *Tfrc*

Increased transcription of *Tfrc*, which encodes the plasma membrane protein transferrin receptor 1 (TFRC), was unexpected. TFRC resides in the plasma membrane as a homodimer and plays a critical role in intracellular iron transport. TFRC binds transferrin and the resultant complex is internalised in vesicles which fuse with endosomes. The transferrin-bound iron is subsequently released and the transferrin-TFRC complex recycled to the plasma membrane. TFRC expression is post-transcriptionally regulated through modification of TFRC mRNA stability, via a regulatory sequence known as the Iron Response Element (IRE) in the 3'-untranslated region (UTR). When intracellular iron levels are low, Iron-Regulatory Proteins (IRP) 1 and 2 bind to the IRE, increasing mRNA stability and TFRC translation. Conversely, when intracellular iron levels are high IRP1 and 2 binding to the IRE is inhibited and TFRC mRNA is degraded [148-150].

The increased transcription of *Tfrc* is consistent with enhanced uptake of iron by the rat hepatocytes. This could potentially exacerbate quinone-induced oxidative stress via the Fenton reaction (discussed in Section 1.2.1). Increases in TFRC mRNA and/or protein levels in response to oxidative stress have been observed *in vitro* previously. Kotamraju *et al* [151] noted that exposure of endothelial cells to 0.5 μ M doxorubicin increased TFRC protein levels between 2 and 16 hours. Exposure of the murine fibroblast B6 cell line to 100 μ M H₂O₂ increased TFRC mRNA levels at 4 and 6 hours [152]. Stabilisation of TFRC mRNA through increased IRP binding to the IRE was confirmed as the mechanism. Conversely, exposure of B6 cells to relatively high levels of MNQ (100 μ M) for 2 hours leads to decreased TFRC mRNA stability [153]. The same group also reported that IRP-1 activity increased within 15-30 minutes of exposure to relatively low concentrations of MNQ (10-50 μ M). This may have resulted in increased TFRC mRNA stability, although it appears this was not assessed. The consistent increase in *Tfrc* transcription observed with quinone exposure in this study is surprising given it may exacerbate the toxicity of quinones, although it is in line with other reports.

Transcription Factors

Five transcription factors (*Egr1*, *Fos*, *Fos11*, *MafK* and *Cebpb*) were increased in the quinone signature gene set. *Egr1*, *Fos* and *Fos11* belong to a group of transcripts collectively known as immediate-early response genes. *Egr1* encodes the early growth

response 1 transcription factor that is transcriptionally induced in response to a range of stress and mitogenic stimuli [154], including oxidative stress [155]. Nair *et al* [156] observed increased *Egr-1* transcription in the neurone-derived PC12-DR2 cell line exposed to 200 μ M H₂O₂. Sub-population analysis identified *Egr1* regulation to be associated with cell survival.

Fos (also known as *c-fos*), *Fos11* (*Fos-like 1*, also known as *Fos-related antigen 1*) and *MafK* (*small Maf K*) encode three of a multitude of subunits that hetero- and homodimerise to form transcription factors collectively known as Activator Protein-1 (AP-1) [157;158]. AP-1 TFs induce transcription of target genes involved in the control of a variety of cellular processes, including proliferation, differentiation, and pro- and anti-apoptotic signalling [157-159]. However the precise roles that different AP-1 dimers play in controlling these cellular processes is poorly understood.

There is an interesting correlation in the transcriptional increases in *Fos* and *Fos11* observed in this study with data published by Venugopal and Jaiswal [160]. Overexpression of *Fos* and *Fos11* in HepG2 cells by transfection with expression plasmids resulted in repression of Nrf2-target genes (e.g. *Nqo1*). They suggested that increased concentrations of AP-1 heterodimers containing either *Fos* or *Fos11* negatively regulate transcription of ARE-containing genes by interfering with binding of the Nrf2 transcription factor. Thus increased transcription of *Fos* and *Fos11* observed in this study may account for the relatively weak transcriptional responses observed for Nrf2-target genes (as discussed in Section 4.3.2.3).

Cebpb encodes C/EBP β (also known as nuclear factor for interleukin 6), a TF belonging to the CCAAT/enhancer-binding protein (C/EBP) family. A role for C/EBP β in GST induction has been demonstrated *in vitro*. Exposure of the rat hepatocyte-derived cell line H4IIE to the cancer chemopreventive agent oltipraz induced GSTA2 mRNA and protein levels via a C/EBP β dependent mechanism [161]. Kang *et al* later proposed C/EBP β augmented induction of GSTA2 via binding to a C/EBP response element upstream of the ARE, also suggesting a role in potentiating Nrf2-ARE pathway induction in response to oxidative stress [84].

Antioxidant Response

Two genes linked to antioxidant generation, *Hmox1* and *Mat2a*, were increased with quinone exposure. As discussed in Section 4.3.2.2, *Hmox1* mediates the detoxification of pro-oxidant heme and generates products with antioxidant properties. *Mat2a* encodes the enzyme methionine-adenosyl transferase 2a, transcription of which is responsive to oxidative stress [74] and the encoded enzyme is part of the homocysteine pathway. The MAT2A enzyme generates adenosyl-methionine, shunting methionine towards homocysteine generation. This has the effect of increasing the availability of cysteine for replenishment of the GSH pool during oxidative stress (as discussed in Section 1.3.1).

Maintenance of Cellular Integrity/Morphology

Changes in cellular morphology, such as plasma membrane blebbing, often precedes cytotoxicity associated with quinone exposure. MNQ exposure has been shown to induce changes in morphology (i.e. blebbing) in a variety of cell lines [162]. Thor *et al* [102] demonstrated that damage to the cytoskeleton is partly responsible for quinone-induced morphological change in hepatocytes. Both arylating and redox-active quinones have been shown to induce cytoskeletal protein (e.g. actin) crosslinking, although the biochemical nature of lesions differ [102]. In addition to the cytoskeleton there are a range of associated structures, including cell adhesion molecules, anchoring domains and microfilaments that are potential targets of quinone-mediated damage. Three genes linked to the organisation of the cytoskeleton, maintenance of cell-cell adhesion and extracellular matrix interactions (*Epha2*, *Mylip* and *Tgm1*) were increased in the quinone signature genes.

Epha2 was the only gene whose transcription was increased at all time points. *Epha2* encodes Ephrin receptor A2, a tyrosine kinase with established roles in neuronal migration and general cell-cell interaction and extracellular matrix attachment [163]. *Epha2* overexpression has also been implicated in promoting cell survival in tumour cells [164;165] and the gene is induced in models of hypoxia [166]. *Tgm1* encodes transglutaminase 1, an enzyme that catalyses the post translational cross-linking of proteins [167]. *Tgm1*, and other transglutaminases are known to be important in cell-cell and cell-matrix adhesion. No association of *Tgm1* induction with oxidative stress has been made. However, *Tgm2* (the so-called 'tissue-type' transglutaminase) has been shown to be induced in primary astrocytes exposed to oxidative stress [168].

Mylip (also known as MIR) encodes an E3 ubiquitin-protein ligase that mediates ubiquitination and subsequent proteasomal degradation of myosin regulatory light chain (MRLC) [169;170]. A role in influencing cytoskeleton interactions, cell morphology and motility have been demonstrated in Swiss 3T3 fibroblasts [170] and neuronal cell lines [169;171]. Transcriptional regulation of *Epha2*, *Tgm1* and *Mylip* may indicate adaptive maintenance of cellular morphology/extracellular matrix interactions in response to quinone challenge.

The increased transcription of *Chka* may be indicative of an adaptive response to quinone-mediated plasma membrane damage. *Chka* encodes one of the subunits of the enzyme choline kinase (CK), which catalyzes the phosphorylation of choline to phosphocholine, the first step in the biosynthesis the membrane lipid phosphatidylcholine (PC) [172;173]. Increased CK activity is observed in many human tumours [172;174] and overexpression in cell lines confers them oncogenic properties [175]. It has also been noted that CK induction occurs in response to cellular stresses, including that evoked in the liver by carbon tetrachloride (CCl₄) exposure [173]. In hepatocytes CCl₄ is metabolized to the trichloromethyl radical, a compound that can initiate lipid peroxidation[51]. As discussed in Section 1.2.2, lipid peroxidation results in extensive damage to lipid membranes and potentiates ROS generation. It is possible that increased transcription of *Ckha* is an attempt to enhance PC synthesis to facilitate repair of plasma membrane damage caused by quinone-induced oxidative stress.

Maintenance of Homeostasis

The increased transcription of *Slc5a3* and *Pdk4* provides some evidence of adaptive responses to perturbed homeostasis with quinone exposure. *Slc5a3* (also known as sodium/*myo*-inositol cotransporter (SMIT)) encodes a symporter protein that plays a critical role in maintaining cell volume through osmotic control [176]. The SLC5A3 symporter effects this control through the transport of *myo*-inositol, a small molecule belonging to a class of compounds known as organic compatible (or nonperturbing) osmolytes [177]. Maintenance of a constant cell volume is important for normal function and survival [176] and *Slc5a3* is induced in cell culture in response to hyperosmotic stress [178]. Indeed, hyperosmotic stress and cell dehydration sensitizes cells to apoptosis [179]. There has also been some suggestion that oxidative stress can induce cell dehydration and shrinkage [177].

Increased transcription of *Slc5a3* with quinone exposure is consistent with an attempt to maintain cell volume in response to oxidative challenge.

Pdk4 encodes one of four isoforms of pyruvate dehydrogenase kinase (PDK) and is strongly upregulated in starvation [180]. PDKs play a critical role in regulating the contribution that glucose and fatty acids (FAs) make to energy production. This is achieved through the PDK-directed inactivation of the pyruvate dehydrogenase complex (PDC). Inactivation of PDC results in glucose conservation and increased utilisation of FAs for energy production. The net effect is increased generation of acetyl-CoA via FA beta-oxidation for utilisation in the tricarboxylic acid cycle [180-183]. The induction of *Pdk4* implies quinone exposure has depleted hepatocyte glucose levels. A possible mechanism for this depletion is quinone-mediated disruption of the respiratory chain. Quinones, including MNQ and doxorubicin, can interfere with electron flow through the respiratory chain, increasing utilisation of reducing equivalents [34]. This would most likely result in glucose depletion necessitating a shift towards utilising FAs as an energy source. Indeed, supplementing hepatocytes with glycolytic substrates (e.g. fructose) has been shown to ameliorate quinone cytotoxicity [20]. Menadione exposure of white fat cells *in vitro* has also been shown to increase glucose oxidation [184].

Growth Arrest Genes

Regulation of genes involved in growth arrest is entirely consistent with oxidative stress and DNA damage. Increased transcription of GADD and DDIT-related genes were observed primarily with quinones inducing marked oxidative challenge (Figure 4.4B). However, two genes implicated in growth arrest and cell cycle control were increased in the quinone signature set. *Dusp5* is a p53-target gene and encodes a protein phosphatase that has been shown to display activity towards mitogen-activated protein kinase 3 (MAPK3) [185] and extracellular response kinase 1 (ERK1) *in vitro* [186]. Dephosphorylation of MAPK3 and ERK1 is believed to negatively regulate cell-cycle progression [185], thus increased *Dusp5* transcription is consistent with growth arrest associated with DNA damage.

Okl38 is a pregnancy-induced growth inhibitory factor first described by Huynh *et al* [187]. Expression was low in breast cancer cell lines and almost completely lost in dimethylbenz(A)anthracene-induced breast tumours. They also demonstrated that

transfection of MCF-7 cells with *Ok138* cDNA resulted in reduced oncogenicity in nude mice. *Ok138* cDNA transfection of Chang liver cells has been shown to induce growth inhibition leading to cell death and loss of expression in hepatocarcinomas is associated with uncontrolled growth [188]. Recently *Ok138* induction has been reported in human aortic endothelial cells (HAEC) exposed to oxidative stress [189]. Microarray analysis of HAEC cells treated with *tert*-butylhydroquinone detected >10-fold induction in *Ok138* transcription at 4 hours. Li *et al* [189] also demonstrated that RNA interference (RNAi) of Nrf2 ablated this response, concluding that *Ok138* is an Nrf2-target gene.

Pro-Survival Signalling

Regulation of three genes (*Pim3*, *Vegfa* and *Gdf15*) with known roles in cell survival was observed. Transcription of the proto-oncogene *Pim3* was increased from 1 hour, indicating an important role in the early response of hepatocytes to quinone exposure. *Pim3* is a member of the PIM family of serine/threonine kinases that are known to negatively regulate apoptosis [190]. *Pim3* has been shown to inhibit apoptosis in several colon cancer cell lines (e.g. SW480, HT29 and HCT116) through inactivation of the pro-apoptotic protein BAD [191]. Aberrant expression of *Pim3* has been observed in hepatocellular carcinoma development and its ablation in human hepatoma cell lines with RNA interference increases apoptosis [192].

Increased transcription of *Vegfa* with quinone exposure was not unexpected. *In vivo Vegfa* plays a critical role in tissue responses to hypoxia, inducing angiogenesis [193].

Overexpression is also associated with increased tumour growth and metastatic spread [194]. *In vitro Vegfa* overexpression is observed in a variety of cells, enhancing cell survival with hypoxic and oxidative challenge [194-197].

Gdf15 is an immediate-early response gene belonging to the tissue growth factor beta (TGF β) superfamily and is thought to play a positive role in cell survival [198-200].

Induction of *Gdf15* has been observed in a number of organs in response to tissue injury, including the brain, lung, kidney and liver [201-205]. Increased transcription of *Gdf15* has been described following ischemic/reperfusion and CCl₄-induced hepatic injury [201;206], both of which have an oxidative stress component. Navarro-Sabate *et al* [206] demonstrated that *Gdf15* was one of the key genes regulated during ischemic preconditioning of a perfused rat liver model.

The induction of *Gdf15*, *Vegfa* and *Pim3* is consistent with positive cell survival signalling. Significantly, transcriptional regulation of *Pim3* has not been reported in response to quinone exposure or oxidative stress.

Pro-Apoptotic Signalling

As well as pro-survival signals, genes with pro-apoptotic function were also increased. *Brd2* (also known as RING3) is a nuclear serine/threonine kinase implicated in transcriptional regulation [207]. Zhou *et al* [208] have suggested a role for *Brd2* in initiating apoptosis in COS7 and HNE1 cells. *In vivo*, *Brd2* has been linked to induction of apoptosis in mammary gland epithelial cells during the reproductive cycle of mice [209]. *Zfp36*, also known as tristetraprolin (TTP), is a zinc finger protein involved in the regulation of inflammatory cytokine levels, for example tumour necrosis factor alpha (TNF α) [210]. This is achieved through binding and destabilisation of target mRNAs. A synergistic role for TTP in TNF α -mediated apoptosis has also been demonstrated [211].

A third transcriptional change suggestive of a pro-apoptotic signal was the decrease in *LOC498331* transcription. *LOC498331* is the rodent orthologue of PTPN13, the human gene that encodes protein tyrosine phosphatase, non-receptor type 13. PTPN13, also known as FAP-1 (CD95 (FAS)-associated phosphatase) is involved in regulation of FAS death receptor-mediated apoptosis [212;213]. PTPN13 is overexpressed in a number of tumours and cell lines and confers resistance to FAS-mediated apoptosis by interfering with signal transduction [213-215]. Decreased expression with quinone exposure may result in increased sensitivity of hepatocytes to apoptosis. The changes observed in *Brd2*, *Zfp36* and *LOC498331* transcription are consistent with pro-apoptotic signalling.

4.3.2.5. Correlating Quinone Signature Genes with the Biology of Quinone Challenge

With the exception of Nrf2-target genes, comprehensive regulation of functional pathways was not observed consistently with quinone exposure. However, the majority of the quinone signature genes do correlate with known biological effects of quinone exposure. The quinone signature genes have been placed into the biological context of quinone challenge and oxidative stress (Figure 4.6). Transcriptional changes in Nrf2-target genes and DNA damage response genes have also been added to the model.

A number of the genes identified are well documented as being regulated in response to oxidative stress, and in some cases quinone exposure (e.g. *Fos*, *Egr1*, *Vegfa*, *Gdf15*, *Hmox1*, *Mat2a* and *Okl38*). The presence of these genes validates the data analysis strategy used, conferring greater confidence in the novel transcriptional changes identified. Significantly, *Pim3*, *Dusp5*, *Mylip*, *Pdk4* and *Slc5a3* have not previously been associated with quinone exposure or oxidative stress. The consistent transcriptional regulation of these novel genes implies a key role in the ameliorative response of hepatocytes to quinone challenge.

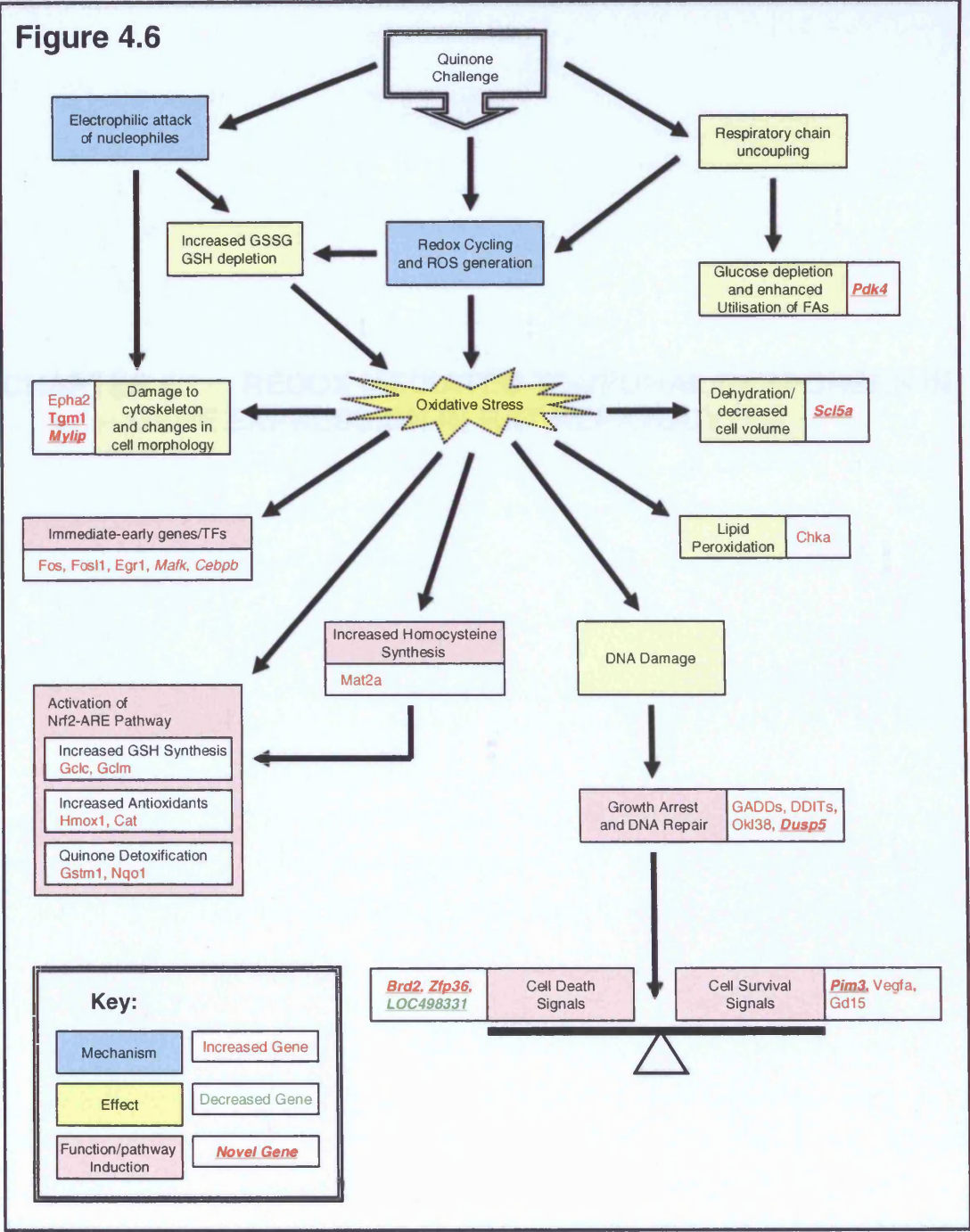


Figure 4.6: Quinone signature genes integrated into a model of quinone challenge

Quinones exert toxicity through two primary reactivities; redox cycling and arylation of cellular nucleophiles, both resulting in increased GSSG levels, GSH depletion, oxidative stress and damage to cellular macromolecules. In addition, redox cycling quinones can disrupt the normal flow of electrons through the respiratory chain, resulting in enhanced ROS generation and perturbed energy metabolism. The downstream effects of these mechanisms of toxicity are highlighted (yellow boxes), with the cellular responses to counter them also indicated (red boxes). Genes consistently regulated with quinone exposure have been overlaid into the context of the cellular responses to oxidative stress and quinone toxicity.

**CHAPTER 5. REDOX MEDIATED TEMPORAL RESPONSES IN
GENE EXPRESSION IN RAT HEPATOCYTES**

5.1. Introduction

Transcriptional investigations in rat hepatocytes exposed to five different quinones with varying reactivity, in terms of arylating and redox cycling potential, enabled the identification of a core set of 'quinone signature genes' (Chapter 4). The majority of 'quinone signature genes' were found to correlate with known biological effects of quinone exposure (i.e. oxidative stress, GSH depletion, DNA damage, cytoskeletal changes). However, with the exception of genes encoding proteins belonging to the nuclear factor (erythroid-derived 2)-like 2-antioxidant response element (Nrf2-ARE) pathway, comprehensive regulation of functional pathways was not consistently observed. This may have been partly due to the diverse reactivity of the five quinones selected (as reviewed in Chapter 3). Thus, it was decided to conduct a more comprehensive transcriptional analysis, focussing on the response of rat hepatocytes to quinone-mediated redox challenge.

To this end transcriptional responses induced by 2,3-dimethoxy-1,4-naphthoquinone (DMNQ) and menadione (MNQ) exposure, the two quinones previously shown to cause the most marked and consistent redox challenge, were investigated. The main aim of this study was to identify key pathways regulated in response to DMNQ and MNQ over a 24 hour exposure period. It was hoped that analysis of responses to the two quinones with such similar redox activities would allow the identification of critical response pathways through which cells seek to counter redox challenge and promote cell survival. In addition, it was envisaged that the transcriptional investigations may provide an improved mechanistic understanding of cellular systems perturbed by quinone exposure and redox stress. Exposure of rat hepatocytes to concentrations of each quinone, previously identified as being on the threshold of causing cytotoxicity following 8 hours exposure (Chapter 3), was carried out. It was anticipated that with an extended exposure period of 24 hours, 150 μ M DMNQ or 25 μ M MNQ would result in an increase in cytotoxicity relative to control cultures. It was hoped that this experimental design would address the question of whether the battery of Nrf2-target genes require more overt cytotoxicity for transcriptional induction.

Transcriptional responses were evaluated using the Rat Whole Genome 230 2.0 Affymetrix GeneChip[®] microarrays. They contain over 31,000 probe sets representing approximately 28,000 rat genes, allowing a far more comprehensive transcriptional readout than the

GSKrat1a GeneChips[®] previously used (Chapters 3 and 4). As before (Chapter 4), biological theme analysis was carried out on transcriptional data to gain insight into the functional effects of DMNQ and MNQ exposure. In addition, clustering analysis was carried out to group regulated genes into clusters that share common temporal profiles for both quinones.

5.2. Results

Rat hepatocyte monolayer cultures were exposed to vehicle control (VC), DMNQ (150 μ M), or MNQ (25 μ M) for up to 24 hours (according to the methodology outlined in Section 2.1). At a number of time points during the 24 hours exposure period cultures were sampled for lactate dehydrogenase (LDH) leakage, cellular reduced glutathione (GSH) and oxidised glutathione (GSSG) levels, media total glutathione and total RNA.

5.2.1. Biochemical Endpoints

LDH leakage, cellular GSH/GSSG levels and total media glutathione were determined as outlined in Sections 2.3 and 2.7.2, respectively. Triplicate or duplicate cultures exposed to either VC, DMNQ or MNQ from two or three replicate experiments were sampled.

LDH leakage was assessed at 1, 2, 4, 6, 8, 12, 18 and 24 hours (Figure 5.1). No significant increases in LDH leakage were observed between 1 and 8 hours with DMNQ or MNQ exposure. A gradual increase in LDH leakage was noted in DMNQ and MNQ exposed cultures compared to the concurrent controls from 12 hours onwards. LDH leakage peaked at 24 hours, with DMNQ and MNQ exposure resulting in approximately 70 and 90 percent total LDH leakage, respectively versus approximately 50 percent in VC exposed cultures.

Cellular GSH levels were assessed at 1, 4, 6, 8, 12, 18 and 24 hours (Figure 5.2). Significant decreases in GSH were observed in DMNQ exposed cultures compared to VC exposed cultures from 4 hours onwards. The decrease in GSH was most marked at 8 hours (approximately 25 percent of VC levels) and plateaued between 12 and 24 hours (at approximately 40 percent of VC levels). Significantly decreased GSH levels were observed in MNQ exposed cultures between 1 and 8 hours compared to VC exposed cultures. From 12 hours onwards no significant decreases in GSH levels were observed in MNQ exposed cultures and a general trend of returning to basal levels was seen.

Cellular GSSG levels were assessed at 1, 4, 8, 18 and 24 hours (Figure 5.3). Significant increases in GSSG levels were observed in DMNQ and MNQ exposed cultures compared to VC exposed cultures at 1 and 4 hours. With DMNQ and MNQ exposed cultures, increases were most marked at the 1 hour time point and returned to control levels by 8 hours.

Media total glutathione levels (expressed as percent of total glutathione) were assessed at 1, 4, 8, 12 and 18 hours (Figure 5.4). Significant increases in media total glutathione levels were observed at all time points (except 18 hours) in DMNQ and MNQ exposed cultures when compared to VC exposed cultures. Proportionately the most marked increases were at the 1 hour time point, with approximately 21 and 17-fold increases in media glutathione levels in DMNQ and MNQ exposed cultures, respectively. There was also a general trend of increased media total glutathione levels with time in VC exposed cultures from 12 hours onwards.

Figure 5.1

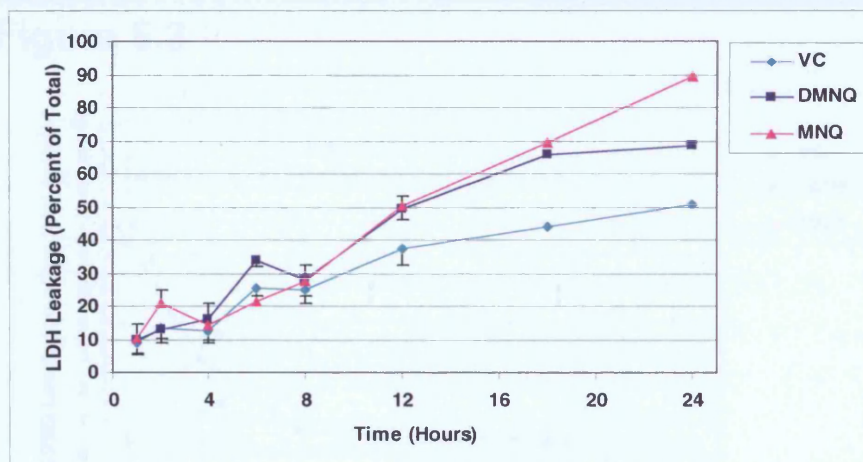


Figure 5.1: Percent LDH leakage in rat hepatocyte monolayers exposed to VC, DMNQ or MNQ for 1, 2, 4, 6, 8, 12, 18 and 24 hours. Results are mean values \pm SD (1 to 12 hours n=3 repeat experiments; 18 and 24 hours n=2 repeat experiments). ANOVA and post-hoc Dunnett's T-test.

Figure 5.2

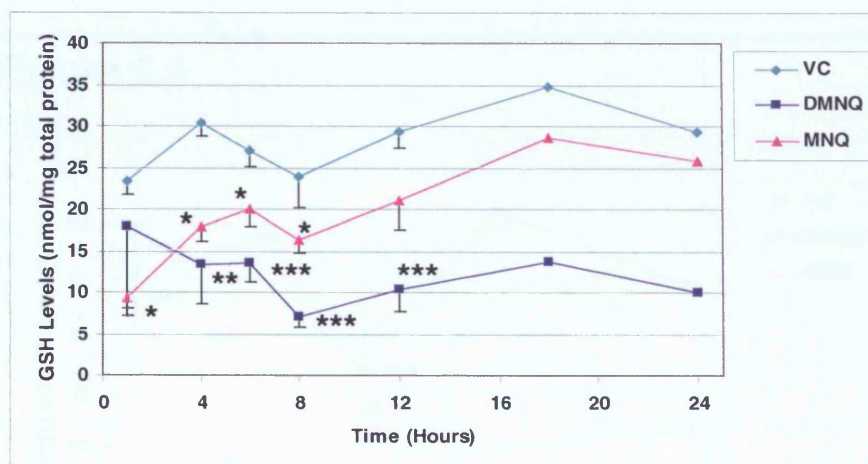


Figure 5.2: GSH levels in rat hepatocyte monolayers exposed to VC, DMNQ or MNQ for 1, 4, 8, 18 and 24 hours. Results are mean values \pm SD (1 to 12 hours n=3 repeat experiments; 18 and 24 hours n=2 repeat experiments). ANOVA and post-hoc Dunnett's T-test. * = $P < 0.05$, ** = $P < 0.01$, *** = $P < 0.001$ versus VC.

Figure 5.3

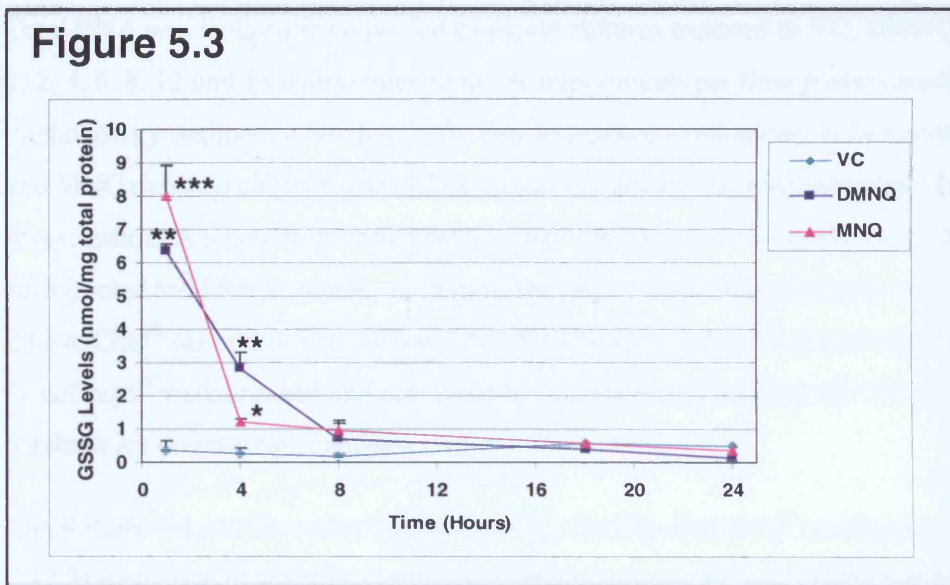


Figure 5.3: GSSG levels in rat hepatocyte monolayers exposed to VC, DMNQ or MNQ for 1, 4, 8, 18 and 24 hours. Results are mean values \pm SD (1 to 8 hours n=3 repeat experiments; 18 and 24 hours n=2 repeat experiments). ANOVA and post-hoc Dunnett's T-test. * = P<0.05, ** = P<0.01 versus VC.

Figure 5.4

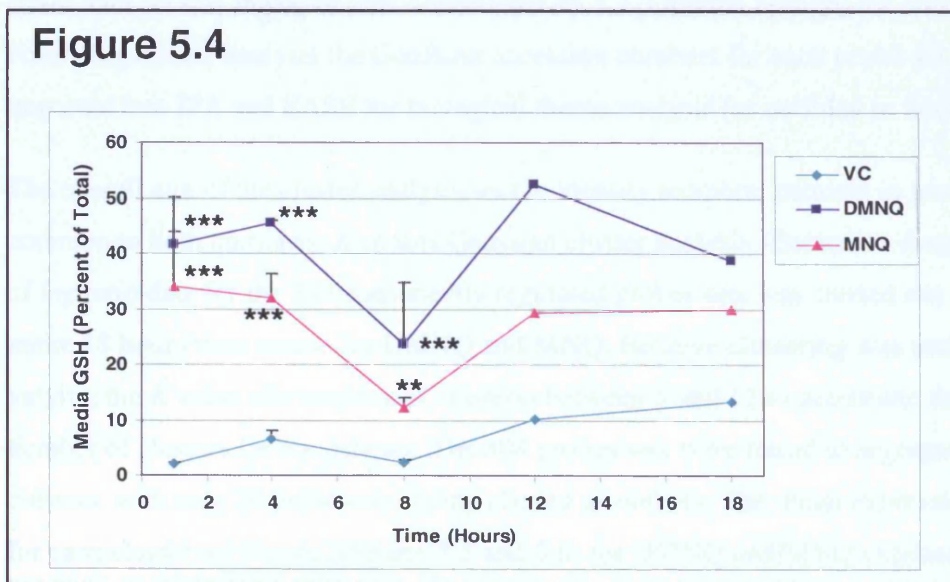


Figure 5.4: Media total glutathione levels in rat hepatocyte monolayers exposed to VC, DMNQ or MNQ for 1, 4, 8, 18 and 24 hours. Results are mean values \pm SD (1 to 12 hours n=3 repeat experiments; 18 hours n=2 repeat experiments). ANOVA and post-hoc Dunnett's T-test. * = P<0.05, ** = P<0.01, *** = P<0.001 versus VC.

5.2.2. Transcriptomic Investigations

Total RNA was isolated from pooled triplicate cultures exposed to VC, DMNQ, or MNQ at 1, 2, 4, 6, 8, 12 and 18 hours (three replicate experiments per time point) (according to the methodology outlined in Section 2.10). Due to marked cytotoxicity at 24 hours in DMNQ and MNQ exposed cultures, total RNA yields and quality were not adequate for GeneChip[®] investigation. A single fragmented biotinylated-cRNA target synthesis was prepared for each pooled total RNA sample and hybridised onto a single Rat Genome Array 230 version 2 GeneChip[®] (as outlined in section 2.12). Following hybridisation and washing, GeneChips[®] were scanned and data pre-analysed prior to transfer to the Rosetta Resolver[®] database for downstream analysis.

The RatioBuild and Trend Set functions within Rosetta Resolver[®] (outlined in section 2.12.3) were used to generate comparison tables between VC and DMNQ or MNQ treated groups. For each time point, a ratio trend set was produced across the entire time course for both quinones and the *log* ratio change in expression and *p*-value exported for all probe sets regulated (threshold values of $> \pm 2$ -fold change and $p \leq 0.05$) at 4 points across the entire data set. A total of 804 probe sets fitted this selection criteria and the *log* ratio data for the entire data set was imported into ArrayMiner v5.3.2 (Optimal Design) for cluster analysis. Following cluster analysis the GenBank accession numbers for each probe set was imported into IPA and EASE for biological theme analysis (as outlined in Section 2.12.3).

The overall aim of the cluster analysis was to identify temporal patterns in gene expression common to both quinones. *K*-means Gaussian cluster analysis (Euclidian distance measure) of *log* ratio data for the 804 consistently regulated probes sets was carried out across the entire 18 hours time course for DMNQ and MNQ. Iterative clustering was undertaken by varying the *K* value (the number of clusters) between 5 and 12 to determine the optimal number of clusters for the data set. The 804 probes sets were found to segregate well into 8 clusters, with only 20 probes sets being classed as outliers. The mean expression profiles for each cluster are shown (Figures 5.5 and 5.6) for DMNQ and MNQ exposed cultures*. Overall the temporal profiles for each quinone were very similar for all 8 clusters.

*A full list of probe sets segregating to each of the eight clusters is presented in the supplementary data disc, Chapter 5 (804_DMNQ_MNQ_probe_sets_clustered.xls).

Probes sets displaying a trend of decreased transcription segregated to clusters C1, C2, C6 and C8 (398 probe sets in total) (Figure 5.5). Cluster C1 contained probe sets that showed a gradual trend in decreased transcription across the entire time course, peaking at 18 hours. Clusters C2 and C6 contained genes that showed slight (C2) or moderate (C6) decreases in transcription from 4 hours, plateauing from 12 hours onwards. Cluster C8 contained genes displaying a transient decrease in transcription between 4 and 8 hours, followed by a return to basal levels for the remainder of the time course. Probe sets displaying a general trend in increased transcription segregated to clusters C3, C4, C5 and C7 (386 probe sets in total) (Figure 5.6). Clusters C3 and C4 contained genes that showed moderate increases in transcription from 4-6 hours, plateauing at 12 to 18 hours. Cluster C5 contained genes that showed slight increases in transcription between 6 and 12 hours. Cluster C7 contained genes displaying the most marked responses, with rapid increases in transcription between 2 and 6 hours that peaked at 12 hours.

The Genbank accession numbers for the probe sets within each of the eight clusters were imported into IPA to gain an overview of the key functional classes of genes within each cluster. The top five molecular functions reported for each cluster are presented in the tables adjacent to each cluster profile within Figures 5.5 and 5.6. Overall similar classes of genes were represented in increased and decreased clusters, with the key themes being cell cycle/growth control, cell death and cell morphology-related molecular functions. The DNA repair-related and energy production functional classes were only represented in the increased clusters.

Figure 5.5

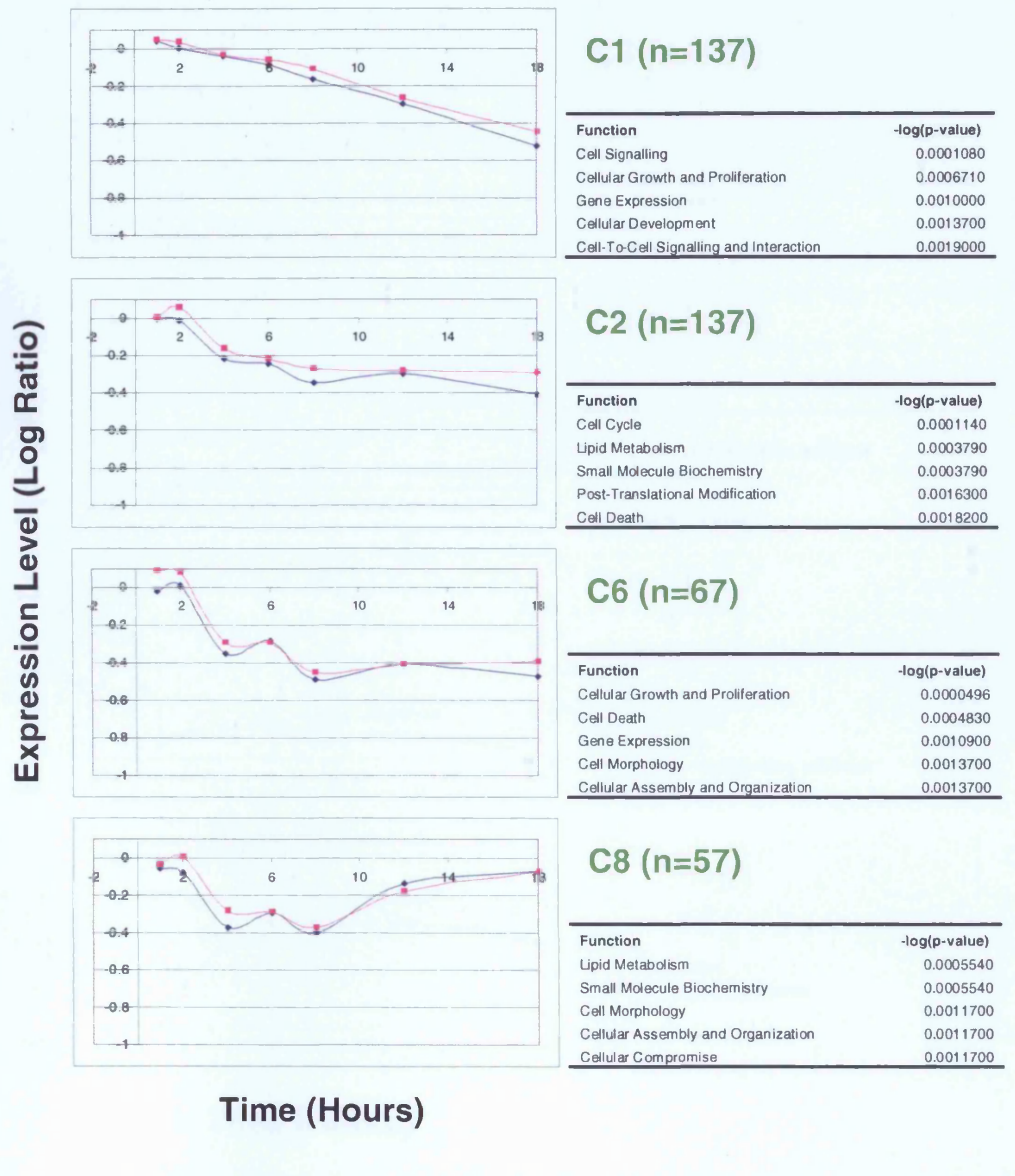


Figure 5.5: Mean profiles of clusters C1, C2, C6 and C8, decreased with DMNQ (blue profiles) and MNQ (pink profiles) exposure.

The cluster size (*n* in parenthesis) indicates the number of probe sets segregating to each cluster. The table to the right of each profile indicates the top five molecular functions associated with each cluster and the significance (expressed as $-\log(p\text{-value})$) assigned by IPA.

Figure 5.6

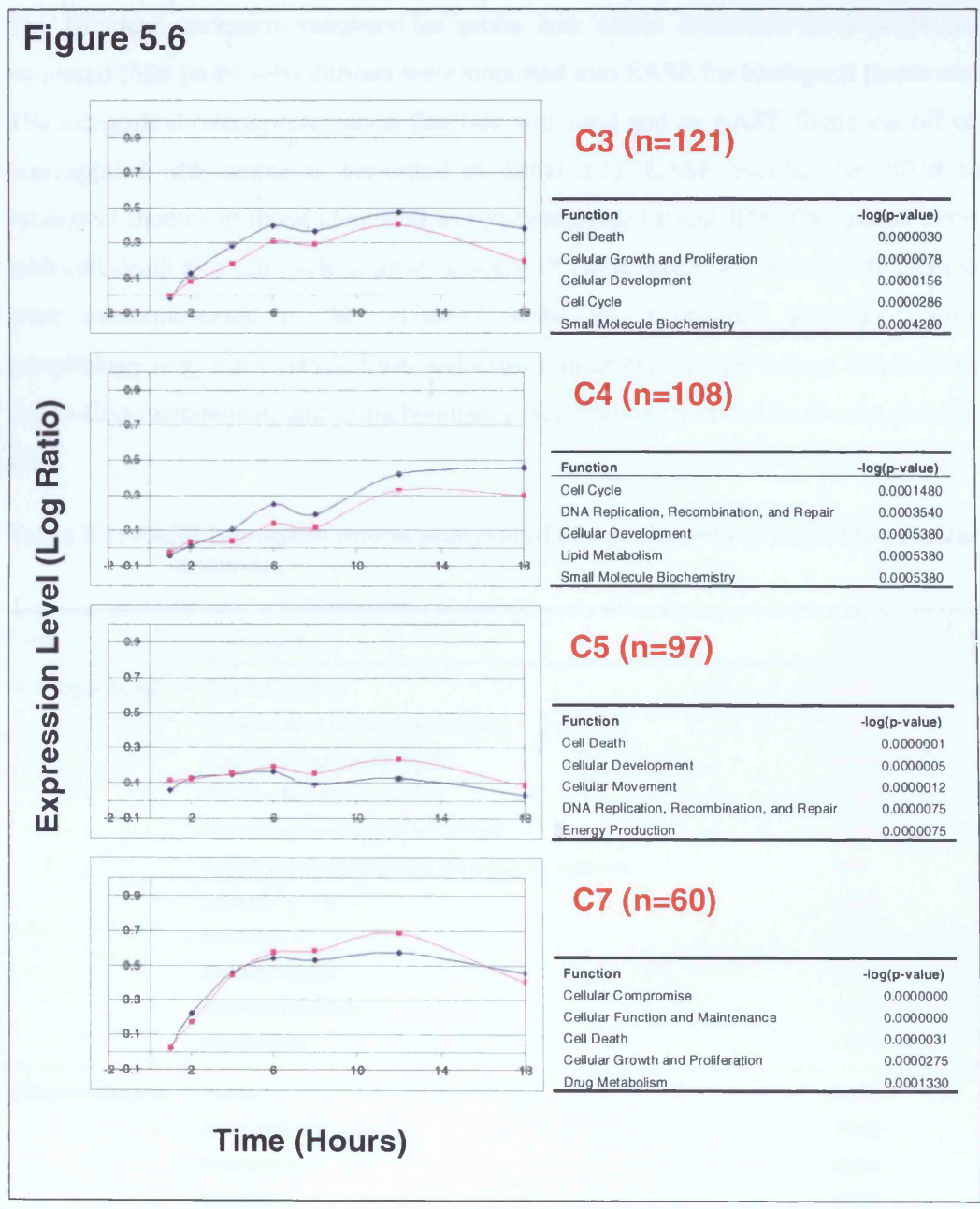


Figure 5.6: Mean profiles of clusters C3, C4, C5 and C7, increased with DMNQ (blue profiles) and MNQ (pink profiles) exposure.

The cluster size (n in parenthesis) indicates the number of probe sets segregating to each cluster. The table to the right of each profile indicates the top five molecular functions associated with each cluster and the significance (expressed as $-\log(p\text{-value})$) assigned by IPA.

The Genbank accession numbers for probe sets within decreased (398 probe sets) or increased (386 probe sets) clusters were imported into EASE for biological theme analysis. The categorical overrepresentation function was used and an EASE Score cut-off of 0.05 was applied (the output is presented in Table 5.1). EASE analysis identified similar biological themes to those identified as overrepresented using IPA. Categories associated with cell death and cell cycle control, along with DNA repair (e.g. nucleotide metabolism) were overrepresented in the increased probe set. Categories associated with cell morphology (e.g. actin cytoskeleton and extracellular matrix) and energy metabolism (e.g. acetyl-CoA metabolism and mitochondrion) were overrepresented in the decreased probe set.

Table 5.1: EASE biological theme analysis of 804 probe sets selected for cluster analysis.

System	Gene Category	EASE Score
GO Biological Process	Physiological process	0.0338
	Induction of apoptosis by intracellular signals	0.0339
	Regulation of programmed cell death	0.0366
	Induction of programmed cell death	0.0366
	Positive regulation of programmed cell death	0.0366
	Nucleobase/nucleoside/nucleotide and nucleic acid metabolism	0.04
	Cell cycle	0.0432
	Metabolism	0.0251
	Alcohol metabolism	0.039
	Acetyl-CoA metabolism	0.0477
	Organogenesis	0.0518
GO Cellular Component	Nucleus	0.0398
	Actin cytoskeleton	0.0232
	Mitochondrion	0.0256
	Intracellular	0.0421
	Extracellular matrix	0.0556
GO Molecular Function	Binding	0.0148
	Cytokine activity	0.0155
	Nucleic acid binding	0.0246
	DNA binding	0.0391
	Transferase activity/transferring acyl groups	0.0543

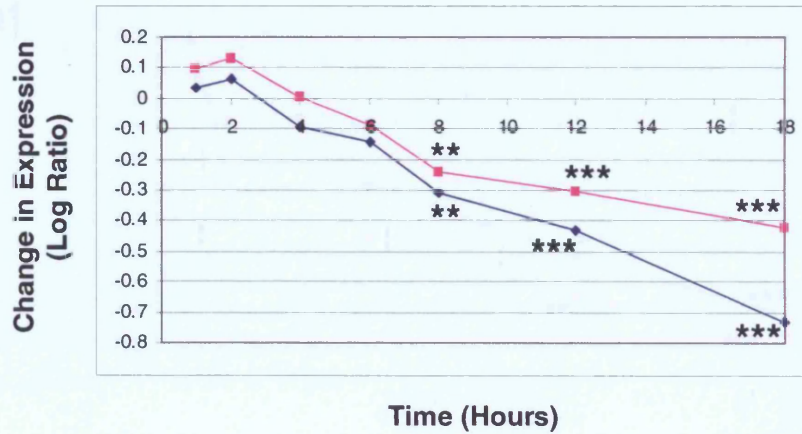
The table shows the results of EASE analysis for the 804 probe sets selected for cluster analysis. GO classes with an EASE score of ≤ 0.05 are shown. Direction of change is indicated by the EASE score font colour (Red = increased, Green = decreased).

In clusters C1 and C6 a large proportion of genes involved in proliferation/cell cycle control and apoptotic signalling were represented. A number of exemplar genes from these clusters, displaying decreased temporal trends in transcription, were selected for more detailed interpretation. In cluster C1, *tissue growth factor beta 2 (Tgfb2)* and *apoptotic peptidase factor 1 (Apaf1)* showed significant decreases in transcription from between 6 and 8 hours, peaking at 18 hours, with both DMNQ and MNQ exposure (Figures 5.7A and B, respectively). Both *Tgfb2* and *Apaf1* were represented in the top two molecular functions identified for cluster C1 (cell signalling and cellular growth/proliferation). More marked decreases in transcription were observed in cluster C6, with *nerve growth factor receptor-associated protein 1 (Ngfrap1)* and *TGF β -inducible early growth response 3 (Tieg3)* (Figures 5.8A and B, respectively) displaying typical profiles for this cluster. Both *Ngfrap1* and *Tieg3* were significantly decreased at 12 and 18 hours with DMNQ and MNQ exposure and grouped in the top molecular function (cellular growth and proliferation) for cluster C6.

The mean profiles of cluster C8 were very different from the other clusters with decreased trends in transcription (Figure 5.9). Exemplar genes such as *Cytochrome p450 1a1 (Cyp1a1)* and *quiescin Q6-like 1 (Qscn6l1)* displayed transient decreases in transcription between 4 and 12 hours (Figures 5.9A and B, respectively). *Cyp1a1* and *Qscn6l1* were present in one of the top two molecular functions identified for cluster C8, small molecule biochemistry.

Figure 5.7

A: Tgfb2



B: Apaf1

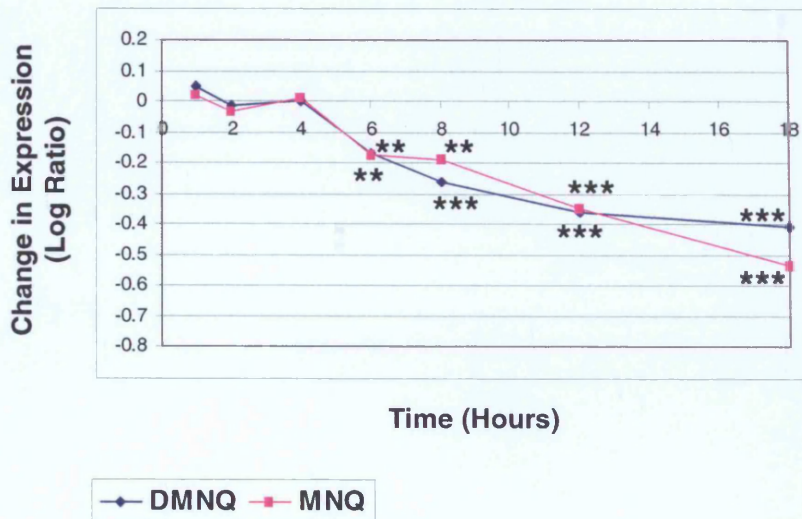
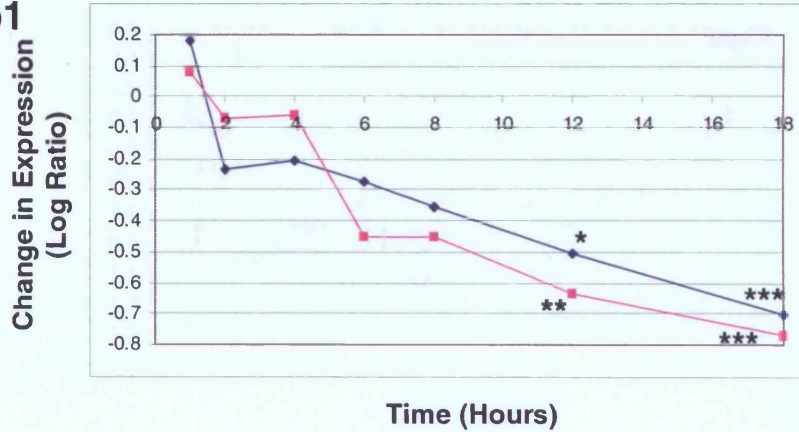


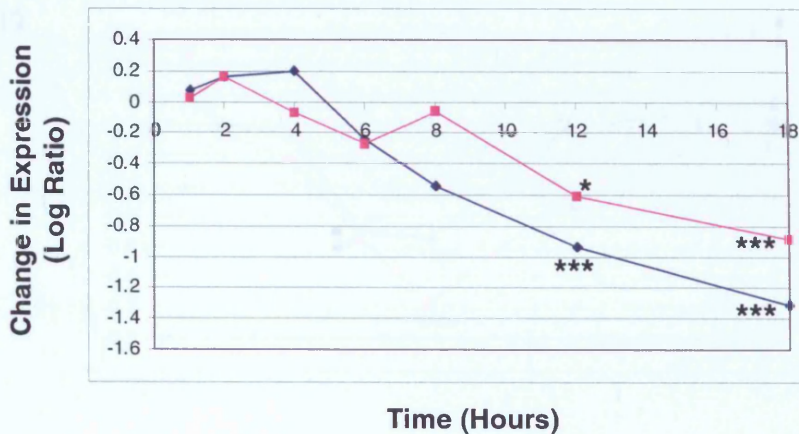
Figure 5.7: Exemplar gene profiles for cluster C1. Results are group mean log ratio of change relative to VC exposed cultures (n=3 repeat experiments). ANOVA and post-hoc T-test (** = P<0.01, *** = P<0.001 versus VC).

Figure 5.8

A: Ngfrap1



B: Tieg3

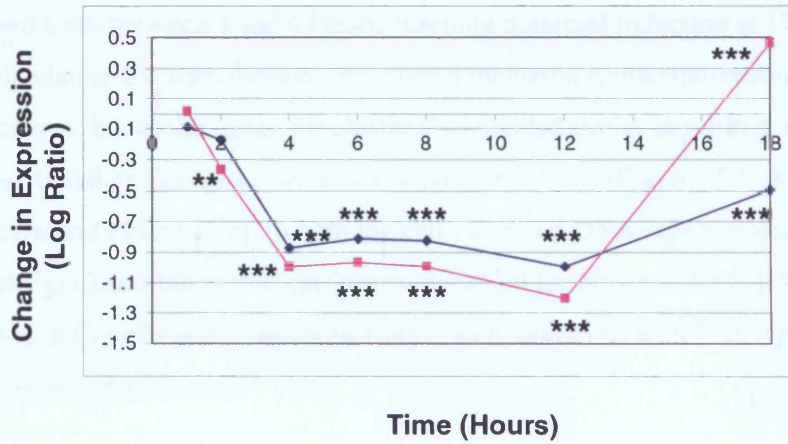


—◆— DMNQ —■— MNQ

Figure 5.8: Exemplar gene profiles for cluster C6. Results are group mean log ratio of change relative to VC exposed cultures (n=3 repeat experiments). ANOVA and post-hoc T-test (* = $P < 0.05$, ** = $P < 0.01$, *** = $P < 0.001$ versus VC).

Figure 5.9

A: Cyp1a1



B: Qscn6l1

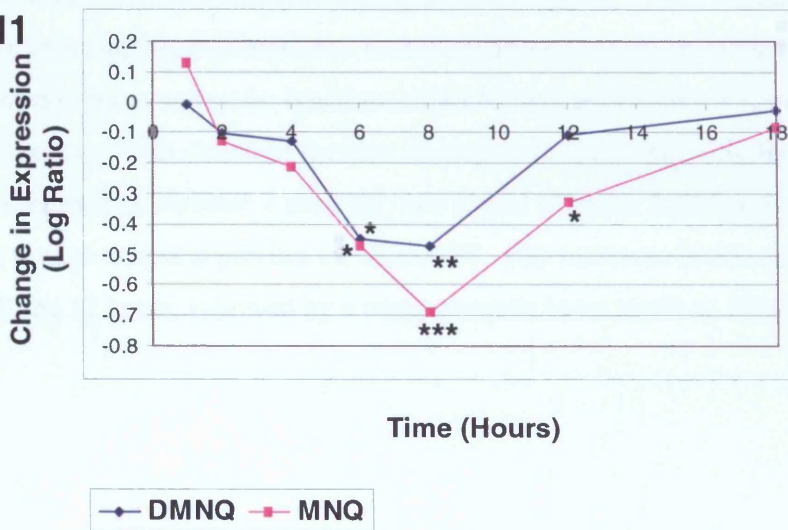


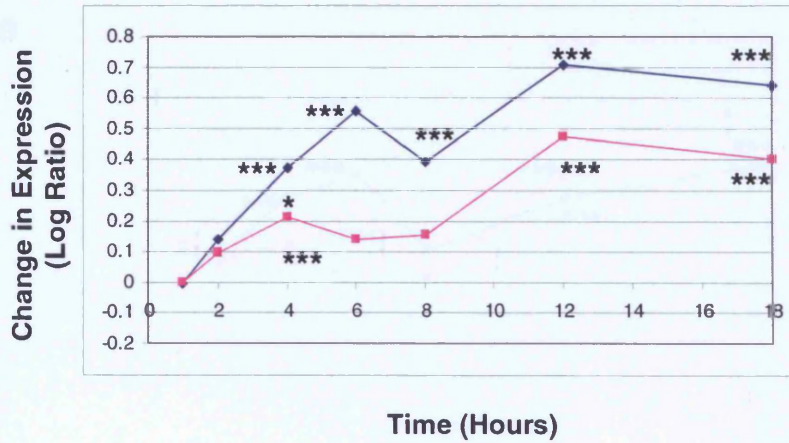
Figure 5.9: Exemplar gene profiles for cluster C8. Results are group mean log ratio of change relative to VC exposed cultures (n=3 repeat experiments). ANOVA and post-hoc T-test (* = P<0.05, ** = P<0.01, * = P<0.001 versus VC).**

In cluster C3 molecular functions such as cell death/proliferation control were well represented, with *Serine/threonine kinases Pim1* and *Pim3* displaying typical profiles for genes within these functional categories (Figures 5.10A and B, respectively). *Pim1* and *Pim3* were increased from between 4 and 6 hours, reaching maximal induction at 12 and 18 hours. Genes within cluster C4 also displayed consistent increased transcription across much of the time course. Exemplar genes for cluster C4 included *cyclin-dependent kinase inhibitor 1A (Cdkn1a)* and *proliferating cell nuclear antigen (Pcna)* (Figures 5.11A and B, respectively). *Cdkn1a* and *Pcna* belong to both the cell cycle and DNA repair molecular functions, the most significant functional categories identified for cluster C4 by IPA. Significant increases in *Cdkn1a* and *Pcna* transcription were observed with DMNQ and MNQ exposure from 4 hours onwards.

The two most significant molecular functions represented in cluster C7 were cellular compromise and cellular function/maintenance. Genes encoding heat shock-related proteins were well represented in these molecular functions. Marked increases within 4 hours of DMNQ and MNQ exposure was observed for *heat shock protein 105 (Hsp105)*, *Hsp2a*, *DnaJ homologue subfamily A, member 1 (Dnajal)* and *Hspb1* (Figures 5.12A to D). All four genes display typical temporal profiles for cluster C7, with increases in transcription peaking between 8 and 12 hours, followed by a return towards basal levels at 18 hours.

Figure 5.10

A: Pim1



B: Pim3

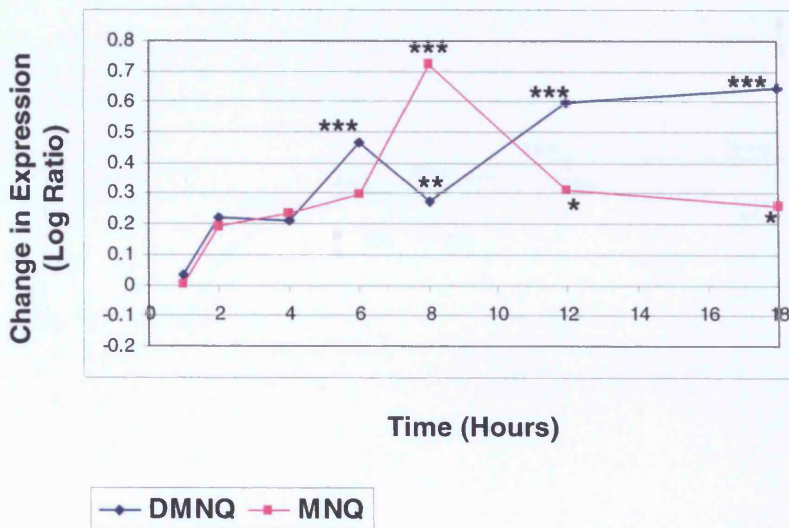
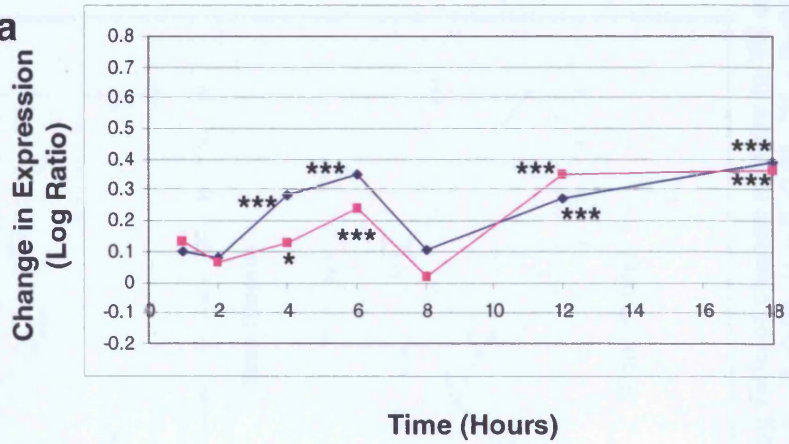


Figure 5.10: Exemplar gene profiles for cluster C3. Results are group mean log ratio of change relative to VC exposed cultures (n=3 repeat experiments). ANOVA and post-hoc T-test (* = $P < 0.05$, *** = $P < 0.001$ versus VC).

Figure 5.11

A: Cdkn1a



B: Pcna

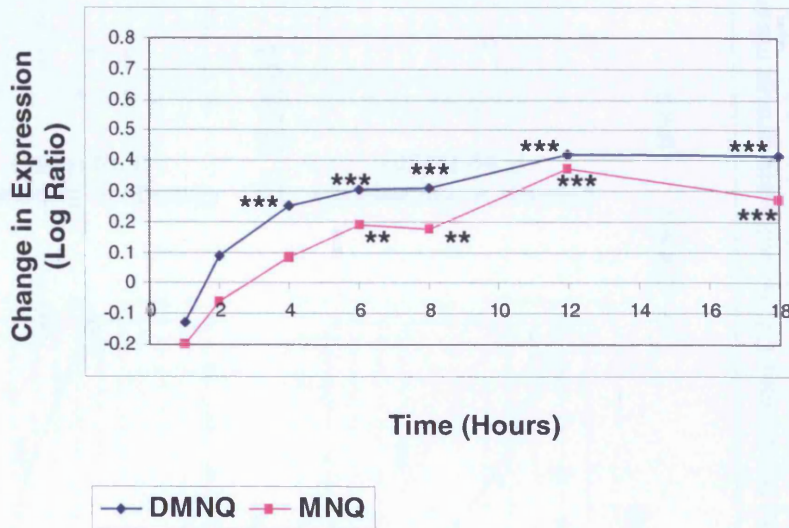
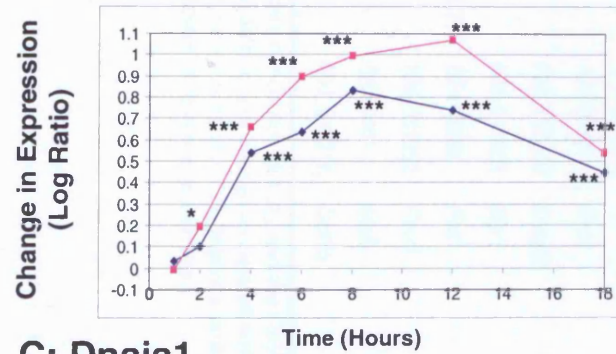


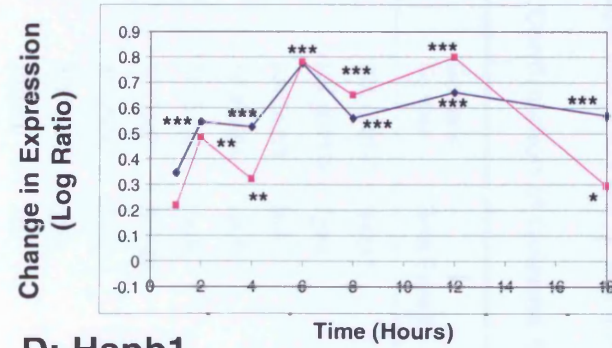
Figure 5.11: Exemplar gene profiles for cluster C4. Results are group mean log ratio of change relative to VC exposed cultures (n=3 repeat experiments). ANOVA and post-hoc T-test (* = P<0.05, ** = P<0.01, *** = P<0.001 versus VC).

Figure 5.12

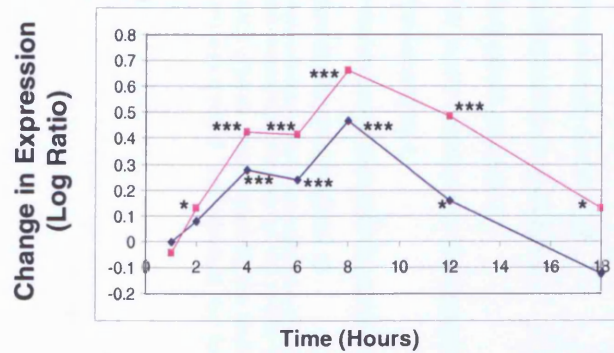
A: Hsp105



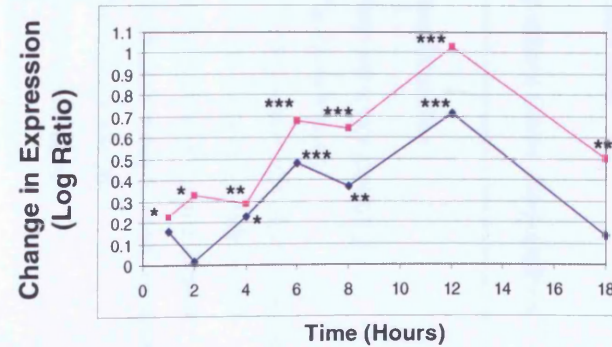
B: Hsp2a



C: Dnaja1



D: Hspb1



—●— DMNQ —■— MNQ

Figure 5.12: Exemplar gene profiles for cluster C7. Results are group mean log ratio of change relative to VC exposed cultures (n=3 repeat experiments). ANOVA and post-hoc T-test (* = $P < 0.05$, ** = $P < 0.01$, *** = $P < 0.001$ versus VC).

5.2.2.1. Confirmation of Quinone Signature Genes

Transcriptional regulation of quinone signature genes identified previously (Chapter 4) was evaluated. Of the 22 genes identified (Table 4.7), quinone-mediated differential regulation of 18 were confirmed in this study (Table 5.2). Differential regulation of *Mat2a*, *Okl38*, *Epha2*, *Cebpb* and *LOC498331* was not confirmed.

Table 5.2: Confirmation of Quinone Signature Gene Regulation

Cluster	GenBank Number	Gene Symbol	Gene Description
C7	NM_012580	<i>Hmox1</i>	<i>Haem oxygenase (decycling) 1</i>
C5	NM_031659	<i>Tgm1</i>	<i>Transglutaminase 1</i>
C3	AA818380	<i>Mylip</i>	<i>Myosin regulatory light chain interacting protein</i>
C3	AF080594	<i>Vegfa</i>	<i>Vascular endothelial growth factor A</i>
C3	AI175732	<i>Vegfa</i>	<i>Vascular endothelial growth factor A</i>
C7	BE116021	<i>Slc5a3</i>	<i>Solute carrier family 5 (inositol transporters), member 3</i>
C3	AB025017	<i>Zfp36</i>	<i>Zinc finger protein 36</i>
C3	AW140851	<i>Chka</i>	<i>Choline kinase alpha</i>
C3	M58040	<i>Tfrc</i>	<i>Transferrin receptor</i>
C7	AI175045	<i>Pdk4</i>	<i>Pyruvate dehydrogenase kinase, isoenzyme 4</i>
C3	NM_022602	<i>Pim3</i>	<i>Serine/threonine-protein kinase pim-3</i>
C4	AA946361	<i>Brd2</i>	<i>Bromodomain containing 2</i>
C7	NM_133578	<i>Dusp5</i>	<i>Dual specificity phosphatase 5</i>
C7	NM_012551	<i>Egr1</i>	<i>Early growth response 1</i>
Unclassified (C7)	BF415939	<i>Fos</i>	<i>FBJ murine osteosarcoma viral oncogene homolog</i>
C7	NM_012953	<i>Fos1</i>	<i>Fos-like antigen 1</i>
C3	BI284461	<i>Mafk</i>	<i>v-maf musculoaponeurotic fibrosarcoma oncogene family, protein K</i>
C3	NM_019216	<i>Gdf15</i>	<i>Growth differentiation factor 15</i>

The table shows the cluster identity and the Genbank accession number of the probe set representing each gene. The direction of change associated with each cluster is indicated by the font colour (**Red** = increased, **Green** = decreased). Where a probe set was termed 'unclassified' by ArrayMiner clustering, the nearest cluster is shown in parentheses.

5.2.2.2. Nrf2-Target Genes and the Antioxidant Response

Increased transcription of three Nrf2-target genes was observed with DMNQ and MNQ exposure (Table 5.3). Two probe sets representing *Gclc* segregated to clusters C3 and C4, indicating a moderate increase in transcription from 4 to 6 hours that was maintained throughout the latter exposure period. *Glutathione reductase (Gsr)* was present in cluster C5, indicating a slight increase in transcription between 6 and 12 hours. *Hmox1* gave the most marked response, as evidenced by its segregation to cluster C7. No other Nrf2-target genes were present in the 804 genes selected for cluster analysis. In addition to the Nrf2-target genes, several other genes involved in the oxidative stress response, or encoding proteins with antioxidant activity, were increased with DMNQ and MNQ exposure (Table 5.3). Decreased transcription of ROS-generating systems was also observed with DMNQ and MNQ exposure. The exemplar genes selected for cluster C8, *Cyp1a1* and *Qscn61l*, being good examples (Figure 5.9A and B).

Table 5.3: Oxidative stress response and Nrf2-target genes regulated with DMNQ and MNQ exposure

Cluster	GenBank Number	Gene Symbol	Gene Description	Pathway/Function
C8	X00469	<i>Cyp1a1</i>	<i>Cytochrome P450 1a1</i>	Phase I drug metabolism
C8	AW535805	<i>Qscn61l</i>	<i>Quiescin 6-like 1</i>	Sulphydryl oxidase/disulphide bond formation
C3	J05181	<i>Gclc</i> [#]	<i>Glutamate-cysteine ligase, catalytic subunit</i>	GSH Biosynthesis
C3	BF555110	<i>Txn1l</i>	<i>Thioredoxin-like 1</i>	Redox homeostasis
C4	AA892770	<i>Gclc</i> [#]	<i>Glutamate-cysteine ligase, catalytic subunit</i>	GSH Biosynthesis
C4	AW532618	<i>Slc7a11</i>	<i>Solute carrier family 7, member 11</i>	Cystine/glutamate transport
C5	AW525915	<i>Gsr</i> [#]	<i>Glutathione reductase</i>	Redox homeostasis
Unclassified (C5)	NM_053968.1	<i>Mt3</i>	<i>Metallothionein 3</i>	Antioxidant/heavy metal binding
C7	NM_012580	<i>Hmox1</i> [#]	<i>Haem oxygenase (decycling) 1</i>	Antioxidant/haem degradation

The table shows the cluster identity and the Genbank accession number of the probe set representing each gene, along with an indication of the pathway/function. The direction of change associated with each cluster is indicated by the font colour (Red = increased, Green = decreased). Where a probe set was termed 'unclassified' by ArrayMiner clustering, the nearest cluster is shown in parentheses. # = Nrf2-target gene.

5.2.2.3. Transcriptional Regulation of Genes Involved in Cell Cycle Control and the Response to DNA Damage

A large number of genes involved in cell cycle control and augmenting the response to DNA damage were regulated with DMNQ and MNQ exposure (Table 5.4). Two key genes involved in this response, *Cdkn1a* and *Pcna*, were the exemplar genes selected for the increased cluster C4 (Figures 5.11A and B). As was previously observed (Chapter 4), quinone-mediated redox challenge of hepatocytes increased the transcription of several DDIT- and GADD-related genes.

Table 5.4: Cell cycle control and DNA damage response genes regulated with DMNQ and MNQ exposure

Cluster	GenBank Number	Gene Symbol	Gene Description	Pathway/Function
C2	AI045459	<i>Ccnt2</i>	<i>Cyclin T2</i>	Regulation of cdk9 activity
C2	AW531623	<i>Cdk7</i>	<i>Cyclin-dependent kinase 7</i>	Component of CDK-activating kinase complex
C3	AA945069	<i>Sertad1</i>	<i>SERTA domain containing 1</i>	Regulation of cyclin D1/CDK4 activity
C3	AA957449	<i>Plk3</i>	<i>Polo-like kinase 3</i>	M-phase regulation
C3	AI177513	<i>Clk1</i>	<i>Cell division cycle-like kinase 1</i>	Cell cycle checkpoint/regulator
C3	BI284349	<i>Myd116</i>	<i>Myeloid differentiation primary response gene 116</i>	DNA damage response
C3	BI287978	<i>Gadd45b</i>	<i>Growth arrest and DNA-damage-inducible 45 beta</i>	DNA damage response
C3	NM_080399.1	<i>Ddit4l</i>	<i>DNA-damage-inducible transcript 4-like</i>	DNA damage response
C3	NM_080906.1	<i>Ddit4</i>	<i>DNA-damage-inducible transcript 4</i>	DNA damage response
C4	U24174	<i>Cdkn1a</i>	<i>Cyclin-dependent kinase inhibitor 1a (p21)</i>	DNA damage response and cell cycle arrest
C4	NM_022381	<i>Pcna</i>	<i>Proliferating cell nuclear antigen</i>	DNA replication and repair
C5	AI100827	<i>Cdk5r</i>	<i>Cyclin-dependent kinase 5, regulatory subunit 1 (p35)</i>	Activates cdk5 promoting G1 to S-phase transition
C5	AW144047	<i>Ccnt1</i>	<i>Cyclin T1</i>	Regulation of cdk9 activity
C7	AI406939	<i>G0s2</i>	<i>G0/G1 switch gene 2</i>	Regulation of progression through cell cycle
C7	AW532628	<i>Cdca2</i>	<i>Cell division cycle associated 2</i>	M-phase regulation
C7	AI599423	<i>Gadd45g</i>	<i>Growth arrest and DNA-damage-inducible 45 gamma</i>	DNA damage response

The table shows the cluster identity and the Genbank accession number of the probe set representing each gene, along with an indication of the pathway/function. The direction of change associated with each cluster is indicated by the font colour (Red = increased, Green = decreased).

5.2.2.4. Transcriptional Regulation of Genes Involved in Energy Metabolism

As discussed previously (Chapter 1 and 4), quinones can interfere with the normal flow of electrons through the mitochondrial respiratory chain[34], adversely affecting ATP synthesis. Consistent with this effect, regulation of a number of genes encoding enzymes and proteins involved energy metabolism and its regulation were modulated with DMNQ and MNQ exposure (Table 5.5). Components of the mitochondrial respiratory chain were decreased and genes involved in short chain fatty acid metabolism were modulated. In addition, glucose metabolism and storage pathways were modulated, with increased transcription of genes involved in glycolysis, gluconeogenesis and glycogen metabolism.

Table 5.5: Energy Metabolism-Related Genes regulated with DMNQ and MNQ Exposure

Cluster	GenBank Number	Gene Symbol	Gene Description	Pathway/Function
C1	NM_012812	<i>Cox6a2</i>	<i>Cytochrome c oxidase, subunit VIa, polypeptide 2</i>	Electron transport chain
C2	AI175767	<i>Ndufa11</i>	<i>NADH dehydrogenase (ubiquinone) 1 alpha subcomplex 11</i>	Electron transport chain
C8	BI291880	<i>Oxsm</i> (RGD1311092)	<i>3-oxoacyl-ACP synthase, mitochondrial</i>	Short chain fatty acid synthesis
C3	BI277460	<i>Pck1</i>	<i>Phosphoenolpyruvate carboxykinase 1</i>	Gluconeogenesis
C4	BF283381	<i>Pfkfb3</i>	<i>6-phosphofructo-2-kinase/fructose-2,6-biphosphatase 3</i>	Regulation of glycolysis
C4	AI233740	<i>Akr1b8</i>	<i>Aldo-keto reductase family 1, member B8</i>	Regulation of glycolysis
C5	BI274037	<i>Ppp1r3b</i>	<i>Protein phosphatase 1, regulatory (inhibitor) subunit 3B</i>	Regulation glycogen metabolism
C7	BM390827	<i>Ppp1r3c</i>	<i>Protein phosphatase 1, regulatory (inhibitor) subunit 3C</i>	Regulation glycogen metabolism
C7	AI175045	<i>Pdk4</i>	<i>Pyruvate dehydrogenase kinase, isoenzyme 4</i>	Regulation of glucose/fatty acid metabolism

The table shows the cluster identity and the Genbank accession number of the probe set representing each gene, along with an indication of the pathway/function. The direction of change associated with each cluster is indicated by the font colour (Red = increased, Green = decreased).

5.2.2.5. Transcriptional Regulation of Genes Involved in Iron Homeostasis

Transcriptional changes were seen in a number of genes involved in iron and haem homeostasis with DMNQ and MNQ exposure (Table 5.6). *Hmox1*, which was in cluster C7, was markedly increased from 4 hours onwards. Moderate increases in the transcription of *aminolevulinic acid synthase 1 (Alas1)*, *solute carrier family 25, member a37 (Slc25a37)* and *Tfrc* were seen at the later time points, as indicated by their segregation to clusters C3 or C4. Decreases in transcription of similar magnitude were observed for *hemochromatosis type 2 (juvenile) homologue (Hfe2)* and *transferrin (Tf)*, which segregated to clusters C1 and C6, respectively.

5.2.6. Biochemical Endpoints

Table 5.6: Iron and Haem Homeostasis-related genes regulated with DMNQ and MNQ exposure

Cluster	GenBank Number	Gene Symbol	Gene Description	Pathway/Function
C7	NM_012580	<i>Hmox1</i>	<i>Haem oxygenase (decycling) 1</i>	Haem degradation
C4	NM_024484.1	<i>Alas1</i>	<i>Aminolevulinic acid synthase 1</i>	Rate limiting step in haem synthesis
C4	AI229706	<i>Slc25a37</i> (RGD1359361)	<i>Solute carrier family 25, member 37</i>	Mitochondrial iron transport
C1	AW434961	<i>Hfe2</i>	<i>Hemochromatosis type 2 (juvenile) homologue</i>	Regulation of iron homeostasis
C3	M58040	<i>Tfrc</i>	<i>Transferrin receptor</i>	Cellular iron transport
C6	AA945548	<i>Tf</i>	<i>Transferrin</i>	Extracellular Iron transport

The table shows the cluster identity and the Genbank accession number of the probe set representing each gene, along with an indication of the pathway/function. The direction of change associated with each cluster is indicated by the font colour (Red = increased, Green = decreased).

5.3. Discussion

The main aim of this study was to utilise Affymetrix GeneChips[®] to identify key response pathways through which rat hepatocytes seek to ameliorate quinone-induced redox stress and promote cell survival. In addition, it was hoped that the investigations would provide an improved mechanistic understanding of cellular systems perturbed under conditions of quinone-mediated redox stress. This was achieved by carrying out a thorough transcriptional analysis of rat hepatocytes exposed to two redox cycling quinones, DMNQ and MNQ, over an 18 hour period.

5.3.1. Biochemical Endpoints

The assessment of cytotoxicity and a thorough evaluation of intra- and extracellular glutathione status were carried out to help place transcriptional changes into context. 150 μ M DMNQ and 25 μ M MNQ exposure did not result in increased LDH leakage relative to VC with up to eight hours exposure, confirming previous findings (Chapters 3 and 4). DMNQ and MNQ exposure did result in a time-related increase in cytotoxicity from 12 hours onwards, relative to concurrent controls. Cytotoxicity peaked at 24 hours, the DMNQ and MNQ exposure resulting in approximately 70 and 90 percent LDH leakage, respectively, compared to 50 percent with VC exposed cultures (Figure 5.1).

Both quinones induced significant effects on GSH levels, although the kinetics were different (Figure 5.2). DMNQ exposure resulted in a gradual decrease in GSH levels, peaking at 8 hours, before plateauing at approximately 40 percent of concurrent controls for the remainder of the 24 hours. MNQ exposure resulted in a marked decrease in GSH levels at 1 hour which slowly recovered to near concurrent control levels by 24 hours. The GSH kinetics fit the known reactivity of the two quinones. DMNQ is a pure redox cyler[26] and causes GSH depletion through redox cycling and GSSG generation. GSH depletion via this route takes time to build, hence the gradual decrease over the early part of the time course. MNQ has the capacity to deplete GSH via redox cycling and arylation[26;27]. The more marked decrease in GSH levels at 1 hour with MNQ is likely due to the additive effect of redox cycling and its capacity to deplete GSH through direct arylation of the thiol moiety. The gradual return of GSH levels to those seen in concurrent controls is a result of the MNQ conjugation depleting its overall reactivity. As DMNQ does not directly bind GSH, due to methoxy substitutions at the reactive 2 and 3 carbon positions, its redox reactivity

remains undiminished. Thus, GSH depletion with DMNQ exposure was maintained throughout the 24 hours exposure.

GSSG levels were significantly increased with both quinones at 1 and 4 hours (Figure 5.3). As seen previously (Chapter 4), GSSG levels returned to concurrent control levels by 8 hours and this effect was maintained for the remainder of the time course. It was previously suggested (Chapter 4) that rat hepatocytes exposed to DMNQ and MNQ exported GSSG to maintain the overall redox balance of the cell. This suggestion fits with the progressive decrease in GSH levels throughout the time course with DMNQ exposure. To confirm this, media total GSH levels were measured (Figure 5.4). Media total GSH levels were significantly increased in DMNQ and MNQ exposed cultures at all time points, although the effect was most marked with DMNQ. The fact that the effect was more pronounced with DMNQ exposed cultures is consistent with redox challenge being maintained throughout the time course. It is possible that the increased media GSH levels were the result of leakage due to plasma membrane damage. This may account for some of the media GSH at the latter time points where increased cytotoxicity/LDH leakage was observed (12 to 24 hours) (Figure 5.1). However, it is unlikely to account for the increased media GSH levels at the earlier time points where the differential between quinone-exposed cultures and concurrent controls was most marked. The marked increase in media GSH levels at 1 to 8 hours is likely to be a direct result of active export of GSSG to redress any redox imbalance.

5.3.2. Transcriptomic Investigations

Transcriptomic analysis has allowed the identification of 804 genes consistently regulated with time in response to DMNQ and MNQ-induced redox challenge. Among these were probe sets representing 18 of the 22 'quinone signature genes' (Table 5.2) previously identified (Chapter 4). This equates to a confirmation rate of approximately 80 percent and underscores the importance of these genes in the response hepatocytes mount to quinone exposure. In general, cluster analysis of the 804 probe sets consistently regulated with DMNQ and MNQ exposure failed to lead to segregation based on function/pathway. Of the eight clusters identified, a high degree of functional overlap was observed based on biological theme analysis. As was seen previously (Chapter 4), the two alternative methods

of biological theme analysis used (IPA and EASE) yielded a similar functional overview of the data (Figures 5.5 and 5.6, and Table 5.1).

It was interesting to note that cluster C7, which displayed the most marked increases in mean expression profile for both DMNQ and MNQ exposure, contained genes typically associated with the general stress response. This is supported by the fact that the top two molecular functions identified by IPA analysis for the cluster were ‘cellular compromise’ and ‘cellular function and maintenance’. Genes represented in these highly significant categories included heat shock-related proteins (as indicated in Figure 5.12A to D), *Hmox1*, *early growth response 1 (Egr1)* and the AP-1-related transcription factors *Fos* and *Fos11*. The latter four genes were previously identified as quinone signature genes (Chapter 4).

In addition to the transcriptional changes observed in general stress response genes, which were entirely expected, genes belonging to several other pathways were co-ordinately regulated with DMNQ and MNQ exposure. The core pathways regulated included intrinsic apoptotic signalling, the antioxidant response, DNA damage repair and cell cycle control, cellular energy metabolism, and iron/haem homeostatic control. An interpretation of the regulation of these key pathways has been made, which provides an overview of the ameliorative response made in response to quinone-induced redox challenge.

5.3.2.1. Pro-survival Signalling - Down Regulation of the Intrinsic Apoptosis Pathway

Genes involved in the regulation of apoptosis were well represented in the 804 probe sets selected for cluster analysis, as evidenced by the IPA and EASE biological theme analysis outputs (Figures 5.5 and 5.6, and Table 5.1). Exemplar genes selected from both decreased and increased gene clusters are integral to the regulation of the intrinsic apoptosis pathway. The regulation of genes involved in the intrinsic apoptotic pathway is not surprising, given that both oxidative stress and quinones have been shown to induce cell death via this mechanism[216-223].

The exemplar genes selected from cluster C1, *Apaf-1* and *Tgfb2*, are both involved in the mitochondrial-mediated ‘intrinsic pathway’ of apoptosis. Decreased transcription of *Apaf-1*, the gene encoding APAF-1 protein was seen from 6 hours onwards with DMNQ and MNQ exposure, peaking at 18 hours (Figure 5.7B). APAF-1 is a key element of the

intrinsic pathway of apoptosis, oligomerising in the presence of cytosolic cytochrome *c* to form the apoptosome complex[224]. The apoptosome recruits and activates caspase-9 and subsequently activates caspases-3 -6 and -7. The latter are known as effector caspases and initiate the proteolytic cascade that leads to apoptotic cell death [225;226]. APAF-1 overexpression sensitises cells to apoptosis[227], thus the decreased transcription observed in DMNQ and MNQ exposed hepatocytes may result in decreased sensitivity to stress-induced apoptosis.

Tgfb2 displayed almost identical kinetics to Apaf-1 (Figure 5.7A). *Tgfb2* encodes one of the three isoforms of transforming growth factor beta (TGF β), a family of cytokines involved in inhibition of proliferation and induction of apoptosis in a variety of cell types[228-231]. Another member of the TGF β family, TGF β 1, has been shown to induce apoptosis in hepatocytes both *in vivo* and *in vitro* [229;232]. TGF β s act through binding to TGF β receptors type I and type II [233]. TGF β -binding signals are transduced via the Smad group of proteins, which form an activated complex that translocates to the nucleus to bring about transcription of TGF β -target genes [233;234]. The pro-apoptotic activity associated with TGF β s is thought to be due to Smad-mediated transcriptional activation of proteins involved in apoptosome-mediated apoptosis [234]. As yet unidentified proteins are thought to trigger the mitochondrial permeability transition, resulting in cytochrome *c* release. In the cytosol, cytochrome *c* binds APAF-1 initiating the formation of the apoptosome and activation of the intrinsic pathway [233].

Tieg3, a downstream effector of TGF β activity, was markedly decreased in transcription at 12 and 18 hours with DMNQ and MNQ exposure (Figure 5.8B). *Tieg3* belongs to TGF β -inducible immediate-early response gene family [235-237]. *Tieg* genes encode Sp1-like transcription factors involved in the early response of TGF β signal transduction[238;239]. *Tiegs* have been shown to possess similar properties to TGF β s, inducing growth arrest and/or apoptosis in CHO cells, pancreatic epithelial cells and the Hep3B hepatoma cell line [239-241]. No direct link between *Tieg3* transcription and TGF β 2 exists. However, Spittau *et al*[236] have demonstrated that TGF β 1 treatment of OLI-neu cells results in marked increases in *Tieg3* transcription within 30 to 60 minutes. Different TGF β s do function through the same signalling system [228], suggesting that the decrease in transcription seen in *Tieg3* is a downstream effect of the decrease seen in *Tgfb2* from 8 hours. The fact that

the decrease in *Tieg3* seen in DMNQ and MNQ exposed hepatocytes occurs 4 hours after the initial decrease in *Tgfβ2* transcription is consistent with this suggestion.

Ngfrap1, the second exemplar gene within cluster C6, was significantly decreased at 12 and 18 hours (Figure 5.8A). *Ngfrap1* encodes the protein also known as NADE (p75^{NTR}-associated cell death executor) and is involved in nerve growth factor (NGF) apoptotic signalling [242;243]. Binding of immature NGF to p75 neurotrophin receptor (p75^{NTR}) induces apoptosis in neuronal cells *in vivo* and *in vitro* and NADE is thought to be a key mediator of this response [242]. Indeed, NADE overexpression results in caspase-3 activation in a range of neuronal cells lines[244;245]. Yoon *et al*[246] have linked NADE activity to modulating the mitochondrial or intrinsic apoptotic pathway. They demonstrated that NADE interacts with a protein released from mitochondria during apoptosis called SMAC (second mitochondria-derived activator of caspase). This interaction prevents SMAC ubiquitination and proteosomal degradation, allowing it to inhibit the activity of IAPs (inhibitor of apoptosis proteins) which would normally block caspase-9 activation[247].

As well as suppression of mediators of the intrinsic apoptotic pathway, simultaneous induction of pro-survival genes was observed. *Pim1* and *Pim3*, both encoding kinases belonging to the PIM family, were significantly increased with DMNQ and MNQ exposure from as early as 4 hours (Figure 5.10A and B). *Pim3* was previously identified as a 'quinone signature gene' (Chapter 4). Segregation of *Pim1* to the same gene cluster (C3) emphasizes the importance of PIM kinases in the response of hepatocytes to quinone exposure and redox stress. Although *Pim3* regulation has not previously been linked to oxidative stress, *Pim1* induction has been. Katakami *et al*[248] demonstrated that exposure of rat aortic smooth muscle cells to H₂O₂ resulted in both increased *Pim1* mRNA and protein levels within 2 to 6 hours.

The PIM kinases are involved in cell survival and proliferation and are overexpressed in a number of cancers and cell lines[191;192;249-251]. One of the main mechanisms through which PIM kinases are known to promote cell survival is via inactivation of BCL2-antagonist of cell death (BAD) [190;191;252;253], a pro-apoptotic member of the Bcl-2 family [254]. BAD binds anti-apoptotic members of the Bcl-2 family (e.g. Bcl-X(L), Bcl-2 and Bcl-W), thereby inhibiting their activity and promoting activation of the intrinsic

apoptosis pathway[254]. Thus, increased transcription of *Pim1* and *Pim3* is also consistent with suppression of the mitochondria-driven intrinsic pathway of apoptosis.

5.3.2.2. The Antioxidant Response

The selected concentrations of DMNQ and MNQ induced a marked oxidative challenge in rat hepatocytes, as evidenced by the increased GSSG levels at 1 to 4 hours (Figure 5.3) and depletion of GSH levels for a large part of the exposure period (Figure 5.2). Given the importance of maintaining the redox balance within the cell, it was no surprise that hepatocytes responded by increasing transcription of genes involved in returning the intracellular environment to a more reduced state (Table 5.3).

As outlined in Section 1.3.2, key to this response is induction of the Nrf2-ARE pathway. Previously it was found that DMNQ and MNQ exposure of rat hepatocytes for up to 8 hours elicited only a minimal induction of Nrf2-target genes (Chapter 4). One of the aims of this study was to determine whether more prolonged exposure of rat hepatocytes to DMNQ or MNQ was required to induce a comprehensive response in Nrf2-target genes. Extending the exposure period to 18 hours, by which time a general trend of increased cytotoxicity was seen (Figure 5.1), failed to result in a more marked induction of Nrf2-target genes (Table 5.3). As was seen previously (Chapter 4), DMNQ and MNQ exposure resulted in increased transcription of *Hmox1* and *Gclc* from 4 hours. The only additional Nrf2-target gene regulated was *Gsr* which segregated to cluster C5, indicating a slight increase between 6 and 12 hours. *Gsr* encodes glutathione reductase (GSHr), an enzyme that forms an integral part of the 'GSH redox cycle' (as discussed in Section 1.3.1). GSHr reduces GSSG, formed as a result glutathione peroxidase-driven H₂O₂ reduction, back to GSH. The increased transcription of *Gsr* is evidence of a compensative response to the elevated levels of GSSG seen in the early phase of the exposure period (Figure 5.3).

There was also a correlative relationship between the GSH depletion observed with DMNQ and MNQ exposure and increased transcription of *Gclc* and *Slc7a11*. As discussed previously (Chapter 4), increased transcription of *Gclc* is likely a direct response to GSH depletion as hepatocytes increase expression of the rate limiting enzyme in GSH biosynthesis. To feed the increased requirement for GSH synthesis, *Slc7a11* was also induced. *Slc7a11* encodes a cysteine/glutamate transporter that is responsible for the import amino acids required for GSH biosynthesis from the extracellular environment.

Increased transcription of *Slc7a11* in response to oxidative stress and quinone exposure has been reported previously [255]. Overall, the increased transcription of antioxidant response genes, including *thioredoxin-like 1* and *metallothionein 3*, correlates with the return of GSSG levels in DMNQ and MNQ exposed hepatocytes towards those seen in VC exposed hepatocytes (Figure 5.4). This balance was maintained for the remainder of the time course even though the redox challenge remained.

In addition to increases in antioxidant genes, decreased transcription of genes encoding proteins that contribute to prooxidant generation was observed. The exemplar genes selected for cluster C8, *Cyp1a1* and *Qscn611*, both encode proteins that can be considered as prooxidant generating systems (Figure 5.9 and Table 5.3). *Cyp1a1* encodes the ROS-generating[256] cytochrome P450 1A1 (CYP1A1) and its transcriptional suppression has been reported in hepatoma cell lines exposed to oxidative stress[95;257-259]. Morel and Barouki[49] suggest that the down regulation of the ROS-generating CYP1A1 during oxidative stress is part of a concerted response to return to a balanced redox state. The transcriptional decrease in *Qscn611* is likely part of the same response.

Qscn611, also known as quiescin Q6 sulphhydryl oxidase 2 (QSOX2), encodes a sulphhydryl oxidase that catalyzes the formation of disulphide bonds in a range of proteins and peptides[260]. Formation of the disulphide bonds is accompanied by the concomitant generation of H₂O₂[260;261], which has the potential to generate ROS via the Fenton reaction (as outlined in Chapter 1). Thus expression of QSOX2 (and other sulphhydryl oxidases) under prooxidant conditions has the potential to exacerbate oxidative stress and the decreased transcription of *Qscn611* is likely a compensative response to quinone-induced redox challenge. No reports have been found correlating decreased transcription of *Qscn611*, or other sulphhydryl oxidases, as an adaptive response to oxidative stress or quinone exposure. However, Mairret-Coello *et al* [262] have hypothesised that dysregulation of sulphhydryl oxidases in the brain could be a contributing factor to neurological diseases with an oxidative stress component (e.g. Alzheimer's diseases or Parkinson's disease).

5.3.2.3. The Response to DNA Damage

Transcriptional changes in a number of genes involved in cell cycle regulation and the response to DNA damage were observed with DMNQ and MNQ exposure (Table 5.4). A

significant observation was that gene changes that can be interpreted as both negative (e.g. increased *Cdkn1a* and *Clk1* and decreased *Cdk7*) and positive (e.g. increased *Sertad1*, *Plk3*, *Cdk5r*, *G0s2* and *Cdca2*) regulation of cell cycle progression were present within the 804 probe sets selected for analysis. This response may be indicative of cell cycle dysregulation and would be consistent with the tumour-promoting activity of chronic oxidative stress[263-266] if such a response was observed *in vivo*.

A critical sensor of oxidative DNA damage that regulates cell cycle arrest is the p53 tumour suppressor[267-271]. A key p53-regulated gene, *Cdkn1a* (also known as *p21*) was increased in transcription with DMNQ and MNQ exposure (Figure 5.11A). The protein encoded by *Cdkn1a* effects cell cycle arrest through binding/inhibiting a number of cyclin dependent kinases (CDKs) involved in controlling the G1-S phase transition (e.g. *Cdk2*, *3*, *4* and *6*)[272;273]. Induction of *Cdkn1a* provides evidence of an active p53-mediated response to DNA damage induced by quinone exposure. This is supported by the increased transcription noted in a number of other DNA damage-inducible genes (i.e. *Ddits* and *Gadds*) (Table 5.4).

Induction of *Cdkn1a* and cell cycle arrest following exposure of a range of cell types to quinone-related compounds is well reported[122;273-275]. Examples where this response was induced by naphthoquinones include work carried out by Markovits *et al*[122], who demonstrated that exposure of HepG2 cells to MNQ or vitamin K₂ (a naturally occurring analogue) increased *Cdkn1a* protein levels. In addition, Kim and Yun [276] reported that exposure of vascular smooth muscle cells to the synthetic naphthoquinone DMNQ-304 increased *Cdkn1a* mRNA levels and induced G₁ cell cycle arrest.

A second gene associated with DNA damage that segregated to the same cluster as *Cdkn1a* was *Pcna* (Figure 5.11B). The protein encoded by *Pcna* homotrimerizes to form a ring that clamps round double-stranded DNA and augments attachment of DNA polymerase- δ during replication[272;277]. The PCNA trimer is also important in DNA repair via the base excision repair (BER) and nucleotide excision repair (NER) pathways[277-279]. Both BER and NER pathways are involved in the repair of ROS-induced DNA damage to some degree[60].

5.3.2.4. Adaptive Changes in Energy Metabolism

DMNQ and MNQ exposure of rat hepatocytes resulted in transcriptional changes in genes that encode enzymes core to the regulation of energy metabolism (Table 5.5). Early in this response was the marked increase in *Pdk4* transcription, as evidenced by its segregation to cluster C7. *Pdk4*, which was one of the 'quinone signature genes' previously identified (Chapter 4), plays an important role in regulating glucose and fatty acid (FA) utilisation for energy production. The increased *Pdk4* transcription is consistent with increased expression of PDK, the enzyme responsible for inactivating the pyruvate dehydrogenase complex (PDC). The net effect is enhanced utilisation of FAs for acetyl-CoA synthesis and glucose conservation[180-182]. The shift towards FA utilisation for acetyl-CoA generation is supported by the concurrent decrease in *RGD1311092* transcription, which segregated to cluster C8. *RG1311092* encodes the rat orthologue of 3-oxoacyl-ACP synthase (mitochondrial) (OXSM), a mitochondrial enzyme involved in the synthesis of short chain FAs from acetyl-CoA. Thus, increased *Pdk4* and decreased *RGD1311092* point towards an overall shift towards FA catabolism for the purpose of supplying acetyl-CoA to the citric acid cycle. As discussed previously (Chapter 4), the underlying cause may be a need to conserve glucose/enhance FA utilisation in energy metabolism as a result of quinone-mediated perturbation of the mitochondrial respiratory chain. This could result in a rapidly enhanced utilisation of glucose without a proportional increase in energy production. The rapid depletion of glucose would then require a shift towards FA utilisation to generate the citric acid cycle substrate, acetyl-CoA.

At the same time, DMNQ and MNQ exposure increased the transcription of *protein phosphatase 1, regulatory (inhibitor) subunit 3c* (*Pppr3c*) and *Pppr3b*, which segregated to clusters C7 and C5, respectively. *Pppr3c* and *Pppr3b* encode the glycogen-targeting regulatory subunits (GSRs) protein targeting to glycogen (PTG) and G_L, respectively. The GSRs modulate the activity of the key glycogenic regulatory protein PP1 (protein phosphatase 1), which activates glycogen synthase (GS) and inactivates glycogen phosphorylase (PS)[280;281]. Overexpression of GSRs is associated with increased glycogenesis[280], as the opposing regulation of GS and PS favours synthesis of glycogen from glucose-6-phosphate derived from glycolysis.

Decreased PDC activity (as a result of the *Pdk4* overexpression) would be predicted to spare pyruvate from acetyl-CoA production. With its route into the citric acid cycle blocked, pyruvate is shunted into oxaloacetate generation by pyruvate carboxylase, the first step in gluconeogenesis[180]. To enhance gluconeogenesis, it appears that hepatocytes increased transcription of *Pck1* from 6 hours onwards (as evidenced by its segregation to cluster C3). *Pck1*, encodes phosphoenolpyruvate carboxykinase 1 (PCK1), a key enzyme in controlling the rate of gluconeogenesis[281]. PCK1 catalyzes the conversion of oxaloacetate to phosphoenolpyruvate[63]. When the increased transcription of *Pck1* is coupled with increased glycogenesis (as evidenced by increases in *Pppr3c* and *Pppr3b* transcription), it appears that hepatocytes are attempting to replenish glucose reserves depleted during the early phase of DMNQ and MNQ exposure.

In the latter part of the exposure period (12 to 18 hours), DMNQ and MNQ exposure resulted in decreased transcription of two subunits of the mitochondrial electron transport chain (*Cox6a2* and *Ndufa11*). As discussed previously (Chapters 1 and 4), naphthoquinones are known to disrupt the smooth flow of electrons along the mitochondrial respiratory chain, resulting in increased electron leakage and ROS generation[34]. Decreases in *Cox6a2* and *Ndufa11* transcription provides some evidence of down-regulation of oxidative phosphorylation with DMNQ and MNQ exposure. To compensate for reduced ATP synthesis via oxidative phosphorylation, it appears that the hepatocytes have responded by enhancing glycolysis, as evidenced by the increased transcription of *Pfkfb3*.

Pfkfb3 segregated to cluster C4, indicating increased transcription at 12 and 18 hours with DMNQ and MNQ exposure. *Pfkfb3* encodes a bifunctional enzyme called 6-phosphofructo-2-kinase/fructose-2,6-biphosphatase (PFKFB3), one of four such isozymes (PFKFB1-4)[282;283]. The PFKFBs both synthesise and degrade fructose-2,6-biphosphate (F-2,6-P2), a key modulator of glycolysis and gluconeogenesis[284]. Increased F-2,6-P2 enhances glycolysis through activation of 6-phosphofructo-1-kinase (PFK-1) and suppresses gluconeogenesis through inhibition of fructose-1,6-biphosphatase[282;285]. The different PFKFB isozymes have varying kinase:phosphatase ratio activities which results in varied control of glycolysis/gluconeogenesis. PFKFB3 has the highest kinase:phosphatase ratio of the four isozymes, favouring the synthesis of F-2,6-P2 and a high glycolytic rate[282;284].

PFKFB3 and PFKFB4 induction is known to occur under hypoxic conditions, such as those found in tumours *in vivo*, where a shift from aerobic to anaerobic respiration is essential for cell survival[282-284]. Minchenko *et al*[283] have also demonstrated that *Pfkfb3* transcription is increased in hepatoma cell lines (such as HepG2 and HepB3 cells) cultured under hypoxia. The induction of *Pfkfb3* has not been previously reported with oxidative stress or quinone exposure. However, perturbation of the mitochondrial respiratory chain (likely caused by DMNQ and MNQ exposure) would mimic the energy imbalance associated with hypoxia. Overall, it appears that DMNQ and MNQ exposed hepatocytes are optimising energy output as a result of quinone challenge. Early on during the exposure period, inefficient mitochondrial respiration leads to glucose depletion and results in a shift towards FA utilisation as an energy source. This is quickly followed by a response to replenish glucose stores by enhancing gluconeogenesis and glycogenesis. In the latter time points, where cytotoxicity is observed (and most likely marked perturbation of mitochondrial function), there is a shift from aerobic respiration to enhanced glycolysis as a source of energy.

5.3.2.5. Dysregulation of Iron/Haem Homeostasis Could Exacerbate Quinone Toxicity

Transcriptional regulation of several genes involved in iron and haem homeostasis was observed with DMNQ and MNQ exposure (Table 5.6). The most marked change was the induction of *Hmox1* from 4 hours onwards, as evidenced by its segregation to cluster C7. As mentioned previously (Chapter 4), *Hmox1* is an Nrf2-target gene and is well documented as being inducible following oxidative stress and/or quinone exposure. Conventionally, induction of *Hmox1* is thought to be an antioxidant response that will result in increased degradation of prooxidant free haem[148]. In addition biliverdin, the degradation product of haem, is thought to have antioxidant properties[137-139]. However, the degradation of haem also results in the production of free iron ions in the form of Fe^{2+} , which in the presence of H_2O_2 can drive ROS generation via the Fenton reaction (as discussed in Section 1.2.1). In the presence of redox cycling agents such as DMNQ and MNQ, which increase intracellular H_2O_2 levels via the cyclic generation of $O_2^{\bullet-}$, a rise in Fe^{2+} levels would exacerbate oxidative stress. Thus, it may be that *Hmox1* induction is an inappropriate response to quinone exposure.

Prolonged induction of *Hmox1* could also lead to depletion of the haem pool. The increased transcription of *Alas1* and *Slc25a37* provides some evidence that this may have occurred in DMNQ and MNQ exposed hepatocytes. Both *Alas1* and *Slc25a37* segregated to cluster C4, indicating increased transcription at later time points (i.e. 12 and 18 hours). *Alas1* encodes the enzyme ALAS1, which carries out the first (and rate-limiting) step in haem synthesis within the mitochondria[286;287]. Transcriptional regulation of *Alas1* occurs via a feedback mechanism as a result of decreased intracellular haem levels[286]. Increased transcription of *Slc25a37* provides supportive evidence for increased haem synthesis. *Slc25a37* encodes a membrane transporter belonging to the large SLC25 family of mitochondrial solute carriers[288]. The transporter encoded by *Slc25a37*, also known as *mitoferrin*, is expressed highly in the liver[288] and is the principle iron ion transporter in the mitochondria[289]. Shaw *et al*[289] demonstrated that its expression is essential for haem synthesis in erythroid cells. Thus, it appears that hepatocytes exposed to DMNQ or MNQ are increasing haem synthesis as a result of sustained *Hmox1* induction.

Three genes encoding proteins involved in iron homeostasis were regulated with DMNQ and MNQ exposure, *Tfrc*, *Tf* and *Hfe2* (Table 5.6). *Tfrc* segregated to cluster C3, indicating increased transcription from 6 hours onwards. As discussed previously (Chapter 4), *Tfrc* encodes the plasma membrane protein TFRC which plays a key role in intracellular iron transport. TFRC expression is normally regulated by intracellular iron levels via Iron Regulatory Protein 1 (IRP1) or IRP2-directed stabilisation of *Tfrc* mRNA[148-150]. Increased *Tfrc* mRNA stabilisation has been reported under certain prooxidant conditions *in vitro* (e.g. exposure of murine B6 fibroblasts to low levels of H₂O₂)[152]. However, due to the potential for intracellular iron loading to occur as a result, this type of response seems counter-intuitive. Iron loading in the presence of elevated H₂O₂ would simply result in increased ROS generation via Fenton chemistry.

Tf segregated to cluster C3, indicating decreased transcription with DMNQ and MNQ exposure at 12 and 18 hours. *Tf* encodes transferrin, the secreted protein ligand of TFRC that carries iron systemically. *In vivo*, decreases in serum transferrin are associated with increased hepatic iron levels [290;291]. Thus the decreased transcription of *Tf* observed with DMNQ and MNQ exposure in this study could contribute to hepatocyte iron loading. Harris *et al*[290] have reported decreased *Tf* transcription, both in rat hepatocytes and in the

livers of rats exposed to aflatoxin B₁, a liver carcinogen that induces hepatic oxidative stress and iron loading *in vivo*. A decrease in *Hfe2* transcription was also observed with DMNQ and MNQ exposure, although segregation to cluster C1 indicates a more gradual decrease peaking at 18 hours. *Hfe2* encodes hemochromatosis type 2 (juvenile) protein (HFE2), also known as haemojuviline (HJV). HFE2 is thought to be a key regulator of iron sensing and controlling hepatic iron levels[292;293]. Indeed, mutations in the *Hfe2* gene are thought to be the main cause of juvenile haemochromatosis in humans, and murine *Hfe2* knockouts model the disease[293;294]. It is believed that HFE2 modulates systemic and hepatic iron levels by regulating hepcidin synthesis, although the precise mechanism is yet to be elucidated. Hepcidin is a peptide hormone that decreases dietary iron absorption in the small intestine and iron recycling by macrophages through enhancing ferroportin internalisation in these tissues/cell types[294;295]. It is possible that the decrease in *Hfe2* transcription is a response to depletion in media iron levels, a possible consequence of the increase in *Tfrc* transcription.

When the increased *Tfrc* transcription is considered in the context of the decreases seen in *Tf* and *Hfe2* transcription, it appears that some form of perturbation in iron homeostasis has occurred with DMNQ and MNQ exposure. A possible mechanism is quinone or ROS-mediated inactivation of the iron sensing apparatus, namely IRP1 and IRP2. Exposure of rat cardiomyocyte H9c2 cells to low levels (<20µM) of doxorubicin, a quinone-related compound, results in inactivation of IRP1 and IRP2[296]. In the case of IRP1, inactivation is driven both by an alcohol metabolite of doxorubicin and ROS generated via redox cycling of its quinone moiety. Inactivation of IRP2 is predominantly caused through excessive ROS generation. Similarly, MNQ exposure of murine B6 fibroblasts causes disruption of the normal function of IRP1[153]. This resulted in an inability of the cells to sense changes in iron availability and coordinate the adaptive changes in key effectors of intracellular iron homeostasis (i.e. TFRC and ferritin proteins).

Overall the transcriptional changes in iron/haem metabolism-related genes are consistent with the idea that exposure of rat hepatocytes to DMNQ and MNQ caused dysregulation of intracellular iron homeostasis (as summarised in Figure 5.13). An initiating event is the early increase in *Hmox1* transcription, part of the antioxidant response to quinone exposure. However, prolonged overexpression of *Hmox1* results in haem depletion, followed by a

compensative increase in haem synthesis (as evidenced by increases *Alas1* and *Slc25a37* transcription). The net result is most likely an increase in intracellular free iron which would exacerbate oxidative stress by enhancing ROS generation via the Fenton reaction. At the same time, quinone and ROS-mediated inactivation of the iron sensing proteins IRP1 and IRP2 results in loss of transcriptional control of *Tfrc*, enhancing iron influx. When this is coupled with decreased transcription of *Tf* and *Hfe2*, overall iron loading of hepatocytes in the later part of the time course may result. This further potentiates the generation of ROS and exacerbation of cytotoxic effects of quinone exposure. With the exception of *Hmox1*, the transcriptional changes observed in iron/haem metabolism genes occur in the later part of the time course (12 to 18 hours). This coincides with the trend in increased cytotoxicity observed from 12 hours onwards with DMNQ and MNQ exposure, as evidenced by the increased LDH leakage (Figure 5.1).

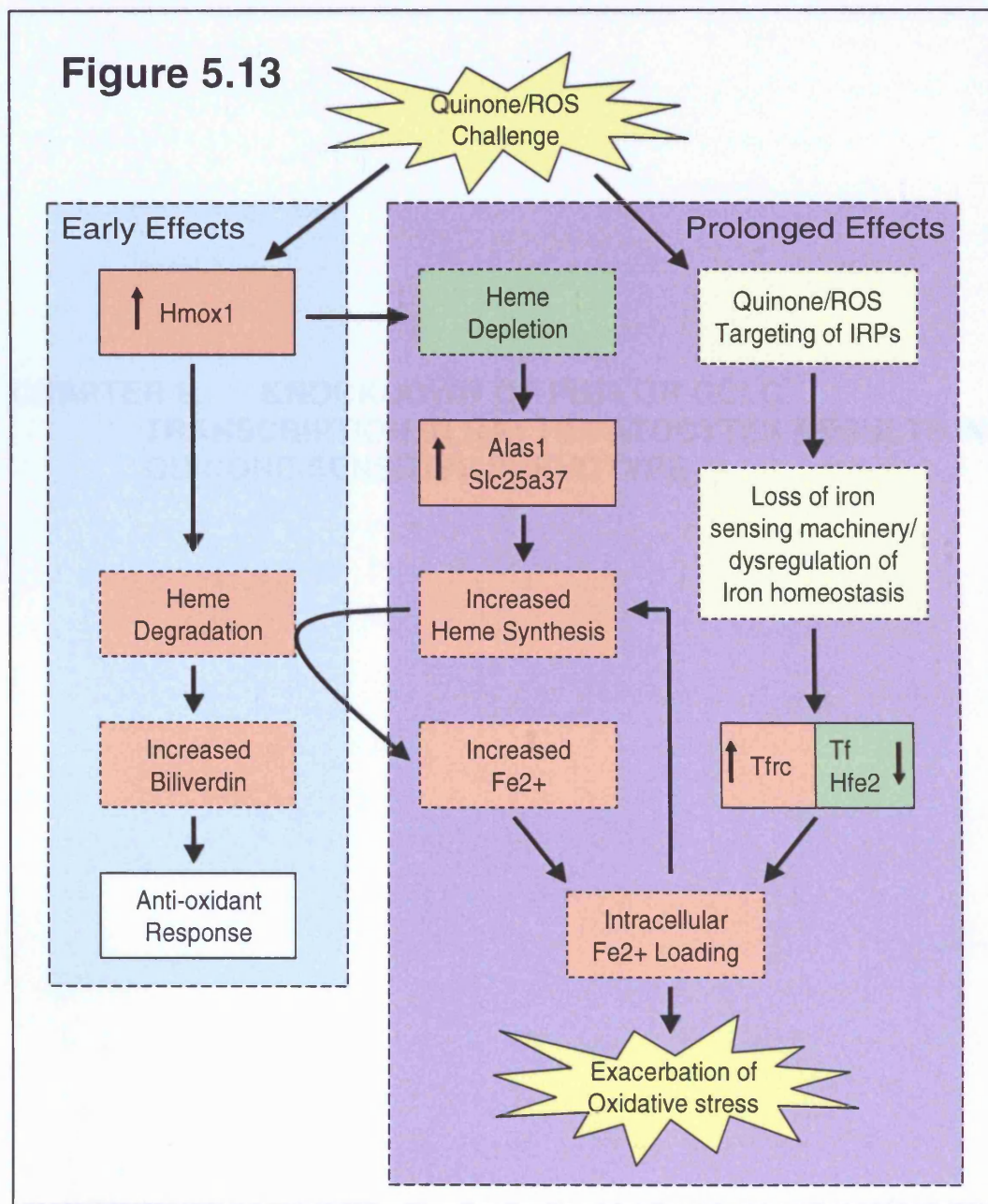


Figure 5.13: DMNQ and MNQ exposure in rat hepatocytes results in dysregulation of iron and haem homeostasis.

Based on transcriptional findings, DMNQ and MNQ exposure in rat hepatocytes results in induction of Hmx1. Initially this regulation forms part of a coordinated antioxidant response to quinone-mediated oxidative stress, resulting in haem degradation and production of the antioxidant biliverdin. Prolonged overexpression of Hmx1 depletes haem whilst increasing intracellular Fe^{2+} , exacerbating oxidative stress through Fenton chemistry. Depletion of haem results in Alas1 and Slc25a37 (mitoferrin) induction to increase haem synthesis, resulting in cyclic production of Fe^{2+} , as indicated. The sustained exposure of the iron sensing machinery to oxidative stress and quinone exposure also results in loss of homeostatic control of iron levels, as evidenced by the dysregulation of Tfrc, Tf and Hfe2. This would add to intracellular iron loading and further exacerbate oxidative stress.

**CHAPTER 6. KNOCKDOWN OF PIM3 OR GCLC
TRANSCRIPTION IN RAT HEPATOCYTES RESULTS IN A
QUINONE-SENSITIVE PHENOTYPE**

6.1. Introduction

Transcriptional investigations in rat hepatocytes exposed to a range of quinones identified *serine/threonine kinase Pim3* as being consistently increased in the absence of cytotoxicity (Chapter 4). A more comprehensive transcriptomic study, focussing on temporal responses to the redox cycling quinones 2,3-dimethoxy-1,4-naphthoquinone (DMNQ) and menadione (MNQ), confirmed the regulation of *Pim3* in rat hepatocytes (Chapter 5). Increased *Pim3* transcription was observed with both quinones between 6 and 18 hours (Figure 5.10B). As discussed previously (Chapters 4 and 5), *Pim3* is a member of the PIM family of serine/threonine kinases[297]. Other members of the PIM family (i.e. *Pim1* and *Pim2*) play a role in regulating anti-apoptotic signalling and *Pim3* mediates apoptosis in the HepG2 cell line[192]. Recently, the pro-apoptotic protein BCL2-antagonist of cell death (BAD) has been identified as a key target of PIM kinases[298]. Taken together, these data imply a role for *Pim3* in modulating the apoptotic response to quinone exposure in rat hepatocytes.

To investigate the role of *Pim3* further, I have sought to test the hypothesis that *Pim3* is an important gene involved in regulating the hepatocytes response to quinone-induced redox stress (and ameliorating associated cytotoxicity). To achieve this, I have employed the gene interference technique known as small interfering RNA (siRNA). siRNA utilises the endogenous RNA interference (RNAi) post-transcriptional control pathway first observed in plants[107] and later in *Caenorhabditis elegans*[108]. The term RNAi was later coined by Ketting and Plasterk[109]. An active RNAi pathway has since been demonstrated in mammalian cells and synthetic siRNAs are routinely exploited as tools for understanding gene function[110;111]. siRNAs are short double-stranded oligoribonucleotides that associate with the RNA-induced silencing complex (RISC) and induce degradation of complementary target mRNA sequences. The result is decreased levels of the target gene mRNA and consequently, decreased protein expression[110;111]. Through the use of conventional transfection techniques, it is possible to introduce siRNAs that target a gene of interest into cells cultured *in vitro*. This can bring about suppression of both the mRNA and protein expression of that gene. Once gene suppression (or 'knockdown') has been achieved, the role of that gene can be inferred by studying phenotypic changes in the cells transfected.

The aim of this study was to investigate whether siRNA-mediated knockdown of *Pim3* in rat hepatocytes results in a quinone-sensitive phenotype. In addition to investigating the role of *Pim3* knockdown in quinone cytotoxicity, the phenotypic changes associated with suppression of *Glutamate-cysteine ligase, catalytic subunit (Gclc)* were also assessed. As discussed previously (Chapter 1), *Gclc* encodes the catalytic subunit of the enzyme that carries out the rate-limiting step in glutathione (GSH) biosynthesis. Increased *Gclc* transcription in response to DMNQ and MNQ exposure was previously shown (Chapter 5). It was concluded that increased *Gclc* transcription is consistent with an adaptive response by rat hepatocytes to increase GSH levels as a consequence of quinone challenge (i.e. redox stress/thiol arylation-induced GSH depletion). Thus, suppression of *Gclc* would be predicted to result in a reduced capacity to synthesise GSH, severely compromising the hepatocytes ability to survive quinone challenge. In this instance, *Gclc* knockdown served as a 'proof of principle' (in terms of the utility of siRNA-mediated gene interference) in primary rat hepatocytes.

At the time this work was undertaken, no published data existed on successful transfection and siRNA-mediated gene knockdown in primary hepatocytes. A number of groups have successfully demonstrated siRNA-mediated gene knockdown in hepatocyte-derived hepatoma cell lines[299-303]. In general, primary cells are a more challenging prospect than cell lines for siRNA transfection (Personal communication, 2005: Dr Neil Clarke, Gene Interference Group, GSK R&D). The conspicuous absence of published work in primary hepatocytes is consistent with this assertion. After consulting with the technical support groups of various specialist manufacturers, *TransIT-TKO*[®] (Mirus Corporation) was identified as the most appropriate transfection reagent to use in this study. Mirus state that *TransIT-TKO*[®] is an efficient transfectant reagent in a range of primary cells and cell lines, including primary mouse hepatocytes (<http://www.mirusbio.com/products/transit/tko/index.asp#data>). Data presented on the Mirus website indicates knockdown of at least 70 percent for two endogenous genes (ABC/A1 and Lamin A/C).

Prior to undertaking *Pim3* or *Gclc* knockdown experiments, it was decided to evaluate the effectiveness of *TransIT-TKO*[®] in suppressing transcription of a housekeeper gene. *Glyceraldehyde-3-phosphate dehydrogenase (Gapdh)* was selected for this and a validated

rat-specific siRNA was obtained from Ambion (Table 6.1). To maintain consistency with previous experiments (Chapters 3, 4 and 5), siRNA transfection was carried out during the course of the routine overnight (16 hours) recovery period that rat hepatocytes were allowed prior to treatment. Any subsequent quinone exposure period (of up to 8 hours) would mean that approximately 24 hours had been allowed for target gene knockdown. To evaluate the cytotoxicity of the *TransIT-TKO*[®] transfection reagent in rat hepatocytes, several concentrations were tested during this experiment and LDH leakage measured. Initial concentration selection was based around the manufactures recommendations.

Similar titration experiments were carried out with *Pim3* and *Gclc* siRNAs to identify the most potent sequences and optimal concentrations. Three pre-designed siRNAs for each gene were ordered from Ambion (Table 6.1) and target gene knockdown assessed at three concentrations (25, 50 and 100nM). Due to the potential for off-target effects with siRNA transfection, it is good practice to demonstrate a phenotype associated with target gene knockdown with more than one siRNA sequence. In addition, the efficiency of target gene knockdown can vary for different siRNAs specific for the same gene. The assessment of knockdown efficiency for three siRNAs per gene allowed the selection of the two most potent sequences for the subsequent quinone-challenge experiments.

Table 6.1: Control and Target Gene siRNA Details

siRNA Name	Ambion Product Code	Sense Sequence (5'→3')	Antisense Sequence (5'→3')
GAPDH siRNA [§]	4631	Not Supplied	Not Supplied
Control siRNA [*]	4611	Not Supplied	Not Supplied
<i>Pim3</i> siRNA 1	16706-52109	GGACACGGUCUACACUGACTt	GUCAGUGUAGACCGUGUCctt
<i>Pim3</i> siRNA 2	16704-192160	GCAGCUUAAUUGAGUGGUGUtt	ACACCACUCAAUAAAGCUGctg
<i>Pim3</i> siRNA 3	16704-192161	CGGUCUCUUUUUAUGGUGtt	CACCAUAAAUAAAGACCGGtg
<i>Gclc</i> siRNA 1	16704-200497	CGAGGUGGAGUACAUGUUGtt	CAACAUGUACUCCACCUCGtc
<i>Gclc</i> siRNA 2	16704-200498	GGACAACAUGAGGAAACGctt	GCGUUUCCUCAUGUUGUCctc
<i>Gclc</i> siRNA 3	16704-200499	CCAUUUUGAGAAUAUUCAGtt	CUGAAUAUUCUCAAAAUGGtc

[§]Silencer[®] GAPDH siRNA (Human, Mouse, Rat), ^{*}Silencer[®] Negative Control #1

Once *Pim3* and *Gclc* siRNAs were selected, quinone challenge experiments were carried out to investigate phenotypic changes associated with target gene knockdown. The redox cycling quinones DMNQ and MNQ were used to challenge rat hepatocytes. Concentrations previously defined as sub-toxic at up to 8 hours exposure (Chapter 3) were used to investigate whether *Pim3* and *Gclc* knockdown resulted in a more sensitive phenotype. To aid interpretation of the resultant phenotypes, relevant endpoints were assessed. LDH leakage was measured to indicate general cytotoxicity and necrotic cell death. As *Pim3* is known to augment the anti-apoptotic response, activated caspase 3 activity was measured. GSH levels were also measured due to the integral role *Gclc* plays in maintaining its biosynthesis.

6.2. Results

Rat hepatocytes were prepared and treated according to the methods outlined in Section 2.1. Transfection of rat hepatocyte monolayers was carried out according to the methods outlined in Section 2.2.

6.2.1. Optimisation Experiments

A titration experiment was carried out to select the optimal concentration of *TransIT-TKO*[®] to use for transfection of rat hepatocytes monolayers, based on efficiency of housekeeper gene knockdown (*Gapdh*) and level of cytotoxicity (LDH Leakage). Following a 2 hours attachment period, hepatocytes were exposed to various transfection conditions for 16 hours (as outlined in Table 6.2). The transfection media were changed for maintenance medium (Williams E Incomplete) and following a further 8 hours incubation (total of 24 hours) *Gapdh* transcription and LDH leakage were measured.

Table 6.2: Transfection media conditions used to determine optimal *TransIT-TKO*[®] conditions for target gene knockdown

Transfection Media	Conditions	Purpose
Media Control	Williams E incomplete media	Control culture conditions
100nM GAPDH siRNA	100nM GAPDH siRNA in WE incomplete media containing 5.0, 7.5, or 10.0 μ L/mL <i>TransIT-TKO</i> [®] reagent	Evaluation of target gene knockdown (<i>Gapdh</i>) efficiency and cytotoxicity
100nM Control siRNA	100nM Control siRNA in WE incomplete media containing 5.0, 7.5, or 10.0 μ L/mL <i>TransIT-TKO</i> [®] reagent	Reference control for <i>Gapdh</i> siRNA exposed cultures
Transfectant Control	WE incomplete media containing 5.0, 7.5, or 10.0 μ L/mL <i>TransIT-TKO</i> [®] reagent	Reference control for evaluating level of cytotoxicity due to transfectant reagent alone

Total RNA was isolated from triplicate cultures and SybrMan[®] quantitative-polymerase chain reaction (RT-QPCR) used to determine the level of *Gapdh* transcription (according to the methods outlined in Sections 2.10 and 2.13, respectively). The level of *Gapdh* transcription in Media Control and Control siRNA exposed cultures were comparable for all three *TransIT-TKO*[®] concentrations used (Figure 6.1A). Transfection of rat hepatocytes with 100nM *Gapdh* siRNA resulted in greater than 95 percent suppression of *Gapdh* expression (relative to Control siRNA exposed cultures) for all three *TransIT-TKO*[®]

concentrations tested (Figure 6.1A). LDH leakage was assessed in triplicate cultures (according to the methodology outlined in Section 2.3) for all transfection conditions detailed in Table 6.2 (Figure 6.1B). There was a general trend of increased LDH leakage with increasing concentration of *TransIT-TKO*[®]. There were no marked differences in the level of LDH leakage observed in cultures exposed to Control siRNA, *Gapdh* siRNA or *TransIT-TKO*[®] alone. Based on the low level of LDH leakage and effective *Gapdh* knockdown, 5.0 μ L/mL was selected as the optimal *TransIT-TKO*[®] reagent transfection concentration.

Based on the successful knockdown of a housekeeper gene in rat hepatocyte monolayers, performance of the *TransIT-TKO*[®] transfectant reagent was evaluated for the selected target genes (i.e. *Pim3* and *Gclc*). Three different siRNAs for each target gene were tested at final concentrations of 25, 50 and 100nM (according to the method outlined in Section 2.2). Following 16 hours of transfection, the media was replaced with fresh maintenance medium and the hepatocytes incubated for a further 8 hours, after which the level of *Pim3/Gclc* transcription and LDH leakage was measured and compared to that observed in control cultures (Media Control, 100nM Control siRNA and 5.0 μ L/mL *TransIT-TKO*[®] Control). Total RNA was isolated from triplicate cultures and SybrMan[®] RT-QPCR used to determine the level of gene transcription (according to the methods outlined in Sections 2.11 and 2.13, respectively). The level of *Pim3* or *Gclc* transcription was normalised to the housekeeper *beta actin* and expressed as percent of Control siRNA transfected cultures. LDH leakage was measured in triplicate cultures as outlined in Section 2.3.

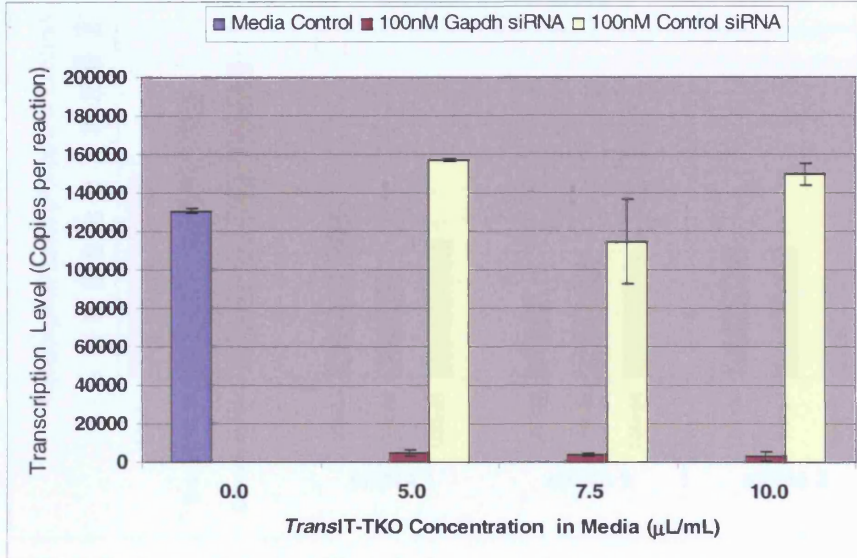
All three *Pim3* siRNAs suppressed *Pim3* transcription relative to the Control siRNA transfected cultures (Figure 6.2A), although there were no clear dose-responses. Overall, *Pim3* siRNA 2 and *Pim3* siRNA 3 performed best, with *Pim3* expression at the 100nM concentration 39 and 32 percent of Control siRNA cultures, respectively. No marked changes in LDH leakage were noted with any of the *Pim3* siRNAs, when compared to the Control siRNA transfected cultures (Figure 6.2B). The level of LDH leakage was approximately 41 percent for Control siRNA transfected cultures versus between 42 and 47 percent for *Pim3* siRNA transfected cultures. No siRNA concentration-related trend in LDH leakage was apparent for *Pim3* siRNA transfection.

All three *Gclc* siRNAs caused suppression of *Gclc* transcription relative to the Control siRNA transfected cultures (Figure 6.3A). Dose-related suppression of *Gclc* transcription was observed for *Gclc* siRNA 1 and *Gclc* siRNA 2, with the 100nM concentration resulting in greater than 90 percent and greater than 85 percent knockdown, respectively. *Gclc* siRNA 3 was less potent, with approximately 65 percent knockdown at 100nM and no clear dose-relationship. LDH leakage for all three concentrations of *Gclc* siRNA 1 and *Gclc* siRNA 2 were comparable to Control siRNA levels (approximately 40 percent leakage). *Gclc* siRNA 3 transfection resulted in a slightly elevated level of LDH leakage at all three concentrations (45 to 50 percent).

Based on the transcription and LDH leakage data, *Pim3* siRNAs 2 and 3, and *Gclc* siRNAs 1 and 2 were selected as the most effective siRNAs for further investigation. Due to the enhanced *Gclc* knockdown observed (and absence of increased cytotoxicity), it was decided to transfect at a consistent siRNA concentration of 100nM for all future experiments.

Figure 6.1

A: GAPDH Transcription



B: LDH Leakage

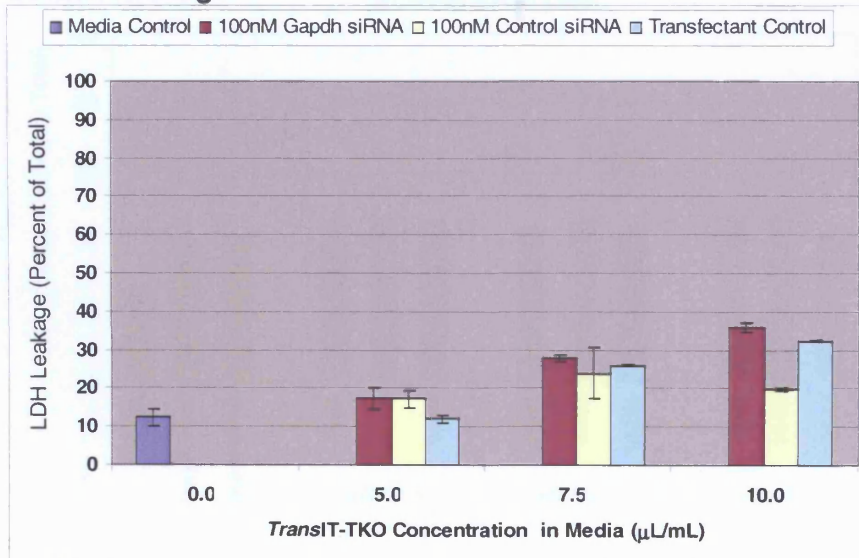
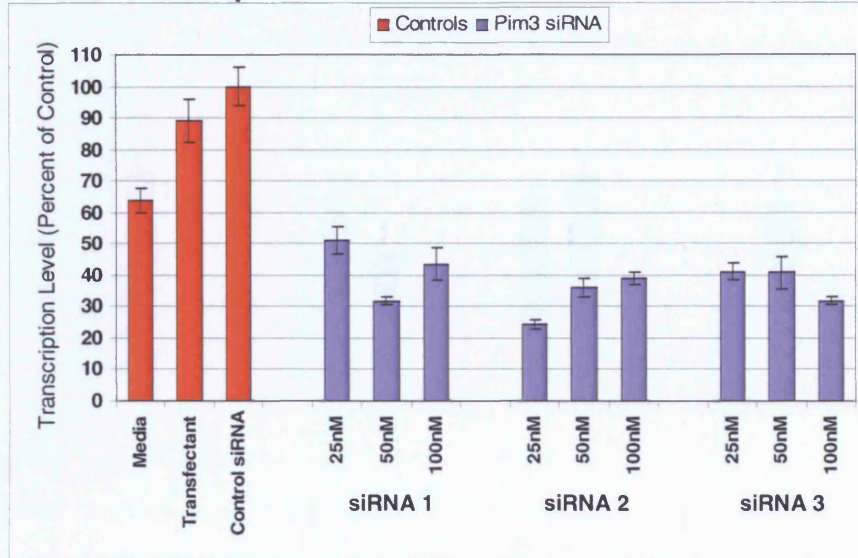


Figure 6.1: *Gapdh* transcription (A) and LDH Leakage (B) in rat hepatocyte monolayers exposed to 0.0, 5.0, 7.5 or 10.0 $\mu\text{L/mL}$ TransIT-TKO[®] in WE incomplete media for 16 hours, followed by 8 hours in fresh WE incomplete media. Results are mean values of triplicate cultures \pm SD (from a single experiment).

Figure 6.2

A: Pim3 Transcription



B: Pim3 LDH Leakage

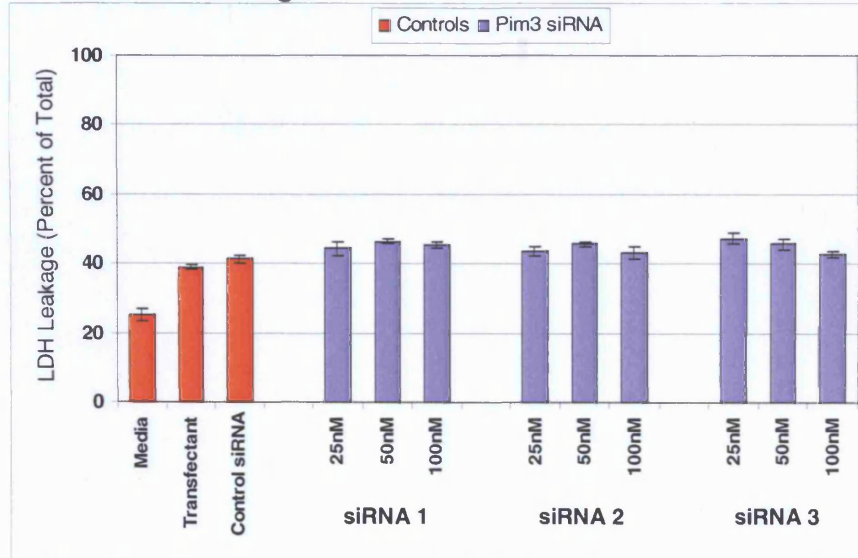
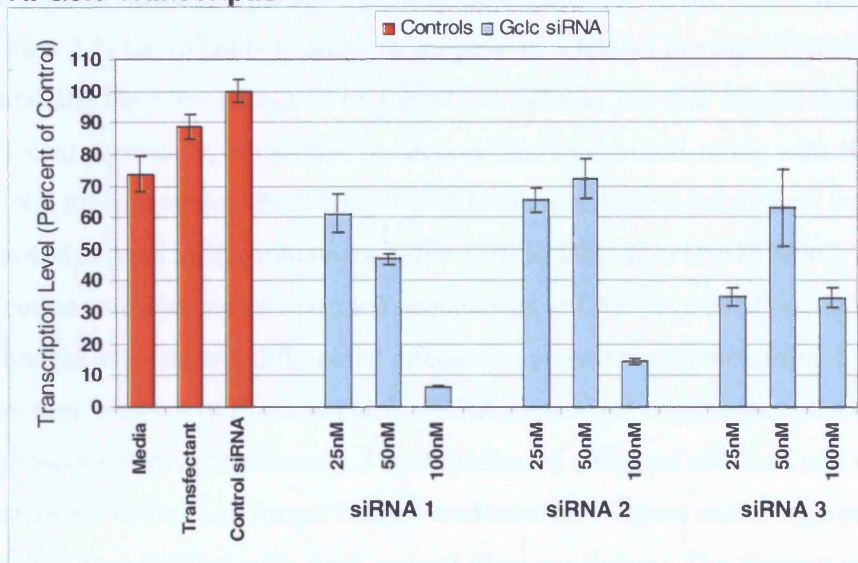


Figure 6.2: *Pim3* transcription (A) and LDH leakage (B) in rat hepatocyte monolayers transfected with three different *Pim3* siRNAs at 25, 50, or 100nM final concentrations (transfection with *TransIT-TKO*[®] at 10.0 μ L/mL in WE incomplete media for 16 hours, followed by 8 hours in fresh WE incomplete media). Results are mean values of triplicate cultures \pm SD (from a single experiment).

Figure 6.3

A: Gclc Transcription



B: GcSc LDH Leakage

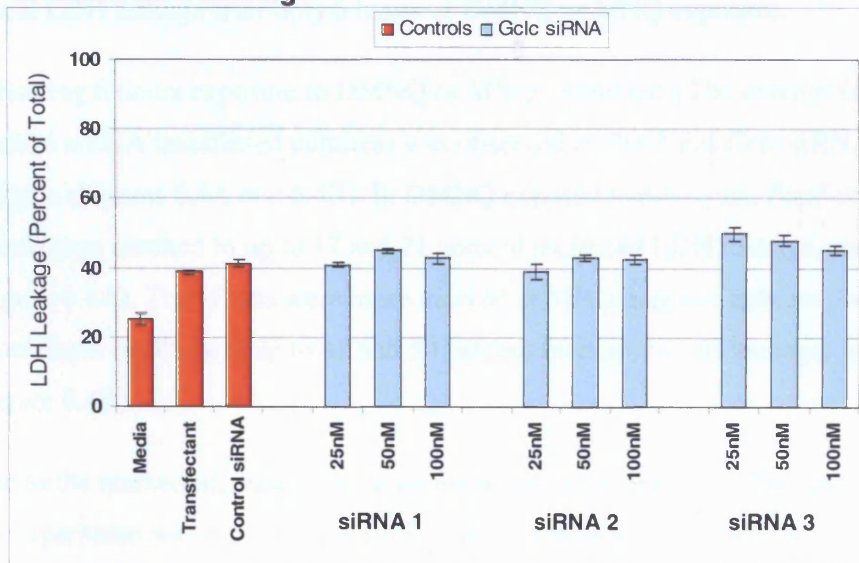


Figure 6.3: Gclc transcription (A) and LDH leakage (B) in rat hepatocyte monolayers transfected with three different Gclc siRNAs at 25, 50, or 100nM final concentrations (transfection with *TransIT-TKO*[®] at 10.0 μ L/mL in WE incomplete media for 16 hours, followed by 8 hours in fresh WE incomplete media). Results are mean values of triplicate cultures \pm SD (from a single experiment).

6.2.2. Quinone Challenge of Rat Hepatocytes Transfected with *Pim3* or *Gclc* siRNAs

Rat hepatocyte monolayer cultures were incubated with transfection media (as outlined in Section 2.2) for 16 hours to allow target gene knockdown to occur. Transfection media containing the *Pim3* siRNAs 2 or 3 and *Gclc* siRNAs 1 or 2 at 100nM final concentration (selected previously, as outlined in Section 6.2.1) were used, along with 100nM Control siRNA for comparison. Following the 16 hours transfection incubation, hepatocytes were exposed to fresh media containing either 150 μ M DMNQ or 25 μ M MNQ. The original intention was to expose transfected hepatocytes to DMNQ or MNQ-containing media for 8 hours and evaluate any differential effects on cytotoxicity by measuring LDH leakage. However, viewing of *Pim3* and *Gclc* siRNA transfected hepatocyte cultures by light microscopy after approximately 5 hours indicated a marked effect on cell viability. Hepatocyte cultures no longer formed confluent monolayers and a large number of rounded, free-floating cells, were present (data not shown). The changes were far more marked in MNQ-exposed cultures. Thus, it was decided to sample triplicate cultures to assess LDH leakage after only 6 hours of DMNQ or MNQ exposure.

Following 6 hours exposure to DMNQ or MNQ, increased LDH leakage (relative to Control siRNA transfected cultures) was observed in *Pim3* and *Gclc* siRNA transfected cultures (Figures 6.4A and 6.4B). In DMNQ exposed hepatocytes, *Pim3* or *Gclc* knockdown resulted in up to 17 and 21 percent increased LDH leakage, respectively (Figure 6.4A). The effects were more marked in MNQ exposed cultures, with *Pim3* or *Gclc* knockdown resulting in up to 48 and 50 percent increased LDH leakage, respectively (Figure 6.4B).

Due to the marked increase in quinone sensitivity observed with *Pim3* or *Gclc* knockdown, the experiment was repeated and LDH leakage assessed following 3 hours of DMNQ or MNQ exposure. In addition to LDH leakage, activated caspase 3 and total GSH levels were assessed (according to the methods outlined in Sections 2.3, 2.7.2 and 2.8, respectively). To determine the level of target gene knockdown, SybrMan[®] RT-QPCR was used to assess *Pim3* and *Gclc* transcription under the same conditions. Following 3 hours exposure to DMNQ or MNQ, increased LDH leakage (relative to Control siRNA transfected cultures) was observed in *Pim3* and *Gclc* siRNA transfected cultures (Figures 6.4C and 6.4D). In DMNQ exposed hepatocytes, *Pim3* or *Gclc* knockdown resulted in up to 13 and 24 percent

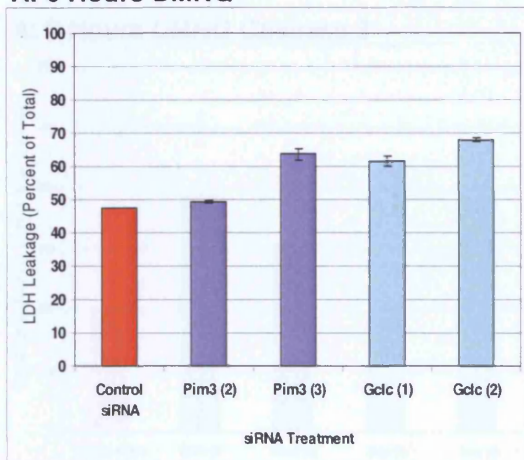
increased LDH leakage, respectively (Figure 6.4C). As was seen at 6 hours, the effects were more marked in MNQ exposed cultures, with *Pim3* or *Gclc* knockdown resulting in up to 48 and 65 percent increased LDH leakage, respectively (Figure 6.4D).

Pim3 knockdown resulted in increased activated caspase 3 activity in rat hepatocyte cultures exposed to DMNQ and MNQ for 3 hours (Figures 6.5A and 6.5B, respectively). Increases of up to 93 percent (DMNQ exposed cultures) and 133 percent (MNQ exposed cultures) over caspase 3 levels found in Control siRNA-transfected cultures were observed. The effects induced by *Pim3* siRNA 2 and 3 were comparable. Activated caspase 3 levels were also increased with *Gclc* knockdown in DMNQ and MNQ exposed hepatocyte cultures (Figures 6.5A and 6.5B, respectively), although the effects were not as consistent as those seen with the *Pim3* siRNAs. Caspase 3 levels were unchanged in DMNQ exposed cultures with *Gclc* siRNA 1 and increased 73 percent with MNQ exposure. The opposite was observed with *Gclc* siRNA 2, where caspase 3 activity was increased by 89 percent in DMNQ exposed cultures and unchanged in MNQ exposed cultures.

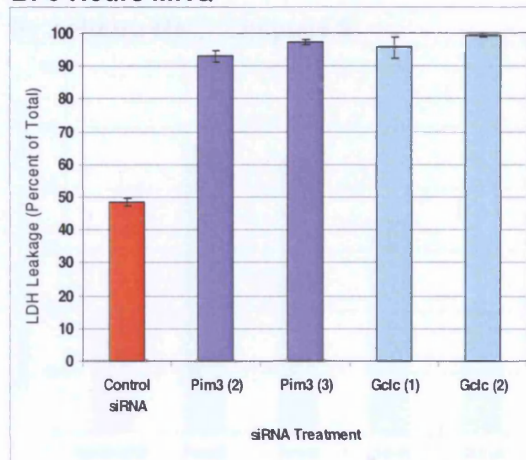
Pim3 and *Gclc* knockdown resulted in different effects on GSH levels following 3 hours DMNQ or MNQ exposure (Figures 6.5C and 6.5D, respectively). In general, GSH levels in hepatocyte cultures transfected with *Pim3* siRNAs remained comparable to those observed in Control siRNA cultures (16 to 23 percent decreases in DMNQ-exposed cultures and no change in MNQ-exposed cultures). GSH levels were markedly decreased with *Gclc* knockdown, with approximately 40 percent less observed in DMNQ-exposed cultures and up to 91 percent less in MNQ-exposed cultures.

Figure 6.4

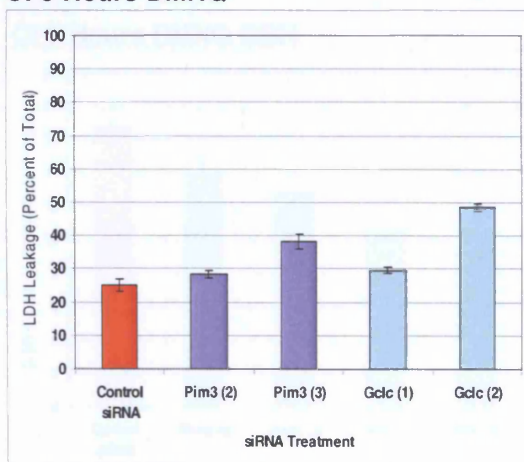
A: 6 Hours DMNQ



B: 6 Hours MNQ



C: 3 Hours DMNQ



D: 3 Hours MNQ

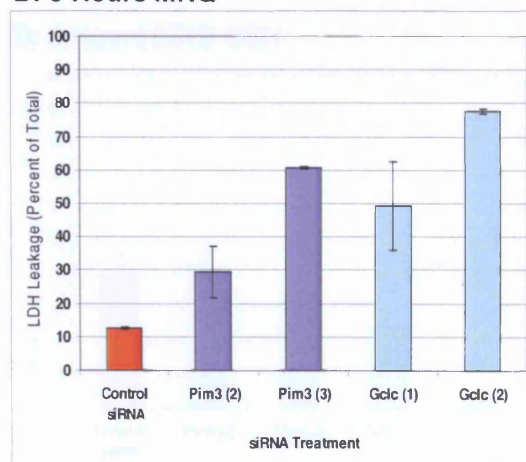
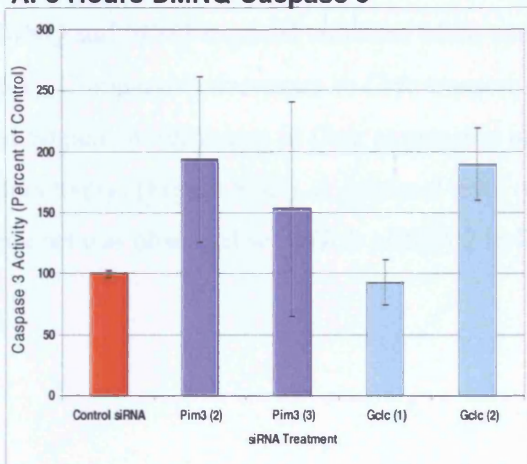


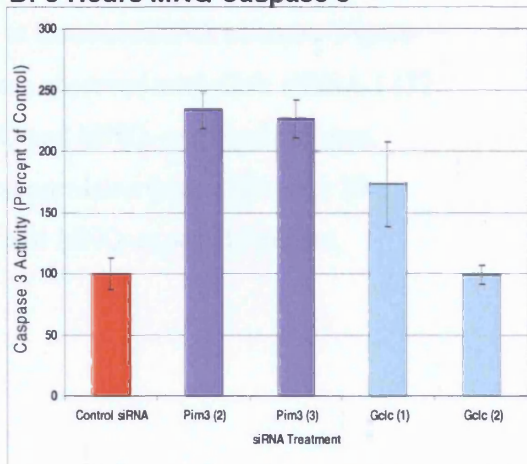
Figure 6.4: LDH leakage in rat hepatocyte monolayers challenged with DMNQ or MNQ following *Pim3* or *Gclc* knockdown. LDH leakage was assessed following 6 hours DMNQ (A) or MNQ (B) exposure in the first experiment. In the second experiment LDH leakage was assessed following 3 hours DMNQ (C) or MNQ (D) exposure. Results are mean values of triplicate cultures \pm SD (from single experiments).

Figure 6.5

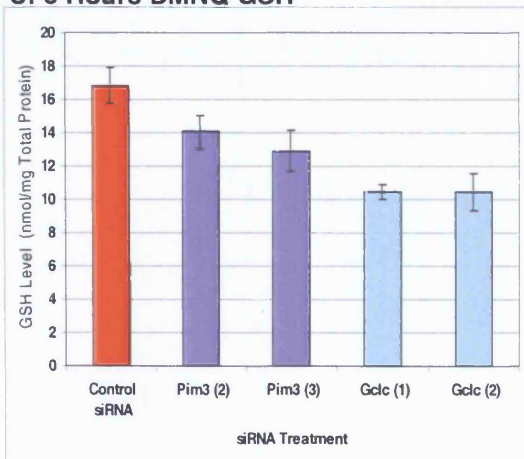
A: 3 Hours DMNQ Caspase 3



B: 3 Hours MNQ Caspase 3



C: 3 Hours DMNQ GSH



D: 3 Hours MNQ GSH

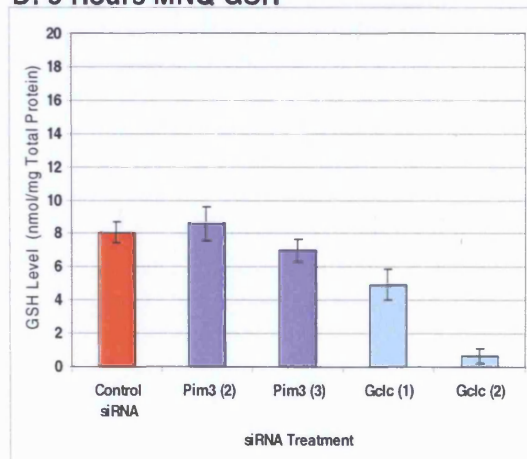
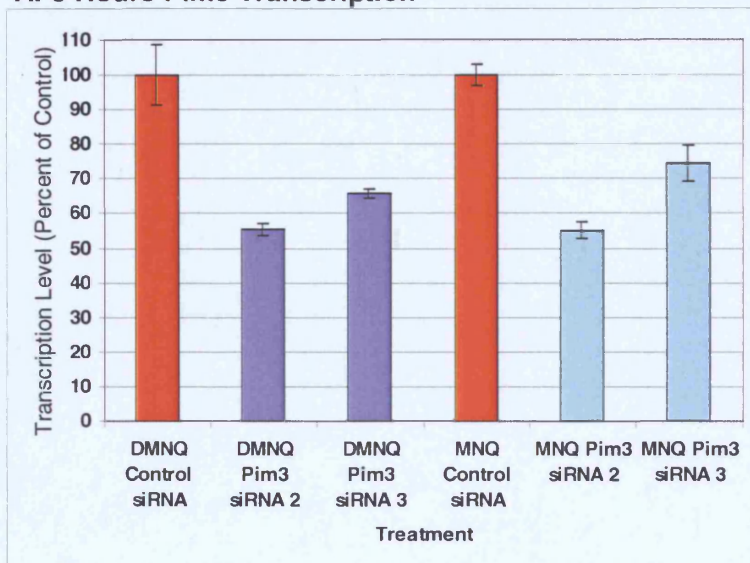


Figure 6.5: Activated caspase 3 activity and GSH levels in rat hepatocyte monolayers challenged with DMNQ or MNQ following *Pim3* or *Gclc* knockdown. Caspase 3 activity was assessed following 3 hours DMNQ (A) or MNQ (B) exposure. In the same experiment GSH levels were assessed following DMNQ (C) or MNQ (D) exposure. Results are mean values of triplicate cultures \pm SD (from a single experiment).

The transcription levels of *Pim3* (Figure 6.6A) and *Gclc* (Figure 6.6B) in transfected hepatocytes following 3 hours DMNQ or MNQ exposure was not suppressed to the same extent as had been seen during the optimisation experiment (Figures 6.2A and 6.3A). Transfection with *Pim3* siRNAs resulted in up to 45 percent decreased *Pim3* expression in DMNQ and MNQ-exposed cultures, when compared to Control siRNA cultures (Figure 6.6A). Comparable decreases in *Gclc* transcription were observed with *Gclc* siRNA 1 (37 and 50 percent decreases in *Gclc* expression in DMNQ and MNQ –exposed cultures, respectively) (Figure 6.6B). A minimal level of *Gclc* suppression (approximately 20 percent) was observed with *Gclc* siRNA 2 in DMNQ and MNQ-exposed cultures.

Figure 6.6

A: 3 Hours Pim3 Transcription



B: 3 Hours Gclc Transcription

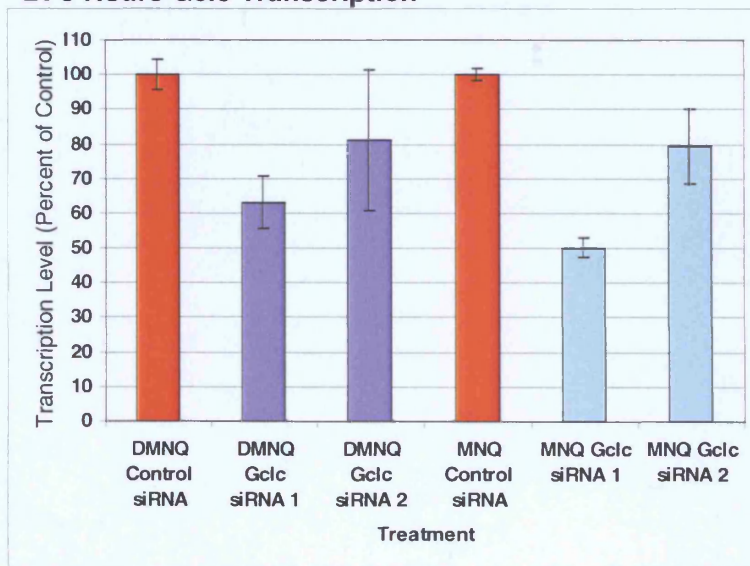


Figure 6.6: *Pim3* (A) and *Gclc* (B) transcription in rat hepatocyte monolayers challenged with DMNQ or MNQ following *Pim3* or *Gclc* knockdown. Results are mean values of triplicate cultures \pm SD (from a single experiment). *Pim3* and *Gclc* expression are expressed as percent of concurrent Control siRNA transfected cultures.

6.3. Discussion

Increased transcription of *Pim3* and *Gclc* in rat hepatocytes exposed to a range of quinones has been consistently demonstrated (Chapters 4 and 5). Based on the literature available, a functional interpretation of consequence of increased *Pim3* or *Gclc* transcription was made. This implicated *Pim3* and *Gclc* in mediating the anti-apoptotic and antioxidant responses in rat hepatocytes exposed to quinones (discussed in Sections 5.3.2.1 and 5.3.2.2, respectively). To confirm this interpretation, the consequence of reduced *Pim3* or *Gclc* transcription on the ability of rat hepatocytes to respond to quinone challenge was investigated using gene interference. The main aim of this study was to utilise siRNA-mediated gene knockdown to investigate the effect of *Pim3* or *Gclc* suppression on the sensitivity of rat hepatocytes to quinone-mediated redox challenge.

6.3.1. Optimisation of Rat Hepatocyte Transfection and Selection of Target Gene siRNAs

Prior to investigating the role of *Pim3* or *Gclc* suppression in quinone-mediated redox stress, it was necessary to demonstrate that siRNA-mediated gene knockdown was possible in rat hepatocytes. The lack of published siRNA-related studies in primary hepatocytes implied that this may prove a significant challenge. *TransIT-TKO*[®] was selected as a promising transfectant reagent, based on indicative data provided by the manufacturer (Mirus Corporation). It was decided to evaluate the performance of *TransIT-TKO*[®] in rat hepatocyte monolayers, both in terms of cytotoxicity and efficiency of knockdown of the housekeeper gene *Gapdh* (using a previously validated siRNA).

Transfection of rat hepatocytes with 100nM GAPDH siRNA (Ambion) at three concentrations of *TransIT-TKO*[®] (5.0, 7.5 and 10.0 μ L/mL) resulted in marked suppression of *Gapdh* mRNA by 24 hours (Figure 6.1A). At all three *TransIT-TKO*[®] concentrations tested, greater than 95 percent suppression of *Gapdh* was observed. This clearly demonstrated the effectiveness of *TransIT-TKO*[®] for siRNA transfection of rat hepatocytes monolayers. Slight increases in LDH leakage (when compared to media control-exposed cultures) under the same conditions at the 7.5 and 10.0 μ L/mL *TransIT-TKO*[®] concentrations were indicative of elevated cytotoxicity (Figure 6.1B). The levels of LDH leakage observed with 5.0 μ L/mL *TransIT-TKO*[®] were in line with those seen in the media

controls. Thus, 5.0 μ L/mL *TransIT-TKO*[®] was selected as the optimal transfection concentration based on the low level of cytotoxicity and efficient *Gapdh* knockdown.

Using the optimal transfection conditions, the potency of three different pre-designed siRNAs per gene for *Pim3* and *Gclc* were tested at concentrations of 25, 50 and 100nM. Very similar levels of potency were observed for all three *Pim3* siRNAs (Figure 6.2A). Overall *Pim3* siRNAs 2 and 3 resulted in the most consistent suppression of *Pim3* mRNA, although there were no clear dose responses. Suppression of *Pim3* mRNA of between 60 to 70 percent of Control siRNA transfected cultures were achieved at 100nM 24 hours after transfection. Similar target gene knockdown was observed for *Gclc* siRNA 3, although *Gclc* siRNAs 1 and 2 were far more potent (Figure 6.3A). *Gclc* mRNA suppression of greater than 80 percent was achieved at the 100nM concentration for *Gclc* siRNAs 1 and 2. None of the target gene siRNAs used for transfection caused a notable increase in cytotoxicity when compared to Control siRNA transfected cultures (Figures 6.2A and 6.3B), at any of the concentrations tested. Based on the potency of target gene suppression (and the absence of any discernable increase in cytotoxicity) *Pim3* siRNAs 2 and 3 and *Gclc* siRNAs 1 and 2 were selected for the quinone challenge studies. Due to the enhanced *Gclc* knockdown observed at the 100nM, it was decided to transfect at this concentration for all future experiments with *Pim3* and *Gclc* siRNAs.

In general, the target level of mRNA suppression for *in vitro* RNAi experiments is greater than 70 percent (Personal communication, 2005: Dr Neil Clarke, Gene Interference Group, GSK R&D). This was attained for *Gclc* but not for *Pim3* under the conditions tested. It is possible that extending the culture period in maintenance media prior to assessing *Pim3* mRNA levels may have resulted in a more marked decrease. However, this would mean markedly extending the culture period prior to quinone challenge compared to the transcriptional studies carried out previously (Chapters 4 and 5). It is possible that the relative sensitivity of hepatocytes to quinone challenge would change as a result of an extended culture period, reducing the comparability of the RNAi experiments to the original transcriptomics studies.

6.3.2. DMNQ and MNQ Challenge of Rat Hepatocytes With Suppressed *Pim3* or *Gclc* Expression

Pim3 knockdown resulted in increased cytotoxicity (as assessed by LDH leakage) within 3 hours of DMNQ or MNQ exposure (Figures 6.4C and D). The increased sensitivity to DMNQ or MNQ-mediated cytotoxicity was even more pronounced by 6 hours (Figures 6.4A and B). The fact that the concentrations of DMNQ and MNQ used had been consistently shown to be sub-toxic with up to 8 hours exposure (Chapters 3, 4 and 5) underscores the importance of *Pim3* induction in protecting rat hepatocytes from quinone-mediated cytotoxicity. Interestingly, the phenotype induced by *Pim3* knockdown was markedly more sensitive to MNQ challenge than DMNQ. As discussed previously (Chapter 3), MNQ redox cycles to a similar extent as DMNQ and also has the capacity to arylate thiol moieties[26]. Thus, it appears that that *Pim3* is not only important in the response to cytotoxicity resulting from redox stress, but also sulphhydryl arylation.

Pim3 knockdown in rat hepatocytes resulted in increases in activated caspase 3 activity after 3 hours exposure to DMNQ and MNQ (Figures 6.5 A and B). This change is indicative of increased apoptosis and is consistent with the known role that *Pim3* plays in mediating the anti-apoptotic response in a range of tissues and cell lines[191;252;304]. The effect that *Pim3* knockdown had on activated caspase 3 levels in rat hepatocytes exposed to redox cycling quinones provides evidence that *Pim3* is important in regulating the anti-apoptotic response to redox stress. A role for *Pim3* in preventing apoptosis and promoting proliferation has been demonstrated in hepatocyte-related systems (e.g. human hepatocarcinomas and hepatoma cell lines)[192]. However, this is the first time that a role for *Pim3* in preventing apoptosis during oxidative stress has been proposed.

Transfection with both *Pim3* siRNAs resulted in minimal effects on GSH levels following 3 hours DMNQ or MNQ challenge, when compared to Control siRNA cultures (Figure 6.5C and D). The lack of any marked decrease in GSH levels suggests that *Pim3* knockdown is not associated with altered glutathione metabolism. This was not the case with *Gclc* knockdown, which resulted in decreased GSH levels relative to Control siRNA transfected cultures with DMNQ and MNQ challenge (Figures 6.5C and D). The effect was more marked with MNQ challenge than DMNQ. This is most likely due to the capacity for MNQ to deplete GSH through both sulphhydryl arylation and redox cycling[26]. As shown previously (Chapters 4 and 5), MNQ can deplete GSH levels far more rapidly than DMNQ

(within 1 hour of exposure). The enhanced depletion of GSH levels observed with *Gclc* knockdown was entirely expected and is consistent with a reduced capacity for transfected hepatocytes to synthesise GSH. Although the *Gclc* mouse knockout is embryolethal, the heterozygotes have a reduced capacity to synthesise GSH (and *Gclc* mRNA and protein is decreased)[305].

Because of the critical role GSH plays in protecting hepatocytes from quinone-mediated toxicity[25;306], *Gclc* knockdown was predicted to result in increased cytotoxicity with DMNQ and MNQ exposure. This was indeed the case, as evidenced by the increased LDH leakage observed with 3 and 6 hours DMNQ or MNQ exposure, relative to Control siRNA transfected cultures (Figures 6.4A to 6.4D). Again, *Gclc* knockdown resulted in greater sensitivity to MNQ challenge than DMNQ.

Overall, the level of *Pim3* or *Gclc* knockdown that was achieved in the quinone challenge experiment was less than originally anticipated. Decreases in mRNA of less than 50 percent were observed with both siRNAs used for each target gene, relative to Control siRNA transfected cultures (Figures 6.6A and B). Although not a marked effect, the phenotypic changes observed were striking. A general trend observed was that the siRNA for each target gene that resulted in the most quinone-sensitive phenotype, *Pim3* siRNA 3 and *Gclc* siRNA 2, had minimal effects on respective mRNA levels. Target gene transcription in hepatocyte cultures transfected with these siRNAs were reduced by only 20-30 percent relative to Control siRNA cultures following DMNQ or MNQ challenge (Figures 6.6A and B). However, following 3 hours exposure to DMNQ or MNQ, the level of cytotoxicity was markedly greater than that seen with *Pim3* siRNA 2 or *Gclc* 1. A possible explanation for this observation is that hepatocytes where *Pim3* or *Gclc* mRNA levels were markedly suppressed were in the dead populations and would not have contributed to the transcriptional readout. As a result, the transcriptional levels of the target genes would appear higher in hepatocyte cultures transfected with the most potent siRNAs (i.e. *Pim3* siRNA 3 and *Gclc* siRNA 2).

The findings of this study indicate that *Pim3* or *Gclc* knockdown sensitises rat hepatocytes to quinone-induced redox stress. The data validates the hypothesis that the increased transcription of these genes in response to quinone exposure (Chapters 4 and 5) are critical elements through which rat hepatocytes attempt to survive quinone challenge and redox

stress. Sensitivity to MNQ exposure was markedly greater than to DMNQ, suggesting that *Pim3* and *Gclc* are also important in the response to cytotoxicity resulting from sulphhydryl arylation. The phenotypic changes observed as a result of *Gclc* knockdown are entirely in-line with the known role that glutathione status plays in a cells ability to survive quinone challenge. Based on the increase in activated caspase 3 observed with DMNQ and MNQ challenge, *Pim3* is most likely involved in mediating the anti-apoptotic response to these chemical stressors.

**CHAPTER 7. TOXICOKINETICS OF DMNQ AND MNQ IN MICE
AND THE UTILITY OF DMNQ FOR STUDYING HEPATIC
REDOX STRESS *IN VIVO***

7.1. Introduction

The redox active quinones 2,3-dimethoxy-1,4-naphthoquinone (DMNQ) and menadione (MNQ) are frequently utilised as tool compounds, enabling the study of redox stress [22;26;26;27;30;52;104;118;119;220;307-314] and the role it plays in the toxicity of quinone-related medicines. The majority of these investigations were carried out using *in vitro* cell models. Recently transcriptomics has been employed to further our understanding of the genes and pathways involved in the response to redox stress[255;315;316]. Transcriptional analysis of rat hepatocytes exposed to DMNQ and MNQ identified a number of common genes/pathways regulated under conditions of redox challenge (Chapter 5). These may be involved in ameliorating the toxicity associated with redox challenge *in vitro*.

To relate the data mentioned above to the *in vivo* situation, equivalent hepatic studies are required in live animals. No such data exists in the public domain for DMNQ or MNQ. Upon literature review it was also found that there was a complete absence of *in vivo* data for DMNQ. This was surprising, given that the utility of DMNQ as a superior tool for studying redox stress *in vitro* was first defined by Gant *et al* in 1988[26]. In order to address the paucity of *in vivo* data, it was decided to undertake a thorough evaluation of DMNQ toxicokinetics and biodistribution in mice. It was hoped that such a study would lay the foundation for utilising DMNQ for the study of redox stress *in vivo*, with an emphasis on hepatic effects for this programme of work. Once the exposure kinetics of DMNQ had been defined, evaluation of the physiological consequences of this quinone in the liver could be undertaken. Such studies would include transcriptional analysis.

The overall aim of this study was to define the toxicokinetics and tissue distribution of DMNQ following a single dose which did not cause acute hepatotoxicity, in male C57BL/6J mice. To add value to this data, equivalent profiling was undertaken in MNQ treated mice. This would fill a knowledge gap, in terms of MNQ toxicokinetics, and also act as a comparator quinone for any physiological endpoints that were assessed. To confirm that the dose level selected for DMNQ was not acutely hepatotoxic, plasma levels of the liver enzymes alanine aminotransferase (ALT) and aspartate aminotransferase (AST) were monitored. Evaluation of whether DMNQ (and MNQ) administration *in vivo* resulted in a hepatic redox challenge was undertaken through the assessment of liver glutathione status

(both reduced glutathione (GSH) and oxidised glutathione (GSSG)). Based on the exposure kinetics and effects observed on glutathione status, it was decided that key time points post treatment would be selected for transcriptional analysis. Transcriptional responses were evaluated using the Mouse Whole Genome 430 2.0 Affymetrix GeneChip[®] microarrays in the livers of DMNQ and MNQ treated mice and compared to baseline readouts (from time matched vehicle control-treated mice).

The in-life phase of all experiments reported within this chapter were conducted by Dr T Gant and Miss A Pointon (MRC Toxicology Unit, University of Leicester under Home Office licences 80/1690, 80/2048 or 80/2146). Either tissues, or appropriate biofluids and tissue extracts, were supplied to me for downstream analysis.

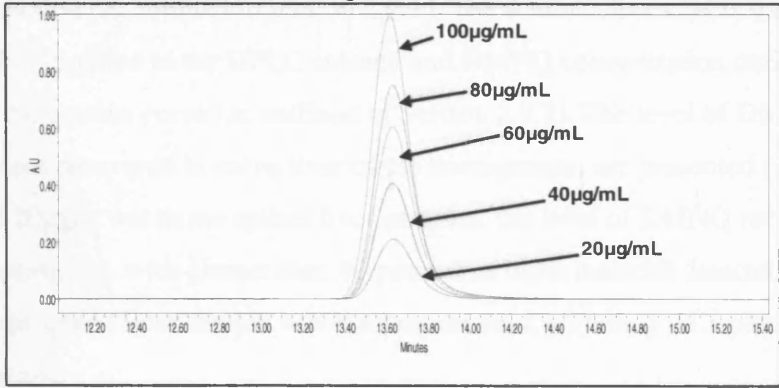
7.2. Results

7.2.1. Quinone Assay Development

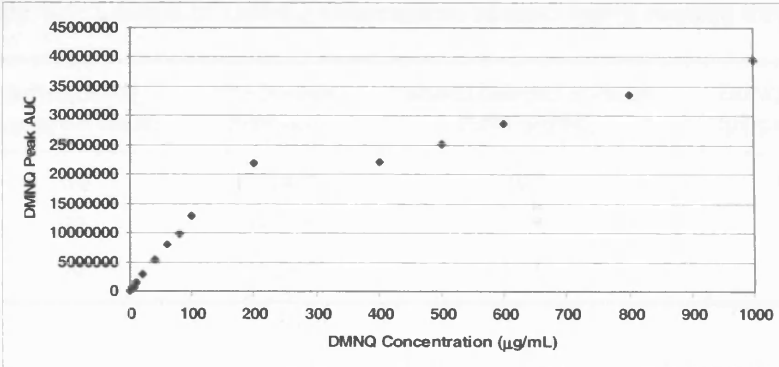
In order to investigate the toxicokinetics, tissue distribution and elimination of DMNQ and MNQ in mice, a high-performance liquid chromatography (HPLC)-based assay was developed (methodology outlined in Section 2.9). Initial experiments involved the dissolution of DMNQ in 50% v/v HPLC grade methanol (Running Buffer) at various concentrations to evaluate the assay performance. A calibration curve with the following concentrations was prepared: 1000, 800, 600, 500, 400, 200, 100, 80, 60, 40, 6.25, 20, 10, 5, 2.5, 1.25 and 0.625 μ g/mL. The calibration curve was applied to the HPLC column and absorbance monitored at 276nm over a 35 minute period. A single peak at approximately 13.5 minutes was consistently detected for each DMNQ dilution (Figure 7.1A) and the peak area under the curve (AUC) was plotted against input DMNQ concentration to evaluate linearity of the calibration curve (Figure 7.1B). The HPLC assay performed well up to 100 μ g/mL, at which point there was loss of linearity (Figure 7.1B). Linear regression analysis of the 0.625 to 100 μ g/mL concentration range gave an R^2 value of 0.9983 (Figure 7.1C).

Figure 7.1

A: DMNQ HPLC Chromatograms



B: DMNQ Calibration Curve



C: DMNQ Linear Regression

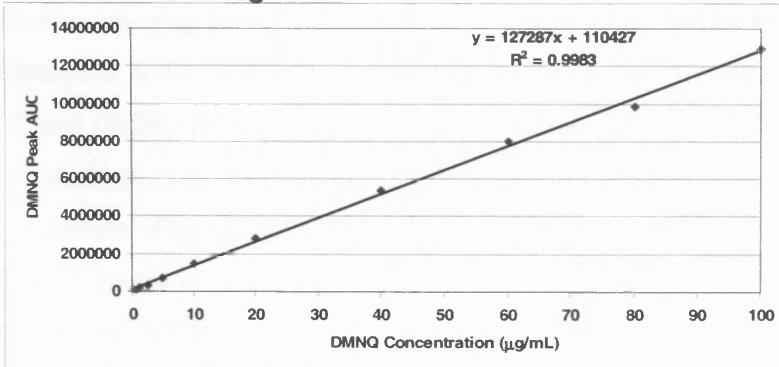


Figure 7.1: DMNQ HPLC assay optimisation. A) Example DMNQ HPLC chromatograms indicating 276nm peak absorbance at 13.5 minutes. B) DMNQ input concentration versus 13.5 minutes peak AUC for 0.625 to 1000µg/mL DMNQ in Assay Buffer. C) Linear regression of linear range of DMNQ calibration curve (0.625 to 100µg/mL).

To evaluate the performance of the HPLC assay, DMNQ was spiked into naïve mouse liver homogenates at equivalent to 100, 20 and 10µg/g of wet tissue prior to acetonitrile extraction (as outlined in section 2.9.1). The acetonitrile extracts were dissolved in Assay Buffer, applied to the HPLC column and DMNQ concentration derived with reference to the calibration curve (as outlined in Section 2.9.2). The level of DMNQ detected and percent recovered in naïve liver tissue homogenates are presented (Table 7.1). For the 10 and 20µg/g wet tissue spiked liver samples, the level of DMNQ recovered was proportional, with greater than 80 percent of input material detected. The 100µg/g wet tissue spiked liver sample was not proportional, with only 62.1 percent of input DMNQ detected.

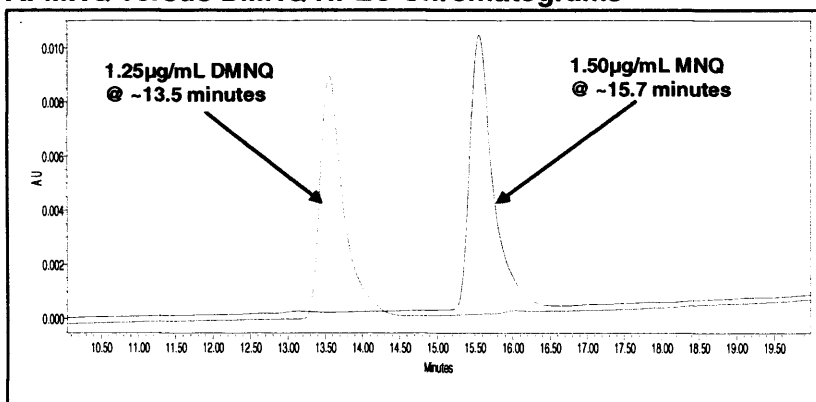
Table 7.1: Levels of DMNQ detected in spiked naïve mouse liver homogenates.

Spiked DMNQ (µg/mg wet tissue)	13.5 Minutes Peak AUC	DMNQ Detected in Assay Buffer (µg/mL)	DMNQ Detected (µg/g wet tissue)	Percent DMNQ Recovered
100	8020407	62.1	62.1	62.1
20	2261978	16.9	16.9	84.5
10	1185920	8.4	8.4	84.5

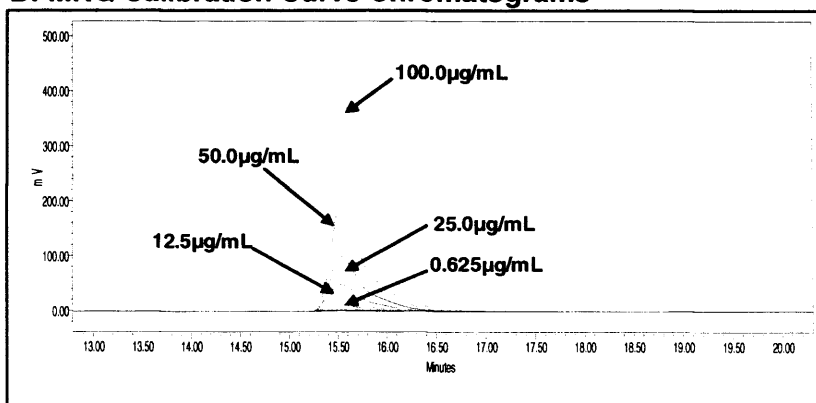
Due to the structural similarity between DMNQ and MNQ, the same assay conditions were applied to detecting MNQ. MNQ was dissolved in Assay Buffer at a starting concentration of 100µg/mL and a calibration curve prepared by double-diluting down to 0.195µg/mL. MNQ and DMNQ peaks at 276nm clearly separated on the HPLC chromatogram (Figure 7.2A). A single peak at approximately 15.7 minutes was consistently detected for each MNQ dilution (Figure 7.2B). Peak AUC was plotted against input MNQ concentration to evaluate linearity of the calibration curve (Figure 7.2C). The MNQ assay performed equally as well as the DMNQ assay, displaying linearity up to 100µg/ml with an R² value of 0.9989 (Figure 7.2C).

Figure 7.2

A: MNQ versus DMNQ HPLC Chromatograms



B: MNQ Calibration Curve Chromatograms



C: MNQ Linear Regression

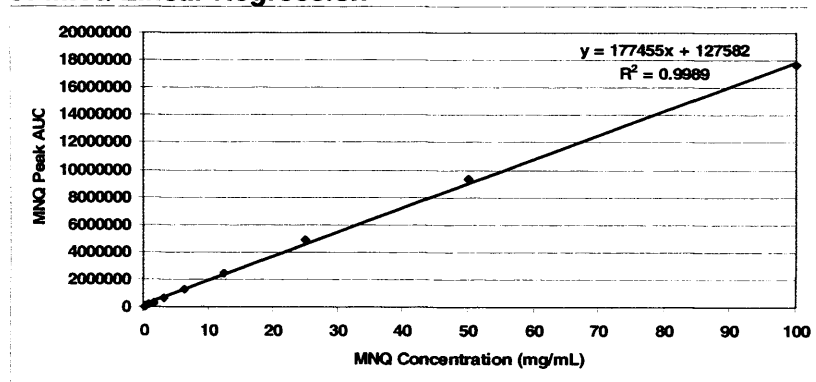


Figure 7.2: MNQ HPLC assay optimisation. A) MNQ versus DMNQ HPLC chromatograms indicating 276nm peak absorbance at 15.7 and 13.5 minutes, respectively. B) MNQ calibration curve HPLC chromatograms. C) Linear regression of MNQ calibration curve (0.195 to 100 µg/mL).

7.2.2. Preliminary Investigations into DMNQ Exposure Kinetics in C57BL/6J Mice

Studies investigating the effects of oral administration of DMNQ to male C57BL/6J mice indicated poor bioavailability via this route when given in a PEG-200 based formulation (data produced by Dr T Gant and not reported as part of this thesis). Oral administration of up to 200mg/kg DMNQ failed to result in detectable liver exposure, or the anticipated effects on GSH/GSSG levels. Thus, it was decided to evaluate intraperitoneal (i.p.) administration of DMNQ as an alternative route to increase systemic exposure.

Initially, male C57BL/6J mice (12 per treatment group) were treated with either 10mL/kg polyethylene glycol 200 (PEG-200, vehicle control) or 200mg/kg DMNQ in PEG-200 i.p.. The intention was to sacrifice one mouse per treatment group at staggered intervals over a 24 hour period to carry out a preliminary evaluation of the toxicokinetics. However, with the exception of a single mouse (animal 21), all animals treated with 200mg/kg DMNQ were found dead within 1 hour after dosing. Vehicle control treated animals were found moribund at the same time and were killed immediately via cervical dislocation. Upon opening the peritoneal cavity, ascites were noted in all animals, with the exception of Animal 21. Animal 21 was treated with the DMNQ dose solution but was given a fractional dose in error (estimated to be less than 1/10 of the appropriate dose volume). This animal displayed no adverse clinical signs and was killed via cervical dislocation approximately 3 hours after dosing.

Acetonitrile extractions were prepared from livers of 6 animals per treatment group (including animal 21) and DMNQ levels determined using the HPLC assay (according to the methods outlined in Section 2.9). No DMNQ was detected in vehicle control treated animals whereas mean liver levels in 200mg/kg DMNQ treated animals were 5.34 μ g/g wet tissue (Figure 7.3A). A small DMNQ peak in the HPLC chromatogram for the liver from animal 21 (misdosed) was observed, equating to 0.04 μ g/g wet tissue. GSH and GSSG levels were measured in the livers from the same animals (according to the method outlined in Section 2.7.2) to determine whether the tissue had received a redox challenge. A significant increase in liver GSH levels was observed in mice treated with 200mg/kg DMNQ compared to vehicle control treated mice (approximately 1.4-fold increase) (Figure 7.3B). Liver GSSG levels were markedly increased in mice treated with 200mg/kg DMNQ versus the vehicle control treated mice (approximately 4.8-fold increase), indicating redox

challenge (Figure 7.3C). GSH levels in the liver of animal 21 were comparable to those observed in vehicle control treated mice (Figure 7.3A), although GSSG levels were elevated slightly (approximately 1.6-fold increase) (Figure 7.3C).

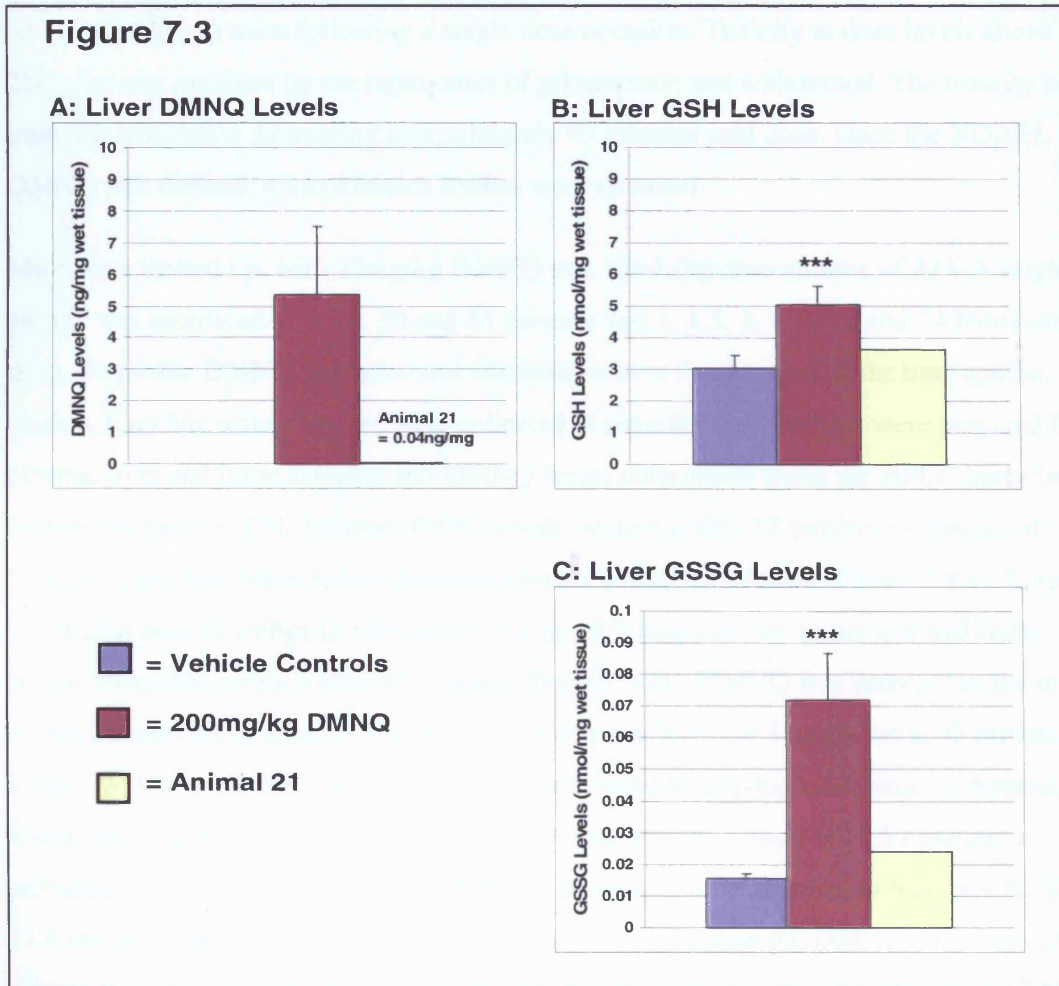


Figure 7.3: Liver tissue DMNQ (A), GSH (B) and GSSG (C) levels in mice treated with Vehicle Control (n=6) or 200mg/kg DMNQ (n=5) i.p. Results are group mean values \pm SD (except for Animal 21). Two-tailed equal variance T-test. * = $P < 0.001$ versus Vehicle Control group.**

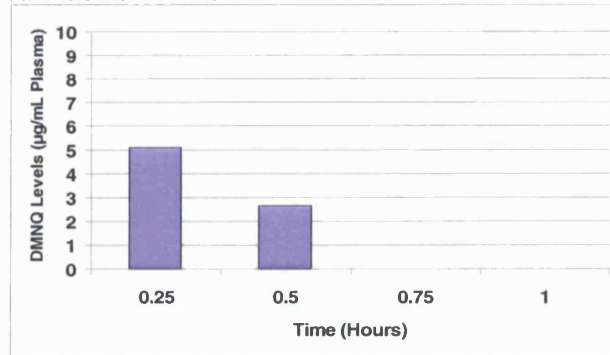
Note: Mice treated with 200mg/kg DMNQ i.p. were found dead approximately 1 hour after dosing. Vehicle control treated animals were killed 1 hour after dosing. Animal 21 received approximately 1/10th of the intended DMNQ dose solution and was killed at 3 hours post dosing.

Due to the poor tolerability of the PEG-200 as a vehicle for i.p. dosing, additional dose ranging studies were conducted using Arachis Oil (AO) as an alternative. These studies were conducted by Dr T Gant and are not reported within this thesis. Subsequently, Dr T Gant identified 25mg/kg DMNQ in AO via the i.p. route as the no observed adverse effect level (NOAEL) in mice following a single dose occasion. Toxicity at dose levels above 25mg/kg was manifest by the rapid onset of piloerection and withdrawal. The toxicity was transient, with mice recovering approximately 45 minutes post dose. Once the NOAEL for DMNQ was defined, toxicokinetics studies were resumed.

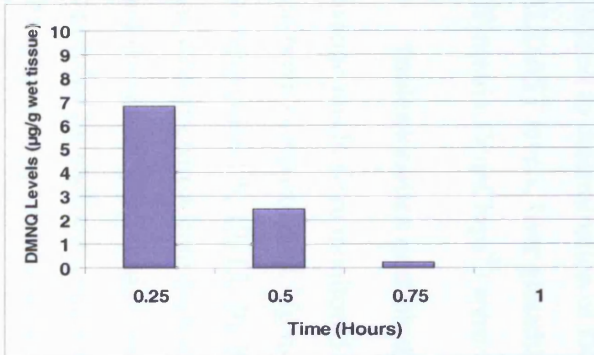
Mice were treated i.p. with 25mg/kg DMNQ in a 10mL/kg dose volume of AO. A single animal was sacrificed at 0, 15, 30 and 45 minutes and 1, 1.5, 3, 4, 8, 12 and 24 hours post dose. To profile DMNQ exposure and elimination over the duration of the time course, plasma, liver and urine samples were collected. Acetonitrile extractions were prepared from plasma, liver and urine samples and DMNQ levels determined using the HPLC assay (as outlined in Section 2.9). Plasma DMNQ levels peaked within 15 minutes of dosing, at 5.1µg/mL and had fallen below detectable levels within 45 minutes (Figure 7.4A). Liver levels also peaked within 15 minutes of dosing, at 6.8µg/g of wet tissue and had fallen below detectable levels within 60 minutes (Figure 7.4B). DMNQ was detected in the urine within 30 minutes of dosing (Figure 7.4C), with peak levels of 4.4µg/hour at 45 minutes. Urine DMNQ levels fell rapidly from 1.5 hours onwards, although remained at detectable levels until 8 hours. In addition to the DMNQ peak at approximately 13.5 minutes, a prominent peak was noted in the urine HPLC chromatograms from early time points. The 11.5 minute peak produced a considerably stronger signal than the DMNQ peak between 30 minutes and 1.5 hours, and was no longer present from 2 hours onwards (Figure 7.4D). This peak was not present in AO-treated mice and is apparently DMNQ-related.

Figure 7.4

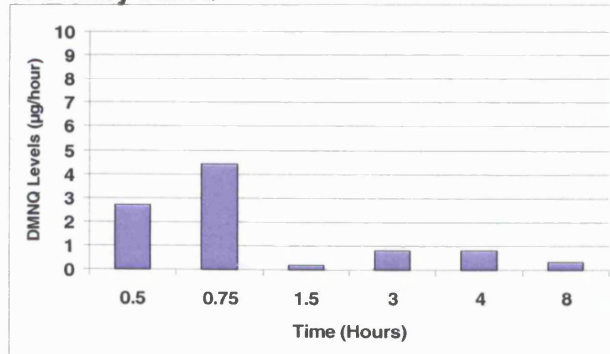
A: Plasma DMNQ



B: Liver DMNQ



C: Urinary DMNQ



D: Urinary DMNQ HPLC Chromatograms

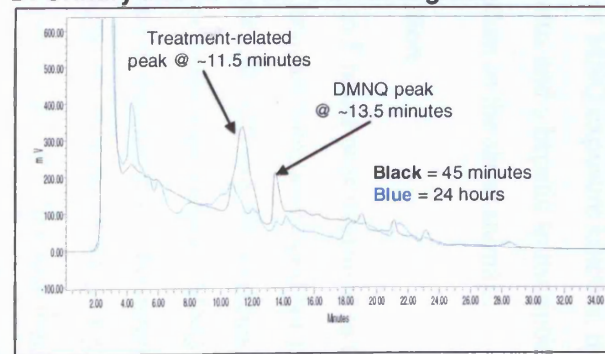


Figure 7.4: DMNQ exposure kinetics in male C57BL/6J mice treated with 25mg/kg DMNQ in AO i.p. (n=1 per time point). DMNQ levels in plasma (A), liver tissue (B) and urine (C). Urinary HPLC chromatograms (D) for DMNQ treated mice at 45 minutes shows the presence of an additional treatment-related peak (24 hours chromatogram shown for comparison).

7.2.3. Toxicokinetics, Biodistribution and Hepatic Effects of Acute DMNQ or MNQ Exposure in C57BL/6J Mice

A comprehensive assessment of the plasma and tissue kinetics of DMNQ and MNQ was carried out using the HPLC assays optimised previously (Section 7.2.1). Based on the initial exposure investigations (Section 7.2.2), it was decided to monitor the kinetics of DMNQ in male C57BL/6J mice for five hours following a single i.p. dose of 25mg/kg in AO. For comparison, a second group of mice were treated i.p. with 25mg/kg of MNQ in AO. In addition to determination of DMNQ or MNQ exposure kinetics, measurement of plasma ALT/AST levels, liver glutathione status and a hepatic transcriptional readout (using Affymetrix GeneChips[®]) were undertaken in the same animals.

7.2.3.1. Toxicokinetics and Biodistribution

Parent quinone levels were monitored for up to 5 hours post treatment in the plasma, liver, kidney and brain compartments. Up to three animals were sacrificed per treatment group at each of 10 time points (5, 10, 15, 20, 30, 45, 60, 90, 120 and 300 minutes). Acetonitrile extractions were prepared from each plasma or tissue sample and DMNQ or MNQ levels determined using the HPLC assays (as outlined in Section 2.9). The mean quinone exposure profiles for each compartment (presented in Figures 7.5A to 7.5D) were imported into WinNonlin version 1.4 (Pharsight Corporation) and the data analysed using non-compartmentalised analysis to derive exposure metrics, including T_{max}, C_{max} and half life (t_{1/2}) (summarised in Table 7.2).

Overall, the plasma kinetics for DMNQ and MNQ were comparable with T_{max} for both quinones being reached by 10 minutes. C_{max} values in this compartment were 8.97µg/mL and 11.1µg/mL for DMNQ and MNQ, respectively and plasma elimination rates were similar (DMNQ t_{1/2} = 18 minutes; MNQ t_{1/2} = 20 minutes). The only plasma exposure metric that differed markedly for the two quinones was plasma AUC, with overall plasma exposure for DMNQ being approximately half that observed for MNQ (AUC_{last} of 246 and 498ng.hr/mL, respectively).

Tissue distribution for the quinones was strikingly different. DMNQ was much more widely and rapidly distributed than MNQ. An absorption phase for DMNQ was barely apparent for any of the tissues assessed, whereas clear absorption kinetics were observed for MNQ in the liver and kidneys (Figures 7.5B, C and D). T_{max} was reached in the liver

and kidney by 10 minutes, whereas MNQ Tmax was not reached until 20 (liver) to 30 (kidneys) minutes after dosing. Liver and kidney MNQ exposure levels were markedly lower than those observed for DMNQ. Cmax values in the liver and kidney were approximately 3-fold higher with DMNQ and tissue AUC values were 2.4-fold (liver) to 4.4-fold (kidneys) higher. DMNQ was also detected in the brain (Cmax = 1.35µg/g; Tmax = 10 minutes), whereas MNQ was not.

Table 7.2: DMNQ and MNQ exposure metrics in male C57BL/6J mice

Quinone	Body Compartment	Cmax (µg/mL or g)	Tmax (Minutes)	AUClast (ng.min/mL or g)	AUCinf. (ng.min/mL)	AUCextrap. (Percent)	Half life (Minutes)
DMNQ	Plasma	8.97	15	246	250	1.9	18
	Liver	9.75	10	287	300	4.2	51
	Kidney	18.7	10	757	789	4.0	122
	Brain	1.35	10	52	57	9.4	70
MNQ	Plasma	11.1	10	498	507	1.8	20
	Liver	3.31	20	119	135	11.7	24
	Kidney	5.91	30	171	172	1.0	15
	Brain	ND	ND	ND	ND	ND	ND

Cmax = maximum concentration achieved. Tmax = time to maximum concentration. AUClast = area under the curve to the last data point. AUCinf. = AUC extrapolated from the last data point. AUCextrap. = percent of AUCinf. derived from extrapolation. Half life = time taken for half of the compound to be cleared from a compartment. ND = not detected; MNQ was not detected in brain tissue.

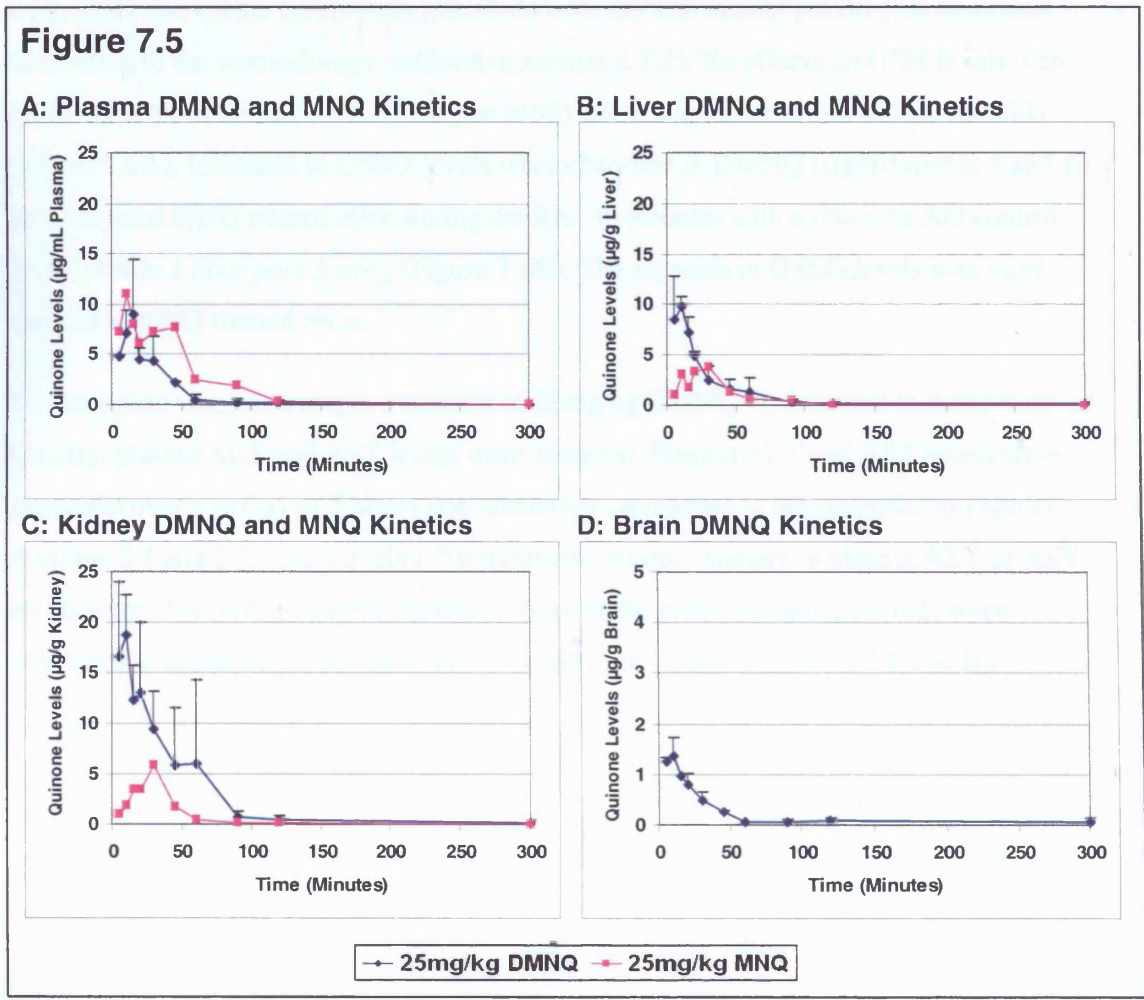


Figure 7.5: DMNQ and MNQ exposure kinetics in male C57BL/6J mice treated with 25mg/kg in AO i.p. Quinone levels were determined in plasma (A), liver (B), kidney (C) and brain (D) tissue. Mean quinone concentrations (\pm SD) are shown for each compartment (DMNQ n=3 per time point; MNQ n=1 to 2 per time point).

Note: MNQ was not detected in brain tissue

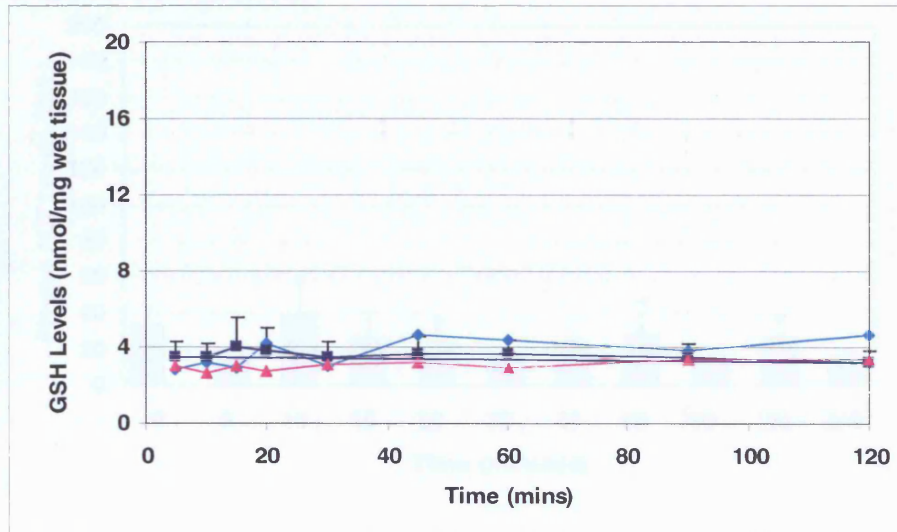
7.2.3.2. Hepatic GSH/GSSG and Plasma ALT/AST Levels

To determine whether 25mg/kg DMNQ and MNQ i.p. resulted in a redox challenge to the liver, GSH and GSSG levels were measured over the 120 minute period post treatment (according to the methodology outlined in section 2.7.2). No effects on GSH levels were observed in mice treated with DMNQ or MNQ when compared to AO treated controls (Figure 7.6A). Increases in GSSG levels were observed in DMNQ (significant at 5 and 10 minutes) and MNQ treated mice during the first 30 minutes with a return to AO control levels within 1 hour post dosing (Figure 7.6B). The increase in GSSG levels was more marked in MNQ treated mice.

To determine whether a single treatment of 25mg/kg DMNQ i.p. resulted in acute liver toxicity, plasma ALT and AST levels were assessed. Plasma ALT and AST levels were measured over a period of 5 hours post treatment (according to the methods outlined in Sections 2.4 and 2.5, respectively). No treatment-related changes in plasma ALT or AST levels were observed in DMNQ treated mice over the entire sampling period, when compared to the levels observed in AO treated control mice (Figures 7.7A and B).

Figure 7.6

A: Liver GSH Levels



B: Liver GSSG Levels

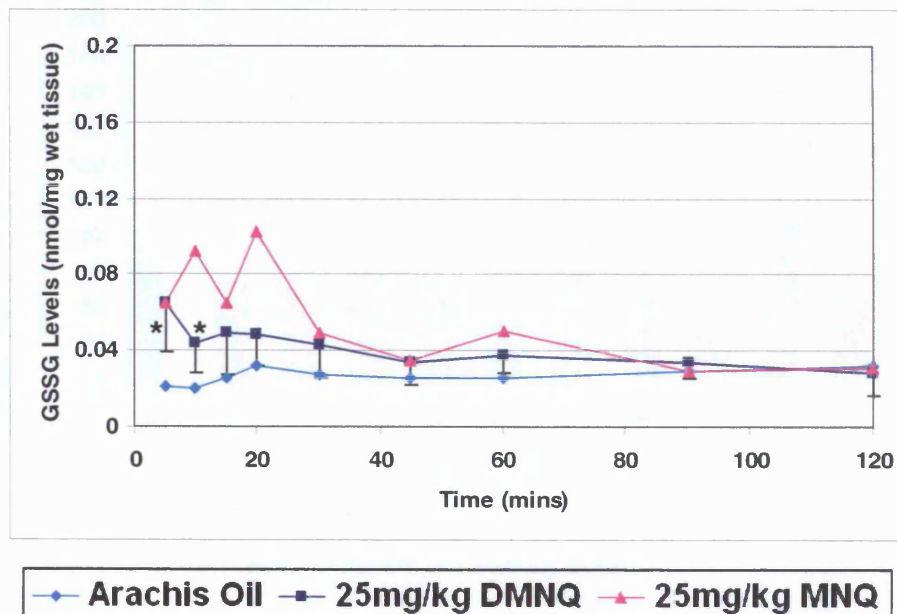
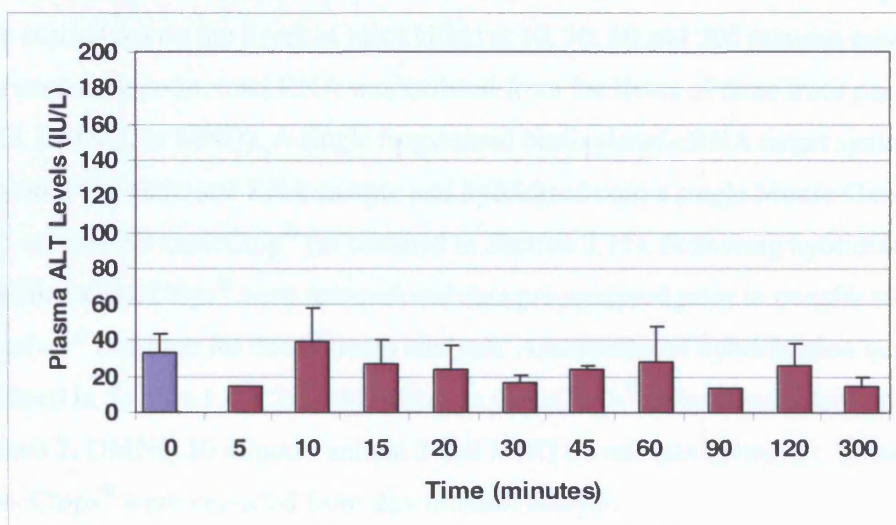


Figure 7.6: Liver GSH (A) and GSSG (B) levels in mice treated with AO (n=2), DMNQ (n=4) or MNQ (n=2). Results are mean values \pm SD. ANOVA and post-hoc Dunnett's T-test. * = $P < 0.05$ versus AO controls.

Figure 7.7

A: Plasma ALT Levels



B: Plasma AST Levels

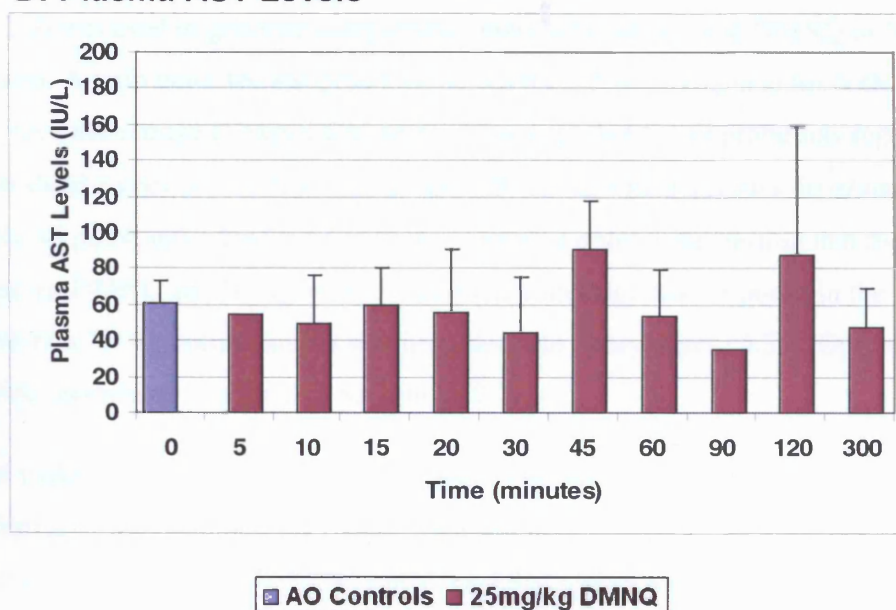


Figure 7.7: Plasma ALT (A) and AST (B) levels in mice treated with AO (n=10) or 25mg/kg DMNQ (n=3 per time point, except 5 and 90 minutes where n=2).

Note: A single AO treated animal was sampled at each time point between 5 and 300 minutes. Data from these mice are represented as a single group (n=10) at 0 minutes for comparison to the DMNQ treated group.

7.2.3.3. Hepatic Transcriptional Investigations

Hepatic transcriptional responses in male C57BL/6J mice resulting from 25mg/kg DMNQ or MNQ i.p. were investigated over a 5 hour period post treatment. Transcriptional analysis was carried out on the livers of mice killed at 10, 30, 60 and 300 minutes post treatment. For each time point, total RNA was isolated from the livers of three mice per treatment (AO, DMNQ, or MNQ). A single fragmented biotinylated-cRNA target synthesis was prepared for each total RNA sample and hybridised onto a single Mouse Genome Array 430 version 2.0 GeneChip[®] (as outlined in Section 2.12). Following hybridisation and washing, GeneChips[®] were scanned and data pre-analysed prior to transfer to the Rosetta Resolver[®] database for downstream analysis. Assessment of hybridisation quality (as outlined in Section 1.4.2.2) identified three GeneChips[®] to be substandard (AO 30 minutes animal 2, DMNQ 30 minutes animal 3 and MNQ 60 minutes animal 3). These three GeneChips[®] were excluded from downstream analysis.

The RatioBuild Trend function within Rosetta Resolver[®] Resolver (outlined in section 2.12.3) was used to generate comparison tables between AO and DMNQ or MNQ treated groups. A ratio trend set was produced across the entire time course for both quinones and the *log* ratio change in expression and *p*-value exported for all probe sets regulated (threshold values of $>\pm 2$ -fold change and $p \leq 0.05$) at 4 points across the entire data set. Only 42 probe sets were found to fit this selection criteria, suggesting that the dose levels used for DMNQ and MNQ evoked a minimal transcriptional response in the liver. The *log* ratio data for the entire data set was imported into ArrayMiner v5.3.2 (Optimal Design) for cluster analysis (as outlined in Section 2.12.3).

The overall aim of the cluster analysis was to identify temporal patterns in gene expression common to both quinones. *K*-means Gaussian cluster analysis (Euclidean distance measure) of *log* ratio data for the 42 consistently regulated probes sets was carried out across the entire 5 hours time course for DMNQ and MNQ. Iterative clustering was undertaken by varying the *K* value (the number of clusters) between 4 and 10 to determine the optimal number of clusters for the data set. The 42 probes sets were found to segregate well into six clusters, with eight probes sets being classed as outliers. The mean expression profiles for each cluster are shown (Figures 7.8 and 7.9) for DMNQ and MNQ exposed cultures. Overall the temporal profiles for each quinone were very similar for all six clusters.

The Genbank accession numbers for the probe sets within each of the six clusters were imported into Ingenuity Pathways Analysis (IPA) to attempt to gain an overview of functional classes of genes regulated (as outlined in Section 2.12.3). Due to the low gene representation within each cluster the IPA analysis failed to confer any meaningful biological interpretation on the transcriptional data. Manual assessment of the functionality of the clustered probes sets (cluster tables within Figures 7.8 and 7.9) indicated an absence of classic redox-regulated genes (e.g. activator protein 1 (AP-1)-related genes, nuclear factor (erythroid-derived 2)-like 2-antioxidant response element (Nrf2-ARE)-pathway genes and DNA damage-related genes).

Figure 7.8

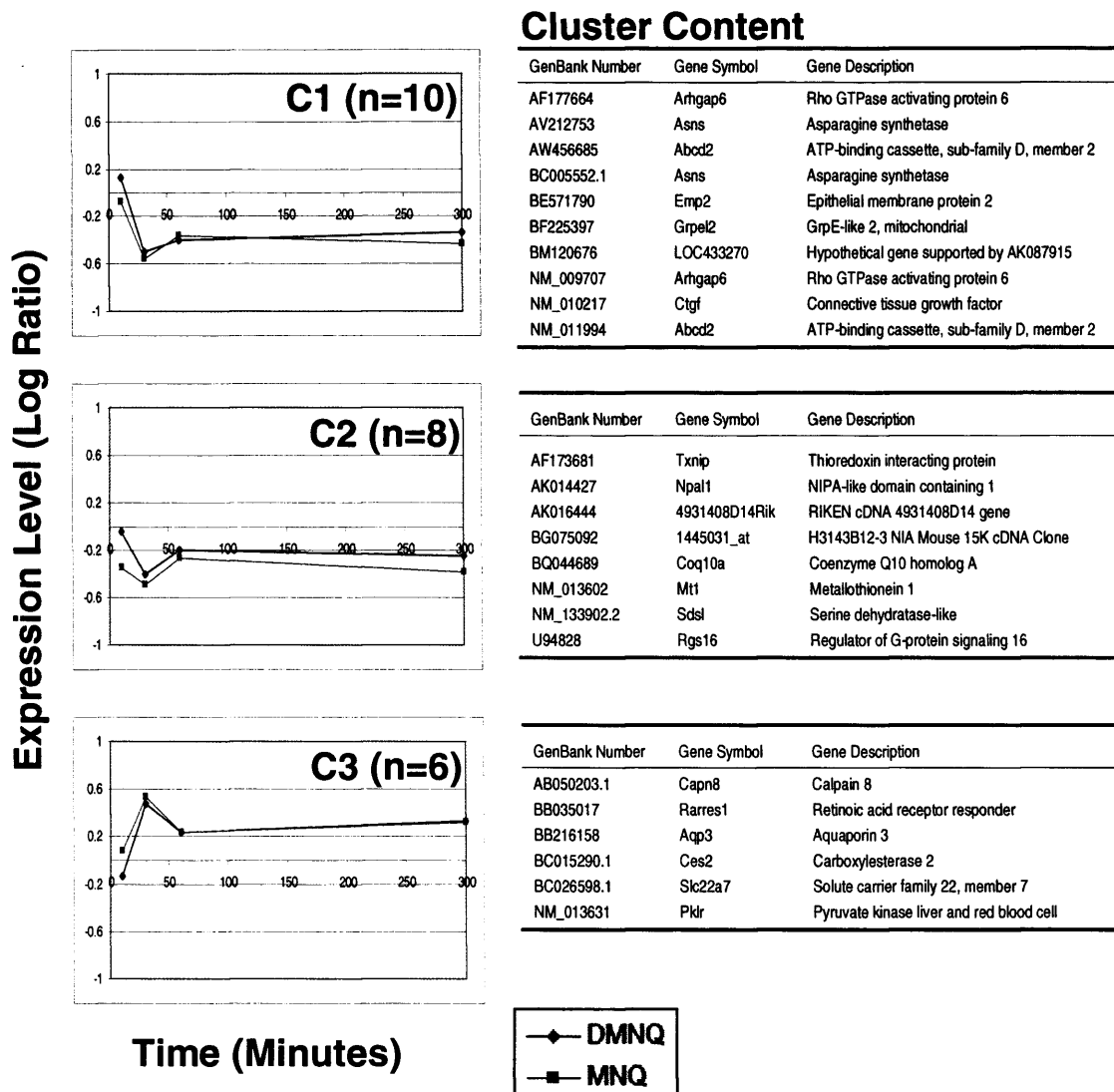


Figure 7.8: Mean profiles of clusters C1, C2 and C3

The cluster size (n in parenthesis) indicates the number of probe sets segregating to each cluster. The table to the right of each profile contains the identity of the probe sets segregating to each cluster. n=3 GeneChips® per data point, except 30 minutes AO group, 30 minutes DMNQ group and 60 minutes MNQ group where n=2 GeneChips® per data point.

Figure 7.9

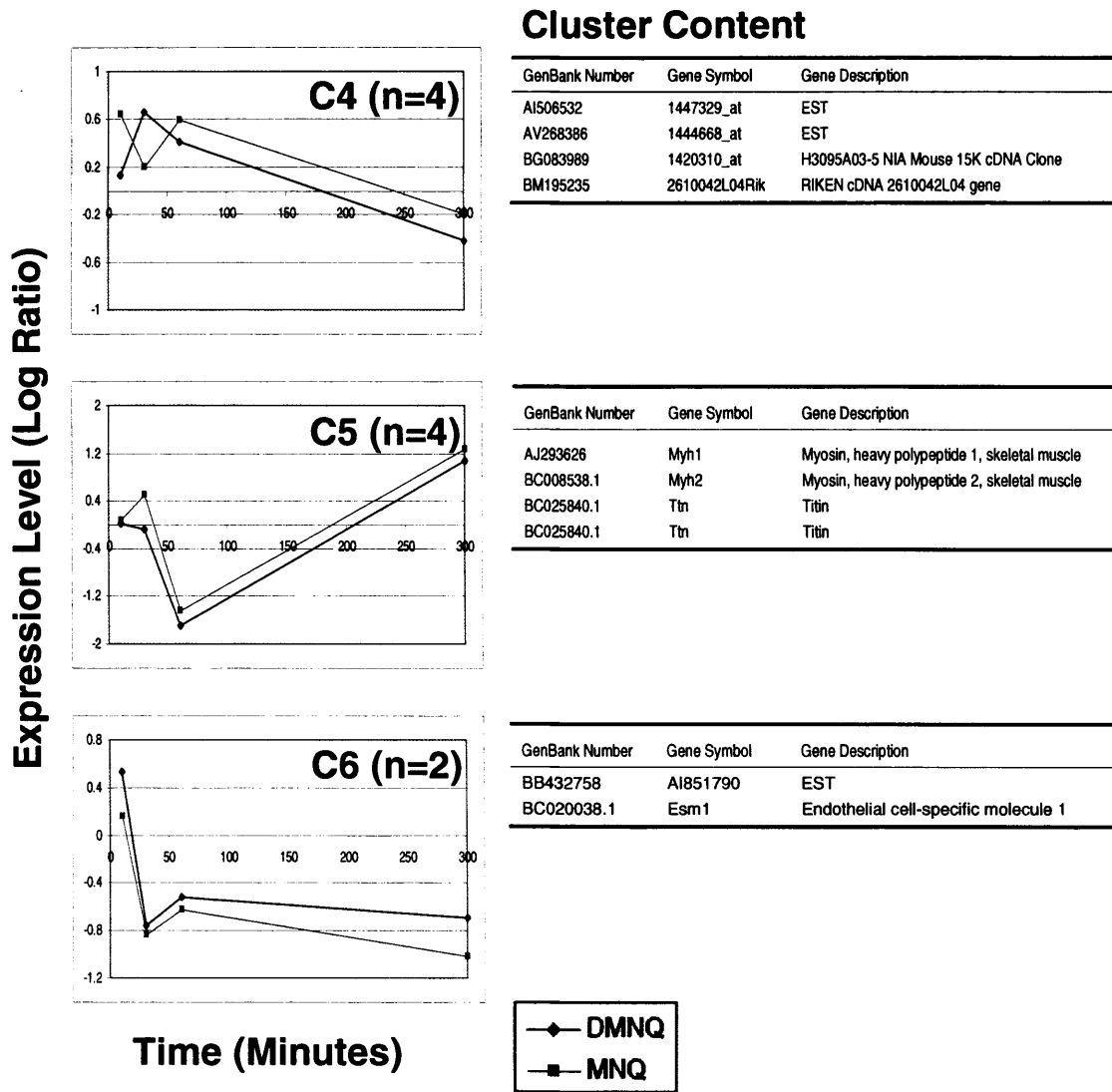


Figure 7.9: Mean profiles of clusters C4, C5 and C6

The cluster size (n in parenthesis) indicates the number of probe sets segregating to each cluster. The table to the right of each profile contains the identity of the probe sets segregating to each cluster. n=3 GeneChips® per data point, except 30 minutes AO group, 30 minutes DMNQ group and 60 minutes MNQ group where n=2 GeneChips® per data point.

7.3. Discussion

The main aim of this study was to carry out a thorough assessment of the toxicokinetics and biodistribution of a single bolus dose of DMNQ in male C57BL/6J mice. Secondly, to evaluate the utility of DMNQ as a tool compound for studying hepatic redox stress *in vivo*, by monitoring changes in the liver glutathione status and transcriptome of DMNQ-treated mice. As discussed previously (Section 7.1), DMNQ has been extensively used to study the effects of redox stress *in vitro*[26;31;308;317-319], however there is a complete lack of *in vivo* data within the public domain. The related naphthoquinone MNQ is also frequently used as a tool for investigating redox-related effects *in vitro*[52;220;312;314;320-323] though unlike DMNQ, a knowledgebase on its *in vivo* toxicity exists[52;324-329]. However, to date no studies on the toxicokinetics of MNQ *in vivo* have been published (only a single study on the distribution of vitamin K₁ in rats, an MNQ analogue [330]). For these reasons, MNQ was included as a comparator compound in this study.

To enable the assessment of the toxicokinetics and biodistribution of DMNQ and MNQ in mice an HPLC assay was successfully developed. Under the same assay conditions (as detailed in Section 2.9) DMNQ and MNQ peaks eluted at approximately 13.5 minutes and 15.7 minutes, respectively. HPLC assay performance was comparable for DMNQ and MNQ solutions, with linearity being maintained up to a concentration of 100µg/mL in assay buffer for both quinones

7.3.1. Preliminary Investigations into DMNQ Exposure Kinetics in C57BL/6J mice

As mentioned previously (Section 7.2.2), due to the absence of any treatment-related findings (in terms of clinical signs, detectable hepatic exposure, and alterations in the liver glutathione status and transcriptome) with up to 200mg/kg DMNQ in PEG-200 via the oral route (data not shown), i.p. administration was utilised to increase exposure. The same dose level and vehicle resulted in 100 percent lethality within 1 hour via the i.p. route. Based on this finding, the LD₁₀₀ for DMNQ would appear to be comparable to that defined for MNQ by Molitor and Robinson, who reported that 200mg/kg MNQ i.p. was 100 percent lethal in mice[329]. These data suggest that DMNQ and MNQ are roughly equitoxic *in vivo*, an unexpected finding given the differential cytotoxicity observed in hepatocytes *in vitro* [26;119;307;331]. MNQ is consistently observed to be approximately an order of

magnitude more cytotoxic *in vitro*. Indeed, dose-ranging studies carried out as part of this thesis (Chapter 3) found the 8 hours EC₅₀ for MNQ in rat hepatocytes to be markedly lower than the DMNQ EC₅₀ (approximately 35µM versus greater than 250µM) (Table 3.4). Initial consideration of these findings suggests a disparity between the relative toxicity of DMNQ and MNQ in the *in vivo* and *in vitro* situation. However, it is important to note that marked toxicity was also observed in the PEG-200 treated control group. This suggests that a proportion of the toxicity observed with 200mg/kg DMNQ i.p. was vehicle-related.

HPLC analysis of acetonitrile extracts from the livers of mice exposed to 200mg/kg DMNQ i.p. in PEG-200 confirmed successful exposure (Figure 7.3A). Hepatic glutathione status in the same mice was significantly different from PEG-200 control mice, with increases in both GSH and GSSG levels (Figures 7.3B and C, respectively). However, the fact that the mice had been dead for an unknown amount of time (up to 30 minutes) prior to tissue being sampled means that the DMNQ exposure and glutathione status data for this study are unreliable. The only conclusion that could be drawn is that DMNQ exposure was markedly improved with i.p. versus oral dosing.

To overcome the poor tolerability of PEG-200 as a vehicle via the i.p. route, subsequent dose-ranging experiments used AO as an alternative. These studies, undertaken by Dr T Gant and not reported in this thesis, identified a dose of 25mg/kg as the NOAEL for DMNQ via the i.p. route in mice (in terms of clinical signs). As DMNQ dose levels were escalated above 25mg/kg, acute toxicity was apparent. This was manifest by piloerection and withdrawal (personal communication, Dr T Gant, 2006). The NOAEL (25mg/kg) dose level was used to undertake an exploratory evaluation of the toxicokinetics of DMNQ in mice to aid the design of a more definitive study. Successful systemic exposure of DMNQ via the i.p. route was confirmed, with detectable levels observed in plasma and liver tissue (Figure 7.4A and B). For both compartments, DMNQ levels peaked at 15 minutes and was cleared by 60 minutes post dose. Analysis of urine samples indicated that a proportion of DMNQ was excreted via the renal route (Figure 7.4C), with peak clearance lagging behind peak systemic levels at 45 minutes post dose.

In addition to the DMNQ peak eluting at approximately 13.5 minutes on the HPLC chromatogram, an additional treatment-related peak was noted in the urine sampled at 30 and 45 minutes post dose (Figure 7.5D). Eluting at approximately 11.5 minutes on the

HPLC chromatogram, the peak had an AUC value markedly greater than the DMNQ peak. It is possible that this peak represented DMNQ-related urinary metabolite. This suggestion initiated urinary metabolic profiling studies in mice treated with DMNQ to identify the putative metabolites. This work, carried out by Dr U Lutz and Dr W Lutz (Department of Toxicology, University of Wuerzburg) in collaboration with Dr T Gant subsequently identified sulphate and glucuronide conjugates of the dihydroquinone as the major urinary metabolites of DMNQ in mice (data awaiting publication).

7.3.2. Toxicokinetics, Biodistribution and Hepatic Effects of Acute DMNQ or MNQ Exposure in C57BL/6J Mice

Based on the preliminary toxicokinetics of DMNQ in mice, a definitive study was designed. It was decided to investigate the kinetics of DMNQ in male C57BL/6J mice for five hours following a single i.p. dose of 25mg/kg in AO. As mentioned previously, MNQ was administered at the same dose level to a second group of mice for comparison. DMNQ and MNQ exposure was monitored in plasma, liver, kidneys and brain at 10 time points during the 5 hours post treatment. Plasma kinetics for both quinones were comparable with similar C_{max}, T_{max} and T_{1/2} metrics (Table 7.2), although the MNQ AUC was higher than DMNQ (plasma AUC_{last} of 498 and 246ng.hr/mL, respectively).

Although plasma kinetics were similar, tissue distribution was strikingly different for the two quinones. DMNQ was more widely distributed than MNQ, both in terms of tissues exposed and the level of exposure (Figures 7.5A to D and Table 7.2). Based on tissue AUC_{last} values, DMNQ exposure in the liver was 2.4-fold greater than that observed with MNQ, and in the kidneys exposure was 4.4-fold greater. An important difference was that DMNQ was also detected in the brain (albeit at much lower levels than those observed in the liver and kidneys), whereas MNQ was not (Figure 7.5D and Table 7.2). Thus DMNQ appears to cross the blood brain barrier whereas MNQ does not. The increased efficiency with which DMNQ distributes to the tissues is puzzling given the difference in lipophilicity between the two quinones. DMNQ has a log P value of 1.67 compared to a value of 2.24 for MNQ[332;333], suggesting that MNQ tissue distribution would be more efficient.

A possible explanation for this unexpected finding is the chemical reactivity of MNQ, which has the capacity to arylate soft nucleophiles such as GSH[334;335]. The formation of GSH-menadiol conjugates upon tissue entry would reduce the level of free MNQ that

could be detected in acetonitrile tissue extracts by the HPLC assay. As DMNQ does not possess this reactivity, due to the methoxy substitutions at the 2, 3- carbon positions[26], tissue levels would remain elevated until metabolism or clearance occurs. As mentioned previously, metabolite profiling for DMNQ (and MNQ) undertaken by Dr U Lutz and Dr W Lutz in collaboration with Dr T Gant has identified sulphate and glucuronide metabolites. These metabolites provide evidence that DMNQ and MNQ undergo two-electron transfer reduction to hydroquinones prior to conjugation reactions and urinary clearance. This route of metabolism is known to be an important detoxification reaction for quinones[9;28]. However, based on the high levels of DMNQ in the kidneys and its presence in the urine (Figure 7.4C), renal clearance appears to be a major route of elimination. Although urine MNQ levels were not measured in this study, the relatively low levels found in the kidneys relative to DMNQ (4.4-fold lower) suggests renal elimination is less important.

So what is the primary route of MNQ elimination? It is likely that GSH-menadiol conjugates were formed in the liver and are subsequently cleared via the biliary route. GSH conjugates formed in the liver can be excreted intact in the bile[28]. Dr T Gant is currently investigating whether such GSH conjugates are present in the bile of mice treated with MNQ to confirm this hypothesis. The urinary metabolite profiling work discussed earlier has also confirmed the presence of a mercapturic acid conjugate of MNQ in mice. Although a minor metabolite, its presence does at least provide some evidence of MNQ-GSH conjugate formation *in vivo*. The alternative route of GSH conjugate elimination is via renal clearance, during which the glutamate and glycine residues of GSH are sequentially cleaved, followed by *N*-acetylation of the cysteine moiety to form a mercapturic acid conjugate[28].

To investigate whether a single bolus 25mg/kg i.p. dose of DMNQ or MNQ resulted in any hepatic effects, the glutathione status and transcriptome of the liver was monitored. GSSG levels were increased during the first 30 minutes post DMNQ and MNQ treatment (significant increases for DMNQ at 5 and 10 minutes), before a gradual return to basal levels by 60 minutes post dose (Figure 7.6B). This finding confirms that DMNQ and MNQ treated mice were exposed to hepatic redox challenge, albeit a short transient one. No

treatment-related changes in GSH levels were observed with either quinone over the 5 hours post dose (Figure 7.6A).

Although no historical data exists for DMNQ, MNQ administration to rats has been shown to rapidly decrease hepatic GSH[324]. Ossola *et al* reported that a single i.p. dose of 750 μ mol/kg of menadione sodium bisulphite (MSB) resulted in a 28 percent decrease in hepatic GSH levels within 1 hour, reaching a maximum effect at 3 hours with approximately 50 percent GSH depletion (versus vehicle control)[324]. A dose of 750 μ mol/kg MSB equates to approximately 130mg/kg of MNQ, a dose level greater than five times that used in this study. Thus, the lack of effect on hepatic GSH levels observed with 25mg/kg MNQ (and DMNQ) is most likely due to the dose level being too low to result in any appreciable GSH depletion. As discussed previously (Section 1.3.1), the concentration of GSH in the liver (4-8mM) is one of the highest of any tissue[42]. Consequently, the liver has the capacity to cope with relatively high concentrations of agents that have the potential to deplete GSH, such as DMNQ and MNQ.

A single bolus dose near 25mg/kg of MNQ (or MSB) to rodents does not result in histopathological changes in the liver[52;329]. In fact, either repeat dosing around this level for at least three consecutive days[327;328] or single bolus doses in the region of 75 to 150mg/kg[52;336] is necessary to induce detectable hepatic toxicity. As equivalent hepatotoxicity reference data did not exist for DMNQ *in vivo*, plasma levels of ALT and AST were assessed to monitor whether a single bolus dose of 25mg/kg DMNQ i.p. resulted in damage to the liver. No treatment related changes in plasma ALT/AST levels were observed during the 5 hours post dose (Figures 7.7A and B). These data indicate that no acute hepatotoxicity is associated with a single 25mg/kg dose of DMNQ i.p., a finding that is in line with the *in vivo* MNQ knowledgebase.

Transcriptome analysis of the livers from DMNQ and MNQ treated mice indicated minimal changes were associated with a 25mg/kg dose of each quinone during the 5 hours post treatment. Only 42 probe sets were consistently regulated across the time course with either quinone. This is a very low grade transcriptional response given the number of genes whose transcription was monitored (approximately 35,000). There was a conspicuous absence of genes typically regulated with quinone exposure or redox stress, such as *NADPH: quinone oxidoreductase 1 (Nqo1)*, *heme oxygenase 1 (Hmox1)*, subunits of glutamate-cysteine

ligase and AP-1-related transcripts. This was surprising, given that the livers had undergone a degree of redox stress, confirmed by the transient increase in GSSG levels observed between 5 and 10 minutes post treatment (Figure 7.6B). The low number of regulated transcripts, and lack of redox 'housekeeper' genes, suggests that only background variation was observed. It is likely that higher dose levels, or even repeat administration of DMNQ (and MNQ) is required to evoke transcriptional responses indicative of redox stress in the liver.

No true transcriptomic studies on the *in vivo* hepatic effects of DMNQ or MNQ treatment have been published to date. A limited amount of data does exist on the hepatic transcriptional responses evoked by MNQ administration, although only for focussed sets of genes. Such studies have generally used dosing regimes that would lead to greater hepatic MNQ exposure (in terms of dose level or frequency). For example, *Hmox1* induction was observed in the livers of rats treated with a single dose of 750 μ mol/kg MSB i.p. (equivalent to approximately 130mg/kg MNQ)[324]. Yoshinari *et al* reported that 40mg/kg MNQ i.p administration to rats on three consecutive days resulted in increased transcription of *Nqo1*[337]. And increased transcription of *cytochrome P450 1A1 (Cyp1a1)* and *Cyp1a2* was observed in the livers of rats treated orally with 15mg/kg MNQ for 4 days[338]. These studies support the assertion that a single i.p. dose of 25mg/kg of MNQ (and DMNQ) is insufficient to evoke a transcriptional response in the livers of mice.

This study provides the first detailed determination of the toxicokinetics and biodistribution of DMNQ and MNQ *in vivo*. Both quinones displayed similar plasma exposure kinetics, although the tissue distribution was strikingly different. DMNQ was more rapidly and widely distributed to the tissues assayed. Notably DMNQ crossed the blood brain barrier, whereas MNQ did not. DMNQ exposure levels were markedly higher in the liver and kidney, both in terms of C_{max} and AUC. It is hypothesised that the reactivity of MNQ may partly account for the apparent reduced tissue distribution. The determination of the presence of GSH-menadiol conjugates in the bile of MNQ treated mice will confirm this (work currently underway within Dr T Gant's group). The increase in liver GSSG levels observed with DMNQ confirms the utility of this compound for studying hepatic redox stress *in vivo*. However, based on minimal hepatic transcriptional responses observed with a single dose of 25mg/kg, future studies will necessitate a repeat dosing approach.

CHAPTER 8. GENERAL DISCUSSION

The overall aim of this thesis was to undertake a thorough transcriptomic study of the response to quinone-induced hepatic redox stress, both *in vitro* and *in vivo*. The study has enabled the identification of genes and control pathways whose differential regulation appears key in the adaptive response to quinone challenge (Chapter 4) and quinone-mediated redox stress (Chapter 5) in rat hepatocytes. In particular the role of *Pim3* kinase in rat hepatocyte survival following quinone-induced redox stress was established and confirmed using RNA interference techniques (Chapter 6). For the first time, the utility of the redox cycling quinone 2,3-dimethoxy-1,4-naphthoquinone (DMNQ) for studying hepatic redox stress *in vivo* was explored (Chapter 7). Comparison of DMNQ *in vivo* exposure kinetics with the structurally-related analogue menadione (MNQ) demonstrates that the former has clear advantages as a tool compound for study redox stress *in vivo*.

8.1. The Utility of Quinone Signature Genes

One of the main aims of this thesis was to investigate the utility of transcriptomics in the recognition and understanding of toxicity, particularly that associated with quinone exposure. Through the use of quinones with varied reactivity (in terms of redox cycling and arylating potential), it was hypothesised that sets of genes that differentiate the reactivity of the quinones (mechanism-based marker genes) would be able to be identified. The transcriptional investigation carried out (Chapter 4) determined that it was not possible to differentiate quinone reactivity based on transcriptomic data (Figure 4.4). This was most likely due to the fact that both reactivities result in similar cellular stress challenges and these are reflected in the transcriptomic data. Redox active quinones induce oxidative stress and arylating quinones mimic oxidative stress (through rapid depletion of GSH resulting in a shift in redox status). Transcriptomic profiles were unable to differentiate these two events.

A core set of genes were consistently regulated in response to the quinones tested, these have been termed 'quinone signature genes' (Table 4.7). A number of these have not previously been associated with quinone exposure or in some cases oxidative stress. However, their regulation makes functional sense based on the known biological consequences of quinone challenge (Figure 4.6). The data presented here indicates potential utility for quinone signature genes in the drug development process. The inclusion of such a gene panel within a screen could aid the detection of quinone-related metabolites prior to

structural identification. During the drug development process, pharmaceutical companies frequently progress lead New Chemical Entities (NCEs) that are subsequently identified to have quinone-related metabolites once metabolism studies are carried out. The reactive nature of quinones means that NCEs with quinone-related metabolites potentially carry an additional safety liability and would be better removed from development earlier[339]. This would assist NCE development because metabolite profiling occurs relatively late in development. The earliest drug metabolism readout typically takes the form of *in vitro* studies in isolated liver microsomes or in hepatocyte cultures (from a variety of relevant mammalian species) and occur in the late stages of lead optimisation or the early stages of preclinical development[340;341]. Due to practical limitations, it is not feasible to carry out metabolite studies any earlier at present. However, there is clear value (in terms of development costs) in being able to discharge the risk of quinone-related metabolites earlier in the lead optimisation/preclinical development cycle if suitable screens existed. A panel of quinone signature genes has the potential to form the basis of such a screening tool.

Although a core set of 22 quinone signature genes was identified (Table 4.6), additional work would be required before they could be confirmed as a quinone marker panel for use in cell-based screening. Many of the genes can be considered markers of a general stress response. For example, *early growth-response 1 (Egr1)*, activator protein-1-related genes (i.e. *Fos*, *Fos-like 1* and *small maf protein K*) and *heme oxygenase 1 (Hmox1)* have been shown to be induced in response to a range of stress stimuli in various cell types[138;139;154;155;157-159;342-346]. Others have been associated with the response to oxidative stress induced by non-quinone entities, including *transglutaminase 1*[168], *choline kinase alpha*[173], *pregnancy-induced growth inhibitor*[189] and *growth differentiation factor 15*[201;206]. However, within the set of 22 quinone signature genes, *serine/threonine kinase Pim3*, *dual specificity phosphatase 5*, *myosin regulatory light chain interacting protein*, *pyruvate dehydrogenase kinase isoenzyme 4* and *solute carrier family 5 member 3* have not previously been linked directly with either oxidative stress or quinone exposure. The lack of response-specificity of individual genes is not necessarily important for a screen. It is the overall responsiveness of the panel that would be used for detecting the presence of quinone metabolites. To determine whether the panel of genes is specific to quinones it would be necessary to carry out additional testing in rat hepatocytes with non-quinone entities that exert similar mechanistic challenges. Equivalent studies with

compounds that have known quinone-related metabolites would also need to be run to assess responsiveness of the gene panel fully. This would allow the utility of the quinone signature genes identified in this thesis to be confirmed as a valuable screening tool for identifying quinone-related metabolites.

8.2. The Efficacy of Thymoquinone in Preventing Aflatoxin B₁-Mediated Hepatocarcinogenesis Warrants Further Investigation

Thymoquinone (TQ), the active constituent of *Nigella sativa* seed extract[125;126], was originally included in the quinones selected for investigation to increase diversity within the test set. Being a benzoquinone analogue, it meant that two compounds of this class of quinone were included (the other being 1,4-benzoquinone). It also has some confounding properties for a quinone, given its capacity to arylate nucleophiles (it reacts non-enzymatically with GSH[129]) while at the same time displaying superoxide anion scavenging properties[126]. The arylating capacity of TQ was confirmed during the dose-ranging study carried out in rat hepatocytes (Chapter 3) in that GSH depletion was observed at 8 hours (Figure 3.5C). Superoxide scavenging has been cited as the mechanism for TQ ameliorating oxidative stress-related toxicity in *in vivo* and *in vitro* systems (reviewed in Section 3.1.1). Two studies have demonstrated that TQ co-administration can protect mice and rats against doxorubicin-induced cardiotoxicity[127;128].

Transcriptional data produced as part of this thesis (Chapter 4) suggests that superoxide scavenging is not the only mechanism through which TQ can ameliorate the effects of oxidative stress. TQ exposure of rat hepatocytes at a sub-cytotoxic concentration for 8 hours resulted in increased transcription of a number of nuclear factor (erythroid-derived 2)-like 2 (Nrf2)-target genes (Figure 4.4A). Although no change in glutathione status was observed with 50 μ M TQ exposure (Figures 4.1B and C), it evoked a far more marked transcriptional induction of Nrf2-target genes than the other quinones tested. The other quinones did adversely affect glutathione status at equitoxic concentrations. This finding suggests that a component of the protective properties of TQ is attributable to its potency as an inducer of Nrf2-target genes.

The potency of TQ for inducing Nrf2-target gene transcription, in the absence of adverse effects on glutathione status, is significant. Compounds with such properties have potential

utility as cancer chemopreventive agents[347;348]. Indeed, TQ co-administration at 10mg/kg (a sub-toxic dose) has been shown to protect mice against benzo[a]pyrene (B[a]P)-induced forestomach carcinogenesis[349]. Similarly Badary *et al*[350] demonstrated that the same dosing regime led to a significant reduction in the mutagenicity of B[a]P in mice (as assessed by a reduced rate of chromosomal aberrations).

Cancer chemoprevention involves the administration of compounds to block the carcinogenic process[351]. There are a number of mechanisms through which these agents exert their anti-cancer activity. One important mode of action is via modulation of metabolism, leading to enhanced detoxification of carcinogenic agents. In this regard, the Nrf2 pathway is of critical importance. As discussed previously (Section 1.3.2), many of the proteins encoded by Nrf2-target genes are involved in detoxification of carcinogenic agents, such as reactive metabolites or reactive oxygen species (ROS). Key Nrf2-target genes include a battery of phase 2 metabolism enzymes that carry out the conjugation of reactive metabolites, facilitating enhanced elimination[49;85;351;352].

To date the dithiolethiones are probably the best studied group of cancer chemopreventive agents. Their efficacy has been demonstrated in a range of chemically-induced experimental models of carcinogenesis[353]. The dithiolethione oltipraz, originally developed as a treatment for parasitic infections, has been shown to markedly reduce the rates of tumour formation in mice exposed to diethylnitrosamine, uracil mustard and B[a]P [354]. In rats oltipraz decreases the rate of colon tumour formation induced by azomethane exposure[355] and aflatoxin-B₁ (AFB₁)-induced hepatocarcinogenesis[356]. Short-term clinical trials on the efficacy of oltipraz in preventing hepatocarcinogenesis have been carried out in populations where dietary exposure to AFB₁ is high (Qidong, China) and resulted in significant increases in urinary excretion of the aflatoxin-mercapturic acid[357]. This indicates that oltipraz enhances phase 2 metabolism of AFB₁ in man, suggesting it may have potential for reducing development of hepatocarcinomas associated with high AFB₁ exposure.

The findings of this study suggest that the utility of TQ as a chemopreventive for AFB₁-induced hepatocarcinogenesis warrants further investigation. It shares the Nrf2-pathway inducing properties of the dithiolethiones[358-360] while at the same time having superoxide scavenging activity[126]. There is obvious potential for these properties to act

in synergy, conferring increased efficacy on TQ for cancer chemoprevention compared to an agent that works solely through Nrf2 pathway induction or has antioxidant activity alone.

8.3. An Insight into the Key Genes Promoting Hepatocyte Survival in the Face of Quinone-Mediated Mitochondrial Toxicity

The study of temporal responses to DMNQ and MNQ exposure in rat hepatocytes (Chapter 5) has offered a detailed insight into the adaptations made by these cells under conditions of marked oxidative stress. Transcriptional changes correlate with the perturbations in cellular metabolism and biochemical lesions that redox cycling quinones are known to induce. The pathways regulated also confirm the central role of mitochondria in the manifestation of the redox cycling quinone toxicity. Redox cycling quinones (including DMNQ and MNQ) act as alternate electron acceptors, disrupting the normal flow of electrons along the respiratory chain[100;361]. This reduces the efficiency of aerobic respiration, leading to depletion of substrates required for energy metabolism, decreased ATP generation and increased electron leakage from the respiratory chain[34;39;362]. The futile redox cycling between the parent quinone and semiquinone radical also leads to additional ROS generation via Fenton chemistry (as outlined in Section 1.1.3). The net result is: 1) perturbed energy homeostasis and 2) ROS-mediated depletion of GSH (and other antioxidants) that can result in oxidative stress. Left unchecked these two intrinsically linked challenges can eventually lead to cell death via apoptosis (if the cell has sufficient reserves of ATP) or necrosis (if the cell does not)[363] (as outlined in Figure 8.1).

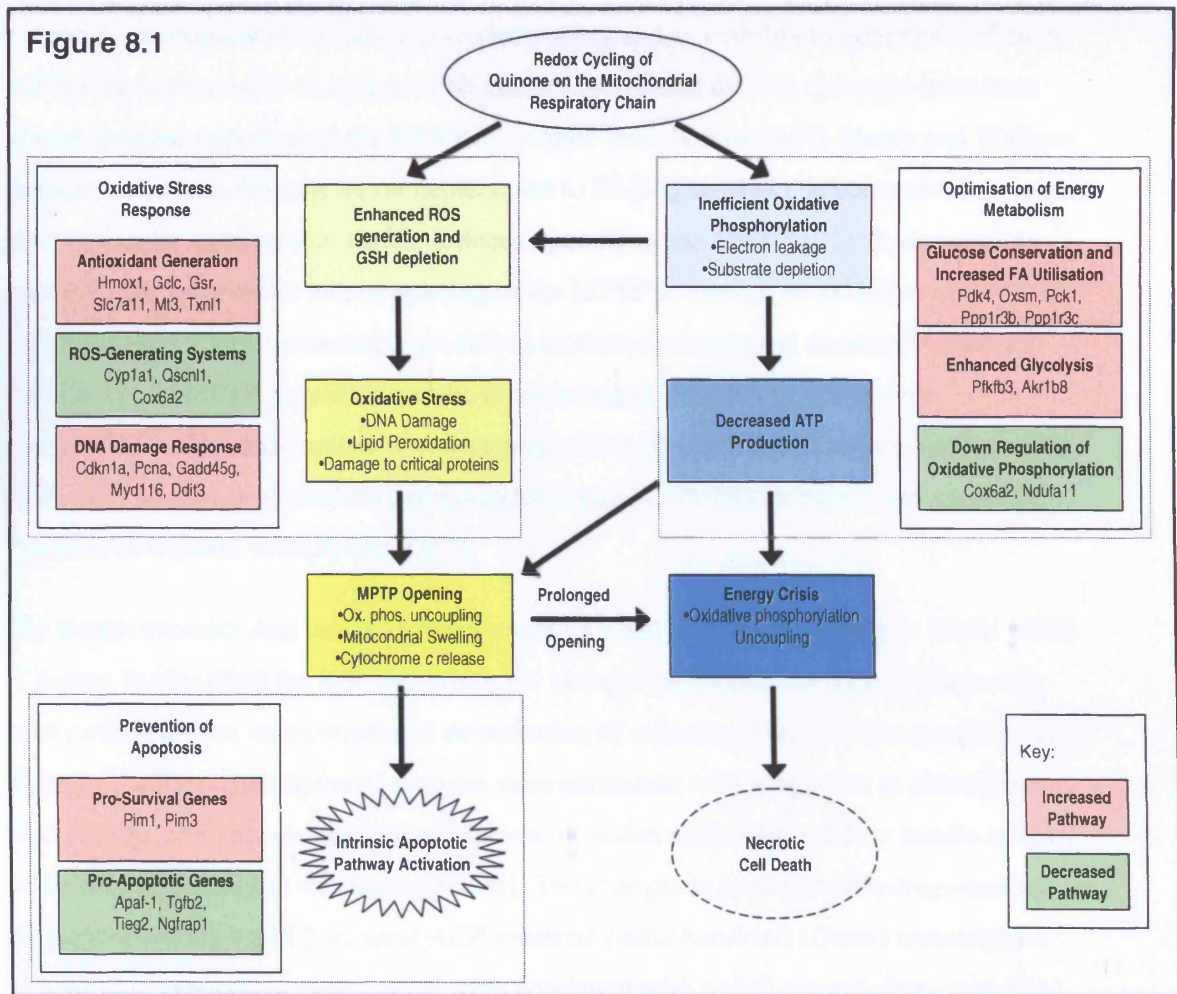


Figure 8.1: Mechanisms of redox cycling quinone-mediated mitochondrial toxicity and the key response pathways regulated by rat hepatocytes to ameliorate these effects and promote survival.

Redox cycling quinones act as alternate electron acceptors, perturbing normal electron flow along the respiratory chain. This leads to a chain of events that increase ROS generation and cause oxidative stress, decrease ATP generation and eventually leads to the MPTP opening. This can result in cell death via apoptosis (if sufficient ATP is available) or necrosis. The key transcriptional responses mounted by rat hepatocytes to counter these effects and promote survival are indicated.

The key route through which redox cycling quinones cause mitochondria-mediated cell death is via 'permeability transition' as a result of opening of the mitochondrial permeability transition pore (MPTP)[364;365]. Mitochondrial permeability transition is characterised as increased non-specific permeability of the inner mitochondrial membrane, loss of the membrane potential and mitochondrial swelling[363]. Transient opening of the MPTP can result in cytochrome *c* release and initiation of cell death via the intrinsic

apoptotic pathway. Prolonged opening of the MPTP can result in loss of membrane potential, uncoupling of oxidative phosphorylation and an inability to generate sufficient ATP leading eventually to necrotic cell death[366]. Redox cycling quinones have been shown to induce opening of the MPTP in isolated mitochondria[367]. Henry and Wallace demonstrated that exposure of rat hepatocytes to DMNQ or MNQ, at concentrations within the same order of those that I used, induced opening of the MPTP[101]. Redox cycling quinones are believed to induce opening of the MPTP as a result of oxidative stress[20;100]. Under prooxidant conditions oxidation of cysteinyl residues that play a critical role in MPTP regulation results in an increased probability of the pore opening[368]. This mechanism was first proposed by Petronelli *et al* who investigated the effect that a number of oxidative stress-inducing agents (MNQ included) had on MPTP function in isolated mitochondria[367].

My transcriptomics data using rat hepatocytes exposed to 150 μ M DMNQ or 25 μ M MNQ (Chapter 5) identified the key transcriptional changes promoting survival of these cells under conditions of redox-mediated perturbation of mitochondrial function (summarised in Figure 8.1). The transcriptional changes were consistent with adaptation to altered energy metabolism. Quinone-mediated perturbation of oxidative phosphorylation results in rapid utilisation of glycolytic substrates[20;184]. The changes in *pyruvate dehydrogenase kinase, isoenzyme 4 (Pdk4)* and *3-oxoacyl-ACP synthase (mitochondrial) (Oxsm)* transcription (Figure 8.1) early in the time course were consistent with a shift towards fatty acid (FA) catabolism to supply acetyl-CoA to the citric acid cycle, allowing glucose conservation. At the same time, increases in transcription of protein *phosphatase 1 regulatory (inhibitor) subunit 3B (Pppr3b)*, *Pppr3c* and *phosphoenolpyruvate carboxykinase 1 (Pck1)* indicate an attempt to replenish glucose stores by shunting pyruvate (spared as a result of FA catabolism) into gluconeogenesis and glycogen storage. As time progresses and reduced mitochondrial ATP generation becomes more critical, increased transcription of *6-phosphofructo-2-kinase/fructose-2,6-biphosphatase 3 (Pfkfb3)* and *aldo-keto reductase family 1, member B8 (Akr1b8)*, and decreased transcription of *cytochrome c oxidase, subunit VIa, polypeptide 2 (Cox6a2)* and *NADH dehydrogenase (ubiquinone) 1 alpha subcomplex 11 (Ndufa11)*, point towards enhanced glycolysis and down-regulation of oxidative phosphorylation. The transcriptional changes indicate how rat hepatocytes optimise energy output in the face of a perturbation of normal mitochondrial function.

In addition to optimisation of energy metabolism, transcriptional changes indicate a coordinated oxidative stress and DNA damage response in the face of enhanced ROS generation within the mitochondria (Figure 8.1). Increased transcription of antioxidant defense genes (e.g. *Hmox1* and *Metallothionein 3 (Mt3)*) and glutathione metabolism genes (*glutamate-cysteine ligase catalytic subunit (Gclc)*, *glutathione reductase (Gsr)* and *solute carrier family 7, member 11 (Slc7a11)*) were accompanied by decreased transcription of ROS-generating systems (e.g. *cytochrome P450 1a1 (Cyp1a1)* and *Quiescin 6-like 1 (Qscn1)*). Increased transcription of a number of tumour suppressor p53-target genes (e.g. *Cyclin-dependent kinase inhibitor 1a (p21) (Cdkn1a)*, growth arrest and *DNA-damage-inducible 45 gamma (Gadd45g)* and *DNA-damage-inducible transcript 3 (Ddit3)*) are indicative of cell cycle arrest in response to ROS-mediated DNA damage[267;369;370]. The proteins and enzymes encoded by this diverse group of genes work in concert to minimise the deleterious effects of excessive ROS generation. However, once these cellular defences are overwhelmed oxidative stress ensues. In the mitochondria this can lead to MPTP opening with the outcomes discussed previously (i.e. apoptosis or cellular energy crisis and necrosis).

Transient opening of the MPTP can result in release of mitochondrial constituents into the cytosol, among them cytochrome *c* which binds to oligomerised APAF-1 forming the apoptosome[363]. The apoptosome recruits and activates caspase-9 which initiates apoptosis through the subsequent activation of effector caspases (i.e. caspase-3, -6 and -7)[225;226]. Changes in apoptosis-related genes in DMNQ and MNQ exposed hepatocytes (Figure 8.1) indicate the core transcriptional response necessary to prevent (or perhaps delay) activation of the intrinsic apoptotic pathway following MPTP opening. There was decreased transcription of several pro-apoptotic genes (i.e. *apoptotic peptidase factor 1 (Apaf1)*, *tissue growth factor beta 2 (Tgfb2)*, *TGFB-inducible early growth response 3 (Tieg3)* and *nerve growth factor receptor-associated protein 1 (Ngfrap1)*), all of which are linked to the intrinsic apoptotic pathway. *Tgfb2* and *Tieg3* have been implicated in potentiation of MPTP opening[233]. APAF-1 is a core component of the apoptosome[226;371;372] and the protein encoded by *Ngfrap1* is involved in blocking the activity of Apoptosis Inhibitor Proteins (AIPs), which would normally prevent activation of Caspase-9[247].

The transcriptional findings indicate that the anti-apoptotic response is primarily mediated by PIM kinase family members. *Pim1* and *Pim3* transcription was increased from 6 hours onwards in rat hepatocytes exposed to DMNQ or MNQ (Figure 5.10). The importance of *Pim3* in hepatocyte survival in response to challenge with redox cycling quinones was confirmed by targeted knockdown of this gene using RNA interference (Chapter 6). At 150 μ M DMNQ and 25 μ M MNQ, hepatocytes transfected with *Pim3*-specific small interfering RNAs (siRNAs) displayed increased sensitivity over those transfected with a non-functional control siRNA. Marked necrotic cell death was noted with 6 hours exposure (increased LDH leakage; Figures 6.4A and B) and evidence of increased apoptosis was observed within 3 hours (activated caspase 3 activity; Figure 6.5A and B). PIM kinases have been shown to promote cell survival through inactivation of the BCL2-agonist of cell death (BAD)[190;191;252;253]. This activity prevents binding of BAD with anti-apoptotic members of the Bcl-2 family (e.g. Bcl-X(L), Bcl-2 and Bcl-W), thereby freeing them to facilitate inhibition of the intrinsic apoptosis pathway[254;298]. Based on the data presented within this thesis, PIM kinases are of central importance in promoting hepatocyte survival in response to challenge with redox cycling quinones. A role for *Pim3* in promoting cell survival in response to oxidative stress, quinone challenge or MPTP opening has not been previously defined.

8.4. Comparability of the *In Vivo* and *In Vitro* Hepatic Responses to DMNQ and its Utility for Studying Oxidative Stress *In Vivo*

One of the achievements of this thesis was to address the paucity of *in vivo* data on DMNQ. DMNQ, and related quinones such as MNQ, are frequently used as tool compounds for studying redox stress *in vitro*. The ability of DMNQ to generate hydrogen peroxide, increase GSSG levels and affect other redox-relevant endpoints have been demonstrated in a host of cell types[219;319;373-376]. The utility of this quinone for equivalent *in vivo* studies are obvious, although apparently no such studies have been undertaken. Analysis carried out on the tissues and biofluids from male C57BL/6J mice treated with a single bolus dose of 25mg/kg DMNQ i.p. has provided a thorough profile of the toxicokinetics and initial biodistribution of this quinone (Table 7.2). Comparison with equivalent data produced for MNQ shows that DMNQ is more widely distributed (Figure 7.5 and Table 7.2). Significantly, DMNQ was distributed to the brain, whereas MNQ was not.

The advantages of DMNQ for studying oxidative stress and quinone-mediated redox effects *in vitro* over other quinones have been recognised by others[365;377]. It has a similar redox potential to MNQ, but does not have the capacity to arylate cellular nucleophiles due to the methoxy substitutions at the 2 and 3 carbon position[377]. Thus, without the added complexity of cytotoxicity derived from protein adduct formation, DMNQ enables the cytotoxic effects of redox stress to be more definitively studied. This assertion is just as relevant to the study of redox stress *in vivo*. When this is considered alongside the superior biodistribution profile demonstrated for DMNQ, the case for this compound being the tool of choice for studying oxidative stress and redox-related toxicity *in vivo* is clear. Indeed, the fact that DMNQ crosses the blood brain barrier (BBB) opens up opportunities for studying the effects of oxidative stress in neuronal tissue *in vivo*. This may be of value in helping to define the role that oxidative stress plays in a number of neurological disease states. For example, it has long been recognised that Alzheimer's and Parkinson's diseases have an oxidative stress component[378;379]. DMNQ may also have utility in studying the effects of respiratory chain perturbation in neuronal tissue.

In vivo work undertaken as part of this thesis focused on the hepatic physiological consequences of DMNQ (and MNQ) exposure (Chapter 7). This was to allow the direct comparison of hepatocyte transcriptomic data to equivalent *in vivo* data, an important step for defining the relevance of changes observed *in vitro*. Transcriptional changes observed in rat hepatocytes exposed to 150 μ M DMNQ or 25 μ M MNQ (summarised in Figure 8.1) indicated a coordinated response to the deleterious effects of redox challenge. There was evidence of induction of antioxidant defence systems, the response to DNA damage, anti-apoptotic signalling and optimisation of energy metabolism to compensate for perturbation of mitochondrial function. It is clear from the changes observed in glutathione status that 150 μ M DMNQ or 25 μ M MNQ resulted in a marked redox challenge to rat hepatocytes (Figures 5.2 to 5.4). No evidence of this type of response was observed in the livers of DMNQ or MNQ treated mice (refer to Section 7.2.3.3). Changes in glutathione status in the livers of mice treated with 25mg/kg i.p DMNQ or MNQ were more subtle (compared to those observed in rat hepatocytes exposed to 150 μ M DMNQ or 25 μ M MNQ), with only transient increases in GSSG being observed (Figure 7.6B). As DMNQ or MNQ was systemically cleared, the redox challenge subsided (refer to plasma and liver quinone kinetics, Figures 7.5A and B). Thus, the lack of hepatic transcriptional response *in vivo* is

most likely a function of insufficient quinone exposure (in terms of levels and time) being achieved.

Equating *in vitro* treatment conditions with *in vivo* exposure is not a simple task, although efforts were made to ensure comparability. *In vitro*, DMNQ and MNQ concentrations that induced an effect on glutathione status, while not causing overt acute (up to 8 hours) cytotoxicity were selected (Chapter 3). *In vivo*, the 25mg/kg i.p. dose was based on the no observed adverse affect levels (NOAEL) defined for DMNQ (based on clinical signs in dose ranging studies, refer to Section 7.3.1) and MNQ[329]. At these dose levels overt liver toxicity was not observed with DMNQ (based on plasma ALT/AST levels, Figures 7.7) but a change in glutathione status was (Figure 7.6B). As DMNQ exposure levels were increased above 25mg/kg dose-limiting toxicity was rapidly observed (as outlined in Section 7.2.2). When this is considered in the context of the minimal changes in liver physiology at the NOAEL (i.e. no redox-related transcriptional changes and only a transient increase in GSSG levels), it must be concluded that the primary target organ for DMNQ toxicity is not the liver.

The differential responses to DMNQ or MNQ-mediated redox challenge in primary hepatocytes and the liver *in vivo* underscores the importance of taking a cautious approach when drawing conclusions based simply on *in vitro* data. An understanding of the *in vivo* situation helps define the relevance of findings seen *in vitro*. Key determinants for the differential response most likely include quinone exposure and environmental conditions. Primary hepatocytes are continuously exposed to DMNQ for the duration of the experiment, whereas *in vivo*, DMNQ is rapidly cleared from the liver (Table 7.2). Additionally the capacity for primary hepatocyte *in vitro* to survive redox challenge is greatly diminished compared to hepatocytes within the *in vivo* environment (Personal communication; Dr Dominic Williams, Pharmacology Department, University of Liverpool). The culture conditions also ensure that hepatocytes endure a higher level of oxygen tension than their *in vivo* counter parts[380], exacerbating the oxidative stress associated with redox cycling quinones.

The rapidity with which toxicity is manifest following i.p. administration of DMNQ above 25mg/kg may point towards the brain as the potential primary target organ. DMNQ certainly penetrated the BBB (Figure 7.5D) and neuronal tissue may well be exquisitely

sensitive to the effects of such a quinone. DMNQ can act as an alternate electron acceptor within the mitochondrial respiratory chain, disrupting electron flow and diminishing energy production[34]. The redox stress it induces also depletes cellular antioxidants. Neurons are highly dependent on aerobic energy production[381]. A second potential DMNQ target organ is the heart, which is also more susceptible to mitochondrial perturbation and oxidative stress than the liver[382;383]. The cardiac effects of DMNQ in the same mice are currently being investigated (within Dr Tim Gant's group, MRC Toxicology Unit, Leicester University). Early findings indicate that acute cardiac toxicity is caused by a DMNQ dose of 25mg/kg i.p. and that this is indeed associated with mitochondrial events (based on transcriptional changes in the heart tissue).

8.5. Future Work

To evaluate the specificity of the 'quinone signature genes' an assessment of the responsiveness of this panel to non-quinones is necessary. This would require the treatment of rat hepatocytes with a number of non-quinone compounds that exert toxicity through arylation or redox cycling. Compounds known to have quinone-related metabolites would also be assessed.

One of the aims of this thesis was to carry out a comparison of the hepatic transcriptional response to quinones *in vitro* and *in vivo*. This was not achieved because DMNQ and MNQ dose levels used in mice were too low to evoke an oxidative stress response. Dose escalation above 25mg/kg DMNQ is not feasible, due to rapid onset of dose-limiting toxicity. This appears to be C_{max}-related as clinical signs subside within 30 minutes (as DMNQ is cleared). Thus a repeat dosing approach at or below 25mg/kg is required, which may include multiple daily dosing due the rapid clearance of DMNQ.

RNA interference (RNAi) experiments confirmed a role for *Pim3* in hepatocyte survival in response to quinone-mediated redox challenge. Additional RNAi experiments are required to confirm the importance of other key genes in ameliorating quinone cytotoxicity. It would also be interesting to define whether PIM kinases play a role in quinone hepatotoxicity *in vivo*. Possible avenues for evaluating such a role would include transcript analysis in the livers of DMNQ or MNQ treated mice. Investigating whether PIM kinase knockout models display increased hepatic sensitivity to redox-cycling quinones would also be of value. *In vivo* RNA interference would be an alternative route of investigation

8.6. Conclusions

During the course of this study I have sought to utilise transcriptomics to identify key genes and control pathways in ameliorating quinone-mediated hepatotoxicity, with a focus on redox stress.

In vitro this was undertaken in primary rat hepatocytes, where transcriptional responses to quinones with a range of reactivities (in terms of arylating and redox cycling capacity) were assessed. It was not possible to differentiate arylating or redox cycling quinones based on transcriptional responses. This is most likely a function of the two mechanisms resulting in similar cellular challenges. However a core set of 22 'quinone signature genes' were identified, which may have utility in screening for quinone-related metabolites.

Significantly, *Pim3*, *Dusp5*, *Myip*, *Pdk4* and *Slc5a3* have not previously been associated with quinone exposure or oxidative stress. As anticipated, Nrf2-target genes were regulated with quinones affecting glutathione status, but also with TQ which did not. TQ's potency for inducing Nrf2-target genes warrants more investigation and may indicate efficacy in hepatic cancer chemoprevention.

Subsequent hepatocyte studies focused on temporal responses to DMNQ and MNQ, both redox cycling quinones. A coordinated response to redox stress and DNA damage was observed, with increased transcription of Nrf2 and p53-target genes and decreased transcription of ROS-generating systems. Changes in genes encoding enzymes central to modulation of energy metabolism indicate a shift towards enhanced glycolysis to compensate for quinone-mediated perturbation of mitochondrial function. Overall, the transcriptional responses confirmed the central role that mitochondria are known to play in redox cycling quinone toxicity, with down regulation of the intrinsic apoptotic pathway to promote cell survival. Key to this response were serine/threonine kinases *Pim1* and *Pim3*, the importance of the latter being confirmed in RNA interference experiments. The role of PIM kinases in ameliorating quinone and mitochondrial toxicity in the liver warrants further investigation.

In vivo studies in mice treated with single doses of 25mg/kg DMNQ or MNQ i.p. provided detailed exposure kinetics that will lay the foundation for further *in vivo* work. DMNQ treatment did result in a redox challenge within the liver, although the response was only transient. Based on transcriptional analysis, this challenge was not sufficient to induce

oxidative stress. Repeat dosing studies are required to investigate hepatic responses to DMNQ-mediated redox stress *in vivo*. Based on the rapidity with which DMNQ-related toxicity is manifest at doses above 25mg/kg i.p., an organ other than the liver is the primary target for toxicity. A possible candidate is the brain as DMNQ crossed the BBB. This opens up possibilities for DMNQ as a tool for investigating oxidative stress and perturbed mitochondrial function in neuronal tissue *in vivo*. This may be of value in defining their role in neurological disease states and toxicity.

The findings of this study add to the knowledgebase of quinone toxicity and key hepatic response pathways for promoting cell survival. In addition, as quinones are frequently used as tool compounds for studying oxidative stress, the data also furthers our understanding of the relationship between oxidative stress and gene expression.

The work in this study indicates that genomics has applicability to identify toxicity soon after chemical exposure. It can perhaps be argued that at the present time it is not the high mechanistic precision tool that was initially anticipated. This was indicated by its inability to differentiate quinones based on their specific reactivities (Chapter 4). It is though sensitive for toxicity and applied early in the drug development pipeline could have the potential to screen out those compounds that have potential to cause toxicity, either intrinsically or via reactive metabolites, in a more timely manner. The lack of understanding of gene functions hinders effective interpretation of genomics data and it is probable that as this knowledge advances then genomics will become a more mechanistically precise tool. For example, of the 804 probe sets selected for cluster analysis following exposure of rat hepatocytes to DMNQ or MNQ (Chapter 5), it was only possible to confer a functional interpretation on a small proportion (226, approximately 30 percent). Therefore as the understanding of individual gene roles in cell biology improves, so will the interpretation of transcriptional profiles and the mechanistic precision of the tool. Genomics as a discipline is still in its relative infancy, so at the present time we are seeing only the first stages of application in toxicology. As the science develops further it will further empower mechanistic toxicology as genomics is applied to its full potential.

REFERENCES

1. Smith, M.T. (1985) Quinones as mutagens, carcinogens, and anticancer agents: introduction and overview. *Journal of Toxicology & Environmental Health*, **16**, 665-672.
2. Vromans, R.M., van de, S.R., Groeneveld, M., Vermeulen, N.P., van de, S.R., Groeneveld, M., and Vermeulen, N.P. (1990) One-electron reduction of mitomycin c by rat liver: role of cytochrome P-450 and NADPH-cytochrome P-450 reductase. *Xenobiotica*, **20**, 967-978.
3. Monks, T.J., Jones, D.C., and Jones, D.C. (2002) The metabolism and toxicity of quinones, quinonimines, quinone methides, and quinone-thioethers. [Review] [145 refs]. *Current Drug Metabolism*, **3**, 425-438.
4. Rotello, V.M. (1999) Model systems for redox cofactor activity. [Review] [23 refs]. *Current Opinion in Chemical Biology*, **3**, 747-751.
5. McIntire, W.S. (1998) Newly discovered redox cofactors: possible nutritional, medical, and pharmacological relevance to higher animals. [Review] [245 refs]. *Annual Review of Nutrition*, **18**, 145-177.
6. Saraste, M. (1999) Oxidative phosphorylation at the fin de siecle. [Review] [50 refs]. *Science*, **283**, 1488-1493.
7. Alberts, B., Bray, D., Lewis, J., Raff, M., Roberts, K., and Watson, J.D. (1989) Energy Conversion: Mitochondria and chloroplasts. In Robertson, M. (ed.) *Molecular Biology of the Cell*. Garland Publishing, pp 341-404.
8. Linnane, A.W., Eastwood, H., and Eastwood, H. (2006) Cellular redox regulation and prooxidant signaling systems: a new perspective on the free radical theory of aging. [Review] [22 refs]. *Annals of the New York Academy of Sciences*, **1067**, 47-55.
9. Munday, R. (2001) Concerted action of DT-diaphorase and superoxide dismutase in preventing redox cycling of naphthoquinones: an evaluation. *Free Radic. Res.*, **35**, 145-158.
10. Mascolo, N., Capasso, R., and Capasso, F. (2007) Senna: A safe and effective drug. *Phytother. Res.*, **12**, S143-S145.
11. Li, N., Venkatesan, M.I., Miguel, A., Kaplan, R., Gujuluva, C., Alam, J., Nel, A., Venkatesan, M., I, Miguel, A., Kaplan, R., Gujuluva, C., Alam, J., and Nel, A. (2000) Induction of heme oxygenase-1 expression in macrophages by diesel exhaust particle chemicals and quinones via the antioxidant-responsive element. *Journal of Immunology*, **165**, 3393-3401.
12. Schneider, G. (2005) Enzymes in the biosynthesis of aromatic polyketide antibiotics. [Review] [37 refs]. *Current Opinion in Structural Biology*, **15**, 629-636.
13. Hrdina, R., Gersl, V., Klimtova, I., Simnek, T., Machackova, J., Adamcova, M., Gersl, V., Klimtova, I., Simnek, T., Machackova, J., and Adamcova, M. (2000) Anthracycline-induced cardiotoxicity. [Review] [68 refs]. *Acta Medica (Hradec Kralove)*, **43**, 75-82.

14. Rabbani,A., Finn,R.M., Ausio,J., Finn,R.M., and Ausio,J. (2005) The anthracycline antibiotics: antitumor drugs that alter chromatin structure. [Review] [73 refs]. *Bioessays*, **27**, 50-56.
15. Patel,S., Sprung,A.U., Keller,B.A., Heaton,V.J., Fisher,L.M., Sprung,A.U., Keller,B.A., Heaton,V.J., and Fisher,L.M. (1997) Identification of yeast DNA topoisomerase II mutants resistant to the antitumor drug doxorubicin: implications for the mechanisms of doxorubicin action and cytotoxicity. *Molecular Pharmacology*, **52**, 658-666.
16. Begleiter,A. (2000) Clinical applications of quinone-containing alkylating agents. [Review] [242 refs]. *Frontiers in Bioscience*, **5**, E153-E171.
17. Beall,H.D., Winski,S.I., and Winski,S., I (2000) Mechanisms of action of quinone-containing alkylating agents. I: NQO1-directed drug development. [Review] [98 refs]. *Frontiers in Bioscience*, **5**, D639-D648.
18. Hargreaves,R.H., Hartley,J.A., Butler,J., Hartley,J.A., and Butler,J. (2000) Mechanisms of action of quinone-containing alkylating agents: DNA alkylation by aziridinylquinones. [Review] [50 refs]. *Frontiers in Bioscience*, **5**, E172-E180.
19. Bolton,J.L., Trush,M.A., Penning,T.M., Dryhurst,G., Monks,T.J., Trush,M.A., Penning,T.M., Dryhurst,G., and Monks,T.J. (2000) Role of quinones in toxicology. [Review] [298 refs]. *Chemical Research in Toxicology*, **13**, 135-160.
20. Henry,T.R., Wallace,K.B., and Wallace,K.B. (1996) Differential mechanisms of cell killing by redox cycling and arylating quinones. *Arch.Toxicol.*, **70**, 482-489.
21. Jarabak,R., Harvey,R.G., Jarabak,J., Harvey,R.G., and Jarabak,J. (1998) Redox cycling of polycyclic aromatic hydrocarbon o-quinones: metal ion-catalyzed oxidation of catechols bypasses inhibition by superoxide dismutase. *Chemico-Biological Interactions*, **115**, 201-213.
22. Seung,S.A., Lee,J.Y., Lee,M.Y., Park,J.S., Chung,J.H., Lee,J.Y., Lee,M.Y., Park,J.S., and Chung,J.H. (1998) The relative importance of oxidative stress versus arylation in the mechanism of quinone-induced cytotoxicity to platelets. *Chemico-Biological Interactions*, **113**, 133-144.
23. O'Brien,P.J. (1991) Molecular mechanisms of quinone cytotoxicity.[erratum appears in Chem Biol Interact 1992 Jan;81(1-2):219]. [Review] [165 refs]. *Chemico-Biological Interactions*, **80**, 1-41.
24. Watanabe,N., Dickinson,D.A., Liu,R.M., Forman,H.J., Dickinson,D.A., Liu,R., and Forman,H.J. (2004) Quinones and glutathione metabolism. [Review] [33 refs]. *Methods in Enzymology*, **378**, 319-340.
25. Shertzer,H.G., Lastbom,L., Sainsbury,M., Moldeus,P., Lastbom,L., Sainsbury,M., and Moldeus,P. (1992) Menadione-mediated membrane fluidity alterations and oxidative damage in rat hepatocytes. *Biochem.Pharmacol.*, **43**, 2135-2141.
26. Gant,T.W., Rao,D.N., Mason,R.P., Cohen,G.M., Rao,D.N., Mason,R.P., and Cohen,G.M. (1988) Redox cycling and sulphhydryl arylation; their relative importance in the mechanism of quinone cytotoxicity to isolated hepatocytes. *Chemico-Biological Interactions*, **65**, 157-173.

27. Miller,M.G., Rodgers,A., Cohen,G.M., Rodgers,A., and Cohen,G.M. (1986) Mechanisms of toxicity of naphthoquinones to isolated hepatocytes. *Biochem.Pharmacol.*, **35**, 1177-1184.
28. Parkinson,A. (1996) Biotransformation of xenobiotics. In Klassen,C.D. (ed.) *Cassarett and Doull's toxicology: The basic science of poisons.*, pp 113-86.
29. Gutierrez,P.L. (2000) The role of NAD(P)H oxidoreductase (DT-Diaphorase) in the bioactivation of quinone-containing antitumor agents: a review. [Review] [117 refs]. *Free Radical Biology & Medicine*, **29**, 263-275.
30. Stubberfield,C.R., Cohen,G.M., and Cohen,G.M. (1989) Interconversion of NAD(H) to NADP(H). A cellular response to quinone-induced oxidative stress in isolated hepatocytes. *Biochem.Pharmacol.*, **38**, 2631-2637.
31. Watanabe,N., Forman,H.J., and Forman,H.J. (2003) Autoxidation of extracellular hydroquinones is a causative event for the cytotoxicity of menadione and DMNQ in A549-S cells. *Archives of Biochemistry & Biophysics*, **411**, 145-157.
32. van Bladeren,P.J. (2000) Glutathione conjugation as a bioactivation reaction. [Review] [86 refs]. *Chemico-Biological Interactions*, **129**, 61-76.
33. Monks,T.J., Lau,S.S., and Lau,S.S. (1997) Biological reactivity of polyphenolic-glutathione conjugates. [Review] [196 refs]. *Chemical Research in Toxicology*, **10**, 1296-1313.
34. Wallace,K.B., Starkov,A.A., and Starkov,A.A. (2000) Mitochondrial targets of drug toxicity. [Review] [192 refs]. *Annual Review of Pharmacology & Toxicology*, **40**, 353-388.
35. Toxopeus,C., van,H., I, Thuring,J.W., Blaauboer,B.J., Noordhoek,J., van,H., I, Thuring,J.W., Blaauboer,B.J., and Noordhoek,J. (1993) Cytotoxicity of menadione and related quinones in freshly isolated rat hepatocytes: effects on thiol homeostasis and energy charge. *Arch.Toxicol.*, **67**, 674-679.
36. Toxopeus,C., van,H., I, de Winther,M.P., van den,D.D., Horbach,G.J., Blaauboer,B.J., Noordhoek,J., van,H., I, de Winther,M.P., van den,D.D., Horbach,G.J., Blaauboer,B.J., and Noordhoek,J. (1994) Role of thiol homeostasis and adenine nucleotide metabolism in the protective effects of fructose in quinone-induced cytotoxicity in rat hepatocytes. *Biochem.Pharmacol.*, **48**, 1682-1692.
37. Herman,E.H., Ferrans,V.J., and Ferrans,V.J. (1998) Preclinical animal models of cardiac protection from anthracycline-induced cardiotoxicity. [Review] [49 refs]. *Seminars in Oncology*, **25**, 15-21.
38. Minotti,G., Menna,P., Salvatorelli,E., Cairo,G., Gianni,L., Menna,P., Salvatorelli,E., Cairo,G., and Gianni,L. (2004) Anthracyclines: molecular advances and pharmacologic developments in antitumor activity and cardiotoxicity. [Review] [525 refs]. *Pharmacological Reviews*, **56**, 185-229.
39. Wallace,K.B. (2003) Doxorubicin-induced cardiac mitochondrionopathy. [Review] [140 refs]. *Pharmacology & Toxicology*, **93**, 105-115.
40. Williams,D.P. (2006) Toxicophores: investigations in drug safety. *Toxicology*, **226**, 1-11.

41. Cheeseman,K.H., Slater,T.F., and Slater,T.F. (1993) An introduction to free radical biochemistry. [Review] [42 refs]. *British Medical Bulletin*, **49**, 481-493.
42. Reed,D.J. (1998) Evaluation of Chemical-Induced Oxidative Stress as a Mechanism of Hepatocyte Death. In Hayes,A.W., Thomas,J.A., and Gardner,D.E. (eds.) *Toxicology of the Liver*. Taylor Francis, pp 187-220.
43. Johnson,I.J., Krishna,M.C., Gandhidasan,R., Murugesan,R., Krishna,M.C., Gandhidasan,R., and Murugesan,R. (1999) Cytotoxicity, redox cycling and photodynamic action of two naturally occurring quinones. *Biochim.Biophys.Acta*, **1472**, 462-470.
44. Gregus,Z. and Klaassen,C.D. (1996) Mechanisms of toxicity. In Klassen,C.D. (ed.) *Casarett and Doull's Toxicology: The basic science of poisons*. Graw Hill, pp 35-74.
45. Gibson,G.G. and Skett,P. (2001) Enzymology and molecular mechanisms of drug metabolism reactions. In Gibson,G.G. and Skett,P. (eds.) *Introduction to drug metabolism*. Nelson Thornes, pp 37-87.
46. Adam,A., Smith,L.L., Cohen,G.M., Smith,L.L., and Cohen,G.M. (1990) An evaluation of the redox cycling potencies of paraquat and nitrofurantoin in microsomal and lung slice systems. *Biochem.Pharmacol.*, **40**, 1533-1539.
47. Gabbita,S.P., Robinson,K.A., Stewart,C.A., Floyd,R.A., Hensley,K., Robinson,K.A., Stewart,C.A., Floyd,R.A., and Hensley,K. (2000) Redox regulatory mechanisms of cellular signal transduction. [Review] [107 refs]. *Archives of Biochemistry & Biophysics*, **376**, 1-13.
48. Stohs,S.J., Bagchi,D., and Bagchi,D. (1995) Oxidative mechanisms in the toxicity of metal ions. [Review] [124 refs]. *Free Radical Biology & Medicine*, **18**, 321-336.
49. Morel,Y., Barouki,R., and Barouki,R. (1999) Repression of gene expression by oxidative stress. [Review] [189 refs]. *Biochemical Journal*, **342 Pt 3**, 481-496.
50. Comporti,M. (1987) Glutathione depleting agents and lipid peroxidation. [Review] [178 refs]. *Chemistry & Physics of Lipids*, **45**, 143-169.
51. Comporti,M. (1998) Lipid peroxidation as a mediator of chemical-induced hepatocyte death. In Hayes,A.W., Thomas,J.A., and Gardner,D.E. (eds.) *Toxicology of the Liver*. Taylor Francis, pp 221-58.
52. Chiou,T.J., Chou,Y.T., Tzeng,W.F., Chou,Y.T., and Tzeng,W.F. (1998) Menadione-induced cell degeneration is related to lipid peroxidation in human cancer cells. *Proceedings of the National Science Council, Republic of China - Part B, Life Sciences*, **22**, 13-21.
53. Sevanian,A., Ursini,F., and Ursini,F. (2000) Lipid peroxidation in membranes and low-density lipoproteins: similarities and differences. [Review] [50 refs]. *Free Radical Biology & Medicine*, **29**, 306-311.
54. Rodriguez,H., Akman,S.A., Holmquist,G.P., Wilson,G.L., Driggers,W.J., LeDoux,S.P., Akman,S.A., Holmquist,G.P., Wilson,G.L., Driggers,W.J., and LeDoux,S.P. (2000) Mapping oxidative DNA damage using ligation-mediated polymerase chain reaction technology. *Methods (Duluth)*, **22**, 148-156.

55. Comporti,M. (1989) Three models of free radical-induced cell injury. [Review] [356 refs]. *Chemico-Biological Interactions*, **72**, 1-56.
56. Yu,T.W., Anderson,D., and Anderson,D. (1997) Reactive oxygen species-induced DNA damage and its modification: a chemical investigation. *Mutat.Res.*, **379**, 201-210.
57. Evans,M.D., Cooke,M.S., Podmore,I.D., Zheng,Q., Herbert,K.E., Lunec,J., Cooke,M.S., Podmore,I.D., Zheng,Q., Herbert,K.E., and Lunec,J. (1999) Discrepancies in the measurement of UVC-induced 8-oxo-2'-deoxyguanosine: implications for the analysis of oxidative DNA damage. *Biochemical & Biophysical Research Communications*, **259**, 374-378.
58. Poulsen,H.E., Loft,S., and Weimann,A. (2000) Urinary measurement of 8-oxodG. In Lunec,J. and Griffiths,H.R. (eds.) *Measuring in vivo oxidative damage: A practical approach.*, pp 69-80.
59. Williams,G.M., Jeffrey,A.M., and Jeffrey,A.M. (2000) Oxidative DNA damage: endogenous and chemically induced. [Review] [108 refs]. *Regulatory Toxicology & Pharmacology*, **32**, 283-292.
60. Slupphaug,G., Kavli,B., Krokan,H.E., Kavli,B., and Krokan,H.E. (2003) The interacting pathways for prevention and repair of oxidative DNA damage. [Review] [148 refs]. *Mutat.Res.*, **531**, 231-251.
61. Timbrell,J. (2000) Toxic response to foreign compounds. In Timbrell,J. (ed.) *Principles of biochemical toxicology*. Taylor Francis, pp 175-258.
62. Kretzschmar,M. (1996) Regulation of hepatic glutathione metabolism and its role in hepatotoxicity. [Review] [85 refs]. *Experimental & Toxicologic Pathology*, **48**, 439-446.
63. Stryer,L. (1988) Oxidative Phosphorylation. In Stryer,L. (ed.) *Biochemistry.*, pp 397-426.
64. Anderson,M.E. (1998) Glutathione: an overview of biosynthesis and modulation. [Review] [88 refs]. *Chemico-Biological Interactions*, **111-112**, 1-14.
65. Ristoff,E., Larsson,A., and Larsson,A. (1998) Patients with genetic defects in the gamma-glutamyl cycle. [Review] [36 refs]. *Chemico-Biological Interactions*, **111-112**, 113-121.
66. Orrenius,S., Ormstad,K., Thor,H., Jewell,S.A., Ormstad,K., Thor,H., and Jewell,S.A. (1983) Turnover and functions of glutathione studied with isolated hepatic and renal cells. *Federation Proceedings*, **42**, 3177-3188.
67. Arscott,L.D., Veine,D.M., Williams,C.H., Jr., Veine,D.M., and Williams,C.H., Jr. (2000) Mixed disulfide with glutathione as an intermediate in the reaction catalyzed by glutathione reductase from yeast and as a major form of the enzyme in the cell. *Biochemistry*, **39**, 4711-4721.
68. Cao,K., Devanesan,P.D., Ramanathan,R., Gross,M.L., Rogan,E.G., Cavalieri,E.L., Devanesan,P.D., Ramanathan,R., Gross,M.L., Rogan,E.G., and Cavalieri,E.L. (1998) Covalent binding of catechol estrogens to glutathione catalyzed by horseradish peroxidase, lactoperoxidase, or rat liver microsomes. *Chemical Research in Toxicology*, **11**, 917-924.

69. Fliege,R., Metzler,M., and Metzler,M. (2000) Electrophilic properties of patulin. N-acetylcysteine and glutathione adducts. *Chemical Research in Toxicology*, **13**, 373-381.
70. Abou-Donia,M.B. (1995) Metabolism and toxicokinetics of xenobiotics. In Derelanko,M.J. and Hollinger,M.A. (eds.) *CRC Handbook of toxicology*. CRC Press, pp 539-89.
71. Butterworth,M., Lau,S.S., Monks,T.J., Lau,S.S., and Monks,T.J. (1996) 17 beta-estradiol metabolism by hamster hepatic microsomes: comparison of catechol estrogen O-methylation with catechol estrogen oxidation and glutathione conjugation. *Chemical Research in Toxicology*, **9**, 793-799.
72. Armstrong,R.N. (1997) Structure, catalytic mechanism, and evolution of the glutathione transferases. [Review] [121 refs]. *Chemical Research in Toxicology*, **10**, 2-18.
73. Timbrell,J. (2000) Toxic responses to foreign compounds. In Timbrell,J. (ed.) *Principles of biochemical toxicology*. Taylor Francis, pp 175-258.
74. Mosharov,E., Cranford,M.R., Banerjee,R., Cranford,M.R., and Banerjee,R. (2000) The quantitatively important relationship between homocysteine metabolism and glutathione synthesis by the transsulfuration pathway and its regulation by redox changes. *Biochemistry*, **39**, 13005-13011.
75. Dalton,T.P., Shertzer,H.G., Puga,A., Shertzer,H.G., and Puga,A. (1999) Regulation of gene expression by reactive oxygen. [Review] [291 refs]. *Annual Review of Pharmacology & Toxicology*, **39**, 67-101.
76. Lunec,J., Holloway,K., Cooke,M., Evans,M., Holloway,K., Cooke,M., and Evans,M. (2003) Redox-regulation of DNA repair. [Review] [22 refs]. *Biofactors*, **17**, 315-324.
77. Gius,D., Botero,A., Shah,S., and Curry,H.A. (1999) Intracellular oxidation/reduction status in the regulation of transcription factors NF-kB and AP-1. *Toxicol.Lett.*, **106**, 93-106.
78. Liu,H., Colavitti,R., Rovira,I.I., Finkel,T., Colavitti,R., Rovira,I., I, and Finkel,T. (2005) Redox-dependent transcriptional regulation. [Review] [65 refs]. *Circulation Research*, **97**, 967-974.
79. Thannickal,V.J. and Fanburg,B.L. (2000) Reactive oxygen species in cell signalling. *American Journal of Physiology - Lung Cellular & Molecular Physiology*, **279**, L1005-L1028.
80. Zhang,D.D. (2006) Mechanistic studies of the Nrf2-Keap1 signaling pathway. [Review] [73 refs]. *Drug Metabolism Reviews*, **38**, 769-789.
81. Nerland,D.E. (2007) The antioxidant/electrophile response element motif. [Review] [74 refs]. *Drug Metabolism Reviews*, **39**, 235-248.
82. Rushmore,T.H., Morton,M.R., Pickett,C.B., Morton,M.R., and Pickett,C.B. (1991) The antioxidant responsive element. Activation by oxidative stress and identification of the DNA consensus sequence required for functional activity. *Journal of Biological Chemistry*, **266**, 11632-11639.
83. Nguyen,T., Sherratt,P.J., Pickett,C.B., Sherratt,P.J., and Pickett,C.B. (2003) Regulatory mechanisms controlling gene expression mediated by the antioxidant response element. [Review] [105 refs]. *Annual Review of Pharmacology & Toxicology*, **43**, 233-260.

84. Kang,K.W., Lee,S.J., Kim,S.G., Lee,S.J., and Kim,S.G. (2005) Molecular mechanism of nrf2 activation by oxidative stress. [Review] [65 refs]. *Antioxidants & Redox Signaling*, **7**, 1664-1673.
85. Lyakhovich,V.V., Vavilin,V.A., Zenkov,N.K., Menshchikova,E.B., Vavilin,V.A., Zenkov,N.K., and Menshchikova,E.B. (2006) Active defense under oxidative stress. The antioxidant responsive element. [Review] [118 refs]. *Biochemistry-Russia*, **71**, 962-974.
86. He,C.H., Gong,P., Hu,B., Stewart,D., Choi,M.E., Choi,A.M., Alam,J., Gong,P., Hu,B., Stewart,D., Choi,M.E., Choi,A.M., and Alam,J. (2001) Identification of activating transcription factor 4 (ATF4) as an Nrf2-interacting protein. Implication for heme oxygenase-1 gene regulation. *Journal of Biological Chemistry*, **276**, 20858-20865.
87. Numazawa,S., Ishikawa,M., Yoshida,A., Tanaka,S., Yoshida,T., Ishikawa,M., Yoshida,A., Tanaka,S., and Yoshida,T. (2003) Atypical protein kinase C mediates activation of NF-E2-related factor 2 in response to oxidative stress. *American Journal of Physiology - Cell Physiology*, **285**, C334-C342.
88. Vollrath,V., Wielandt,A.M., Iruretagoyena,M., Chianale,J., Wielandt,A.M., Iruretagoyena,M., and Chianale,J. (2006) Role of Nrf2 in the regulation of the Mrp2 (ABCC2) gene. *Biochemical Journal*, **395**, 599-609.
89. Nguyen,T., Sherratt,P.J., Pickett,C.B., Sherratt,P.J., and Pickett,C.B. (2003) Regulatory mechanisms controlling gene expression mediated by the antioxidant response element. [Review] [105 refs]. *Annual Review of Pharmacology & Toxicology*, **43**, 233-260.
90. Scheel,J., Von Brevern,M.C., Horlein,A., Fischer,A., Schneider,A., Bach,A., Von Brevern,M., Horlein,A., Fischer,A., Schneider,A., and Bach,A. (2002) Yellow pages to the transcriptome. [Review] [101 refs]. *Pharmacogenomics*, **3**, 791-807.
91. Burczynski,M.E., McMillian,M., Ciervo,J., Li,L., Parker,J.B., Dunn,R.T., Hicken,S., Farr,S., Johnson,M.D., McMillian,M., Ciervo,J., Li,L., Parker,J.B., Dunn,R.T., Hicken,S., Farr,S., and Johnson,M.D. (2000) Toxicogenomics-based discrimination of toxic mechanism in HepG2 human hepatoma cells.[see comment]. *Toxicological Sciences*, **58**, 399-415.
92. Marin-Kuan,M., Nestler,S., Verguet,C., Bezencon,C., Piguet,D., Mansourian,R., Holzwarth,J., Grigorov,M., Delatour,T., Mantle,P., Cavin,C., Schilter,B., Nestler,S., Verguet,C., Bezencon,C., Piguet,D., Mansourian,R., Holzwarth,J., Grigorov,M., Delatour,T., Mantle,P., Cavin,C., and Schilter,B. (2006) A toxicogenomics approach to identify new plausible epigenetic mechanisms of ochratoxin a carcinogenicity in rat. *Toxicological Sciences*, **89**, 120-134.
93. Sarrif,A., van Delft,J.H., van Schooten,F.J., Gant,T.W., Elliott,B.M., van Ravenzwaay,B., van Steeg,H., Vrijhof,H., Delft Joost,H.M., van Schooten,F., Gant,T.W., Elliott,B.M., van Ravenzwaay,B., van Steeg,H., and Vrijhof,H. (2005) Toxicogenomics in genetic toxicology and hazard determination: introduction and overview. *Mutat.Res.*, **575**, 1-3.
94. Merrill,C.L., Ni,H., Yoon,L.W., Tirmenstein,M.A., Narayanan,P., Benavides,G.R., Easton,M.J., Creech,D.R., Hu,C.X., McFarland,D.C., Hahn,L.M., Thomas,H.C., Morgan,K.T., Ni,H., Yoon,L.W., Tirmenstein,M.A., Narayanan,P., Benavides,G.R., Easton,M.J., Creech,D.R., Hu,C., X, McFarland,D.C., Hahn,L.M., Thomas,H.C., and Morgan,K.T. (2002) Etomoxir-induced oxidative stress in HepG2 cells detected by

differential gene expression is confirmed biochemically. *Toxicological Sciences*, **68**, 93-101.

95. Morgan, K.T., Ni, H., Brown, H.R., Yoon, L., Qualls, C.W., Jr., Crosby, L.M., Reynolds, R., Gaskill, B., Anderson, S.P., Kepler, T.B., Brainard, T., Liv, N., Easton, M., Merrill, C., Creech, D., Sprenger, D., Conner, G., Johnson, P.R., Fox, T., Sartor, M., Richard, E., Kuruvilla, S., Casey, W., Benavides, G., Ni, H., Brown, H.R., Yoon, L., Qualls, C.W., Jr., Crosby, L.M., Reynolds, R., Gaskill, B., Anderson, S.P., Kepler, T.B., Brainard, T., Liv, N., Easton, M., Merrill, C., Creech, D., Sprenger, D., Conner, G., Johnson, P.R., Fox, T., Sartor, M., Richard, E., Kuruvilla, S., Casey, W., and Benavides, G. (2002) Application of cDNA microarray technology to in vitro toxicology and the selection of genes for a real-time RT-PCR-based screen for oxidative stress in Hep-G2 cells. *Toxicologic Pathology*, **30**, 435-451.
96. Schena, M., Shalon, D., Davis, R.W., Brown, P.O., Shalon, D., Davis, R.W., and Brown, P.O. (1995) Quantitative monitoring of gene expression patterns with a complementary DNA microarray. [see comment]. *Science*, **270**, 467-470.
97. DeRisi, J., Penland, L., Brown, P.O., Bittner, M.L., Meltzer, P.S., Ray, M., Chen, Y., Su, Y.A., Trent, J.M., Penland, L., Brown, P.O., Bittner, M.L., Meltzer, P.S., Ray, M., Chen, Y., Su, Y.A., and Trent, J.M. (1996) Use of a cDNA microarray to analyse gene expression patterns in human cancer. [see comment]. *Nature Genetics*, **14**, 457-460.
98. Duggan, D.J., Bittner, M., Chen, Y., Meltzer, P., Trent, J.M., Bittner, M., Chen, Y., Meltzer, P., and Trent, J.M. (1999) Expression profiling using cDNA microarrays. [Review] [33 refs]. *Nature Genetics*, **21**, 10-14.
99. Ross, D., Thor, H., Threadgill, M.D., Sandy, M.S., Smith, M.T., Moldeus, P., Orrenius, S., Thor, H., Threadgill, M.D., Sandy, M.S., Smith, M.T., Moldeus, P., and Orrenius, S. (1986) The role of oxidative processes in the cytotoxicity of substituted 1,4-naphthoquinones in isolated hepatocytes. *Archives of Biochemistry & Biophysics*, **248**, 460-466.
100. Henry, T.R., Wallace, K.B., and Wallace, K.B. (1995) The role of redox cycling versus arylation in quinone-induced mitochondrial dysfunction: a mechanistic approach in classifying reactive toxicants. *Sar & Qsar in Environmental Research*, **4**, 97-108.
101. Henry, T.R., Wallace, K.B., and Wallace, K.B. (1995) Differential mechanisms of induction of the mitochondrial permeability transition by quinones of varying chemical reactivities. *Toxicology & Applied Pharmacology*, **134**, 195-203.
102. Thor, H., Mirabelli, F., Salis, A., Cohen, G.M., Bellomo, G., Orrenius, S., Mirabelli, F., Salis, A., Cohen, G.M., Bellomo, G., and Orrenius, S. (1988) Alterations in hepatocyte cytoskeleton caused by redox cycling and alkylating quinones. *Archives of Biochemistry & Biophysics*, **266**, 397-407.
103. D'Odorico, A., Sturniolo, G.C., Bilton, R.F., Morris, A.I., Gilmore, I.T., Naccarato, R., Sturniolo, G.C., Bilton, R.F., Morris, A., I, Gilmore, I.T., and Naccarato, R. (1997) Quinone-induced DNA single strand breaks in a human colon carcinoma cell line. *Carcinogenesis*, **18**, 43-46.
104. Morgan, W.A., Hartley, J.A., Cohen, G.M., Hartley, J.A., and Cohen, G.M. (1992) Quinone-induced DNA single strand breaks in rat hepatocytes and human chronic myelogenous leukaemic K562 cells. *Biochem. Pharmacol.*, **44**, 215-221.

105. Morgan,W.A. (1995) DNA single-strand breakage in mammalian cells induced by redox cycling quinones in the absence of oxidative stress. *Journal of Biochemical Toxicology*, **10**, 227-232.
106. Seglen,P.O. (1976) Preparation of isolated rat liver cells. [Review] [189 refs]. *Methods in Cell Biology*, **13**, 29-83.
107. C.Napoli, C.Lemieux, and R.Jorgensen (1990) Introduction of a Chimeric Chalcone Synthase Gene into Petunia Results in Reversible Co-Suppression of Homologous Genes in trans. *THE PLANT CELL*, **2**, 279-289.
108. Fire,A., Xu,S., Montgomery,M.K., Kostas,S.A., Driver,S.E., Mello,C.C., Xu,S., Montgomery,M.K., Kostas,S.A., Driver,S.E., and Mello,C.C. (1998) Potent and specific genetic interference by double-stranded RNA in *Caenorhabditis elegans*. [see comment]. *Nature*, **391**, 806-811.
109. Ketting,R.F., Plasterk,R.H., and Plasterk,R.H. (2000) A genetic link between co-suppression and RNA interference in *C. elegans*. *Nature*, **404**, 296-298.
110. Svoboda,P. (2007) Off-targeting and other non-specific effects of RNAi experiments in mammalian cells. [Review] [75 refs]. *Current Opinion in Molecular Therapeutics*, **9**, 248-257.
111. Martineau,H.M., Pyrah,I.T., and Pyrah,I.T. (2007) Review of the application of RNA interference technology in the pharmaceutical industry. [Review] [82 refs]. *Toxicologic Pathology*, **35**, 327-336.
112. Zou,H., Li,Y., Liu,X., Wang,X., Li,Y., Liu,X., and Wang,X. (1999) An APAF-1.cytochrome c multimeric complex is a functional apoptosome that activates procaspase-9. *Journal of Biological Chemistry*, **274**, 11549-11556.
113. Vardhanabhuti,S., Blakemore,S.J., Clark,S.M., Ghosh,S., Stephens,R.J., Rajagopalan,D., Blakemore,S.J., Clark,S.M., Ghosh,S., Stephens,R.J., and Rajagopalan,D. (2006) A comparison of statistical tests for detecting differential expression using Affymetrix oligonucleotide microarrays. *Omics a Journal of Integrative Biology*, **10**, 555-566.
114. Rajagopalan,D. (2003) A comparison of statistical methods for analysis of high density oligonucleotide array data. *Bioinformatics*, **19**, 1469-1476.
115. Hosack,D.A., Dennis,G., Jr., Sherman,B.T., Lane,H.C., Lempicki,R.A., Dennis,G., Jr., Sherman,B.T., Lane,H.C., and Lempicki,R.A. (2003) Identifying biological themes within lists of genes with EASE. *Genome Biology*, **4**, R70.
116. Ishigami,T., Uzawa,K., Higo,M., Nomura,H., Saito,K., Kato,Y., Nakashima,D., Shiiba,M., Bukawa,H., Yokoe,H., Kawata,T., Ito,H., Tanzawa,H., Uzawa,K., Higo,M., Nomura,H., Saito,K., Kato,Y., Nakashima,D., Shiiba,M., Bukawa,H., Yokoe,H., Kawata,T., Ito,H., and Tanzawa,H. (2007) Genes and molecular pathways related to radioresistance of oral squamous cell carcinoma cells. *Int.J.Cancer*, **120**, 2262-2270.
117. Mayburd,A.L., Martlinez,A., Sackett,D., Liu,H., Shih,J., Tauler,J., Avis,I., Mulshine,J.L., Martlinez,A., Sackett,D., Liu,H., Shih,J., Tauler,J., Avis,I., and Mulshine,J.L. (2006) Ingenuity network-assisted transcription profiling: Identification of a new pharmacologic mechanism for MK886. *Clinical Cancer Research*, **12**, 1820-1827.

118. Stone,V., Coleman,R., Chipman,J.K., Coleman,R., and Chipman,J.K. (1996) Comparison of the effects of redox cycling and arylating quinones on hepatobiliary function and glutathione homeostasis in rat hepatocyte couplets. *Toxicology & Applied Pharmacology*, **138**, 195-200.
119. Schmieder,P.K., Tapper,M.A., Kolanczyk,R.C., Hammermeister,D.E., Sheedy,B.R., Denny,J.S., Tapper,M.A., Kolanczyk,R.C., Hammermeister,D.E., Sheedy,B.R., and Denny,J.S. (2003) Discriminating redox cycling and arylation pathways of reactive chemical toxicity in trout hepatocytes. *Toxicological Sciences*, **72**, 66-76.
120. Ollinger,K., Buffinton,G.D., Ernster,L., Cadenas,E., Buffinton,G.D., Ernster,L., and Cadenas,E. (1990) Effect of superoxide dismutase on the autoxidation of substituted hydro- and semi-naphthoquinones. *Chemico-Biological Interactions*, **73**, 53-76.
121. Seung,S.A., Lee,J.Y., Lee,M.Y., Park,J.S., Chung,J.H., Lee,J.Y., Lee,M.Y., Park,J.S., and Chung,J.H. (1998) The relative importance of oxidative stress versus arylation in the mechanism of quinone-induced cytotoxicity to platelets. *Chemico-Biological Interactions*, **113**, 133-144.
122. Markovits,J., Wang,Z., Carr,B.I., Sun,T.P., Mintz,P., Le Bret,M., Wu,C.W., Wu,F.Y., Wang,Z., Carr,B., I, Sun,T.P., Mintz,P., Le Bret,M., Wu,C., and Wu,F.Y.H. (2003) Differential effects of two growth inhibitory K vitamin analogs on cell cycle regulating proteins in human hepatoma cells. *Life Sci.*, **72**, 2769-2784.
123. Adams,J., Pepping,J., and Pepping,J. (2005) Vitamin K in the treatment and prevention of osteoporosis and arterial calcification. [Review] [66 refs]. *American Journal of Health-System Pharmacy*, **62**, 1574-1581.
124. Ross,D., Thor,H., Threadgill,M.D., Sandy,M.S., Smith,M.T., Moldeus,P., Orrenius,S., Thor,H., Threadgill,M.D., Sandy,M.S., Smith,M.T., Moldeus,P., and Orrenius,S. (1986) The role of oxidative processes in the cytotoxicity of substituted 1,4-naphthoquinones in isolated hepatocytes. *Archives of Biochemistry & Biophysics*, **248**, 460-466.
125. Daba,M.H., Abdel-Rahman,M.S., and Abdel-Rahman,M.S. (1998) Hepatoprotective activity of thymoquinone in isolated rat hepatocytes. *Toxicol.Lett.*, **95**, 23-29.
126. Badary,O.A., Taha,R.A., Gamal el-Din,A.M., Abdel-Wahab,M.H., Taha,R.A., Gamal el-Din,A.M., and Abdel-Wahab,M.H. (2003) Thymoquinone is a potent superoxide anion scavenger. *Drug Chem.Toxicol.*, **26**, 87-98.
127. Nagi,M.N., Mansour,M.A., and Mansour,M.A. (2000) Protective effect of thymoquinone against doxorubicin-induced cardiotoxicity in rats: a possible mechanism of protection. *Pharmacol.Res.*, **41**, 283-289.
128. Al Shabanah,O.A., Badary,O.A., Nagi,M.N., al Gharably,N.M., Al Rikabi,A.C., Al Bekairi,A.M., Badary,O.A., Nagi,M.N., al Gharably,N.M., Al Rikabi,A.C., and Al Bekairi,A.M. (1998) Thymoquinone protects against doxorubicin-induced cardiotoxicity without compromising its antitumor activity. *J.Exp.Clin.Cancer Res.*, **17**, 193-198.
129. Khalife,K.H., Lupidi,G., and Lupidi,G. (2007) Nonenzymatic reduction of thymoquinone in physiological conditions. *Free Radic.Res.*, **41**, 153-161.

130. Worthen,D.R., Ghosheh,O.A., Crooks,P.A., Ghosheh,O.A., and Crooks,P.A. (1998) The in vitro anti-tumor activity of some crude and purified components of blackseed, *Nigella sativa* L. *Anticancer Res.*, **18**, 1527-1532.
131. Rooney,S., Ryan,M.F., and Ryan,M.F. (2005) Modes of action of alpha-hederin and thymoquinone, active constituents of *Nigella sativa*, against HEP-2 cancer cells. *Anticancer Res.*, **25**, 4255-4259.
132. Rooney,S., Ryan,M.F., and Ryan,M.F. (2005) Effects of alpha-hederin and thymoquinone, constituents of *Nigella sativa*, on human cancer cell lines. *Anticancer Res.*, **25**, 2199-2204.
133. Ivankovic,S., Stojkovic,R., Jukic,M., Milos,M., Milos,M., Jurin,M., Stojkovic,R., Jukic,M., Milos,M., Milos,M., and Jurin,M. (2006) The antitumor activity of thymoquinone and thymohydroquinone in vitro and in vivo. *Exp.Oncol.*, **28**, 220-224.
134. Baker,T.K., Carfagna,M.A., Gao,H., Dow,E.R., Li,Q., Searfoss,G.H., Ryan,T.P., Carfagna,M.A., Gao,H., Dow,E.R., Li,Q., Searfoss,G.H., and Ryan,T.P. (2001) Temporal gene expression analysis of monolayer cultured rat hepatocytes. *Chemical Research in Toxicology*, **14**, 1218-1231.
135. Munday,R., Smith,B.L., Munday,C.M., Smith,B.L., and Munday,C.M. (2001) Effects of modulation of tissue activities of DT-diaphorase on the toxicity of 2,3-dimethyl-1,4-naphthoquinone to rats. *Chemico-Biological Interactions*, **134**, 87-100.
136. Nagi,M.N., Alam,K., Badary,O.A., Al Shabanah,O.A., Al Sawaf,H.A., Al Bekairi,A.M., Alam,K., Badary,O.A., Al Shabanah,O.A., Al Sawaf,H.A., and Al Bekairi,A.M. (1999) Thymoquinone protects against carbon tetrachloride hepatotoxicity in mice via an antioxidant mechanism. *Biochem.Mol.Biol.Int.*, **47**, 153-159.
137. Kato,Y., Shimazu,M., Kondo,M., Uchida,K., Kumamoto,Y., Wakabayashi,G., Kitajima,M., Suematsu,M., Shimazu,M., Kondo,M., Uchida,K., Kumamoto,Y., Wakabayashi,G., Kitajima,M., and Suematsu,M. (2003) Bilirubin rinse: A simple protectant against the rat liver graft injury mimicking heme oxygenase-1 preconditioning.[see comment]. *Hepatology*, **38**, 364-373.
138. Alam,J., Cook,J.L., and Cook,J.L. (2003) Transcriptional regulation of the heme oxygenase-1 gene via the stress response element pathway. [Review] [96 refs]. *Current Pharmaceutical Design*, **9**, 2499-2511.
139. Ohlmann,A., Giffhorn-Katz,S., Becker,I., Katz,N., Immenschuh,S., Giffhorn-Katz,S., Becker,I., Katz,N., and Immenschuh,S. (2003) Regulation of heme oxygenase-1 gene expression by anoxia and reoxygenation in primary rat hepatocyte cultures. *Experimental Biology & Medicine*, **228**, 584-589.
140. Desaint,S., Luriau,S., Aude,J.C., Rousselet,G., Toledano,M.B., Luriau,S., Aude,J., Rousselet,G., and Toledano,M.B. (2004) Mammalian antioxidant defenses are not inducible by H₂O₂. *Journal of Biological Chemistry*, **279**, 31157-31163.
141. Liebermann,D.A., Hoffman,B., and Hoffman,B. (2002) Myeloid differentiation (MyD)/growth arrest DNA damage (GADD) genes in tumor suppression, immunity and inflammation. [Review] [226 refs]. *Leukemia*, **16**, 527-541.

142. Shiloh, Y. (2001) ATM (ataxia telangiectasia mutated): expanding roles in the DNA damage response and cellular homeostasis. [Review] [26 refs]. *Biochemical Society Transactions*, **29**, 661-666.
143. Norbury, C.J., Zhivotovsky, B., and Zhivotovsky, B. (2004) DNA damage-induced apoptosis. [Review] [137 refs]. *Oncogene*, **23**, 2797-2808.
144. Patton, G.W., Paciga, J.E., Shelley, S.A., Paciga, J.E., and Shelley, S.A. (1997) NR8383 alveolar macrophage toxic growth arrest by hydrogen peroxide is associated with induction of growth-arrest and DNA damage-inducible genes GADD45 and GADD153. *Toxicology & Applied Pharmacology*, **147**, 126-134.
145. Fischer-Nielsen, A., Corcoran, G.B., Poulsen, H.E., Kamendulis, L.M., Loft, S., Corcoran, G.B., Poulsen, H.E., Kamendulis, L.M., and Loft, S. (1995) Menadione-induced DNA fragmentation without 8-oxo-2'-deoxyguanosine formation in isolated rat hepatocytes. *Biochem. Pharmacol.*, **49**, 1469-1474.
146. Shoshani, T., Faerman, A., Mett, I., Zelin, E., Tenne, T., Gorodin, S., Moshel, Y., Elbaz, S., Budanov, A., Chajut, A., Kalinski, H., Kamer, I., Rozen, A., Mor, O., Keshet, E., Leshkowitz, D., Einat, P., Skaliter, R., Feinstein, E., Faerman, A., Mett, I., Zelin, E., Tenne, T., Gorodin, S., Moshel, Y., Elbaz, S., Budanov, A., Chajut, A., Kalinski, H., Kamer, I., Rozen, A., Mor, O., Keshet, E., Leshkowitz, D., Einat, P., Skaliter, R., and Feinstein, E. (2002) Identification of a novel hypoxia-inducible factor 1-responsive gene, RTP801, involved in apoptosis. *Molecular & Cellular Biology*, **22**, 2283-2293.
147. Papeleu, P., Loyer, P., Vanhaecke, T., Henkens, T., Elaut, G., and Rogiers, V. (2004) Proliferation of epidermal growth factor-stimulated hepatocytes in a hormonally defined serum-free medium. *ATLA*, **32**, 57-64.
148. Crichton, R.R., Wilmet, S., Legssyer, R., Ward, R.J., Wilmet, S., Legssyer, R., and Ward, R.J. (2002) Molecular and cellular mechanisms of iron homeostasis and toxicity in mammalian cells. [Review] [40 refs]. *Journal of Inorganic Biochemistry*, **91**, 9-18.
149. Pantopoulos, K. (2004) Iron metabolism and the IRE/IRP regulatory system: an update. [Review] [76 refs]. *Annals of the New York Academy of Sciences*, **1012**, 1-13.
150. Mueller, S. (2005) Iron regulatory protein 1 as a sensor of reactive oxygen species. *Biofactors*, **24**, 171-181.
151. Kotamraju, S., Chitambar, C.R., Kalivendi, S.V., Joseph, J., Kalyanaraman, B., Chitambar, C.R., Kalivendi, S., V, Joseph, J., and Kalyanaraman, B. (2002) Transferrin receptor-dependent iron uptake is responsible for doxorubicin-mediated apoptosis in endothelial cells: role of oxidant-induced iron signaling in apoptosis. *Journal of Biological Chemistry*, **277**, 17179-17187.
152. Pantopoulos, K., Hentze, M.W., and Hentze, M.W. (1995) Rapid responses to oxidative stress mediated by iron regulatory protein. *EMBO Journal*, **14**, 2917-2924.
153. Gehring, N.H., Hentze, M.W., Pantopoulos, K., Hentze, M.W., and Pantopoulos, K. (1999) Inactivation of both RNA binding and aconitase activities of iron regulatory protein-1 by quinone-induced oxidative stress. *Journal of Biological Chemistry*, **274**, 6219-6225.
154. Tsai, J.C., Liu, L., Zhang, J., Spokes, K.C., Topper, J.N., Aird, W.C., Liu, L., Zhang, J., Spokes, K.C., Topper, J.N., and Aird, W.C. (2001) Epidermal growth factor induces Egr-1

- promoter activity in hepatocytes in vitro and in vivo. *American Journal of Physiology - Gastrointestinal & Liver Physiology*, **281**, G1271-G1278.
155. Wang,C.C., Sharma,G., Draznin,B., Sharma,G., and Draznin,B. (2006) Early growth response gene-1 expression in vascular smooth muscle cells effects of insulin and oxidant stress. *American Journal of Hypertension*, **19**, 366-372.
 156. Nair,V.D., Yuen,T., Olanow,C.W., Sealfon,S.C., Yuen,T., Olanow,C.W., and Sealfon,S.C. (2004) Early single cell bifurcation of pro- and antiapoptotic states during oxidative stress. *Journal of Biological Chemistry*, **279**, 27494-27501.
 157. Karin,M., Liu,Z., Zandi,E., Liu,Z., and Zandi,E. (1997) AP-1 function and regulation. [Review] [83 refs]. *Current Opinion in Cell Biology*, **9**, 240-246.
 158. Shaulian,E., Karin,M., and Karin,M. (2002) AP-1 as a regulator of cell life and death. [Review] [98 refs]. *Nature Cell Biology*, **4**, E131-E136.
 159. Leaner,V.D., Donniger,H., Ellis,C.A., Clark,G.J., Birrer,M.J., Donniger,H., Ellis,C.A., Clark,G.J., and Birrer,M.J. (2005) p75-Ras-GRF1 is a c-Jun/AP-1 target protein: its up regulation results in increased Ras activity and is necessary for c-Jun-induced nonadherent growth of Rat1a cells. *Molecular & Cellular Biology*, **25**, 3324-3337.
 160. Venugopal,R., Jaiswal,A.K., and Jaiswal,A.K. (1996) Nrf1 and Nrf2 positively and c-Fos and Fra1 negatively regulate the human antioxidant response element-mediated expression of NAD(P)H:quinone oxidoreductase1 gene. *Proceedings of the National Academy of Sciences of the United States of America*, **93**, 14960-14965.
 161. Kang,K.W., Cho,I.J., Lee,C.H., Kim,S.G., Cho,I.J., Lee,C.H., and Kim,S.G. (2003) Essential role of phosphatidylinositol 3-kinase-dependent CCAAT/enhancer binding protein beta activation in the induction of glutathione S-transferase by oltipraz. *Journal of the National Cancer Institute*, **95**, 53-66.
 162. Malorni,W., Iosi,F., Mirabelli,F., Bellomo,G., Iosi,F., Mirabelli,F., and Bellomo,G. (1991) Cytoskeleton as a target in menadione-induced oxidative stress in cultured mammalian cells: alterations underlying surface bleb formation. *Chemico-Biological Interactions*, **80**, 217-236.
 163. Xu,H., Tian,W., Lindsley,J.N., Oyama,T.T., Capasso,J.M., Rivard,C.J., Cohen,H.T., Bagnasco,S.M., Anderson,S., Cohen,D.M., Tian,W., Lindsley,J.N., Oyama,T.T., Capasso,J.M., Rivard,C.J., Cohen,H.T., Bagnasco,S.M., Anderson,S., and Cohen,D.M. (2005) EphA2: expression in the renal medulla and regulation by hypertonicity and urea stress in vitro and in vivo. *American Journal of Physiology - Renal Physiology*, **288**, F855-F866.
 164. Lu,M., Miller,K.D., Gokmen-Polar,Y., Jeng,M.H., Kinch,M.S., Miller,K.D., Gokmen-Polar,Y., Jeng,M., and Kinch,M.S. (2003) EphA2 overexpression decreases estrogen dependence and tamoxifen sensitivity. *Cancer Research*, **63**, 3425-3429.
 165. Walker-Daniels,J., Hess,A.R., Hendrix,M.J., Kinch,M.S., Hess,A.R., Hendrix Mary,J.C., and Kinch,M.S. (2003) Differential regulation of EphA2 in normal and malignant cells. [Review] [74 refs]. *American Journal of Pathology*, **162**, 1037-1042.

166. Vihanto,M.M., Plock,J., Erni,D., Frey,B.M., Frey,F.J., Huynh-Do,U., Plock,J., Erni,D., Frey,B.M., Frey,F.J., and Huynh-Do,U. (2005) Hypoxia up-regulates expression of Eph receptors and ephrins in mouse skin. *FASEB Journal*, **19**, 1689-1691.
167. Ientile,R., Caccamo,D., Marciano,M.C., Curro,M., Mannucci,C., Campisi,A., Calapai,G., Caccamo,D., Marciano,M.C., Curro,M., Mannucci,C., Campisi,A., and Calapai,G. (2004) Transglutaminase activity and transglutaminase mRNA transcripts in gerbil brain ischemia. *Neuroscience Letters*, **363**, 173-177.
168. Campisi,A., Caccamo,D., Li,V.G., Curro,M., Parisi,G., Avola,R., Vanella,A., Ientile,R., Caccamo,D., Li,V.G., Curro,M., Parisi,G., Avola,R., Vanella,A., and Ientile,R. (2004) Glutamate-evoked redox state alterations are involved in tissue transglutaminase upregulation in primary astrocyte cultures. *FEBS Letters*, **578**, 80-84.
169. Bornhauser,B.C., Johansson,C., Lindholm,D., Johansson,C., and Lindholm,D. (2003) Functional activities and cellular localization of the ezrin, radixin, moesin (ERM) and RING zinc finger domains in MIR. *FEBS Letters*, **553**, 195-199.
170. Nagano,K., Bornhauser,B.C., Warnasuriya,G., Entwistle,A., Cramer,R., Lindholm,D., Naaby-Hansen,S., Bornhauser,B.C., Warnasuriya,G., Entwistle,A., Cramer,R., Lindholm,D., and Naaby-Hansen,S. (2006) PDGF regulates the actin cytoskeleton through hnRNP-K-mediated activation of the ubiquitin E3-ligase MIR. *EMBO Journal*, **25**, 1871-1882.
171. Olsson,P.A., Korhonen,L., Mercer,E.A., Lindholm,D., Korhonen,L., Mercer,E.A., and Lindholm,D. (1999) MIR is a novel ERM-like protein that interacts with myosin regulatory light chain and inhibits neurite outgrowth. *Journal of Biological Chemistry*, **274**, 36288-36292.
172. Nakagami,K., Uchida,T., Ohwada,S., Koibuchi,Y., Suda,Y., Sekine,T., Morishita,Y., Uchida,T., Ohwada,S., Koibuchi,Y., Suda,Y., Sekine,T., and Morishita,Y. (1999) Increased choline kinase activity and elevated phosphocholine levels in human colon cancer. *Japanese Journal of Cancer Research*, **90**, 419-424.
173. Liao,H., Aoyama,C., Ishidate,K., Teraoka,H., Aoyama,C., Ishidate,K., and Teraoka,H. (2006) Deletion and alanine mutation analyses for the formation of active homo- or hetero-dimer complexes of mouse choline kinase-alpha and -beta. *Biochim.Biophys.Acta*, **1761**, 111-120.
174. Janardhan,S., Srivani,P., Sastry,G.N., Srivani,P., and Sastry,G.N. (2006) Choline kinase: an important target for cancer. [Review] [322 refs]. *Current Medicinal Chemistry*, **13**, 1169-1186.
175. Gallego-Ortega,D., Ramirez,D.M., Gutierrez,R., Ramos,M.A., Sarmentero,J., Cejas,P., Nistal,M., Gonzalez,B.M., Lacal,J.C., Ramirez,D.M.A., Gutierrez,R., Ramos,M.A., Sarmentero,J., Cejas,P., Nistal,M., Gonzalez,B.M., and Lacal,J.C. (2006) Generation and characterization of monoclonal antibodies against choline kinase alpha and their potential use as diagnostic tools in cancer. *Int.J.Oncol.*, **29**, 335-340.
176. Atta,M.G., Dahl,S.C., Kwon,H.M., Handler,J.S., Dahl,S.C., Kwon,H.M., and Handler,J.S. (1999) Tyrosine kinase inhibitors and immunosuppressants perturb the myo-inositol but not the betaine cotransporter in isotonic and hypertonic MDCK cells. *Kidney International*, **55**, 956-962.

177. Warskulat,U., Reinen,A., Grether-Beck,S., Krutmann,J., Haussinger,D., Reinen,A., Grether-Beck,S., Krutmann,J., and Haussinger,D. (2004) The osmolyte strategy of normal human keratinocytes in maintaining cell homeostasis. *Journal of Investigative Dermatology*, **123**, 516-521.
178. Denkert,C., Warskulat,U., Hensel,F., Haussinger,D., Warskulat,U., Hensel,F., and Haussinger,D. (1998) Osmolyte strategy in human monocytes and macrophages: involvement of p38MAPK in hyperosmotic induction of betaine and myoinositol transporters. *Archives of Biochemistry & Biophysics*, **354**, 172-180.
179. Reinehr,R., Haussinger,D., and Haussinger,D. (2006) Hyperosmotic activation of the CD95 death receptor system. [Review] [42 refs]. *Acta Physiologica*, **187**, 199-203.
180. Sugden,M.C., Bulmer,K., Holness,M.J., Bulmer,K., and Holness,M.J. (2001) Fuel-sensing mechanisms integrating lipid and carbohydrate utilization. *Biochemical Society Transactions*, **29**, 272-278.
181. Holness,M.J., Sugden,M.C., and Sugden,M.C. (2003) Regulation of pyruvate dehydrogenase complex activity by reversible phosphorylation. [Review] [78 refs]. *Biochemical Society Transactions*, **31**, 1143-1151.
182. Sugden,M.C., Holness,M.J., and Holness,M.J. (2003) Recent advances in mechanisms regulating glucose oxidation at the level of the pyruvate dehydrogenase complex by PDKs. [Review] [72 refs]. *American Journal of Physiology - Endocrinology & Metabolism*, **284**, E855-E862.
183. Ma,K., Zhang,Y., Elam,M.B., Cook,G.A., Park,E.A., Zhang,Y., Elam,M.B., Cook,G.A., and Park,E.A. (2005) Cloning of the rat pyruvate dehydrogenase kinase 4 gene promoter: activation of pyruvate dehydrogenase kinase 4 by the peroxisome proliferator-activated receptor gamma coactivator. *Journal of Biological Chemistry*, **280**, 29525-29532.
184. Fain,J.N. (1971) Effects of menadione and vitamin K 5 on glucose metabolism, respiration, lipolysis, cyclic 3',5'-adenylic acid accumulation, and adenylyl cyclase in white fat cells. *Molecular Pharmacology*, **7**, 465-479.
185. Ueda,K., Arakawa,H., Nakamura,Y., Arakawa,H., and Nakamura,Y. (2003) Dual-specificity phosphatase 5 (DUSP5) as a direct transcriptional target of tumor suppressor p53. *Oncogene*, **22**, 5586-5591.
186. Mandl,M., Slack,D.N., Keyse,S.M., Slack,D.N., and Keyse,S.M. (2005) Specific inactivation and nuclear anchoring of extracellular signal-regulated kinase 2 by the inducible dual-specificity protein phosphatase DUSP5. *Molecular & Cellular Biology*, **25**, 1830-1845.
187. Huynh,H., Ng,C.Y., Ong,C.K., Lim,K.B., Chan,T.W., Ng,C.Y., Ong,C.K., Lim,K.B., and Chan,T.W. (2001) Cloning and characterization of a novel pregnancy-induced growth inhibitor in mammary gland. *Endocrinology*, **142**, 3607-3615.
188. Ong,C.K., Leong,C., Tan,P.H., Van,T., Huynh,H., Leong,C., Tan,P.H., Van,T., and Huynh,H. (2007) The role of 5' untranslated region in translational suppression of OKL38 mRNA in hepatocellular carcinoma. *Oncogene*, **26**, 1155-1165.

189. Li,R., Chen,W., Yanes,R., Lee,S., Berliner,J.A., Chen,W., Yanes,R., Lee,S., and Berliner,J.A. (2007) OKL38 is an oxidative stress response gene stimulated by oxidized phospholipids. *Journal of Lipid Research*, **48**, 709-715.
190. Yan,B., Zemskova,M., Holder,S., Chin,V., Kraft,A., Koskinen,P.J., Lilly,M., Zemskova,M., Holder,S., Chin,V., Kraft,A., Koskinen,P.J., and Lilly,M. (2003) The PIM-2 kinase phosphorylates BAD on serine 112 and reverses BAD-induced cell death. *Journal of Biological Chemistry*, **278**, 45358-45367.
191. Popivanova,B.K., Li,Y.Y., Zheng,H., Omura,K., Fujii,C., Tsuneyama,K., Mukaida,N., Li,Y., Zheng,H., Omura,K., Fujii,C., Tsuneyama,K., and Mukaida,N. (2007) Proto-oncogene, Pim-3 with serine/threonine kinase activity, is aberrantly expressed in human colon cancer cells and can prevent Bad-mediated apoptosis. *Cancer Science*, **98**, 321-328.
192. Fujii,C., Nakamoto,Y., Lu,P., Tsuneyama,K., Popivanova,B.K., Kaneko,S., Mukaida,N., Nakamoto,Y., Lu,P., Tsuneyama,K., Popivanova,B.K., Kaneko,S., and Mukaida,N. (2005) Aberrant expression of serine/threonine kinase Pim-3 in hepatocellular carcinoma development and its role in the proliferation of human hepatoma cell lines. *Int.J.Cancer*, **114**, 209-218.
193. Otrrock,Z.K., Makarem,J.A., Shamseddine,A.I., Makarem,J.A., and Shamseddine,A., I (2007) Vascular endothelial growth factor family of ligands and receptors: review. [Review] [143 refs]. *Blood Cells Molecules & Diseases*, **38**, 258-268.
194. Schafer,G., Cramer,T., Suske,G., Kemmner,W., Wiedenmann,B., Hocker,M., Cramer,T., Suske,G., Kemmner,W., Wiedenmann,B., and Hocker,M. (2003) Oxidative stress regulates vascular endothelial growth factor-A gene transcription through Sp1- and Sp3-dependent activation of two proximal GC-rich promoter elements. *Journal of Biological Chemistry*, **278**, 8190-8198.
195. Sandner,P., Wolf,K., Bergmaier,U., Gess,B., Kurtz,A., Wolf,K., Bergmaier,U., Gess,B., and Kurtz,A. (1997) Induction of VEGF and VEGF receptor gene expression by hypoxia: divergent regulation in vivo and in vitro. *Kidney International*, **51**, 448-453.
196. Abid,M.R., Schoots,I.G., Spokes,K.C., Wu,S.Q., Mawhinney,C., Aird,W.C., Schoots,I.G., Spokes,K.C., Wu,S., Mawhinney,C., and Aird,W.C. (2004) Vascular endothelial growth factor-mediated induction of manganese superoxide dismutase occurs through redox-dependent regulation of forkhead and IkappaB/NF-kappaB. *Journal of Biological Chemistry*, **279**, 44030-44038.
197. Osada,S., Imai,H., Tomita,H., Tokuyama,Y., Okumura,N., Sakashita,F., Nonoka,K., Sugiyama,Y., Imai,H., Tomita,H., Tokuyama,Y., Okumura,N., Sakashita,F., Nonoka,K., and Sugiyama,Y. (2006) Vascular endothelial growth factor protects hepatoma cells against oxidative stress-induced cell death. *Journal of Gastroenterology & Hepatology*, **21**, 988-993.
198. Strelau,J., Bottner,M., Lingor,P., Suter-Crazzolara,C., Galter,D., Jaszai,J., Sullivan,A., Schober,A., Krieglstein,K., Unsicker,K., Bottner,M., Lingor,P., Suter-Crazzolara,C., Galter,D., Jaszai,J., Sullivan,A., Schober,A., Krieglstein,K., and Unsicker,K. (2000) GDF-15/MIC-1 a novel member of the TGF-beta superfamily. [Review] [12 refs]. *Journal of Neural Transmission, Supplementum.*, 273-276.

199. Subramaniam,S., Strelau,J., Unsicker,K., Strelau,J., and Unsicker,K. (2003) Growth differentiation factor-15 prevents low potassium-induced cell death of cerebellar granule neurons by differential regulation of Akt and ERK pathways. *Journal of Biological Chemistry*, **278**, 8904-8912.
200. Zimmers,T.A., Jin,X., Hsiao,E.C., McGrath,S.A., Esquela,A.F., Koniaris,L.G., Jin,X., Hsiao,E.C., McGrath,S.A., Esquela,A.F., and Koniaris,L.G. (2005) Growth differentiation factor-15/macrophage inhibitory cytokine-1 induction after kidney and lung injury. *Shock*, **23**, 543-548.
201. Hsiao,E.C., Koniaris,L.G., Zimmers-Koniaris,T., Sebald,S.M., Huynh,T.V., Lee,S.J., Koniaris,L.G., Zimmers-Koniaris,T., Sebald,S.M., Huynh,T., V, and Lee,S.J. (2000) Characterization of growth-differentiation factor 15, a transforming growth factor beta superfamily member induced following liver injury. *Molecular & Cellular Biology*, **20**, 3742-3751.
202. Strelau,J., Schober,A., Sullivan,A., Schilling,L., Unsicker,K., Schober,A., Sullivan,A., Schilling,L., and Unsicker,K. (2003) Growth/differentiation factor-15 (GDF-15), a novel member of the TGF-beta superfamily, promotes survival of lesioned mesencephalic dopaminergic neurons in vitro and in vivo and is induced in neurons following cortical lesioning. [Review] [13 refs]. *Journal of Neural Transmission, Supplementum.*, 197-203.
203. Strelau,J., Sullivan,A., Bottner,M., Lingor,P., Falkenstein,E., Suter-Crazzolara,C., Galter,D., Jaszai,J., Krieglstein,K., Unsicker,K., Sullivan,A., Bottner,M., Lingor,P., Falkenstein,E., Suter-Crazzolara,C., Galter,D., Jaszai,J., Krieglstein,K., and Unsicker,K. (2000) Growth/differentiation factor-15/macrophage inhibitory cytokine-1 is a novel trophic factor for midbrain dopaminergic neurons in vivo. *Journal of Neuroscience*, **20**, 8597-8603.
204. Zimmers,T.A., Jin,X., Hsiao,E.C., Perez,E.A., Pierce,R.H., Chavin,K.D., Koniaris,L.G., Jin,X., Hsiao,E.C., Perez,E.A., Pierce,R.H., Chavin,K.D., and Koniaris,L.G. (2006) Growth differentiation factor-15: induction in liver injury through p53 and tumor necrosis factor-independent mechanisms. *Journal of Surgical Research*, **130**, 45-51.
205. Zimmers,T.A., Jin,X., Hsiao,E.C., McGrath,S.A., Esquela,A.F., Koniaris,L.G., Jin,X., Hsiao,E.C., McGrath,S.A., Esquela,A.F., and Koniaris,L.G. (2005) Growth differentiation factor-15/macrophage inhibitory cytokine-1 induction after kidney and lung injury. *Shock*, **23**, 543-548.
206. Navarro-Sabate,A., Peralta,C., Calvo,M.N., Manzano,A., Massip-Salcedo,M., Rosello-Catafau,J., Bartrons,R., Peralta,C., Calvo,M.N., Manzano,A., Massip-Salcedo,M., Rosello-Catafau,J., and Bartrons,R. (2006) Mediators of rat ischemic hepatic preconditioning after cold preservation identified by microarray analysis. *Liver Transplantation*, **12**, 1615-1625.
207. Wu,S.Y., Chiang,C.M., and Chiang,C. (2007) The double bromodomain-containing chromatin adaptor Brd4 and transcriptional regulation. [Review] [34 refs]. *Journal of Biological Chemistry*, **282**, 13141-13145.
208. Zhou,M., Xu,X.J., Zhou,H.D., Liu,H.Y., He,J.J., Li,X.L., Peng,C., Xiong,W., Fan,S.Q., Lu,J.H., Ouyang,J., Shen,S.R., Xiang,B., Li,G.Y., Xu,X., Zhou,H., Liu,H., He,J., Li,X., Peng,C., Xiong,W., Fan,S., Lu,J., Ouyang,J., Shen,S., Xiang,B., and Li,G. (2006) BRD2

is one of BRD7-interacting proteins and its over-expression could initiate apoptosis. *Molecular & Cellular Biochemistry*, **292**, 205-212.

209. Crowley,T.E., Kaine,E.M., Yoshida,M., Nandi,A., Wolgemuth,D.J., Kaine,E.M., Yoshida,M., Nandi,A., and Wolgemuth,D.J. (2002) Reproductive cycle regulation of nuclear import, euchromatic localization, and association with components of Pol II mediator of a mammalian double-bromodomain protein. *Molecular Endocrinology*, **16**, 1727-1737.
210. Johnson,B.A., Geha,M., Blackwell,T.K., Geha,M., and Blackwell,T.K. (2000) Similar but distinct effects of the tristetraprolin/TIS11 immediate-early proteins on cell survival. *Oncogene*, **19**, 1657-1664.
211. Johnson,B.A., Blackwell,T.K., and Blackwell,T.K. (2002) Multiple tristetraprolin sequence domains required to induce apoptosis and modulate responses to TNFalpha through distinct pathways. *Oncogene*, **21**, 4237-4246.
212. Foehr,E.D., Lorente,G., Vincent,V., Nikolich,K., Urfer,R., Lorente,G., Vincent,V., Nikolich,K., and Urfer,R. (2005) FAS associated phosphatase (FAP-1) blocks apoptosis of astrocytomas through dephosphorylation of FAS. *Journal of Neuro-Oncology*, **74**, 241-248.
213. Ivanov,V.N., Ronai,Z., Hei,T.K., Ronai,Z., and Hei,T.K. (2006) Opposite roles of FAP-1 and dynamin in the regulation of Fas (CD95) translocation to the cell surface and susceptibility to Fas ligand-mediated apoptosis. *Journal of Biological Chemistry*, **281**, 1840-1852.
214. Lee,S.H., Shin,M.S., Park,W.S., Kim,S.Y., Kim,H.S., Lee,J.H., Han,S.Y., Lee,H.K., Park,J.Y., Oh,R.R., Jang,J.J., Lee,J.Y., Yoo,N.J., Shin,M.S., Park,W.S., Kim,S.Y., Kim,H.S., Lee,J.H., Han,S.Y., Lee,H.K., Park,J.Y., Oh,R.R., Jang,J.J., Lee,J.Y., and Yoo,N.J. (1999) Immunohistochemical localization of FAP-1, an inhibitor of Fas-mediated apoptosis, in normal and neoplastic human tissues. *APMIS*, **107**, 1101-1108.
215. Yao,H., Song,E., Chen,J., Hamar,P., Song,E., Chen,J., and Hamar,P. (2004) Expression of FAP-1 by human colon adenocarcinoma: implication for resistance against Fas-mediated apoptosis in cancer. *British Journal of Cancer*, **91**, 1718-1725.
216. El Mahdy,M.A., Zhu,Q., Wang,Q.E., Wani,G., Wani,A.A., Zhu,Q., Wang,Q., Wani,G., and Wani,A.A. (2005) Thymoquinone induces apoptosis through activation of caspase-8 and mitochondrial events in p53-null myeloblastic leukemia HL-60 cells. *Int.J.Cancer*, **117**, 409-417.
217. Hsu,Y.L., Cho,C.Y., Kuo,P.L., Huang,Y.T., Lin,C.C., Cho,C., Kuo,P., Huang,Y., and Lin,C. (2006) Plumbagin (5-hydroxy-2-methyl-1,4-naphthoquinone) induces apoptosis and cell cycle arrest in A549 cells through p53 accumulation via c-Jun NH2-terminal kinase-mediated phosphorylation at serine 15 in vitro and in vivo. *Journal of Pharmacology & Experimental Therapeutics*, **318**, 484-494.
218. Qiu,X.B., Schonthal,A.H., Cadenas,E., Schonthal,A.H., and Cadenas,E. (1998) Anticancer quinones induce pRb-preventable G2/M cell cycle arrest and apoptosis. *Free Radical Biology & Medicine*, **24**, 848-854.
219. Bresgen,N., Karlhuber,G., Krizbai,I., Bauer,H., Bauer,H.C., Eckl,P.M., Karlhuber,G., Krizbai,I., Bauer,H., Bauer,H.C., and Eckl,P.M. (2003) Oxidative stress in cultured

cerebral endothelial cells induces chromosomal aberrations, micronuclei, and apoptosis. *Journal of Neuroscience Research*, **72**, 327-333.

220. Criddle,D.N., Gillies,S., Baumgartner-Wilson,H.K., Jaffar,M., Chinje,E.C., Passmore,S., Chvanov,M., Barrow,S., Gerasimenko,O.V., Tepikin,A.V., Sutton,R., Petersen,O.H., Gillies,S., Baumgartner-Wilson,H.K., Jaffar,M., Chinje,E.C., Passmore,S., Chvanov,M., Barrow,S., Gerasimenko,O., V, Tepikin,A., V, Sutton,R., and Petersen,O.H. (2006) Menadione-induced reactive oxygen species generation via redox cycling promotes apoptosis of murine pancreatic acinar cells. *Journal of Biological Chemistry*, **281**, 40485-40492.
221. Harrison,J.F., Hollensworth,S.B., Spitz,D.R., Copeland,W.C., Wilson,G.L., LeDoux,S.P., Hollensworth,S.B., Spitz,D.R., Copeland,W.C., Wilson,G.L., and LeDoux,S.P. (2005) Oxidative stress-induced apoptosis in neurons correlates with mitochondrial DNA base excision repair pathway imbalance. *Nucleic Acids Research*, **33**, 4660-4671.
222. Laux,I., Nel,A., and Nel,A. (2001) Evidence that oxidative stress-induced apoptosis by menadione involves Fas-dependent and Fas-independent pathways. *Clinical Immunology*, **101**, 335-344.
223. Ryan,L., O'Callaghan,Y.C., O'Brien,N.M., O'Callaghan,Y.C., and O'Brien,N.M. (2004) Generation of an oxidative stress precedes caspase activation during 7beta-hydroxycholesterol-induced apoptosis in U937 cells. *Journal of Biochemical & Molecular Toxicology*, **18**, 50-59.
224. Chim,C.S., Fung,T.K., Wong,K.F., Lau,J.S., Liang,R., Fung,T.K., Wong,K.F., Lau,J.S., and Liang,R. (2006) Frequent DAP kinase but not p14 or Apaf-1 hypermethylation in B-cell chronic lymphocytic leukemia. *Journal of Human Genetics*, **51**, 832-838.
225. Cain,K. (2003) Chemical-induced apoptosis: formation of the Apaf-1 apoptosome. [Review] [95 refs]. *Drug Metabolism Reviews*, **35**, 337-363.
226. Cecconi,F., Gruss,P., and Gruss,P. (2001) Apaf1 in developmental apoptosis and cancer: how many ways to die?. [Review] [54 refs]. *Cellular & Molecular Life Sciences*, **58**, 1688-1697.
227. Perkins,C., Kim,C.N., Fang,G., Bhalla,K.N., Kim,C.N., Fang,G., and Bhalla,K.N. (1998) Overexpression of Apaf-1 promotes apoptosis of untreated and paclitaxel- or etoposide-treated HL-60 cells. *Cancer Research*, **58**, 4561-4566.
228. Samatar,A.A., Wang,L., Mirza,A., Koseoglu,S., Liu,S., Kumar,C.C., Wang,L., Mirza,A., Koseoglu,S., Liu,S., and Kumar,C.C. (2002) Transforming growth factor-beta 2 is a transcriptional target for Akt/protein kinase B via forkhead transcription factor. *Journal of Biological Chemistry*, **277**, 28118-28126.
229. Oberhammer,F.A., Pavelka,M., Sharma,S., Tiefenbacher,R., Purchio,A.F., Bursch,W., Schulte-Hermann,R., Pavelka,M., Sharma,S., Tiefenbacher,R., Purchio,A.F., Bursch,W., and Schulte-Hermann,R. (1992) Induction of apoptosis in cultured hepatocytes and in regressing liver by transforming growth factor beta 1. *Proceedings of the National Academy of Sciences of the United States of America*, **89**, 5408-5412.
230. Ponchel,F., Puisieux,A., Tabone,E., Michot,J.P., Froschl,G., Morel,A.P., Frebourg,T., Fontaniere,B., Oberhammer,F., Ozturk,M., Puisieux,A., Tabone,E., Michot,J.P., Froschl,G., Morel,A.P., Frebourg,T., Fontaniere,B., Oberhammer,F., and Ozturk,M.

- (1994) Hepatocarcinoma-specific mutant p53-249ser induces mitotic activity but has no effect on transforming growth factor beta 1-mediated apoptosis. *Cancer Research*, **54**, 2064-2068.
231. Lu,T., Burdelya,L.G., Swiatkowski,S.M., Boiko,A.D., Howe,P.H., Stark,G.R., Gudkov,A.V., Burdelya,L.G., Swiatkowski,S.M., Boiko,A.D., Howe,P.H., Stark,G.R., and Gudkov,A., V (2004) Secreted transforming growth factor beta2 activates NF-kappaB, blocks apoptosis, and is essential for the survival of some tumor cells. *Proceedings of the National Academy of Sciences of the United States of America*, **101**, 7112-7117.
 232. Oberhammer,F., Bursch,W., Parzefall,W., Breit,P., Erber,E., Stadler,M., Schulte-Hermann,R., Bursch,W., Parzefall,W., Breit,P., Erber,E., Stadler,M., and Schulte-Hermann,R. (1991) Effect of transforming growth factor beta on cell death of cultured rat hepatocytes. *Cancer Research*, **51**, 2478-2485.
 233. Hibino,T., Nishiyama,T., and Nishiyama,T. (2004) Role of TGF-beta2 in the human hair cycle. [Review] [57 refs]. *Journal of Dermatological Science*, **35**, 9-18.
 234. Cain,K., Freathy,C., and Freathy,C. (2001) Liver toxicity and apoptosis: role of TGF-beta1, cytochrome c and the apoptosome. [Review] [38 refs]. *Toxicol.Lett.*, **120**, 307-315.
 235. Wang,B., Liu,K., Lin,F.T., Lin,W.C., Liu,K., Lin,F., and Lin,W. (2004) A role for 14-3-3 tau in E2F1 stabilization and DNA damage-induced apoptosis. *Journal of Biological Chemistry*, **279**, 54140-54152.
 236. Spittau,B., Wang,Z., Boinska,D., Krieglstein,K., Wang,Z., Boinska,D., and Krieglstein,K. (2007) Functional domains of the TGF-beta-inducible transcription factor Tieg3 and detection of two putative nuclear localization signals within the zinc finger DNA-binding domain. *Journal of Cellular Biochemistry*, **101**, 712-722.
 237. Wang,Z., Peters,B., Klussmann,S., Bender,H., Herb,A., Krieglstein,K., Peters,B., Klussmann,S., Bender,H., Herb,A., and Krieglstein,K. (2004) Gene structure and evolution of Tieg3, a new member of the Tieg family of proteins. *Gene*, **325**, 25-34.
 238. Wang,Z., Peters,B., Klussmann,S., Bender,H., Herb,A., Krieglstein,K., Peters,B., Klussmann,S., Bender,H., Herb,A., and Krieglstein,K. (2004) Gene structure and evolution of Tieg3, a new member of the Tieg family of proteins. *Gene*, **325**, 25-34.
 239. Ribeiro,A., Bronk,S.F., Roberts,P.J., Urrutia,R., Gores,G.J., Bronk,S.F., Roberts,P.J., Urrutia,R., and Gores,G.J. (1999) The transforming growth factor beta(1)-inducible transcription factor TIEG1, mediates apoptosis through oxidative stress. *Hepatology*, **30**, 1490-1497.
 240. Cook,T., Gebelein,B., Mesa,K., Mladek,A., Urrutia,R., Gebelein,B., Mesa,K., Mladek,A., and Urrutia,R. (1998) Molecular cloning and characterization of TIEG2 reveals a new subfamily of transforming growth factor-beta-inducible Sp1-like zinc finger-encoding genes involved in the regulation of cell growth. *Journal of Biological Chemistry*, **273**, 25929-25936.
 241. Tachibana,I., Imoto,M., Adjei,P.N., Gores,G.J., Subramaniam,M., Spelsberg,T.C., Urrutia,R., Imoto,M., Adjei,P.N., Gores,G.J., Subramaniam,M., Spelsberg,T.C., and Urrutia,R. (1997) Overexpression of the TGFbeta-regulated zinc finger encoding gene,

- TIEG, induces apoptosis in pancreatic epithelial cells. *Journal of Clinical Investigation*, **99**, 2365-2374.
242. Mukai,J., Suvant,P., Sato,T.A., Suvant,P., and Sato,T. (2003) Nerve growth factor-dependent regulation of NADE-induced apoptosis. [Review] [73 refs]. *Vitamins & Hormones*, **66**, 385-402.
 243. Mukai,J., Shoji,S., Kimura,M.T., Okubo,S., Sano,H., Suvanto,P., Li,Y., Irie,S., Sato,T.A., Shoji,S., Kimura,M.T., Okubo,S., Sano,H., Suvanto,P., Li,Y., Irie,S., and Sato,T. (2002) Structure-function analysis of NADE: identification of regions that mediate nerve growth factor-induced apoptosis. *Journal of Biological Chemistry*, **277**, 13973-13982.
 244. Mukai,J., Hachiya,T., Shoji-Hoshino,S., Kimura,M.T., Nadano,D., Suvanto,P., Hanaoka,T., Li,Y., Irie,S., Greene,L.A., Sato,T.A., Hachiya,T., Shoji-Hoshino,S., Kimura,M.T., Nadano,D., Suvanto,P., Hanaoka,T., Li,Y., Irie,S., Greene,L.A., and Sato,T.A. (2000) NADE, a p75NTR-associated cell death executor, is involved in signal transduction mediated by the common neurotrophin receptor p75NTR. *Journal of Biological Chemistry*, **275**, 17566-17570.
 245. Gu C, Casaccia-Bonofil P, Srinivasan A, and Chao MV (1999) Oligodendrocyte apoptosis mediated by caspase activation. *J Neurosci*, **19**, 3043-3049.
 246. Yoon,K., Jang,H.D., Lee,S.Y., Jang,H.D., and Lee,S.Y. (2004) Direct interaction of Smac with NADE promotes TRAIL-induced apoptosis. *Biochemical & Biophysical Research Communications*, **319**, 649-654.
 247. Lindholm,D., Arumae,U., and Arumae,U. (2004) Cell differentiation: reciprocal regulation of Apaf-1 and the inhibitor of apoptosis proteins.[comment]. [Review] [23 refs]. *Journal of Cell Biology*, **167**, 193-195.
 248. Katakami,N., Kaneto,H., Hao,H., Umayahara,Y., Fujitani,Y., Sakamoto,K., Gorogawa,S., Yasuda,T., Kawamori,D., Kajimoto,Y., Matsuhisa,M., Yutani,C., Hori,M., Yamasaki,Y., Kaneto,H., Hao,H., Umayahara,Y., Fujitani,Y., Sakamoto,K., Gorogawa,S., Yasuda,T., Kawamori,D., Kajimoto,Y., Matsuhisa,M., Yutani,C., Hori,M., and Yamasaki,Y. (2004) Role of pim-1 in smooth muscle cell proliferation. *Journal of Biological Chemistry*, **279**, 54742-54749.
 249. Holder,S., Zemskova,M., Zhang,C., Tabrizizad,M., Bremer,R., Neidigh,J.W., Lilly,M.B., Zemskova,M., Zhang,C., Tabrizizad,M., Bremer,R., Neidigh,J.W., and Lilly,M.B. (2007) Characterization of a potent and selective small-molecule inhibitor of the PIM1 kinase. *Molecular Cancer Therapeutics*, **6**, 163-172.
 250. Wang,Z., Bhattacharya,N., Weaver,M., Petersen,K., Meyer,M., Gapter,L., Magnuson,N.S., Bhattacharya,N., Weaver,M., Petersen,K., Meyer,M., Gapter,L., and Magnuson,N.S. (2001) Pim-1: a serine/threonine kinase with a role in cell survival, proliferation, differentiation and tumorigenesis. [Review] [121 refs]. *Journal of Veterinary Science*, **2**, 167-179.
 251. Wang,Z., Bhattacharya,N., Meyer,M.K., Seimiya,H., Tsuruo,T., Tonani,J.A., Magnuson,N.S., Bhattacharya,N., Meyer,M.K., Seimiya,H., Tsuruo,T., Tonani,J.A., and Magnuson,N.S. (2001) Pim-1 negatively regulates the activity of PTP-U2S phosphatase and influences terminal differentiation and apoptosis of monoblastoid leukemia cells. *Archives of Biochemistry & Biophysics*, **390**, 9-18.

252. Li, Y.Y., Popivanova, B.K., Nagai, Y., Ishikura, H., Fujii, C., Mukaida, N., Popivanova, B.K., Nagai, Y., Ishikura, H., Fujii, C., and Mukaida, N. (2006) Pim-3, a proto-oncogene with serine/threonine kinase activity, is aberrantly expressed in human pancreatic cancer and phosphorylates bad to block bad-mediated apoptosis in human pancreatic cancer cell lines. *Cancer Research*, **66**, 6741-6747.
253. Peng, C., Knebel, A., Morrice, N.A., Li, X., Barringer, K., Li, J., Jakes, S., Werneburg, B., Wang, L., Knebel, A., Morrice, N.A., Li, X., Barringer, K., Li, J., Jakes, S., Werneburg, B., and Wang, L. (2007) Pim kinase substrate identification and specificity. *Journal of Biochemistry*, **141**, 353-362.
254. Lee, J.W., Soung, Y.H., Kim, S.Y., Nam, S.W., Kim, C.J., Cho, Y.G., Lee, J.H., Kim, H.S., Park, W.S., Kim, S.H., Lee, J.Y., Yoo, N.J., Lee, S.H., Soung, Y.H., Kim, S.Y., Nam, S.W., Kim, C.J., Cho, Y.G., Lee, J.H., Kim, H.S., Park, W.S., Kim, S.H., Lee, J.Y., Yoo, N.J., and Lee, S.H. (2004) Inactivating mutations of proapoptotic Bad gene in human colon cancers. *Carcinogenesis*, **25**, 1371-1376.
255. Chuang, Y.Y., Chen, Y., Gadisetti, Chandramouli, V.R., Cook, J.A., Coffin, D., Tsai, M.H., DeGraff, W., Yan, H., Zhao, S., Russo, A., Liu, E.T., Mitchell, J.B., Chen, Y., Gadisetti, Chandramouli, V.R., Cook, J.A., Coffin, D., Tsai, M., DeGraff, W., Yan, H., Zhao, S., Russo, A., Liu, E.T., and Mitchell, J.B. (2002) Gene expression after treatment with hydrogen peroxide, menadione, or t-butyl hydroperoxide in breast cancer cells. *Cancer Research*, **62**, 6246-6254.
256. Marchand, A., Barouki, R., Garlatti, M., Barouki, R., and Garlatti, M. (2004) Regulation of NAD(P)H:quinone oxidoreductase 1 gene expression by CYP1A1 activity. *Molecular Pharmacology*, **65**, 1029-1037.
257. Abdel-Razzak, Z., Corcos, L., Fautrel, A., Guillouzo, A., Corcos, L., Fautrel, A., and Guillouzo, A. (1995) Interleukin-1 beta antagonizes phenobarbital induction of several major cytochromes P450 in adult rat hepatocytes in primary culture. *FEBS Letters*, **366**, 159-164.
258. Abdel-Razzak, Z., Corcos, L., Fautrel, A., Champion, J.P., Guillouzo, A., Corcos, L., Fautrel, A., Champion, J.P., and Guillouzo, A. (1994) Transforming growth factor-beta 1 down-regulates basal and polycyclic aromatic hydrocarbon-induced cytochromes P-450 1A1 and 1A2 in adult human hepatocytes in primary culture. *Molecular Pharmacology*, **46**, 1100-1110.
259. Sewer, M.B., Morgan, E.T., and Morgan, E.T. (1998) Down-regulation of the expression of three major rat liver cytochrome P450s by endotoxin in vivo occurs independently of nitric oxide production. *Journal of Pharmacology & Experimental Therapeutics*, **287**, 352-358.
260. Raje, S., Thorpe, C., and Thorpe, C. (2003) Inter-domain redox communication in flavoenzymes of the quiescin/sulfhydryl oxidase family: role of a thioredoxin domain in disulfide bond formation. *Biochemistry*, **42**, 4560-4568.
261. Tury, A., Mairet-Coello, G., Poncet, F., Jacquemard, C., Risold, P.Y., Fellmann, D., Griffond, B., Mairet-Coello, G., Poncet, F., Jacquemard, C., Risold, P.Y., Fellmann, D., and Griffond, B. (2004) QSOX sulfhydryl oxidase in rat adenohypophysis: localization and regulation by estrogens. *Journal of Endocrinology*, **183**, 353-363.

262. Mairet-Coello,G., Tury,A., Fellmann,D., Jouvenot,M., Griffond,B., Tury,A., Fellmann,D., Jouvenot,M., and Griffond,B. (2002) Expression of SOx-2, a member of the FAD-dependent sulfhydryl oxidase/quiescin Q6 gene family, in rat brain. *Neuroreport*, **13**, 2049-2051.
263. Shi,H., Hudson,L.G., Liu,K.J., Hudson,L.G., and Liu,K.J. (2004) Oxidative stress and apoptosis in metal ion-induced carcinogenesis. [Review] [107 refs]. *Free Radical Biology & Medicine*, **37**, 582-593.
264. Shi,H., Shi,X., Liu,K.J., Shi,X., and Liu,K.J. (2004) Oxidative mechanism of arsenic toxicity and carcinogenesis. [Review] [124 refs]. *Molecular & Cellular Biochemistry*, **255**, 67-78.
265. Athar,M. (2002) Oxidative stress and experimental carcinogenesis. [Review] [166 refs]. *Indian Journal of Experimental Biology*, **40**, 656-667.
266. Epe,B. (2002) Role of endogenous oxidative DNA damage in carcinogenesis: what can we learn from repair-deficient mice?. [Review] [95 refs]. *Biological Chemistry*, **383**, 467-475.
267. Chao,C., Saito,S., Kang,J., Anderson,C.W., Appella,E., Xu,Y., Saito,S., Kang,J., Anderson,C.W., Appella,E., and Xu,Y. (2000) p53 transcriptional activity is essential for p53-dependent apoptosis following DNA damage. *EMBO Journal*, **19**, 4967-4975.
268. Crowe,D.L., Sinha,U.K., and Sinha,U.K. (2006) p53 apoptotic response to DNA damage dependent on bcl2 but not bax in head and neck squamous cell carcinoma lines. *Head & Neck*, **28**, 15-23.
269. Fuchs,E.J., McKenna,K.A., Bedi,A., McKenna,K.A., and Bedi,A. (1997) p53-dependent DNA damage-induced apoptosis requires Fas/APO-1-independent activation of CPP32beta. *Cancer Research*, **57**, 2550-2554.
270. Guillouf,C., Rosselli,F., Krishnaraju,K., Moustacchi,E., Hoffman,B., Liebermann,D.A., Rosselli,F., Krishnaraju,K., Moustacchi,E., Hoffman,B., and Liebermann,D.A. (1995) p53 involvement in control of G2 exit of the cell cycle: role in DNA damage-induced apoptosis. *Oncogene*, **10**, 2263-2270.
271. Hirao,A., Kong,Y.Y., Matsuoka,S., Wakeham,A., Ruland,J., Yoshida,H., Liu,D., Elledge,S.J., Mak,T.W., Kong,Y.Y., Matsuoka,S., Wakeham,A., Ruland,J., Yoshida,H., Liu,D., Elledge,S.J., and Mak,T.W. (2000) DNA damage-induced activation of p53 by the checkpoint kinase Chk2.[see comment]. *Science*, **287**, 1824-1827.
272. Gartel,A.L., Serfas,M.S., Tyner,A.L., Serfas,M.S., and Tyner,A.L. (1996) p21--negative regulator of the cell cycle. [Review] [126 refs]. *Proceedings of the Society for Experimental Biology & Medicine*, **213**, 138-149.
273. Wu,R.C., Hohenstein,A., Park,J.M., Qiu,X., Mueller,S., Cadenas,E., Schonthal,A.H., Hohenstein,A., Park,J.M., Qiu,X., Mueller,S., Cadenas,E., and Schonthal,A.H. (1998) Role of p53 in aziridinybenzoquinone-induced p21 waf1 expression. *Oncogene*, **17**, 357-365.
274. Qiu,X., Forman,H.J., Schonthal,A.H., Cadenas,E., Forman,H.J., Schonthal,A.H., and Cadenas,E. (1996) Induction of p21 mediated by reactive oxygen species formed during

the metabolism of aziridinybenzoquinones by HCT116 cells. *Journal of Biological Chemistry*, **271**, 31915-31921.

275. Lim, E.S., Rhee, Y.H., Park, M.K., Shim, B.S., Ahn, K.S., Kang, H., Yoo, H.S., Kim, S.H., Rhee, Y., Park, M., Shim, B., Ahn, K., Kang, H., Yoo, H., and Kim, S. (2007) DMNQ S-64 induces apoptosis via caspase activation and cyclooxygenase-2 inhibition in human nonsmall lung cancer cells. *Annals of the New York Academy of Sciences*, **1095**, 7-18.
276. Kim, T.J., Yun, Y.P., and Yun, Y. (2007) Antiproliferative activity of NQ304, a synthetic 1,4-naphthoquinone, is mediated via the suppressions of the PI3K/Akt and ERK1/2 signaling pathways in PDGF-BB-stimulated vascular smooth muscle cells. *Vascular Pharmacology*, **46**, 43-51.
277. Essers, J., Theil, A.F., Baldeyron, C., van Cappellen, W.A., Houtsmuller, A.B., Kanaar, R., Vermeulen, W., Theil, A.F., Baldeyron, C., van Cappellen, W.A., Houtsmuller, A.B., Kanaar, R., and Vermeulen, W. (2005) Nuclear dynamics of PCNA in DNA replication and repair. *Molecular & Cellular Biology*, **25**, 9350-9359.
278. Fotedar, R., Bendjennat, M., Fotedar, A., Bendjennat, M., and Fotedar, A. (2004) Role of p21WAF1 in the cellular response to UV. [Review] [68 refs]. *Cell Cycle*, **3**, 134-137.
279. Savio, M., Stivala, L.A., Bianchi, L., Vannini, V., Prosperi, E., Stivala, L.A., Bianchi, L., Vannini, V., and Prosperi, E. (1998) Involvement of the proliferating cell nuclear antigen (PCNA) in DNA repair induced by alkylating agents and oxidative damage in human fibroblasts. *Carcinogenesis*, **19**, 591-596.
280. Montori-Grau, M., Guitart, M., Lerin, C., Andreu, A.L., Newgard, C.B., Garcia-Martinez, C., Gomez-Foix, A.M., Guitart, M., Lerin, C., Andreu, A.L., Newgard, C.B., Garcia-Martinez, C., and Gomez-Foix, A.M. (2007) Expression and glycogenic effect of glycogen-targeting protein phosphatase 1 regulatory subunit GL in cultured human muscle. *Biochemical Journal*, **405**, 107-113.
281. Postic, C., Dentin, R., Girard, J., Dentin, R., and Girard, J. (2004) Role of the liver in the control of carbohydrate and lipid homeostasis. [Review] [91 refs]. *Diabetes & Metabolism*, **30**, 398-408.
282. Minchenko, A., Leshchinsky, I., Opentanova, I., Sang, N., Srinivas, V., Armstead, V., Caro, J., Leshchinsky, I., Opentanova, I., Sang, N., Srinivas, V., Armstead, V., and Caro, J. (2002) Hypoxia-inducible factor-1-mediated expression of the 6-phosphofructo-2-kinase/fructose-2,6-bisphosphatase-3 (PFKFB3) gene. Its possible role in the Warburg effect. *Journal of Biological Chemistry*, **277**, 6183-6187.
283. Minchenko, O., Opentanova, I., Minchenko, D., Ogura, T., Esumi, H., Opentanova, I., Minchenko, D., Ogura, T., and Esumi, H. (2004) Hypoxia induces transcription of 6-phosphofructo-2-kinase/fructose-2,6-bisphosphatase-4 gene via hypoxia-inducible factor-1 α activation. *FEBS Letters*, **576**, 14-20.
284. Mahlknecht, U., Chesney, J., Hoelzer, D., Bucala, R., Chesney, J., Hoelzer, D., and Bucala, R. (2003) Cloning and chromosomal characterization of the 6-phosphofructo-2-kinase/fructose-2,6-bisphosphatase-3 gene (PFKFB3, iPFK2). *Int. J. Oncol.*, **23**, 883-891.
285. Lind, P. (2004) Interdependence of hepatic lipid and glucose metabolism: novel pharmacological targets for diabetes. [Review] [51 refs]. *Current Opinion in Investigational Drugs*, **5**, 395-401.

286. Podvinec,M., Handschin,C., Looser,R., Meyer,U.A., Handschin,C., Looser,R., and Meyer,U.A. (2004) Identification of the xenosensors regulating human 5-aminolevulinic acid synthase. *Proceedings of the National Academy of Sciences of the United States of America*, **101**, 9127-9132.
287. Schranzhofer,M., Schiffrer,M., Cabrera,J.A., Kopp,S., Chiba,P., Beug,H., Mullner,E.W., Schiffrer,M., Cabrera,J.A., Kopp,S., Chiba,P., Beug,H., and Mullner,E.W. (2006) Remodeling the regulation of iron metabolism during erythroid differentiation to ensure efficient heme biosynthesis. *Blood*, **107**, 4159-4167.
288. Haitina,T., Lindblom,J., Renstrom,T., Fredriksson,R., Lindblom,J., Renstrom,T., and Fredriksson,R. (2006) Fourteen novel human members of mitochondrial solute carrier family 25 (SLC25) widely expressed in the central nervous system. *Genomics*, **88**, 779-790.
289. Shaw,G.C., Cope,J.J., Li,L., Corson,K., Hersey,C., Ackermann,G.E., Gwynn,B., Lambert,A.J., Wingert,R.A., Traver,D., Trede,N.S., Barut,B.A., Zhou,Y., Minet,E., Donovan,A., Brownlie,A., Balzan,R., Weiss,M.J., Peters,L.L., Kaplan,J., Zon,L.I., Paw,B.H., Cope,J.J., Li,L., Corson,K., Hersey,C., Ackermann,G.E., Gwynn,B., Lambert,A.J., Wingert,R.A., Traver,D., Trede,N.S., Barut,B.A., Zhou,Y., Minet,E., Donovan,A., Brownlie,A., Balzan,R., Weiss,M.J., Peters,L.L., Kaplan,J., Zon,L., I, and Paw,B.H. (2006) Mitoferrin is essential for erythroid iron assimilation. *Nature*, **440**, 96-100.
290. Harris,A.J., Shaddock,J.G., Manjanatha,M.G., Lisenbey,J.A., Casciano,D.A., Shaddock,J.G., Manjanatha,M.G., Lisenbey,J.A., and Casciano,D.A. (1998) Identification of differentially expressed genes in aflatoxin B1-treated cultured primary rat hepatocytes and Fischer 344 rats. *Carcinogenesis*, **19**, 1451-1458.
291. Mori,N., Hirayama,K., and Hirayama,K. (2000) Long-term consumption of a methionine-supplemented diet increases iron and lipid peroxide levels in rat liver. *Journal of Nutrition*, **130**, 2349-2355.
292. Rodriguez,M.A., Niemela,O., Parkkila,S., Niemela,O., and Parkkila,S. (2004) Hepatic and extrahepatic expression of the new iron regulatory protein hemojuvelin. *Haematologica*, **89**, 1441-1445.
293. Niederkofler,V., Salie,R., Arber,S., Salie,R., and Arber,S. (2005) Hemojuvelin is essential for dietary iron sensing, and its mutation leads to severe iron overload.[see comment]. *Journal of Clinical Investigation*, **115**, 2180-2186.
294. Vaulont,S., Lou,D.Q., Viatte,L., Kahn,A., Lou,D., Viatte,L., and Kahn,A. (2005) Of mice and men: the iron age.[comment]. *Journal of Clinical Investigation*, **115**, 2079-2082.
295. Lin,L., Goldberg,Y.P., Ganz,T., Goldberg,Y.P., and Ganz,T. (2005) Competitive regulation of hepcidin mRNA by soluble and cell-associated hemojuvelin. *Blood*, **106**, 2884-2889.
296. Minotti,G., Ronchi,R., Salvatorelli,E., Menna,P., Cairo,G., Ronchi,R., Salvatorelli,E., Menna,P., and Cairo,G. (2001) Doxorubicin irreversibly inactivates iron regulatory proteins 1 and 2 in cardiomyocytes: evidence for distinct metabolic pathways and implications for iron-mediated cardiotoxicity of antitumor therapy. *Cancer Research*, **61**, 8422-8428.

297. Bachmann,M., Moroy,T., and Moroy,T. (2005) The serine/threonine kinase Pim-1. [Review] [25 refs]. *Int.J.Biochem.Cell Biol.*, **37**, 726-730.
298. Macdonald,A., Campbell,D.G., Toth,R., McLauchlan,H., Hastie,C.J., Arthur,J.S., Campbell,D.G., Toth,R., McLauchlan,H., Hastie,C.J., and Arthur,J.S. (2006) Pim kinases phosphorylate multiple sites on Bad and promote 14-3-3 binding and dissociation from Bcl-XL. *BMC Cell Biology*, **7**, 1.
299. Kodama,S., Koike,C., Negishi,M., Yamamoto,Y., Koike,C., Negishi,M., and Yamamoto,Y. (2004) Nuclear receptors CAR and PXR cross talk with FOXO1 to regulate genes that encode drug-metabolizing and gluconeogenic enzymes. *Molecular & Cellular Biology*, **24**, 7931-7940.
300. Qiu,W., Avramoglu,R.K., Dube,N., Chong,T.M., Naples,M., Au,C., Sidiropoulos,K.G., Lewis,G.F., Cohn,J.S., Tremblay,M.L., Adeli,K., Avramoglu,R.K., Dube,N., Chong,T.M., Naples,M., Au,C., Sidiropoulos,K.G., Lewis,G.F., Cohn,J.S., Tremblay,M.L., and Adeli,K. (2004) Hepatic PTP-1B expression regulates the assembly and secretion of apolipoprotein B-containing lipoproteins: evidence from protein tyrosine phosphatase-1B overexpression, knockout, and RNAi studies. *Diabetes*, **53**, 3057-3066.
301. Zhang,S., Yang,J.H., Guo,C.K., Cai,P.C., Yang,J., Guo,C., and Cai,P. (2007) Gene silencing of TKTL1 by RNAi inhibits cell proliferation in human hepatoma cells. *Cancer Letters*, **253**, 108-114.
302. Dong,J., Fujii,S., Imagawa,S., Matsumoto,S., Matsushita,M., Todo,S., Tsutsui,H., Sobel,B.E., Fujii,S., Imagawa,S., Matsumoto,S., Matsushita,M., Todo,S., Tsutsui,H., and Sobel,B.E. (2007) IL-1 and IL-6 induce hepatocyte plasminogen activator inhibitor-1 expression through independent signaling pathways converging on C/EBPdelta. *American Journal of Physiology - Cell Physiology*, **292**, C209-C215.
303. Fujii,C., Nakamoto,Y., Lu,P., Tsuneyama,K., Popivanova,B.K., Kaneko,S., Mukaida,N., Nakamoto,Y., Lu,P., Tsuneyama,K., Popivanova,B.K., Kaneko,S., and Mukaida,N. (2005) Aberrant expression of serine/threonine kinase Pim-3 in hepatocellular carcinoma development and its role in the proliferation of human hepatoma cell lines. *Int.J.Cancer*, **114**, 209-218.
304. Fujii,C., Nakamoto,Y., Lu,P., Tsuneyama,K., Popivanova,B.K., Kaneko,S., Mukaida,N., Nakamoto,Y., Lu,P., Tsuneyama,K., Popivanova,B.K., Kaneko,S., and Mukaida,N. (2005) Aberrant expression of serine/threonine kinase Pim-3 in hepatocellular carcinoma development and its role in the proliferation of human hepatoma cell lines. *Int.J.Cancer*, **114**, 209-218.
305. Dalton,T.P., Dieter,M.Z., Yang,Y., Shertzer,H.G., Nebert,D.W., Dieter,M.Z., Yang,Y., Shertzer,H.G., and Nebert,D.W. (2000) Knockout of the mouse glutamate cysteine ligase catalytic subunit (Gclc) gene: embryonic lethal when homozygous, and proposed model for moderate glutathione deficiency when heterozygous. *Biochemical & Biophysical Research Communications*, **279**, 324-329.
306. Hayes,J.D., McLeod,R., Ellis,E.M., Pulford,D.J., Ireland,L.S., McLellan,L.I., Judah,D.J., Manson,M.M., Neal,G.E., McLeod,R., Ellis,E.M., Pulford,D.J., Ireland,L.S., McLellan,L. I, Judah,D.J., Manson,M.M., and Neal,G.E. (1996) Regulation of glutathione S-transferases and aldehyde reductase by chemoprotectors: studies of

mechanisms responsible for inducible resistance to aflatoxin B1. [Review] [75 refs].
IARC Scientific Publications, 175-187.

307. Thor,H., Mirabelli,F., Salis,A., Cohen,G.M., Bellomo,G., Orrenius,S., Mirabelli,F., Salis,A., Cohen,G.M., Bellomo,G., and Orrenius,S. (1988) Alterations in hepatocyte cytoskeleton caused by redox cycling and alkylating quinones. *Archives of Biochemistry & Biophysics*, **266**, 397-407.
308. Shi,M., Gozal,E., Choy,H.A., Forman,H.J., Gozal,E., Choy,H.A., and Forman,H.J. (1993) Extracellular glutathione and gamma-glutamyl transpeptidase prevent H₂O₂-induced injury by 2,3-dimethoxy-1,4-naphthoquinone. *Free Radical Biology & Medicine*, **15**, 57-67.
309. Badr,M., Yoshihara,H., Kauffman,F., Thurman,R., Yoshihara,H., Kauffman,F., and Thurman,R. (1987) Menadione causes selective toxicity to periportal regions of the liver lobule. *Toxicol.Lett.*, **35**, 241-246.
310. Badr,M.Z., Ganey,P.E., Yoshihara,H., Kauffman,F.C., Thurman,R.G., Ganey,P.E., Yoshihara,H., Kauffman,F.C., and Thurman,R.G. (1989) Hepatotoxicity of menadione predominates in oxygen-rich zones of the liver lobule. *Journal of Pharmacology & Experimental Therapeutics*, **248**, 1317-1322.
311. Bagchi,D., Bagchi,M., Hassoun,E., Moser,J., Stohs,S.J., Bagchi,M., Hassoun,E., Moser,J., and Stohs,S.J. (1993) Effects of carbon tetrachloride, menadione, and paraquat on the urinary excretion of malondialdehyde, formaldehyde, acetaldehyde, and acetone in rats. *Journal of Biochemical Toxicology*, **8**, 101-106.
312. Bellomo,G., Mirabelli,F., Vairetti,M., Iosi,F., Malorni,W., Mirabelli,F., Vairetti,M., Iosi,F., and Malorni,W. (1990) Cytoskeleton as a target in menadione-induced oxidative stress in cultured mammalian cells. I. Biochemical and immunocytochemical features. *Journal of Cellular Physiology*, **143**, 118-128.
313. Chan,H.M., Tabarrok,R., Tamura,Y., Cherian,M.G., Tabarrok,R., Tamura,Y., and Cherian,M.G. (1992) The relative importance of glutathione and metallothionein on protection of hepatotoxicity of menadione in rats. *Chemico-Biological Interactions*, **84**, 113-124.
314. Chen,Q., Cederbaum,A.I., and Cederbaum,A. I (1997) Menadione cytotoxicity to Hep G2 cells and protection by activation of nuclear factor-kappaB. *Molecular Pharmacology*, **52**, 648-657.
315. Efferth,T., Oesch,F., and Oesch,F. (2004) Oxidative stress response of tumor cells: microarray-based comparison between artemisinin and anthracyclines. *Biochem.Pharmacol.*, **68**, 3-10.
316. Lee,J.M., Calkins,M.J., Chan,K., Kan,Y.W., Johnson,J.A., Calkins,M.J., Chan,K., Kan,Y.W., and Johnson,J.A. (2003) Identification of the NF-E2-related factor-2-dependent genes conferring protection against oxidative stress in primary cortical astrocytes using oligonucleotide microarray analysis. *Journal of Biological Chemistry*, **278**, 12029-12038.
317. Gao,F., Yi,J., Shi,G., Li,H., Shi,X., Wang,Z., Tang,X., Yi,J., Shi,G., Li,H., Shi,X., Wang,Z., and Tang,X. (2002) [Ascorbic acid enhances the apoptosis of U937 cells

induced by arsenic trioxide in combination with DMNQ and its mechanism]. [Chinese]. *Chung-Hua Hsueh Yeh Hsueh Tsa Chih: Chinese Journal of Hematology*, **23**, 9-11.

318. Ishihara, Y., Shiba, D., Shimamoto, N., Shiba, D., and Shimamoto, N. (2006) Enhancement of DMNQ-induced hepatocyte toxicity by cytochrome P450 inhibition. *Toxicology & Applied Pharmacology*, **214**, 109-117.
319. Chen, Y., Chan, T.M., and Chan, T.M. (1993) Orthovanadate and 2,3-dimethoxy-1,4-naphthoquinone augment growth factor-induced cell proliferation and c-fos gene expression in 3T3-L1 cells. *Archives of Biochemistry & Biophysics*, **305**, 9-16.
320. Brown, P.C., Dulik, D.M., Jones, T.W., Dulik, D.M., and Jones, T.W. (1991) The toxicity of menadione (2-methyl-1,4-naphthoquinone) and two thioether conjugates studied with isolated renal epithelial cells. *Archives of Biochemistry & Biophysics*, **285**, 187-196.
321. Czaja, M.J., Liu, H., Wang, Y., Liu, H., and Wang, Y. (2003) Oxidant-induced hepatocyte injury from menadione is regulated by ERK and AP-1 signaling. *Hepatology*, **37**, 1405-1413.
322. Di Monte, D., Bellomo, G., Thor, H., Nicotera, P., Orrenius, S., Bellomo, G., Thor, H., Nicotera, P., and Orrenius, S. (1984) Menadione-induced cytotoxicity is associated with protein thiol oxidation and alteration in intracellular Ca²⁺ homeostasis. *Archives of Biochemistry & Biophysics*, **235**, 343-350.
323. Frei, B., Winterhalter, K.H., Richter, C., Winterhalter, K.H., and Richter, C. (1986) Menadione- (2-methyl-1,4-naphthoquinone-) dependent enzymatic redox cycling and calcium release by mitochondria. *Biochemistry*, **25**, 4438-4443.
324. Ossola, J.O., Kristoff, G., Tomaro, M.L., Kristoff, G., and Tomaro, M.L. (2000) Heme oxygenase induction by menadione bisulfite adduct-generated oxidative stress in rat liver. *Comparative Biochemistry & Physiology, Toxicology & Pharmacology*, 91-99.
325. Min, K.S., Terano, Y., Onosaka, S., Tanaka, K., Terano, Y., Onosaka, S., and Tanaka, K. (1991) Induction of hepatic metallothionein by nonmetallic compounds associated with acute-phase response in inflammation. *Toxicology & Applied Pharmacology*, **111**, 152-162.
326. Munday, R., Smith, B.L., Munday, C.M., Smith, B.L., and Munday, C.M. (1998) Effects of butylated hydroxyanisole and dicoumarol on the toxicity of menadione to rats. *Chemico-Biological Interactions*, **108**, 155-170.
327. Radjendirane, V., Joseph, P., Lee, Y.H., Kimura, S., Klein-Szanto, A.J., Gonzalez, F.J., Jaiswal, A.K., Joseph, P., Lee, Y.H., Kimura, S., Klein-Szanto, A.J., Gonzalez, F.J., and Jaiswal, A.K. (1998) Disruption of the DT diaphorase (NQO1) gene in mice leads to increased menadione toxicity. *Journal of Biological Chemistry*, **273**, 7382-7389.
328. Alarcon, O.M., Reinoso, F.A., Silva, L., Padron, F., Reinoso, F.A., Silva, L., and Padron, F. (1995) Changes of serum lipids in vitamin K3 (menadione) treated rats. *Archivos Latinoamericanos de Nutricion*, **45**, 286-289.
329. Molitor, H. and Robinson, H.J. (1940) Oral and Parenteral Toxicity of Vitamin K1, Phthiocol and 2 Methyl 1,4 Naphthoquinone. *Proceedings of the Society for Experimental Biology & Medicine*, **43**, 125-128.

330. Taylor, J.D., Millar, G.J., Jaques, L.B., and Spinks, J.W.T. (1956) The Distribution of Administered Vitamin K1-C14 in Rats. *Canadian Journal of Biochemistry*, **34**, 1143-1152.
331. Stone, V., Coleman, R., Chipman, J.K., Coleman, R., and Chipman, J.K. (1996) Comparison of the effects of redox cycling and arylating quinones on hepatobiliary function and glutathione homeostasis in rat hepatocyte couplets. *Toxicology & Applied Pharmacology*, **138**, 195-200.
332. Hodnett, E.M., Wongwiechintana, C., Dunn, W.J., III, Marrs, P., Wongwiechintana, C., Dunn, W.J., III, and Marrs, P. (1983) Substituted 1,4-naphthoquinones vs. the ascitic sarcoma 180 of mice. *J. Med. Chem.*, **26**, 570-574.
333. Buffinton, G.D., Ollinger, K., Brunmark, A., Cadenas, E., Ollinger, K., Brunmark, A., and Cadenas, E. (1989) DT-diaphorase-catalysed reduction of 1,4-naphthoquinone derivatives and glutathionyl-quinone conjugates. Effect of substituents on autoxidation rates. *Biochemical Journal*, **257**, 561-571.
334. Bellomo, G., Mirabelli, F., DiMonte, D., Richelmi, P., Thor, H., Orrenius, C., Orrenius, S., Mirabelli, F., DiMonte, D., Richelmi, P., Thor, H., Orrenius, C., and Orrenius, S. (1987) Formation and reduction of glutathione-protein mixed disulfides during oxidative stress. A study with isolated hepatocytes and menadione (2-methyl-1,4-naphthoquinone). *Biochem. Pharmacol.*, **36**, 1313-1320.
335. Ross, D., Thor, H., Orrenius, S., Moldeus, P., Thor, H., Orrenius, S., and Moldeus, P. (1985) Interaction of menadione (2-methyl-1,4-naphthoquinone) with glutathione. *Chemico-Biological Interactions*, **55**, 177-184.
336. Saxena, K., Henry, T.R., Solem, L.E., Wallace, K.B., Henry, T.R., Solem, L.E., and Wallace, K.B. (1995) Enhanced induction of the mitochondrial permeability transition following acute menadione administration. *Archives of Biochemistry & Biophysics*, **317**, 79-84.
337. Yoshinari, K., Okino, N., Sato, T., Sugatani, J., Miwa, M., Okino, N., Sato, T., Sugatani, J., and Miwa, M. (2006) Induction of detoxifying enzymes in rodent white adipose tissue by aryl hydrocarbon receptor agonists and antioxidants. *Drug Metabolism & Disposition*, **34**, 1081-1089.
338. Sidorova, Y.A., Grishanova, A.Y., Lyakhovich, V.V., Grishanova, A.Y., and Lyakhovich, V., V (2005) Rat hepatic CYP1A1 and CYP1A2 induction by menadione. *Toxicol. Lett.*, **155**, 253-258.
339. Petersen, K.U. (2002) From toxic precursors to safe drugs. Mechanisms and relevance of idiosyncratic drug reactions. [Review] [30 refs]. *Arzneimittelforschung.*, **52**, 423-429.
340. Lee, M.Y., Dordick, J.S., and Dordick, J.S. (2006) High-throughput human metabolism and toxicity analysis. [Review] [44 refs]. *Current Opinion in Biotechnology*, **17**, 619-627.
341. Baranczewski, P., Staczak, A., Sundberg, K., Svensson, R., Wallin, A., Jansson, J., Garberg, P., Postlind, H., Staczak, A., Sundberg, K., Svensson, R., Wallin, A., Jansson, J., Garberg, P., and Postlind, H. (2006) Introduction to in vitro estimation of metabolic stability and drug interactions of new chemical entities in drug discovery and development. [Review] [96 refs]. *Pharmacological Reports: PR*, **58**, 453-472.

342. Applegate,L.A., Luscher,P., Tyrrell,R.M., Luscher,P., and Tyrrell,R.M. (1991) Induction of heme oxygenase: a general response to oxidant stress in cultured mammalian cells. *Cancer Research*, **51**, 974-978.
343. Lee,B.S., Heo,J., Kim,Y.M., Shim,S.M., Pae,H.O., Kim,Y.M., Chung,H.T., Heo,J., Kim,Y., Shim,S.M., Pae,H., Kim,Y., and Chung,H. (2006) Carbon monoxide mediates heme oxygenase 1 induction via Nrf2 activation in hepatoma cells. *Biochemical & Biophysical Research Communications*, **343**, 965-972.
344. Liu,X.M., Peyton,K.J., Ensenat,D., Wang,H., Schafer,A.I., Alam,J., Durante,W., Peyton,K.J., Ensenat,D., Wang,H., Schafer,A., I, Alam,J., and Durante,W. (2005) Endoplasmic reticulum stress stimulates heme oxygenase-1 gene expression in vascular smooth muscle. Role in cell survival. *Journal of Biological Chemistry*, **280**, 872-877.
345. Rushworth,S.A., Chen,X.L., Mackman,N., Ogborne,R.M., O'Connell,M.A., Chen,X., Mackman,N., Ogborne,R.M., and O'Connell,M.A. (2005) Lipopolysaccharide-induced heme oxygenase-1 expression in human monocytic cells is mediated via Nrf2 and protein kinase C. *Journal of Immunology*, **175**, 4408-4415.
346. Dhakshinamoorthy,S., Jaiswal,A.K., and Jaiswal,A.K. (2000) Small maf (MafG and MafK) proteins negatively regulate antioxidant response element-mediated expression and antioxidant induction of the NAD(P)H:Quinone oxidoreductase1 gene. *Journal of Biological Chemistry*, **275**, 40134-40141.
347. Kwak,M.K., Itoh,K., Yamamoto,M., Kensler,T.W., Itoh,K., Yamamoto,M., and Kensler,T.W. (2002) Enhanced expression of the transcription factor Nrf2 by cancer chemopreventive agents: role of antioxidant response element-like sequences in the nrf2 promoter. *Molecular & Cellular Biology*, **22**, 2883-2892.
348. Hong,W.K., Sporn,M.B., and Sporn,M.B. (1997) Recent advances in chemoprevention of cancer. [Review] [37 refs]. *Science*, **278**, 1073-1077.
349. Badary,O.A., Al Shabanah,O.A., Nagi,M.N., Al Rikabi,A.C., Elmazar,M.M., Al Shabanah,O.A., Nagi,M.N., Al Rikabi,A.C., and Elmazar,M.M. (1999) Inhibition of benzo(a)pyrene-induced forestomach carcinogenesis in mice by thymoquinone. *Eur.J.Cancer Prev.*, **8**, 435-440.
350. Badary,O.A., Abd-Ellah,M.F., El Mahdy,M.A., Salama,S.A., Hamada,F.M., Abd-Ellah,M.F., El Mahdy,M.A., Salama,S.A., and Hamada,F.M. (2007) Anticlastogenic activity of thymoquinone against benzo(a)pyrene in mice. *Food Chem. Toxicol.*, **45**, 88-92.
351. Kwak,M.K., Wakabayashi,N., Kensler,T.W., Wakabayashi,N., and Kensler,T.W. (2004) Chemoprevention through the Keap1-Nrf2 signaling pathway by phase 2 enzyme inducers. [Review] [121 refs]. *Mutat.Res.*, **555**, 133-148.
352. Kohle,C., Bock,K.W., and Bock,K.W. (2007) Coordinate regulation of Phase I and II xenobiotic metabolisms by the Ah receptor and Nrf2. [Review] [96 refs]. *Biochem.Pharmacol.*, **73**, 1853-1862.
353. Kwak,M.K., Egner,P.A., Dolan,P.M., Ramos-Gomez,M., Groopman,J.D., Itoh,K., Yamamoto,M., Kensler,T.W., Egner,P.A., Dolan,P.M., Ramos-Gomez,M., Groopman,J.D., Itoh,K., Yamamoto,M., and Kensler,T.W. (2001) Role of phase 2

enzyme induction in chemoprotection by dithiolethiones. [Review] [62 refs]. *Mutat.Res.*, **480-481**, 305-315.

354. Wattenberg,L.W., Bueding,E., and Bueding,E. (1986) Inhibitory effects of 5-(2-pyrazinyl)-4-methyl-1,2-dithiol-3-thione (Oltipraz) on carcinogenesis induced by benzo[a]pyrene, diethylnitrosamine and uracil mustard. *Carcinogenesis*, **7**, 1379-1381.
355. Rao,C.V., Rivenson,A., Katiwalla,M., Kelloff,G.J., Reddy,B.S., Rivenson,A., Katiwalla,M., Kelloff,G.J., and Reddy,B.S. (1993) Chemopreventive effect of oltipraz during different stages of experimental colon carcinogenesis induced by azoxymethane in male F344 rats. *Cancer Research*, **53**, 2502-2506.
356. Roebuck,B.D., Liu,Y.L., Rogers,A.E., Groopman,J.D., Kensler,T.W., Liu,Y.L., Rogers,A.E., Groopman,J.D., and Kensler,T.W. (1991) Protection against aflatoxin B1-induced hepatocarcinogenesis in F344 rats by 5-(2-pyrazinyl)-4-methyl-1,2-dithiole-3-thione (oltipraz): predictive role for short-term molecular dosimetry. *Cancer Research*, **51**, 5501-5506.
357. Wang,J.S., Shen,X., He,X., Zhu,Y.R., Zhang,B.C., Wang,J.B., Qian,G.S., Kuang,S.Y., Zarba,A., Egner,P.A., Jacobson,L.P., Munoz,A., Helzlsouer,K.J., Groopman,J.D., Kensler,T.W., Shen,X., He,X., Zhu,Y.R., Zhang,B.C., Wang,J.B., Qian,G.S., Kuang,S.Y., Zarba,A., Egner,P.A., Jacobson,L.P., Munoz,A., Helzlsouer,K.J., Groopman,J.D., and Kensler,T.W. (1999) Protective alterations in phase 1 and 2 metabolism of aflatoxin B1 by oltipraz in residents of Qidong, People's Republic of China. *Journal of the National Cancer Institute*, **91**, 347-354.
358. Iida,K., Itoh,K., Kumagai,Y., Oyasu,R., Hattori,K., Kawai,K., Shimazui,T., Akaza,H., Yamamoto,M., Itoh,K., Kumagai,Y., Oyasu,R., Hattori,K., Kawai,K., Shimazui,T., Akaza,H., and Yamamoto,M. (2004) Nrf2 is essential for the chemopreventive efficacy of oltipraz against urinary bladder carcinogenesis. *Cancer Research*, **64**, 6424-6431.
359. Ramos-Gomez,M., Dolan,P.M., Itoh,K., Yamamoto,M., Kensler,T.W., Dolan,P.M., Itoh,K., Yamamoto,M., and Kensler,T.W. (2003) Interactive effects of nrf2 genotype and oltipraz on benzo[a]pyrene-DNA adducts and tumor yield in mice. *Carcinogenesis*, **24**, 461-467.
360. Kwak,M.K., Wakabayashi,N., Itoh,K., Motohashi,H., Yamamoto,M., Kensler,T.W., Wakabayashi,N., Itoh,K., Motohashi,H., Yamamoto,M., and Kensler,T.W. (2003) Modulation of gene expression by cancer chemopreventive dithiolethiones through the Keap1-Nrf2 pathway. Identification of novel gene clusters for cell survival. *Journal of Biological Chemistry*, **278**, 8135-8145.
361. Phelps,D.C., Crane,F.L., and Crane,F.L. (1975) Inhibition of mitochondrial electron transport by hydroxy-substituted 1,4-quinones. *Biochemistry*, **14**, 116-122.
362. Wallace,K.B., Eells,J.T., Madeira,V.M., Cortopassi,G., Jones,D.P., Eells,J.T., Madeira,V.M., Cortopassi,G., and Jones,D.P. (1997) Mitochondria-mediated cell injury. Symposium overview. *Fundamental & Applied Toxicology*, **38**, 23-37.
363. Halestrap,A.P. (2006) Calcium, mitochondria and reperfusion injury: a pore way to die. [Review] [49 refs]. *Biochemical Society Transactions*, **34**, 232-237.

364. Henry, T.R., Wallace, K.B., and Wallace, K.B. (1995) The role of redox cycling versus arylation in quinone-induced mitochondrial dysfunction: a mechanistic approach in classifying reactive toxicants. *Sar & Qsar in Environmental Research*, **4**, 97-108.
365. Henry, T.R., Wallace, K.B., and Wallace, K.B. (1995) Differential mechanisms of induction of the mitochondrial permeability transition by quinones of varying chemical reactivities. *Toxicology & Applied Pharmacology*, **134**, 195-203.
366. Halestrap, A.P., Doran, E., Gillespie, J.P., O'Toole, A., Doran, E., Gillespie, J.P., and O'Toole, A. (2000) Mitochondria and cell death. [Review] [48 refs]. *Biochemical Society Transactions*, **28**, 170-177.
367. Petronilli, V., Costantini, P., Scorrano, L., Colonna, R., Passamonti, S., Bernardi, P., Costantini, P., Scorrano, L., Colonna, R., Passamonti, S., and Bernardi, P. (1994) The voltage sensor of the mitochondrial permeability transition pore is tuned by the oxidation-reduction state of vicinal thiols. Increase of the gating potential by oxidants and its reversal by reducing agents. *Journal of Biological Chemistry*, **269**, 16638-16642.
368. McStay, G.P., Clarke, S.J., Halestrap, A.P., Clarke, S.J., and Halestrap, A.P. (2002) Role of critical thiol groups on the matrix surface of the adenine nucleotide translocase in the mechanism of the mitochondrial permeability transition pore. *Biochemical Journal*, **367**, 541-548.
369. Wyllie, F.S., Haughton, M.F., Bond, J.A., Rowson, J.M., Jones, C.J., Wynford-Thomas, D., Haughton, M.F., Bond, J.A., Rowson, J.M., Jones, C.J., and Wynford-Thomas, D. (1996) S phase cell-cycle arrest following DNA damage is independent of the p53/p21(WAF1) signalling pathway. *Oncogene*, **12**, 1077-1082.
370. Zhan, Q. (2005) Gadd45a, a p53- and BRCA1-regulated stress protein, in cellular response to DNA damage. [Review] [54 refs]. *Mutat. Res.*, **569**, 133-143.
371. Cecconi, F. (1999) Apaf1 and the apoptotic machinery. [Review] [92 refs]. *Cell Death & Differentiation*, **6**, 1087-1098.
372. Chauhan, D., Hideshima, T., Rosen, S., Reed, J.C., Kharbanda, S., Anderson, K.C., Hideshima, T., Rosen, S., Reed, J.C., Kharbanda, S., and Anderson, K.C. (2001) Apaf-1/cytochrome c-independent and Smac-dependent induction of apoptosis in multiple myeloma (MM) cells. *Journal of Biological Chemistry*, **276**, 24453-24456.
373. Morgan, W.A. (1995) Naphthoquinone-induced DNA damage in the absence of oxidative stress. *Biochemical Society Transactions*, **23**, 225S.
374. Shi, M., Gozal, E., Choy, H.A., Forman, H.J., Gozal, E., Choy, H.A., and Forman, H.J. (1993) Extracellular glutathione and gamma-glutamyl transpeptidase prevent H₂O₂-induced injury by 2,3-dimethoxy-1,4-naphthoquinone. *Free Radical Biology & Medicine*, **15**, 57-67.
375. Castillo, S.S., Levy, M., Thaikootathil, J.V., Goldkorn, T., Levy, M., Thaikootathil, J., V, and Goldkorn, T. (2007) Reactive nitrogen and oxygen species activate different sphingomyelinases to induce apoptosis in airway epithelial cells. *Experimental Cell Research*, **313**, 2680-2686.
376. Bresgen, N., Jaksch, H., Bauer, H.C., Eckl, P., Krizbai, I., Tempfer, H., Jaksch, H., Bauer, H., Eckl, P., Krizbai, I., and Tempfer, H. (2006) Astrocytes are more resistant than cerebral

endothelial cells toward geno- and cytotoxicity mediated by short-term oxidative stress. *Journal of Neuroscience Research*, **84**, 1821-1828.

377. Gant, T.W., Rao, D.N., Mason, R.P., Cohen, G.M., Rao, D.N., Mason, R.P., and Cohen, G.M. (1988) Redox cycling and sulphhydryl arylation; their relative importance in the mechanism of quinone cytotoxicity to isolated hepatocytes. *Chemico-Biological Interactions*, **65**, 157-173.
378. Markesbery, W.R. (1997) Oxidative stress hypothesis in Alzheimer's disease. [Review] [155 refs]. *Free Radical Biology & Medicine*, **23**, 134-147.
379. Castellani, R., Smith, M.A., Richey, P.L., Perry, G., Smith, M.A., Richey, P.L., and Perry, G. (1996) Glycooxidation and oxidative stress in Parkinson disease and diffuse Lewy body disease. *Brain Research*, **737**, 195-200.
380. Hirsch-Ernst, K.I., Kietzmann, T., Ziemann, C., Jungermann, K., Kahl, G.F., Kietzmann, T., Ziemann, C., Jungermann, K., and Kahl, G.F. (2000) Physiological oxygen tensions modulate expression of the *mdr1b* multidrug-resistance gene in primary rat hepatocyte cultures. *Biochemical Journal*, **350 Pt 2**, 443-451.
381. Anthony, D.C., Montine, T.J., and Graham, D.G. (1996) Toxic Responses of the Nervous System. In Klaassen, C.D. (ed.) *Cassarett and Doull's Toxicology*. McGraw-Hill, pp 463-86.
382. Wallace, K.B. (1983) Hepatic redox homeostasis following acute adriamycin intoxication in rats. *Biochem. Pharmacol.*, **32**, 2577-2582.
383. Rojas, C., Cadenas, S., Lopez-Torres, M., Perez-Campo, R., Barja, G., Cadenas, S., Lopez-Torres, M., Perez-Campo, R., and Barja, G. (1996) Increase in heart glutathione redox ratio and total antioxidant capacity and decrease in lipid peroxidation after vitamin E dietary supplementation in guinea pigs. *Free Radical Biology & Medicine*, **21**, 907-915.